Connecting Visual Perception, Attention, and Probabilistic Models of Task Performance with EEG Measured Brain Activity

by

Sarah S. Sheldon

A thesis submitted in partial fulfillment of the requirements for the degree of

Doctor of Philosophy

Department of Psychology
University of Alberta

Abstract

The neural mechanisms underlying visual perception and attention continue to elude researchers despite decades of research. Developing novel methodology and improved analytical techniques may provide key insights into these processes that traditional approaches have been unable to reveal. In this dissertation, we pursue this idea in a series of studies whose overall aim is to better understand visual perception, attention, and their underlying neural mechanisms. First, we demonstrate how the novel adaptation of visual working memory probabilistic models can turn simple performance measures into metrics that quantify the quality of participants' internal perceptual representations. When paired with EEG analysis, we find evidence that perceptual representations will vary only within a fixed range of values, but where in that range its precision falls changes from trial-to-trial as a function of post-stimulus neural activity. Next, we extend this approach to test the effects of covert attention modulation while simultaneously questioning previous assumptions about the role of periodic oscillatory activity, particularly in the alpha (8-14 Hz) frequency, during the cued version of the orientation perception task. From this novel combination, we find evidence that the conflicting reports on the role of alpha oscillations in visual perception and attention are, at least partially, due to measures being confounded by the overlapping and task-related 1/f aperiodic activity. Finally, we used multivariate pattern analysis (MVPA) to address a long-standing question regarding how alpha-related brain activity prior to the presentation of a visual stimulus corresponds to attention, perception, and subsequent task performance. Our results suggest that it is the complex spatiotemporal dynamics of alpha amplitude that best represents what makes trials with covert spatial attention distinguishable from trials without. However, we found little evidence that those same spatiotemporal patterns of activity are predictive of subsequent behavioral responses.

Overall, this series of studies demonstrate the value of using novel techniques that can take full advantage of the inherent multidimensionality of EEG data as well as highlights the opportunities these methods present for future research.

Preface

The research project, of which this thesis is a part, received research ethics approval from the University of Alberta Research Ethics Board, Project Name “Electrophysiological markers of cognitive processes”, Study ID: Pro00050069, 08/08/2014 to 03/29/2022.

The content of Chapters 1 and 3 are my own original work. Initial development of the methodology in Chapter 4 was done with advice from Professor A. Fyshe at the University of Alberta. Chapter 2 of this thesis has been published as Sheldon, S. S., and Mathewson, K. E. (2021). To see, not to see or to see poorly: Perceptual quality and guess rate as a function of electroencephalography (EEG) brain activity in an orientation perception task. *European Journal of Neuroscience*, 1– 24. KEM and I conceived of the experiment in Chapter 2 and 3. I was responsible for the data collection and analysis as well as the manuscript composition. KEM facilitated the results interpretation and contributed to manuscript edits.

Acknowledgements

First and foremost, I would like to thank my advisor Kyle Mathewson who has been everything I wanted in an advisor and everything I needed in a mentor. Thank you for helping me restore my belief in myself. I also want to thank all the past and present members of the MathLab, but especially Daniel Robles, Jon Kuziek, and Joanna Scanlon. Your support has meant the world to me, and I am pretty sure I would have crashed a long time ago without it. Also, a huge thanks to my husband Jim who has put up with long distance, late nights, ordering delivery a little too often, and the unending skull cave. Finally, I want to thank my mom and dad, my brother Dusty, and my sisters Shannon, Nicole, Stacie, and Sami for the years of love and support that helped me get to this point.

Table of Contents

List of Tables

List of Figures

1

INTRODUCTION

Our brain consistently deals with a dynamic and continuous stream of information about the world around us. It is so effective and efficient at this task that we do not notice it happening. Yet, a small disruption to this process can have devastating effects. Vision, in particular, is fundamental to our ability to interact with and thrive in the world. It is important enough that 54% of (macaque) primates' neocortex is involved in visual information processing (Van Essen *et al.*, 1990) and 20% of the human cortical surface is dedicated to processing just the most basic visual features of stimuli (Wandell, Dumoulin and Brewer, 2009). While the mechanisms underlying the sensory experience of vision (*i.e.,* the conversion of light into neural signals) are relatively well understood, how that sensory experience is transformed into visual perception is still unknown. Part of this lack of knowledge is due to the difficulty in developing tasks that change what a participant perceives without changing the sensory information. One approach is to use stimuli that have two or more possible perceptual interpretations. For example, a Necker cube is a reversible or ambiguous figure consisting of an invariant stimulus pattern that can alternate between at least two different perceptual interpretations. This allows for dissociation between low-level stimulus processing and the mechanisms involved in conscious perceptions (İşoğlu-Alkaç and Strüber, 2006). However, this approach has limitations including the inability to determine where in the visual pathway the reversal takes places, especially if low-level visual processing fluctuates along with the observer's interpretation (Hogendoorn, 2015).

Another popular approach is to present participants near-threshold stimuli and then compare brain activity between trials with different performance outcomes (*e.g.,* correct vs

incorrect). Traditionally, near-threshold stimuli are part of a two-alternative forced-choice (2-AFC) task or similar discrete response paradigm. In these types of paradigms, participants are required to select one out of two or more possible responses. Sometimes they are asked to choose the correct stimulus out of an array of different stimuli or to simply report whether they detected a visual stimulus. While these paradigms are powerful and easy to use, they might not be the best choice for investigating certain aspects of visual perception that are easier to measure with a continuous scale. For example, the question of whether the quality of visual perception varies from trial to trial or has a precision that remains constant for a given level of visibility would be difficult to answer without a way to directly measure the variability of a response, something that cannot be done with categorical data (in regard to the traditional concept of variability; see Kader and Perry (2007) for a discussion on variability in categorical data).

Another reason the mechanisms underlying visual perception have remained elusive is that certain fundamental questions have yet to be answered. It is still unknown whether visual perception is an all-or-none process or is a continuum of degrees in perception quality. Previous research has found that variations in neural activity give rise to variations in our visual perception (Mathewson et al., 2011; Chaumon & Busch, 2014; Samaha et al., 2020). However, it is unclear whether this is because of variation in stimulus detection, variation in the quality of perception, or a combination of both. To answer this question, we adapted the orientation memory task by Bae and Luck's (2018) into an orientation perception task so that visual perception could be measured on a continuous scale. The researchers originally used their task to investigate how well information held in working memory can be decoded from brain activity. What makes the task useful for the current study is that it allows participants to give a continuous response when asked to report the orientation of the target. Performance can then be quantified

as the angular difference between the orientation of the target and the orientation reported by the participants, referred to as response error. Even better, these distributions of continuous measure of response errors can be modeled with low parameter working memory models such as the standard mixture model introduced by Zhang and Luck (2008) or the variable precision model by Fougnie and colleagues (2012) to quantify parameters of interest such as guess rate and precision. Furthermore, it is relatively easy to add an attentional component to this type of task without altering the visual characteristics of the stimuli. This makes it especially suitable to dissociate sensory and perceptual processes from attentional mechanisms. By extending this method to orientation perception, one can look at how target detection, perceptual variability, and attention are individually related to electrical brain activity during the task.

The rationale for extending working memory models to visual perception is that many working memory models makes similar assumptions about the outcome of target stimuli. Specifically, they both assume, at least superficially, two distinct states: remembered items are analogous to seen targets (which should produce responses clustered around the correct value, with some variability) and forgotten items parallel unseen targets (which should produce random guessing across all values uniformly). This assumption is the essence of the popular mixture modelling technique where a distribution of responses is fit with a probabilistic model representing a mixture of response types (see Figure 1.1 for examples of mixture models). In this way, the mixture model is used to differentiate the response types (*i.e.,* accurate and guesses), and quantify response variability and guess rate as separate and meaningful parameters (Dube and Golomb, 2020).

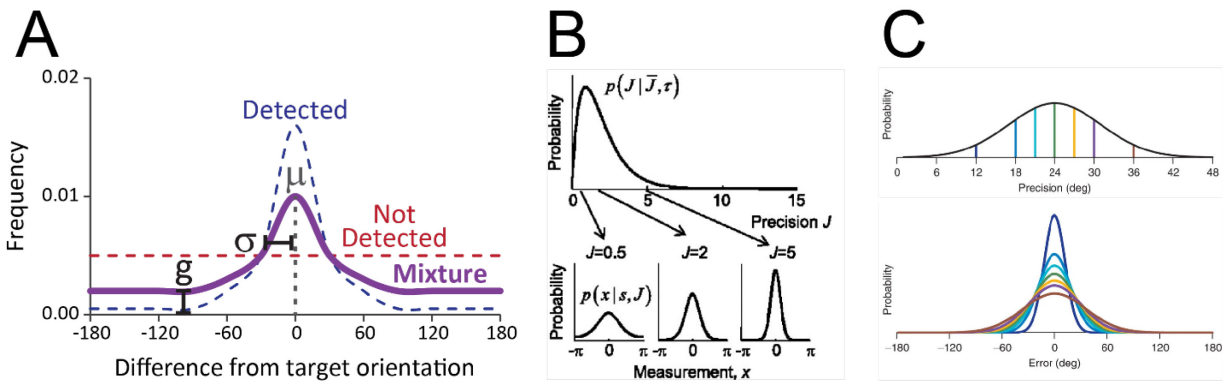

Figure 1.1. ***Examples of visual working memory models***

A) Standard mixture model of performance, showing the probability of reporting each orientation value relative to the original orientation (*i.e.,* amount of response error). When the target was detected, the reported orientation tends to be near the target's orientation (blue broken line). When the target was not detected, the participant is equally likely to report any orientation value (red broken line). When collapsed across trials, the data comprise a mixture of these two trial types (solid purple line), weighted by the probability that probed item was stored in memory. The distribution of the combined trial type can be described by three parameters: g represents guess rate, σ represents response variability, and μ represents response bias which can be fixed at 0 or allowed to vary (adapted from Zhang and Luck, 2008). **B)** (*Upper*) In the variable precision model, the amount of resources dedicated to a target, thus its encoding precision or *J,* is a variable assumed to vary according to (in this example) a gamma distribution. *(Lower*) Von Mises (circular normal) noise distributions correspond to three values of precision (two values when set size, *N*, is equal to 1) and $s = 0$ (adapted from van den Berg, et al., 2012). **C)** (*Upper*) A variable-precision model can be thought of as a higher-order distribution produced by mixing different distributions from fixed-precision models with different precision values. (*Lower*) Each curve shows the distribution of precision for a different fixed-precision model (adapted from Fougnie *et al*., 2012).

Another reason for using working memory models is that there is a strong relationship between perception and working memory. Visual working memory tasks have a visual

perception component that might be a larger contributor to working memory performance than first thought. For example, Schurgin *et al* (2020) recently proposed that working memory performance can be explained by a relatively simple signal detection framework using a single parameter (memory strength, d-prime) once perceptual similarity within the stimulus space is accounted for (Dube and Golomb, 2020). Similarly, Bays (2014) found that recall errors could be better explained by the kind of neural population encoding that explains responses to basic visual features than in terms of allocating limited memory resources. Working memory performance can be well accounted for by basic visual and perceptual processes, therefore it is logical to assume that at least some working memory models are able to capture perceptual processes.

The goals of the current work is first, to ask the question whether working memory probabilistic models can accurately account for performance on an orientation perception task, and, if so, what brain activity is associated with that model's parameters? Next, is how attention and attention-related changes in brain activity affect task performance and whether the working memory model can account for this change, and, if so, how does it affect the model's parameters? Finally, a long-standing question is addressed regarding how brain activity prior to the presentation of a visual stimulus affects perception and subsequent performance.

1.2 Brain Oscillations and Electroencephalography (EEG)

Brain oscillations are the proposed mechanism by which different brain areas communicate and coordinate their activity. It is through the synchronization of rhythmic activity within and between brain regions that cortical excitability and propagation of neural signals are modulated (Buzsáki and Draguhn, 2004; Bonnefond, Kastner and Jensen, 2017). Many cognitive functions are comprised of different component processes that originate in different brain areas. For example, object recognition involves visual processing, feature detection, extracting relevant

information from memory, and decision making. Understanding when and how these operations occur and interact can give insight into mechanisms underlying cognitive functioning (van de Vijver and Cohen, 2019).

The oldest and most well-established method for non-invasive measurements of brain oscillations is electroencephalography (EEG). The first use of EEG in humans was by Hans Berger in 1929. EEG has remained a popular method for studying brain activity because it is non-invasive and has excellent temporal resolution. EEG is considered a direct measure of brain activity, so it lacks the temporal delay associated with measuring changes in blood flow like functional magnetic resonance imaging (fMRI) and functional near-infrared spectroscopy (fNIRS). Specifically, EEG measures synchronized postsynaptic activity of populations of pyramidal neurons. The flow of charged particles across the extracellular membrane causes changes in the polarity of the extracellular fluid. These polarity changes result in dipoles which are instances where a region of a positive charge is separated from a region of a negative charge by some distance. If enough neurons are active at the same time and are oriented so that their dipoles do not cancel each other out (*i.e.,* arranged in parallel), their net activity will sum together creating a dipole whose magnitude is large enough to be measured by electrodes on the scalp (Buzsáki, Anastassiou and Koch, 2012; Jackson and Bolger, 2014; Luck, 2014).

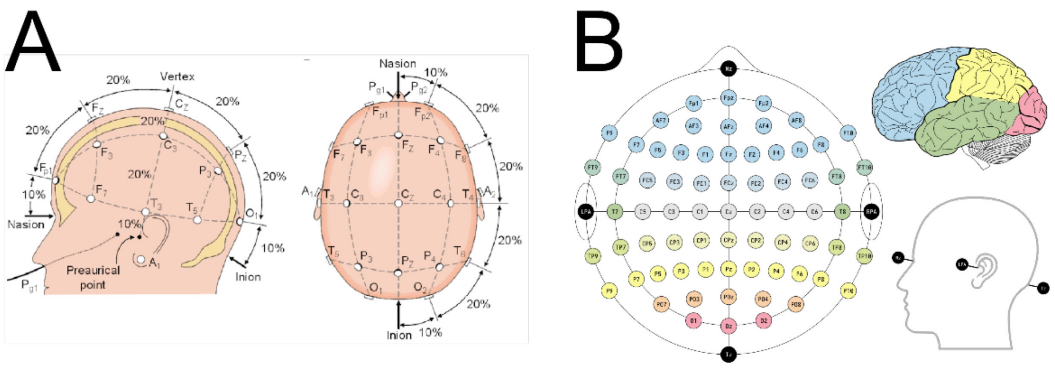

Figure 1.2. ***International standard for EEG electrode placement***

A) EEG electrode positions in the 10-20 system (original image located here: https://blog.adafruit.com/2017/06/19/tdcs-electrode-positioning-the-10-20-system/tdcs-2-2/). **B)** EEG electrode positions in the 10-10 system. The electrode sites are color-coded according to the lobes of the brain which their labels (F, C, P, O, and T) represent (original image by Laurens R. Krol - Own work, CC0, https://commons.wikimedia.org/w/index.php?curid=96859272).

The location of the EEG electrodes has been standardized according to the distance from certain anatomical markers on the head such as the inion and nasion. This standardized system is called the international 10-20, 10-10, or 10-5 system (see Figure 1.2). Twenty, ten, and five are referring to the percentage used for determining the distance between electrodes and anatomical markers. The smaller the percentage, the smaller the distance between electrodes and greater the density of electrode positions across the head. All the relative distances from the anatomical markers are associated with the locations of different functional cortical regions such as the frontal and parietal areas. Odd numbers are assigned to positions left of the center line and even numbers are assigned to positions right of the center line. The more lateral the electrode position, the larger the number.

EEG is recorded as rhythmic activity containing a combination of oscillations fluctuating at different frequencies. The raw EEG signal can be separated into its oscillatory components using one of the various signal-processing methods. These oscillations can be described by three measures: frequency, phase, and power (see Figure 1.3).

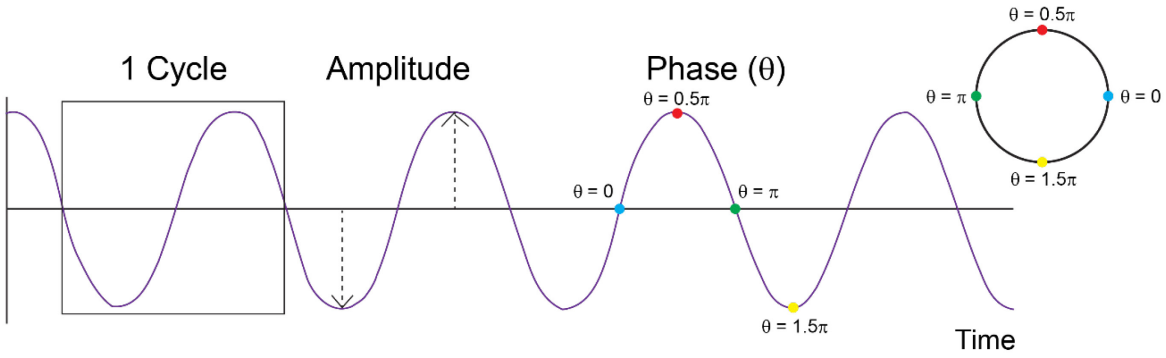

Figure 1.3. ***Example of oscillation characteristics***

Oscillations are characterized by their frequency (the number of cycles per unit time), amplitude or power (power = amplitude^2), and instantaneous phase which fluctuates between 0 and 2p (adapted from van de Vijver & Cohen, 2019).

Power or amplitude (power = amplitude^2) of the waveform can be thought of as the magnitude of the activity. Phase is where in the excitation and inhibition cycle the oscillation is at a given time point (Klimesch, Sauseng and Hanslmayr, 2007; van de Vijver and Cohen, 2019). Logically, phase should relate to when a neural process is more or less optimal because it signifies a phasic change in neural firing probability (VanRullen, 2016b). Inputs arriving during the optimal phase should generate relatively large responses and have a higher probability of firing; whereas inputs arriving during a less optimal phase generate relatively smaller responses and have a lower probability of firing. This enables oscillations to temporally modulate and coordinate information processing by imposing excitability windows that facilitate interactions with appropriate phase and suppressing inputs from out-of-phase neural assemblies (Schroeder and Lakatos, 2009; VanRullen, 2016b). Buzsáki summed this up nicely: "Each oscillatory cycle is a temporal processing window…*"* (Buzsaki and Buzsáki, 2006).

The frequency or speed at which brain oscillations occur have become associated with various functions. Activity at different frequencies is often separated into pre-defined bands to

make it easier to communicate and compare results from different studies. Although the definition of these frequency bands is somewhat arbitrary, they have a basis in the biophysical properties of neurons that constrain the temporal windows at which various functions can occur (Buzsaki and Buzsáki, 2006). Also, pre-defined bands make it easier to form *a priori* hypotheses and use group-level averages. Naturally, this is at the cost of individual differences and sensitivity to performance-related fluctuations within each frequency band. Furthermore, using pre-defined frequency bands requires the assumption that the band limits do not change across individuals and the experiment– an assumption that has been shown to be false under various conditions (Bazanova and Vernon, 2014; Haegens *et al.*, 2014; Mierau, Klimesch and Lefebvre, 2017; Benwell *et al.*, 2019). However, the pre-defined frequency bands have their advantages which often out-weights that potential disadvantages, especially when they are used with a certain degree of caution.

Although there is some small disagreement about what the exact cut-off are, listed are the ranges of the five frequency bands relevant to the current discussion: delta, 1-3 Hz; theta, 4-7 Hz; alpha, 8-14 Hz; beta, 15-30 Hz; and, gamma, >30 Hz. It is common to see these bands separated further, especially in the faster frequencies, but their use usually depends on the hypotheses and experimental design.

An even more controversial question than how to define frequency bands is what role different frequencies have in cognitive functioning. For example, while delta oscillations are often seen during deep sleep, an accumulation of evidence has led investigators to associate waking delta activity with top-down control, attention, memory, motivation, and response inhibition (Harmony, 2013; Başar and Düzgün, 2016; De Vries *et al.*, 2018; Rawls, Miskovic and Lamm, 2020). Delta oscillations have also been implicated in various cognitive dysfunctions

including Alzheimer's disease, schizophrenia, mild cognitive impairment, and alcoholism (Güntekin and Başar, 2016). Since delta activity is a characteristic of sleep, it has been proposed that these oscillations provide prolonged periods of inhibition so that the activity of brain areas that may interfere with mental tasks are inactive (Harmony, 2013). However, there is still a lot unknown about how delta oscillations are related to normal and impaired cognitive processes.

In contrast, theta oscillations have been associated with memory processes though recent studies have found evidence suggesting it has a role in cognitive monitoring and attentional control processes as well (Clayton, Yeung and Cohen Kadosh, 2015; Herweg, Solomon and Kahana, 2020). Theta oscillations can be found in the human cortex and hippocampus. Interactions between cortical and hippocampal theta activity have been associated with virtual navigation, declarative memory, episodic memory, memory encoding, and working memory maintenance (Sauseng *et al.*, 2004; Sauseng and Klimesch, 2008). Theta activity has also been observed in the frontal and parietal cortices during attention tasks though whether it reflects an active mechanism related to prioritization and environmental exploration, or a passive physiological feature emerging from the underlying organization of the attention network (Fiebelkorn and Kastner, 2019; Helfrich, Breska and Knight, 2019) remains unknown.

Alpha oscillations, on the other hand, is the first frequency band identified almost a century ago by Hans Berger (1929). This is because alpha oscillations can have amplitudes large enough to be detected in the raw EEG traces. Also, compared to the other frequency bands, alpha is ubiquitous across the cortex. While alpha oscillations are most prominent over the visual regions, they can often be found at any electrode location regardless of task or stimuli. Alpha is at its maximum in the visual cortex when the participant has their eyes closed. This originally led researchers to conclude that alpha is an 'idling' rhythm (Adrian and Mathews, 1934;

Pfurtscheller, Stancák and Neuper, 1996). That is, it represents the brain being at rest. Since then, the role of alpha oscillations has expanded from a 'cortical idling' brain rhythm to one involved in a range of functions including attention, working memory, and perception (Klimesch, Sauseng and Hanslmayr, 2007; Foxe and Snyder, 2011; Mathewson *et al.*, 2011, 2012; Klimesch, 2012; Clayton, Yeung and Cohen Kadosh, 2015; Frey, Ruhnau and Weisz, 2015; VanRullen, 2016b).

There is also an accumulation of evidence that alpha activity is related to changes in cortical excitability. For example, Laufs and colleagues (2003) used continuous and simultaneous EEG-fMRI to correlate alpha EEG power with blood oxygenation level-dependent (BOLD) signal changes over time. A strong negative correlation of parietal and frontal cortical activity with alpha power was found. In a similar study, the authors found that pre-stimulus alpha phase correlated with cortical excitability fluctuation in the early visual cortex as indexed by the magnitude of visually evoked blood oxygen level dependent (BOLD) response (Scheeringa *et al.*, 2011). A study using EEG-fMRI and EEG-NIRS also found that spontaneous EEG alpha activity in the occipital cortex had an inverse relationship with the fMRI BOLD signal. In addition, the authors reported a positive cross-correlation between alpha and the concentration changes of deoxygenated hemoglobin (Moosmann *et al.*, 2003). This suggests that posterior alpha activity is associated with metabolic deactivation. Finally, some compelling evidence comes from a study using transcranial magnetic stimulation (TMS). In the study, the authors found that phosphenes were more likely to be evoked using TMS over the visual cortex in blindfolded participants when alpha power was low before stimulation rather than high, suggesting that higher alpha power in the visual cortex reduces cortical excitability (Romei *et al.*, 2008; Samaha, Gosseries and Postle, 2017). While these studies provide strong support for alpha

activity being related to cortical excitability, it is still unclear whether alpha modulates cortical excitability or is a consequence of these cortical fluctuations.

Beta has often been associated with motor activity. For example, primary motor cortex exhibits a decrease in beta amplitude during movement and a strong beta rebound when the movement is stopped (Sauseng and Klimesch, 2008). Finally, gamma oscillations have a frequency above 30 Hz and are thought to synchronize local patterns of neuronal population activity and indicate a state of high cortical excitability (Miller *et al.*, 2014; Seymour, Rippon and Kessler, 2017). Gamma activity is often studied (especially frequencies faster than 50 Hz) using more invasive electrophysiological methods such as electrocorticography (ECoG). This is because the faster the frequency, the less distance over which synchronization can occur due to limits imposed by axon conductance and synaptic delays (Buzsaki and Buzsáki, 2006).

1.3 VISUAL PERCEPTION

As mentioned previously, one of the goals of the research studies covered in Chapters 2, 3 and 4 is to investigate the mechanism underlying visual perception. An influential, and particularly controversial issue is the idea that perceptual outcome is determined, or at least influenced, by brain activity prior to the presentation of a stimulus. Some researchers have proposed that the power of oscillatory alpha-band activity can determine perceptual outcome (Hanslmayr *et al.*, 2007; van Dijk *et al.*, 2008). In line with this idea, studies have reported that whether or not a visual stimulus will be perceived can be predicted on a trial-by-trial basis by prestimulus alpha amplitude (Ergenoglu *et al.*, 2004; van Dijk *et al.*, 2008). However, a study looking at discrimination accuracy and its confidence in a two-alternative forced choice (2-AFC) discrimination task found that pre-stimulus alpha activity was not associated with discrimination

accuracy, but instead was related to participants' confidence in the accuracy they reported (Samaha, Iemi and Postle, 2017).

Recently, it has been proposed that spontaneous alpha activity (*i.e.,* ongoing alpha activity that occurs in the absence of sensory input) modulates the probability of responding rather than the probability of perceiving a visual stimulus (Iemi *et al.*, 2017). This is supported by findings that suggest alpha power before stimulus onset predict the probability of reporting the presence of a stimulus, even when no stimulus was presented, with an increased likelihood of reporting stimulus detection during states of low alpha power prior to stimulus onset (Limbach and Corballis, 2016; Benwell *et al.*, 2017, 2021; Iemi *et al.*, 2017; Iemi and Busch, 2018). Furthermore, a study looking at whether the temporal resolution of sequential stimuli varied as a function of prestimulus alpha power found that participants were more likely to report seeing two visual stimuli when occipital alpha power was low regardless of whether there was one or two visual stimuli presented (Lange, Oostenveld and Fries, 2013). It seems alpha power therefore predicts a change in *response threshold* rather than changes to *perceptual sensitivity*.

Other researchers proposed that perceptual outcome depends on the phase of alpha oscillations at the moment of stimulus onset, which is explained as alpha acting as a pulsating inhibition in the brain (Mathewson *et al.*, 2009; Busch, Dubois and VanRullen, 2009; VanRullen, 2016). This theory stems from the idea that there is an "ideal" brain state for optimal stimulus processing which is reflected in the phase of the oscillations. For example, the stimulus being presented at peak of an oscillation leads to better processing than if the stimulus was presented while the oscillation was in its trough or midway between peak and trough. In this way, alpha can use pulses of cortical inhibition to modulate incoming sensory information into perception as a function of the phase within the alpha cycle (Mathewson *et al.*, 2011).

Support for this idea comes from a study using EEG and fMRI simultaneously to look at the covariation between alpha oscillations and blood oxygenation level-dependent (BOLD) signal during visual stimulation. It was found that stimuli arriving at the peak of an alpha cycle corresponded to a lower BOLD signal in the early visual cortex than stimuli presented at the trough. In contrast, pre-stimulus alpha power had no significant relationship to the visually evoked BOLD signal. This evidence suggests that alpha phase reflects periodic fluctuations in cortical excitability, as indexed by the BOLD signal, which, in turn, modulates the strength of the visually evoked response (Scheeringa *et al.*, 2011).

Further evidence comes from a series of studies in which alpha oscillations were rhythmically entrained with visual stimulation resulting in phase locking at the same frequency in the EEG, as well as rhythmic modulation of target detectability and temporal feature integration (Mathewson *et al.*, 2014; Kizuk and Mathewson, 2017; Ronconi and Melcher, 2017; Ronconi, Busch and Melcher, 2018). Using fast optical imaging, it was also found that these alpha oscillations relevant for detection can be localized to the posterior parietal cortex (Mathewson *et al.*, 2014).

However, recent studies have raised questions about the role of alpha phase in perception. Zazio and colleagues (2021) found a strong association between pre-stimulus alpha power, post-stimulus neural correlates of conscious perception, and performance on a near-threshold visual detection task such that Hit trials were preceded by weaker pre-stimulus alpha power and greater post-stimulus evoked responses. By contrast, no influence of pre-stimulus alpha phase was found. A pre-registered study by Ruzzoli and colleagues (2019) also found no significant correlation between perceptual behavior and phase of 5-15 Hz EEG activity despite using a

hypothesis-driven design based on prior studies that had found a significant effect of alpha phase.

Alternatively, these results do not preclude alpha phase from being involved in visual perception. Instead, they might hint at a more complex mechanism where phase and amplitude interact to produce the observed effects on perception. Mathewson *et al* (2011) proposed such a mechanism. The idea was that when alpha amplitude is low, cortical excitability is high enough that a stimulus will always be detected regardless of phase. In contrast, when alpha power is high, cortical excitability fluctuations as a function phase are now cycling between being above and below the excitability threshold required to detect a stimulus. Thus, stimulus detection depends on when in the phase cycle the stimulus was presented only when alpha power is above a certain threshold. Along the same lines, Schalk (2015) proposed a function-through-biased-oscillations (FBO) framework in which the mean voltage of an alpha cycle varies with the amplitude of alpha oscillations. Greater alpha amplitude corresponds to a more negative voltage level and higher inhibition. In turn, this results in shorter time windows for sensory processing (*i.e.,* the duty cycle). This mechanism would provide a parsimonious explanation for the disparate results from previous studies.

Another possible explanation for the conflicting findings on alpha oscillations is based on a model presented by Zazio and colleagues (2020) named the oscillation-based probability of response (OPR). They propose that alpha oscillations modulate gamma activity by decreasing the amplitude and/or synchronization of gamma oscillations thereby affecting visual perception. This idea is supported by research into the role of gamma oscillations for sensory enhancement (Pritchett *et al.*, 2015; Ni *et al.*, 2016) and the inverse relationship between alpha activity, cortical excitability and sensory perception (Samuel *et al.*, 2018; de Graaf *et al.*, 2020). For

example, Fries et al (2008) found that during the prestimulus period, attention within the receptive field of a recorded neural population enhanced gamma band synchronization and reduced alpha band synchronization. Adding to the evidence is research using transcranial stimulation that found stimulation at alpha frequency modulated gamma oscillation activity (Hamidi, 2009; Herring *et al.*, 2019; Okazaki, Mizuno and Kitajo, 2020). Specifically, it was found that applying a weak alternating current at the participant's individual alpha frequency to the occipital cortex induced rhythmically suppressed visual stimulus-induced gamma band power. Furthermore, the degree of gamma band power reduction predicted the decrease in visual detection performance (Herring *et al.*, 2019).

It seems that dynamic interactions between alpha and gamma oscillations might also provide a parsimonious explanation for the disparate results from previous studies (Jensen and Mazaheri, 2010; Zazio *et al.*, 2020). However, it is important to point out that theories based on the interactions between the phase and power of alpha oscillations and those based on coupling between alpha and gamma activity are not mutually exclusive. In fact, the most recent proposals go out of their way to point out that their ideas are complimentary to the previous theories (Schalk, 2015; Zazio *et al.*, 2020). Therefore, it is likely that the alpha cycle could rhythmically shift neurons' membrane potential so that gamma bursts occur only during "excitability windows" where the alpha phase is at its trough, and when the amplitude of alpha activity is sufficiently low. In this way, alpha oscillations would modulate variations in the sensitivity and temporal resolution of visual perception (Wagner *et al.*, 2019).

Finally, it should be noted that alpha and gamma oscillations are not the only frequency bands associated with visual perception. Visual target detection has also been found to vary as a function of prestimulus delta and theta oscillations. In a study by Fiebelkorn et al (2013), they

found that low theta and delta phase modulated visual target detection prior to stimulus onset. Furthermore, the effects of higher frequencies on perceptual outcome, particularly for beta band activity, was almost entirely dependent on their interaction with delta and theta phase. Many studies do not have a long enough interstimulus interval to measure frequencies as low as delta, so this has been a relatively unexplored area. Future research is needed to better understand the role of these lower frequencies in visual perception.

1.4 VISUAL ATTENTION

In addition to visual perception, attention is another focus of the research covered in Chapters 3 and 4. The mechanisms underlying attention have been particularly difficult to elucidate even though it is relevant to a variety of cognitive functions and psychopathologies. This is partly due to the complexity of attention. Even when the focus is only on the visual domain, excluding other sensory or cross-sensory modalities, researchers have distinguished multiple types of attention. These include top-down attention, bottom-up attention, covert attention, overt attention, spatial attention, object-based attention, and feature-based attention (Carrasco, 2011).

Top-down attention is thought as endogenously generated allocation of attention according to internal, behavioral goals. In contrast, bottom-up attention is automatic, driven by exogenous orientating towards physical salience. Overt attention involves moving the eyes towards the attended location whereas covert attention requires allocating attention without moving the eyes. In studies using functional imaging, covert attention has an advantage compared to overt attention because eye movements can be a source of noise during electrophysiological recordings (causes voltage deflections much larger than typical brain-related activity) and a confound due to an uncontrolled change in the visual input during the task (Luck,

2014). Object-based attention involves focusing on certain objects categories like chairs or dogs. Feature-based attention focuses on an object's characteristics like color and orientation. Visual search paradigms are often used to study object- and feature-based attention. Spatial attention is where attention is allocated to different locations in space, often using visual or auditory cues to direct attention during the task. Presumably, attention should enable a relative improvement in task-related sensory processing and subsequent behavioral responses. The two mechanisms associated with attentional modulation of information processing are enhancement and inhibition (Carrasco, 2011; Tallon-Baudry, 2012).

Attentional enhancement is where the task-related sensory signal is amplified by a relative increase in the neuronal response (Luck *et al.*, 1997; Hillyard and Anllo-Vento, 1998; Hillyard, Vogel and Luck, 1998; Kastner and Ungerleider, 2000). Studies in non-human primates have found that attention directed to a location in a neuron's receptive field enhances the neuron's response to a single stimulus presented within the receptive field compared to when attention is directed outside the receptive field (Spitzer, Desimone and Moran, 1988; Motter, 1993; Luck *et al.*, 1997). Using a delayed match-to-sample task with oriented stimuli, researchers were able to construct orientation-tuning curves from neuronal responses when stimuli were attended to and when stimuli were ignored. From this, the researchers found that attention enhanced the responses of V1 and V4 neurons selectively but did not alter the width of their orientation-tuning curve suggesting that visual spatial attention amplifies neural responses to stimuli at attended locations rather than change the preferred orientation or sharpness of tuning, thus prioritizing information processing for stimuli appearing at that location (McAdams and Maunsell, 1999). A similar type of attention modulation is seen for features in that responses

are enhanced for neurons that prefer the feature currently being attended to (Martinez-Trujillo and Treue, 2004; Maunsell and Treue, 2006).

Furthermore, in a study investigating the link between pre-stimulus brain activity and behavioral performance, it was found that discrimination performance and reaction time were predicted on a trial-by-trial basis by the relative decrease in alpha amplitude over the contralateral visual cortex about 500 ms before target onset (Kelly, Gomez-Ramirez and Foxe, 2009). The decrease in contralateral alpha activity was believed to reflect enhanced excitability in the visual processing areas (Sauseng *et al.*, 2005; Thut *et al.*, 2006; Kelly, Gomez-Ramirez and Foxe, 2009). This finding implies that the attention-related enhancement observed at the single-neuron level also occurs at the macroscale level through alpha-related modulation.

The other attentional mechanism, inhibition, is where neurons unrelated to the task are in a state of decreased receptivity so that distracting or competing information does not interfere with the relevant information. This inhibitory attentional mechanism is thought to be mediated by alpha oscillatory activity. For example, with regards to visual spatial attention, numerous studies have found that alpha amplitude is enhanced in the areas contralateral to an ignored location (Kelly *et al.*, 2006) or a location with distracting stimuli (Worden *et al.*, 2000; Foxe and Snyder, 2011). These findings were interpreted as attention-driven modulation of cortical excitability by alpha so that the brain areas irrelevant to the task were selectively suppressed.

Interestingly, this selective functional inhibition or suppression by alpha activity is also observed during feature-based attention. For example, in a delayed-match-to-sample task, participants had an increase in alpha power in the parieto-occipital area during retention of face identities compared with the retention of face orientation. This finding supports the idea of feature-selective attention in that the dorsal stream (maintaining orientation information) was

selectively suppressed by alpha activity when the ventral stream (maintaining face identity) was engaged (Jokisch and Jensen, 2007). In line with these results, it was found that attending to words led to increased power of parieto-occipital alpha oscillations over the right hemisphere as compared to when faces were attended. This object-selective lateralization of alpha oscillations was maintained during sustained selective attention while sequentially presented with face and word stimuli (Knakker, Weiss and Vidnyánszky, 2015). Like spatial and feature-based attention, object-based attention selection also seems to involve alpha oscillations modulating information processing.

So far, the focus has been on attentional mechanisms within separate brain regions. However, there has also been a lot of work looking at synchronous activity between brain areas as a means for mediating attentional modulation. Specifically, posterior parietal and frontal brain regions have been suggested to coordinate attentional modulation of the visual cortex via low-frequency oscillations (Miller and Buschman, 2013; Fiebelkorn and Kastner, 2019). In one study, during the cue-target interval of a cued visual spatial attention task, increased alpha phase synchronization was observed between the prefrontal cortex and the posterior parietal area that was contralateral to the attended visual hemifield. In addition, a significant reduction in alpha amplitude was observed at the parieto-occipital brain areas contralateral to the attended visual hemifield compared to the ipsilateral brain areas (Sauseng *et al.*, 2005). In another study on visuospatial attention, sustained long-range synchronization of high alpha (10-14 Hz) oscillations was observed in the frontal, parietal, and visual areas along with amplitude suppression of low alpha (6-9 Hz) oscillations in the visual cortex. Importantly, stronger high alpha phase synchronization was associated with decreased reaction times to attended stimuli and larger alpha amplitude suppression (Lobier, Palva and Palva, 2018). Finally, collaborating evidence

also comes from a study correlating single-trial EEG alpha power with BOLD activity. The researchers report that the BOLD in the intraparietal sulcus (IPS) had a stronger inverse correlation with occipital alpha power within the hemisphere contralateral to the attended hemifield. Furthermore, the magnitude of this alpha lateralization was positively correlated with BOLD in the dorsal anterior cingulate cortex and dorsolateral prefrontal cortex (Liu *et al.*, 2016). These findings suggest alpha synchronization has an important role in supporting frontoparietal visuospatial attention and possibly cortical excitability of visual brain areas as indicated by modulated alpha amplitude (Peylo, Hilla and Sauseng, 2021).

Although the focus has been mostly on alpha-band activity, it is important to note that many studies have found that theta-band activity is also involved in visual attention, particularly through the engagement of frontocentral areas. For example, Helfrich *et al* (2018) found that perceptual outcome at the single-participant level varied as a function of theta phase even in states of sustained spatial attention. They suggest that neuronal excitability fluctuations at around theta shapes the attentional sampling rhythm of the frontoparietal attention network and the corresponding behavior (Helfrich *et al.*, 2018). Similarly, the variability of attention processing has been associated with theta phase coherence in frontal and parieto-occipital brain regions (Lutz *et al.*, 2009; Reteig *et al.*, 2019). Finally, in a rhythmic transcranial magnetic stimulation (TMS) study designed to establish a causal role for parietal alpha and frontal theta oscillations in the maintenance of working memory representations, the authors found that alpha in the parietal cortex was involved in suppressing task-irrelevant information while prefrontal theta supported task-relevant prioritization (Riddle *et al.*, 2020). This suggests that inhibition by alpha oscillations is only half of a balanced excitatory-inhibitory network supporting successful behavioral performance.

While studies have found attention being mediated by a network of different brain areas, at the local level, there is also recent evidence that suggests attention modulation is more anatomically selective than once thought. Using a linear support vector machine (SVM) classifier, Samaha *et al* (2016) found that the topography of alpha power could be used to identify the one location out of six attended to during sustained spatial attention. In a similar study where a cue was presented briefly in one of 16 locations directing covert spatial attention, it was found that the distribution of posterior alpha sources approximated retinotopic organization and that better performance was associated with the magnitude of the spatial tuning (Popov *et al.*, 2019). These results suggest that attending to specific spatial locations involves selective topographic cortical modulation by alpha oscillations which is much more spatially constrained than the hemispheric or regional changes observed previously. However, it should be noted that the reconstructed tuning function representing the spatial focus of attention by Samaha et al (2016) showed alpha power to be higher at the attended location and falling off for locations further away. In contrast, the tuning function by Popov *et al* (2019) had the inverse with a depression of alpha power at the attended location. While this could be explained by differences in task design and type of recorded brain activity (notable, one study used EEG and the other used MEG), this still highlights how the neural mechanisms underlying visual attention are still largely unknown.

Together, the evidence points toward visual attention relying on both enhancement and inhibition mechanisms which, in turn, are associated with alpha oscillatory activity. This could be because alpha modulates information processing, either directly or indirectly, through fluctuations in cortical excitability using similar mechanisms discussed in the section on visual perception. In this way, changes in alpha activity would result in enhancement or inhibition of

sensory processing since an increase or decrease in cortical excitability would either facilitate or suppress neuronal responses, respectively. Within the larger attentional network, long-range phase synchronization could coordinate, across different brain regions, the top-down prioritization provided by theta with the task-irrelevant suppression provided by alpha oscillations as well as the modulation of local sensory processing through selective enhancement of task-relevant neuronal responses via coupling with gamma oscillations.

1.5 The Unknowns of Alpha Oscillations

Although the mechanisms underlying visual perception and attention remain unclear, it seems that alpha activity has an important role in both functions. However, despite nearly a century of research, there is still a lot about alpha oscillations that remains relatively unknown. For example, in addition to not knowing how alpha is involved in a variety of cognitive functions, the circuits that generate alpha are also unclear. Originally, there was a strong belief that alpha band activity came from a thalamo-cortical loop involving the lateral geniculate nucleus (LGN) and visual cortex and cortico-cortical interactions across different brain regions. In a study by Lopes da Silva and colleagues (1980), strong coherence between the pulvinar nuclei and visual cortex was found; at the same time, there was high cortico-cortical coherence even after partializing the thalamic contribution. Together this suggests independent thalamic and cortical sources of alpha generation (Lopes da Silva, 1991).

In support of independent thalamic and cortical alpha generators, later research pointed to the thalamus as the primary alpha pacemaker, with the classic posterior alpha rhythm driven by the pulvinar (Saalmann *et al.*, 2012). It was also found that the cortex could still generate alpha activity in isolation and in vitro when the pulvinar is inactivated (Lopes da Silva, 1991; Zhou, Schafer and Desimone, 2016). From this, it was proposed that alpha rhythms were the result of a

"diffuse and distributed" system (Silva, Amitai and Connors, 1991; Başar *et al.*, 1997; Bourgeois *et al.*, 2020). However, more recent findings have complicated these prevailing theories. Using microelectrodes and macroelectrodes in surgical epilepsy patient, Halgren and colleagues (2019) found that alpha propagates from higher-order to lower-order cortical areas, and that cortical alpha leads pulvinar alpha, contradicting theories of a thalamic pacemaker. Taken together, the neural circuitry generating alpha oscillations seem rather complex, with independent contributions from thalamic and cortical sources that are likely interacting across different brain areas though the details of where and how still needs to be determined.

While there is a plethora of evidence suggesting that alpha has a role in a variety of cognitive functions across and between different modalities (Klimesch, Sauseng and Hanslmayr, 2007; Foxe and Snyder, 2011; Mathewson *et al.*, 2011, 2012; Klimesch, 2012; Clayton, Yeung and Cohen Kadosh, 2015, 2018; Frey, Ruhnau and Weisz, 2015; VanRullen, 2016b), exactly what that role is, and how it can be involved in so many different functions is still debated. For example, some researchers believe alpha oscillations control the flow of information into sensory areas or from sensory areas to higher order cortical locations via amplitude and phase modulating the time windows at which information can be accessed (Klimesch, Sauseng and Hanslmayr, 2007; Jensen and Mazaheri, 2010; Foxe and Snyder, 2011; Mathewson *et al.*, 2011; Chaumon and Busch, 2014). Others think alpha oscillations indirectly control perception and attention by modulating the higher frequencies (e.g., gamma oscillations, >30 Hz) involved in information processing (Voytek, 2010; Jensen *et al.*, 2014; Zazio *et al.*, 2020). All these explanations seem to point towards alpha oscillations reflecting changes in cortical excitability. In this way, alpha activity would be associated with fluctuations in the level of information processing since an increase or decrease in cortical excitability would facilitate or suppress task-related neural

activity, respectively. Whether this means a mechanism where alpha oscillations are directly modulating via amplitude and phase, indirectly modulating through interactions with gamma activity, or simply an index or consequence of cortical fluctuations remains to be seen.

Overall, the sources of alpha oscillations are still relatively unknown. It is also unclear how (even if) alpha is involved in the brain's functioning. It is up to future researchers to elucidate where in the brain alpha activity is generated. However, the following work will help address some of the mysteries around alpha's involvement in cognitive functions, specifically, perception and attention.

1.6 SUMMARY

To better understand visual perception, attention and their underlying neural mechanisms, a series of experiments were conducted using EEG and probabilistic modelling. The first experiment in Chapter 2 focuses on using visual working memory models to quantify perceptual performance and associated changes in brain activity. The next two experiments reported on in Chapters 3 and 4 extend the results from Chapter 2 by adding a visual spatial attention component. Specifically, Chapter 3 focuses on the visual working models and whether they can be used to quantify the effects of visual spatial attention on orientation perception performance and corresponding changes in brain activity. In contrast, Chapter 4 is addressing the questions regarding pre-stimulus alpha activity and its relationship to visual spatial attention, visual perception, and perceptual outcome. This chapter is dedicated to determining how well alpha power, alpha-gamma coupling, and alpha-based functional connectivity can predict orientation perception performance with and without covert attention. In summary, the following work will investigate the neural mechanisms that connect visual perception and attention to perceptual performance.

References

Adrian, E. D. and Mathews, B. H. (1934) 'The Berger rhythm: potential changes from the occipital lobes in man', *Brain*, 57(4), pp. 355–385. Available at: https://backyardbrains.com/experiments/files/AdrianMathews-1934-EEG-recordings.pdf.

Başar, E. *et al.* (1997) 'Alpha oscillations in brain functioning: an integrative theory', *International Journal of Psychophysiology*, 26(1), pp. 5–29. doi: https://doi.org/10.1016/S0167-8760(97)00753-8.

Başar, E. and Düzgün, A. (2016) 'Links of Consciousness, Perception, and Memory by Means of Delta Oscillations of Brain', *Frontiers in Psychology*, 7, p. Article 275. doi: 10.3389/fpsyg.2016.00275.

Bays, P. M. (2014) 'Noise in Neural Populations Accounts for Errors in Working Memory', *The Journal of Neuroscience*, 34(10), pp. 3632–3645. doi: 10.1523/JNEUROSCI.3204-13.2014.

Bazanova, O. M. and Vernon, D. J. (2014) 'Interpreting EEG alpha activity', *Neuroscience & Biobehavioral Reviews*, 44, pp. 94–110. doi: 10.1016/j.neubiorev.2013.05.007.

Benwell, C. S. Y. *et al.* (2017) 'Prestimulus EEG Power Predicts Conscious Awareness But Not Objective Visual Performance.', *eNeuro*. Society for Neuroscience, 4(6). doi: 10.1523/ENEURO.0182-17.2017.

Benwell, C. S. Y. *et al.* (2019) 'Frequency and power of human alpha oscillations drift systematically with time-on-task', *NeuroImage*. Academic Press, 192, pp. 101–114. doi: 10.1016/J.NEUROIMAGE.2019.02.067.

Benwell, C. S. Y. *et al.* (2021) 'Low pre-stimulus EEG alpha power amplifies visual awareness but not visual sensitivity', *European Journal of Neuroscience*. John Wiley & Sons, Ltd,

00, pp. 1–16. doi: 10.1111/EJN.15166.

van den Berg, R. *et al.* (2012) 'Variability in encoding precision accounts for visual short-term memory limitations', *Proceedings of the National Academy of Sciences of the United States of America*. National Academy of Sciences, 109(22), pp. 8780–8785. doi: 10.1073/pnas.1117465109.

Berger, H. (1929) 'Über das Elektrenkephalogramm des Menschen', *Archiv für Psychiatrie und Nervenkrankheiten*. Springer-Verlag, 87(1), pp. 527–570. doi: 10.1007/BF01797193.

Bonnefond, M., Kastner, S. and Jensen, O. (2017) 'Communication between brain areas based on nested oscillations', *eNeuro*, 4(2). doi: 10.1523/ENEURO.0153-16.2017.

Bourgeois, A. *et al.* (2020) 'Pulvino-cortical interaction: An integrative role in the control of attention', *Neuroscience & Biobehavioral Reviews*, 111, pp. 104–113. doi: https://doi.org/10.1016/j.neubiorev.2020.01.005.

Busch, N. A., Dubois, J. and VanRullen, R. (2009) 'The phase of ongoing EEG oscillations predicts visual perception', *Journal of Neuroscience*, 29(24), pp. 7869–7876. doi: https://doi.org/10.1523/JNEUROSCI.0113-09.2009.

Buzsáki, G., Anastassiou, C. A. and Koch, C. (2012) 'The origin of extracellular fields and currents — EEG, ECoG, LFP and spikes', *Nature Reviews Neuroscience*, 13(6), pp. 407–420. doi: 10.1038/nrn3241.

Buzsaki, G. and Buzsáki, G. (2006) *Rhythms of the Brain*. Oxford, UK: Oxford university press. doi: 10.1093/acprof:oso/9780195301069.001.0001.

Buzsáki, G. and Draguhn, A. (2004) 'Neuronal oscillations in cortical networks', *Science*. American Association for the Advancement of Science, 304(5679), pp. 1926–1929. doi: 10.1126/science.1099745.

Carrasco, M. (2011) 'Visual attention: The past 25 years', *Vision Research*. Pergamon, 51(13), pp. 1484–1525. doi: 10.1016/J.VISRES.2011.04.012.

Chaumon, M. and Busch, N. A. (2014) 'Prestimulus neural oscillations inhibit visual perception via modulation of response gain', *Journal of Cognitive Neuroscience*. MIT Press Journals, 26(11), pp. 2514–2529. doi: 10.1162/jocn_a_00653.

Clayton, M. S., Yeung, N. and Cohen Kadosh, R. (2015) 'The roles of cortical oscillations in sustained attention', *Trends in Cognitive Sciences*. Elsevier Ltd, pp. 188–195. doi: 10.1016/j.tics.2015.02.004.

Clayton, M. S., Yeung, N. and Cohen Kadosh, R. (2018) 'The many characters of visual alpha oscillations', *European Journal of Neuroscience*. Blackwell Publishing Ltd, 48(7), pp. 2498–2508. doi: 10.1111/ejn.13747.

van Dijk, H. *et al.* (2008) 'Prestimulus Oscillatory Activity in the Alpha Band Predicts Visual Discrimination Ability', *The Journal of Neuroscience*, 28(8), pp. 1816–1823. doi: 10.1523/JNEUROSCI.1853-07.2008.

Dube, B. and Golomb, J. D. (2020) 'Revisiting mixture models of memory', *Nature Human Behaviour*, 4(11), pp. 1098–1099. doi: 10.1038/s41562-020-00947-z.

Ergenoglu, T. *et al.* (2004) 'Alpha rhythm of the EEG modulates visual detection performance in humans', *Cognitive Brain Research*, 20(3), pp. 376–383. doi: https://doi.org/10.1016/j.cogbrainres.2004.03.009.

Van Essen, D. C. *et al.* (1990) 'Modular and hierarchical organization of extrastriate visual cortex in the macaque monkey', *Cold Spring Harbor symposia on quantitative biology*, 55, pp. 679–696. Available at: https://www-webofscience-com.login.ezproxy.library.ualberta.ca/wos/woscc/full-record/WOS:A1990HB91800063.

Fiebelkorn, I. C. *et al.* (2013) 'Cortical cross-frequency coupling predicts perceptual outcomes', *NeuroImage*. Academic Press, 69, pp. 126–137. doi: 10.1016/j.neuroimage.2012.11.021.

Fiebelkorn, I. C. and Kastner, S. (2019) 'A Rhythmic Theory of Attention', *Trends in Cognitive Sciences*. Elsevier Current Trends, 23(2), pp. 87–101. doi: 10.1016/j.tics.2018.11.009.

Fougnie, D., Suchow, J. W. and Alvarez, G. A. (2012) 'Variability in the quality of visual working memory', *Nature Communications*. NIH Public Access, 3, p. 1229. doi: 10.1038/ncomms2237.

Foxe, J. J. and Snyder, A. C. (2011) 'The role of alpha-band brain oscillations as a sensory suppression mechanism during selective attention', *Frontiers in Psychology*. Frontiers Media SA, 2, p. Article 154. doi: 10.3389/fpsyg.2011.00154.

Frey, J. N., Ruhnau, P. and Weisz, N. (2015) 'Not so different after all: The same oscillatory processes support different types of attention', *Brain Research*. Elsevier, 1626, pp. 183–197. doi: 10.1016/J.BRAINRES.2015.02.017.

Fries, P. *et al.* (2008) 'The Effects of Visual Stimulation and Selective Visual Attention on Rhythmic Neuronal Synchronization in Macaque Area V4', *The Journal of Neuroscience*, 28(18), pp. 4823–4835. doi: 10.1523/JNEUROSCI.4499-07.2008.

de Graaf, T. A. *et al.* (2020) 'Does alpha phase modulate visual target detection? Three experiments with tACS-phase-based stimulus presentation', *European Journal of Neuroscience*. Blackwell Publishing Ltd, 51(11), pp. 2299–2313. doi: 10.1111/ejn.14677.

Güntekin, B. and Başar, E. (2016) 'Review of evoked and event-related delta responses in the human brain', *International Journal of Psychophysiology*, 103, pp. 43–52. doi: https://doi.org/10.1016/j.ijpsycho.2015.02.001.

Haegens, S. *et al.* (2014) 'Inter- and intra-individual variability in alpha peak frequency',

NeuroImage. Academic Press, 92, pp. 46–55. doi: 10.1016/J.NEUROIMAGE.2014.01.049.

Halgren, M. *et al.* (2019) 'The generation and propagation of the human alpha rhythm', *Proceedings of the National Academy of Sciences*. National Academy of Sciences, 116(47), pp. 23772–23782. doi: 10.1073/pnas.1913092116.

Hamidi, M. (2009) 'Repetitive transcranial magnetic stimulation affects behavior by biasing endogenous cortical oscillations', *Frontiers in Integrative Neuroscience*. Frontiers, 3(JUN), p. 14. doi: 10.3389/neuro.07.014.2009.

Hanslmayr, S. *et al.* (2007) 'Prestimulus oscillations predict visual perception performance between and within subjects', *NeuroImage*, 37(4), pp. 1465–1473. doi: https://doi.org/10.1016/j.neuroimage.2007.07.011.

Harmony, T. (2013) 'The functional significance of delta oscillations in cognitive processing', *Frontiers in Integrative Neuroscience*. Frontiers, 7, p. Article 83. doi: 10.3389/fnint.2013.00083.

Helfrich, R. F. *et al.* (2018) 'Neural mechanisms of sustained attention are rhythmic', *Neuron*. Elsevier Inc., 99(4), pp. 854–865. doi: 10.1016/j.neuron.2018.07.032.

Helfrich, R. F., Breska, A. and Knight, R. T. (2019) 'Neural Entrainment and Network Resonance in Support of Top-down guided Attention', *Current Opinion in Psychology*. Elsevier. doi: 10.1016/J.COPSYC.2018.12.016.

Herring, J. D. *et al.* (2019) 'Low-frequency alternating current stimulation rhythmically suppresses gamma-band oscillations and impairs perceptual performance', *NeuroImage*, 184, pp. 440–449. Available at: https://www.sciencedirect.com/science/article/pii/S1053811918318469 (Accessed: 27

November 2018).

Herweg, N. A., Solomon, E. A. and Kahana, M. J. (2020) 'Theta Oscillations in Human Memory', *Trends in Cognitive Sciences*, 24(3), pp. 208–227. doi: https://doi.org/10.1016/j.tics.2019.12.006.

Hillyard, S. A. and Anllo-Vento, L. (1998) 'Event-related brain potentials in the study of visual selective attention.', *Proceedings of the National Academy of Sciences of the United States of America*. National Academy of Sciences, 95(3), pp. 781–787. doi: 10.1073/pnas.95.3.781.

Hillyard, S. A., Vogel, E. K. and Luck, S. J. (1998) 'Sensory gain control (amplification) as a mechanism of selective attention: electrophysiological and neuroimaging evidence', *Philosophical Transactions of the Royal Society of London. Series B: Biological Sciences*. The Royal Society, 353(1373), pp. 1257–1270. doi: 10.1098/RSTB.1998.0281.

Hogendoorn, H. (2015) 'From sensation to perception: Using multivariate classification of visual illusions to identify neural correlates of conscious awareness in space and time', *Perception*, 44(1), pp. 71–78. doi: 10.1068/p7832.

Iemi, L. *et al.* (2017) 'Spontaneous neural oscillations bias perception by modulating baseline excitability', *Journal of Neuroscience*. Society for Neuroscience, 37(4), pp. 807–819. doi: 10.1523/JNEUROSCI.1432-16.2016.

Iemi, L. and Busch, N. A. (2018) 'Moment-to-moment fluctuations in neuronal excitability bias subjective perception rather than strategic decision-making', *eNeuro*. Society for Neuroscience, 5(3). doi: 10.1523/ENEURO.0430-17.2018.

İşoğlu-Alkaç, Ü. and Strüber, D. (2006) 'Necker cube reversals during long-term EEG recordings: Sub-bands of alpha activity', *International Journal of Psychophysiology*,

59(2), pp. 179–189. doi: https://doi.org/10.1016/j.ijpsycho.2005.05.002.

Jackson, A. F. and Bolger, D. J. (2014) 'The neurophysiological bases of EEG and EEG measurement: A review for the rest of us', *Psychophysiology*. John Wiley & Sons, Ltd, 51(11), pp. 1061–1071. doi: 10.1111/PSYP.12283.

Jensen, O. *et al.* (2014) 'Temporal coding organized by coupled alpha and gamma oscillations prioritize visual processing', *Trends in Neurosciences*. Elsevier Ltd, 37(7), pp. 357–369. doi: 10.1016/j.tins.2014.04.001.

Jensen, O. and Mazaheri, A. (2010) 'Shaping functional architecture by oscillatory alpha activity: Gating by inhibition', *Frontiers in Human Neuroscience*. Frontiers Media S. A., 4, p. 186. doi: 10.3389/fnhum.2010.00186.

Jokisch, D. and Jensen, O. (2007) 'Modulation of Gamma and Alpha Activity during a Working Memory Task Engaging the Dorsal or Ventral Stream', *Journal of Neuroscience*. Society for Neuroscience, 27(12), pp. 3244–3251. doi: 10.1523/JNEUROSCI.5399-06.2007.

Kastner, S. and Ungerleider, L. G. (2000) 'Mechanisms of visual attention in the human cortex', *Annual Review of Neuroscience*. Annual Reviews 4139 El Camino Way, P.O. Box 10139, Palo Alto, CA 94303-0139, USA, pp. 315–341. doi: 10.1146/annurev.neuro.23.1.315.

Kelly, S. P. *et al.* (2006) 'Increases in Alpha Oscillatory Power Reflect an Active Retinotopic Mechanism for Distracter Suppression During Sustained Visuospatial Attention', *Journal of Neurophysiology*, 95(6), pp. 3844–3851. doi: 10.1152/jn.01234.2005.

Kelly, S. P., Gomez-Ramirez, M. and Foxe, J. J. (2009) 'The strength of anticipatory spatial biasing predicts target discrimination at attended locations: a high-density EEG study', *European Journal of Neuroscience*. John Wiley & Sons, Ltd, 30(11), pp. 2224–2234. doi:

https://doi.org/10.1111/j.1460-9568.2009.06980.x.

Kizuk, S. A. D. and Mathewson, K. E. (2017) 'Power and Phase of Alpha Oscillations Reveal an Interaction between Spatial and Temporal Visual Attention', *Journal of Cognitive Neuroscience*. MIT PressOne Rogers Street, Cambridge, MA 02142-1209USAjournals-info@mit.edu, 29(3), pp. 480–494. doi: 10.1162/jocn_a_01058.

Klimesch, W. (2012) 'Alpha-band oscillations, attention, and controlled access to stored information', *Trends in Cognitive Sciences*. Elsevier, 16(12), pp. 606–617. doi: 10.1016/j.tics.2012.10.007.

Klimesch, W., Sauseng, P. and Hanslmayr, S. (2007) 'EEG alpha oscillations: the inhibition–timing hypothesis', *Brain Research Reviews*, 53(1), pp. 63–88. doi: 10.1016/j.brainresrev.2006.06.003.

Knakker, B., Weiss, B. and Vidnyánszky, Z. (2015) 'Object-based attentional selection modulates anticipatory alpha oscillations', *Frontiers in Human Neuroscience*, 8, p. Article 1048. doi: 10.3389/fnhum.2014.01048.

Lange, J., Oostenveld, R. and Fries, P. (2013) 'Reduced Occipital Alpha Power Indexes Enhanced Excitability Rather than Improved Visual Perception', *The Journal of Neuroscience*, 33(7), pp. 3212–3220. doi: 10.1523/JNEUROSCI.3755-12.2013.

Laufs, H. *et al.* (2003) 'EEG-correlated fMRI of human alpha activity', *NeuroImage*, 19(4), pp. 1463–1476. doi: 10.1016/S1053-8119(03)00286-6.

Limbach, K. and Corballis, P. M. (2016) 'Prestimulus alpha power influences response criterion in a detection task', *Psychophysiology*. Blackwell Publishing Inc., 53(8), pp. 1154–1164. doi: 10.1111/psyp.12666.

Liu, Y. *et al.* (2016) 'Top-down Modulation of Neural Activity in Anticipatory Visual Attention:

Control Mechanisms Revealed by Simultaneous EEG-fMRI.', *Cerebral cortex*. Oxford University Press, 26(2), pp. 517–529. doi: 10.1093/cercor/bhu204.

Lobier, M., Palva, J. M. and Palva, S. (2018) 'High-alpha band synchronization across frontal, parietal and visual cortex mediates behavioral and neuronal effects of visuospatial attention', *NeuroImage*, 165, pp. 222–237. doi: https://doi.org/10.1016/j.neuroimage.2017.10.044.

Lopes da Silva, F. (1991) 'Neural mechanisms underlying brain waves: from neural membranes to networks', *Electroencephalography and Clinical Neurophysiology*, 79(2), pp. 81–93. doi: https://doi.org/10.1016/0013-4694(91)90044-5.

Lopes da Silva, F. H. *et al.* (1980) 'Relative contributions of intracortical and thalamo-cortical processes in the generation of alpha rhythms, revealed by partial coherence analysis', *Electroencephalography and Clinical Neurophysiology*, 50(5), pp. 449–456. doi: https://doi.org/10.1016/0013-4694(80)90011-5.

Luck, S. J. *et al.* (1997) 'Neural Mechanisms of Spatial Selective Attention in Areas V1, V2, and V4 of Macaque Visual Cortex', *Journal of Neurophysiology*, 77(1), pp. 24–42. doi: 10.1152/jn.1997.77.1.24.

Luck, S. J. (2014) *An introduction to the event-related potential technique*. 2nd edn. Cambridge, Massachusetts: MIT Press. Available at: https://www.library.ualberta.ca/catalog/7776529 (Accessed: 9 November 2017).

Lutz, A. *et al.* (2009) 'Mental Training Enhances Attentional Stability: Neural and Behavioral Evidence', *Journal of Neuroscience*. Society for Neuroscience, 29(42), pp. 13418–13427. doi: 10.1523/JNEUROSCI.1614-09.2009.

Martinez-Trujillo, J. C. and Treue, S. (2004) 'Feature-Based Attention Increases the Selectivity

of Population Responses in Primate Visual Cortex', *Current Biology*, 14(9), pp. 744–751. doi: https://doi.org/10.1016/j.cub.2004.04.028.

Mathewson, K. E. *et al.* (2009) 'To See or Not to See: Prestimulus Phase Predicts Visual Awareness', *Journal of Neuroscience*, 29(9), pp. 2725–2732. doi: 10.1523/JNEUROSCI.3963-08.2009.

Mathewson, K. E. *et al.* (2011) 'Pulsed out of awareness: EEG alpha oscillations represent a pulsed-inhibition of ongoing cortical processing.', *Frontiers in Psychology*, 2, p. Article 99. doi: 10.3389/fpsyg.2011.00099.

Mathewson, K. E. *et al.* (2012) 'Making waves in the stream of consciousness: entraining oscillations in EEG alpha and fluctuations in visual awareness with rhythmic visual stimulation', *Journal of Cognitive Neuroscience*. MIT Press, 24(12), pp. 2321–2333. doi: 10.1162/jocn_a_00288.

Mathewson, K. E. *et al.* (2014) 'Dynamics of Alpha Control: Preparatory Suppression of Posterior Alpha Oscillations by Frontal Modulators Revealed with Combined EEG and Event-related Optical Signal', *Journal of Cognitive Neuroscience*. MIT PressOne Rogers Street, Cambridge, MA 02142-1209USAjournals-info@mit.edu, 26(10), pp. 2400–2415. doi: 10.1162/jocn_a_00637.

Maunsell, J. H. R. and Treue, S. (2006) 'Feature-based attention in visual cortex', *Trends in Neurosciences*, 29(6), pp. 317–322. doi: https://doi.org/10.1016/j.tins.2006.04.001.

McAdams, C. J. and Maunsell, J. H. R. (1999) 'Effects of Attention on Orientation-Tuning Functions of Single Neurons in Macaque Cortical Area V4', *Journal of Neuroscience*. Society for Neuroscience, 19(1), pp. 431–441. doi: 10.1523/JNEUROSCI.19-01-00431.1999.

Mierau, A., Klimesch, W. and Lefebvre, J. (2017) 'State-dependent alpha peak frequency shifts: experimental evidence, potential mechanisms and functional implications', *Neuroscience*. Pergamon, 360, pp. 146–154. doi: 10.1016/J.NEUROSCIENCE.2017.07.037.

Miller, E. K. and Buschman, T. J. (2013) 'Cortical circuits for the control of attention', *Current Opinion in Neurobiology*, 23(2), pp. 216–222. doi: https://doi.org/10.1016/j.conb.2012.11.011.

Miller, K. J. *et al.* (2014) 'Broadband changes in the cortical surface potential track activation of functionally diverse neuronal populations', *NeuroImage*, 85, pp. 711–720. doi: https://doi.org/10.1016/j.neuroimage.2013.08.070.

Moosmann, M. *et al.* (2003) 'Correlates of alpha rhythm in functional magnetic resonance imaging and near infrared spectroscopy', *NeuroImage*, 20(1), pp. 145–158. doi: 10.1016/S1053-8119(03)00344-6.

Motter, B. C. (1993) 'Focal attention produces spatially selective processing in visual cortical areas V1, V2, and V4 in the presence of competing stimuli', *Journal of Neurophysiology*. American Physiological Society, 70(3), pp. 909–919. doi: 10.1152/jn.1993.70.3.909.

Ni, J. *et al.* (2016) 'Gamma-Rhythmic Gain Modulation', *Neuron*. Cell Press, 92(1), pp. 240–251. doi: 10.1016/j.neuron.2016.09.003.

Okazaki, Y. O., Mizuno, Y. and Kitajo, K. (2020) 'Probing dynamical cortical gating of attention with concurrent TMS-EEG', *Scientific Reports*. Nature Research, 10(1), pp. 1–10. doi: 10.1038/s41598-020-61590-2.

Peylo, C., Hilla, Y. and Sauseng, P. (2021) 'Cause or consequence? Alpha oscillations in visuospatial attention', *Trends in Neurosciences*, 44(9), pp. 705–713. doi: https://doi.org/10.1016/j.tins.2021.05.004.

Pfurtscheller, G., Stancák, A. and Neuper, C. (1996) 'Event-related synchronization (ERS) in the alpha band - An electrophysiological correlate of cortical idling: A review', *International Journal of Psychophysiology*. Elsevier B.V., 24(1–2), pp. 39–46. doi: 10.1016/S0167-8760(96)00066-9.

Popov, T. *et al.* (2019) 'Spatial specificity of alpha oscillations in the human visual system', *Human Brain Mapping*. John Wiley & Sons, Ltd, 40(15), pp. 4432–4440. doi: https://doi.org/10.1002/hbm.24712.

Pritchett, D. L. *et al.* (2015) 'For things needing your attention: The role of neocortical gamma in sensory perception', *Current Opinion in Neurobiology*. Elsevier Ltd, pp. 254–263. doi: 10.1016/j.conb.2015.02.004.

Rawls, E., Miskovic, V. and Lamm, C. (2020) 'Delta phase reset predicts conflict-related changes in P3 amplitude and behavior', *Brain Research*. Elsevier B.V., 1730, p. 146662. doi: 10.1016/j.brainres.2020.146662.

Reteig, L. C. *et al.* (2019) 'Sustaining attention for a prolonged period of time increases temporal variability in cortical responses', *Cortex*, 117, pp. 16–32. doi: https://doi.org/10.1016/j.cortex.2019.02.016.

Riddle, J. *et al.* (2020) 'Causal Evidence for a Role of Theta and Alpha Oscillations in the Control of Working Memory', *Current Biology*, 30(9), pp. 1748–1754. doi: https://doi.org/10.1016/j.cub.2020.02.065.

Romei, V. *et al.* (2008) 'Spontaneous Fluctuations in Posterior α-Band EEG Activity Reflect Variability in Excitability of Human Visual Areas', *Cerebral Cortex*, 18(9), pp. 2010–2018. doi: 10.1093/cercor/bhm229.

Ronconi, L., Busch, N. A. and Melcher, D. (2018) 'Alpha-band sensory entrainment alters the

duration of temporal windows in visual perception', *Scientific Reports*. Nature Publishing Group, 8(1), p. 11810. doi: 10.1038/s41598-018-29671-5.

Ronconi, L. and Melcher, D. (2017) 'Alpha oscillation phase determines the timing of perception: evidence from sensory entrainment', *Journal of Vision*, 17(10), p. 726. doi: 10.1167/17.10.726.

Ruzzoli, M. *et al.* (2019) 'The relevance of alpha phase in human perception', *Cortex*. Elsevier BV, 120, pp. 249–268. doi: 10.1016/j.cortex.2019.05.012.

Saalmann, Y. B. *et al.* (2012) 'The Pulvinar Regulates Information Transmission Between Cortical Areas Based on Attention Demands', *Science*, 337(6095), pp. 753–756. doi: 10.1126/science.1223082.

Samaha, J., Gosseries, O. and Postle, B. R. (2017) 'Distinct Oscillatory Frequencies Underlie Excitability of Human Occipital and Parietal Cortex', *Journal of Neuroscience*. Society for Neuroscience, 37(11), pp. 2824–2833. doi: 10.1523/JNEUROSCI.3413-16.2017.

Samaha, J., Iemi, L. and Postle, B. R. (2017) 'Prestimulus alpha-band power biases visual discrimination confidence, but not accuracy', *Consciousness and Cognition*. Academic Press, 54, pp. 47–55. doi: 10.1016/J.CONCOG.2017.02.005.

Samaha, J., Sprague, T. C. and Postle, B. R. (2016) 'Decoding and Reconstructing the Focus of Spatial Attention from the Topography of Alpha-band Oscillations', *Journal of Cognitive Neuroscience*. MIT PressOne Rogers Street, Cambridge, MA 02142-1209USAjournals-info@mit.edu, 28(8), pp. 1090–1097. doi: 10.1162/jocn_a_00955.

Samuel, I. B. H. *et al.* (2018) 'The frequency of alpha oscillations: Task-dependent modulation and its functional significance', *NeuroImage*. Academic Press Inc., 183, pp. 897–906. doi: 10.1016/j.neuroimage.2018.08.063.

Sauseng, P. *et al.* (2004) 'Theta coupling in the human electroencephalogram during a working memory task', *Neuroscience Letters*. Elsevier Ireland Ltd, 354(2), pp. 123–126. doi: 10.1016/j.neulet.2003.10.002.

Sauseng, P. *et al.* (2005) 'A shift of visual spatial attention is selectively associated with human EEG alpha activity', *European Journal of Neuroscience*. John Wiley & Sons, Ltd, 22(11), pp. 2917–2926. doi: https://doi.org/10.1111/j.1460-9568.2005.04482.x.

Sauseng, P. and Klimesch, W. (2008) 'What does phase information of oscillatory brain activity tell us about cognitive processes?', *Neuroscience & Biobehavioral Reviews*, 32(5), pp. 1001–1013. doi: https://doi.org/10.1016/j.neubiorev.2008.03.014.

Schalk, G. (2015) 'A general framework for dynamic cortical function: the function-through-biased-oscillations (FBO) hypothesis', *Frontiers in Human Neuroscience*, 9, p. Article 352. doi: 10.3389/fnhum.2015.00352.

Scheeringa, R. *et al.* (2011) 'Modulation of Visually Evoked Cortical fMRI Responses by Phase of Ongoing Occipital Alpha Oscillations', *The Journal of Neuroscience*, 31(10), pp. 3813–3820. doi: 10.1523/JNEUROSCI.4697-10.2011.

Schroeder, C. E. and Lakatos, P. (2009) 'Low-frequency neuronal oscillations as instruments of sensory selection', *Trends in Neurosciences*, 32(1), pp. 9–18. doi: https://doi.org/10.1016/j.tins.2008.09.012.

Schurgin, M. W., Wixted, J. T. and Brady, T. F. (2020) 'Psychophysical scaling reveals a unified theory of visual memory strength', *Nature Human Behaviour*, 4(11), pp. 1156–1172. doi: 10.1038/s41562-020-00938-0.

Seymour, R. A., Rippon, G. and Kessler, K. (2017) 'The Detection of Phase Amplitude Coupling during Sensory Processing', *Frontiers in Neuroscience*. Frontiers Media S.A., 11(SEP),

p. 487. doi: 10.3389/fnins.2017.00487.

Silva, L. R., Amitai, Y. and Connors, B. W. (1991) 'Intrinsic Oscillations of Neocortex Generated by Layer 5 Pyramidal Neurons', *Science*, 251(4992), pp. 432–435. doi: 10.1126/science.1824881.

Spitzer, H., Desimone, R. and Moran, J. (1988) 'Increased Attention Enhances Both Behavioral and Neuronal Performance', *Science*. American Association for the Advancement of Science, 240(4850), pp. 338–340. doi: 10.1126/science.3353728.

Tallon-Baudry, C. (2012) 'On the neural mechanisms subserving consciousness and attention', *Frontiers in Psychology*. Frontiers, 2, p. 397. doi: 10.3389/fpsyg.2011.00397.

Thut, G. *et al.* (2006) 'α-Band Electroencephalographic Activity over Occipital Cortex Indexes Visuospatial Attention Bias and Predicts Visual Target Detection', *Journal of Neuroscience*. Society for Neuroscience, 26(37), pp. 9494–9502. doi: 10.1523/JNEUROSCI.0875-06.2006.

VanRullen, R. (2016) 'Perceptual cycles', *Trends in Cognitive Sciences*. Elsevier Current Trends, 20(10), pp. 723–735. doi: 10.1016/j.tics.2016.07.006.

van de Vijver, I. and Cohen, M. X. (2019) *Electrophysiological phase synchrony in distributed brain networks as a promising tool in the study of cognition*, *New Methods in Cognitive Psychology*. doi: 10.4324/9780429318405-8.

Voytek, B. (2010) 'Shifts in gamma phase–amplitude coupling frequency from theta to alpha over posterior cortex during visual tasks', *Frontiers in Human Neuroscience*. Frontiers Media S. A., 4, p. 191. doi: 10.3389/fnhum.2010.00191.

De Vries, I. E. J. *et al.* (2018) 'Priority switches in visual working memory are supported by frontal delta and posterior alpha interactions', *Cerebral Cortex*. Oxford University Press,

28(11), pp. 4090–4104. doi: 10.1093/cercor/bhy223.

Wagner, J. *et al.* (2019) 'Can Oscillatory Alpha-Gamma Phase-Amplitude Coupling be Used to Understand and Enhance TMS Effects?', *Frontiers in Human Neuroscience*, 13, p. Article 263. doi: 10.3389/fnhum.2019.00263.

Wandell, B. A., Dumoulin, S. O. and Brewer, A. A. (2009) 'Visual cortex in humans', *Encyclopedia of Neuroscience*, 10, pp. 251–257. Available at: https://www.spinozacentre.nl/dumoulin/PDFs/Wandell-Encyclopedia-2009.pdf.

Worden, M. S. *et al.* (2000) 'Anticipatory Biasing of Visuospatial Attention Indexed by Retinotopically Specific α-Bank Electroencephalography Increases over Occipital Cortex', *Journal of Neuroscience*. Society for Neuroscience, 20(6), p. RC63. doi: 10.1523/JNEUROSCI.20-06-j0002.2000.

Zazio, A. *et al.* (2020) 'Modelling the effects of ongoing alpha activity on visual perception: The oscillation-based probability of response', *Neuroscience & Biobehavioral Reviews*. Elsevier Ltd, 112, pp. 242–253. doi: 10.1016/j.neubiorev.2020.01.037.

Zazio, A. *et al.* (2021) 'Pre-stimulus alpha-band power and phase fluctuations originate from different neural sources and exert distinct impact on stimulus-evoked responses', *European Journal of Neuroscience*. John Wiley & Sons, Ltd, 00, pp. 1–13. doi: https://doi.org/10.1111/ejn.15138.

Zhang, W. and Luck, S. J. (2008) 'Discrete fixed-resolution representations in visual working memory.', *Nature*. NIH Public Access, 453(7192), pp. 233–235. doi: 10.1038/nature06860.

Zhou, H., Schafer, R. J. and Desimone, R. (2016) ‘Pulvinar-Cortex Interactions in Vision and Attention’, *Neuron*, 89(1), pp. 209–220. doi: https://doi.org/10.1016/j.neuron.2015.11.034.

2

PERCEPTUAL QUALITY AND GUESS RATE AS A FUNCTION OF ELECTROENCEPHALOGRAPHY (EEG) BRAIN ACTIVITY IN AN ORIENTATION PERCEPTION TASK

2.1 INTRODUCTION

Variations in neural activity give rise to observed variations in our visual perception (Mathewson *et al.*, 2011; Chaumon and Busch, 2014; Samaha *et al.*, 2020). While there has been a plethora of research into the brain activity that drives this process, there remains noticeable gaps in our understanding of how these processes work. One of the reasons for this might be because investigators have left basic questions about the underlying mechanisms unanswered. Specifically, and the question the current research will address, does a perceptual representation always form with the same precision or does the quality depend on the state of the neural activity?

Traditionally, visual perception has been studied with two-alternative forced-choice (2-AFC) tasks or similar discrete response paradigms. In these types of paradigms, participants are required to select one out of two or more possible responses. Sometimes they are asked to choose the correct stimulus out of an array of different stimuli or to simply report whether they detected a visual stimulus. While these paradigms are powerful and easy to use, they might not be the best choice for investigating certain aspects of visual perception that are easier to measure with a continuous scale. For example, the question of whether the quality of visual perception varies from trial to trial or has a precision that remains constant for a given level of visibility would be

difficult to answer without a way to directly measure the variability of a response, something that cannot be done with categorical data (in regards to the traditional concept of variability; see Kader and Perry (2007) for a discussion on variability in categorical data). To answer this question about the nature of perceptual processes, we chose a task that can measure visual perception on a continuous scale and a model that can quantify perceptual responses in a way that will inform our question (it should be noted that this can be done by using categorical responses (see Shen and Ma (2019) for 11 experiments of this type), but it relies on the model describing the relationship between a target stimulus and the underlying probability of a correct or positive response rather than simply having the model describe the probability of response errors). With this goal in mind, we adapted the orientation memory task by Bae and Luck (2018) into an orientation perception task. The researchers originally used their task to investigate how well information held in working memory can be decoded from brain activity. What makes the task useful for the current study is that it allows participants to give a continuous response when asked to report the orientation of the target. Performance can then be quantified as the angular difference between the orientation of the target and the orientation reported by the participants, referred to as response errors. This continuous measure of response errors can utilize models such as the standard mixture model introduced by Zhang and Luck (2008) or the variable precision model by Fougnie and colleagues (2012) to quantify parameters of interest such as guess rate and precision. By extending this method to orientation perception, we can look at how target detection and perceptual variability are individually related to electrical brain activity during the task.

To address the question about the type of process underlying visual perception, we combined our adapted version of the visual orientation task with the standard mixture model and

electroencephalography (EEG). Orientation estimation tasks are common in the visual perception literature (Fischer and Whitney, 2014) and the application of the standard mixture model to perception, and orientation perception, in particular, has been previously studied (Bays, 2016; Samaha, Switzky and Postle, 2019). However, to our knowledge, this is a novel approach to quantify the effects of EEG brain activity on visual orientation perception using the standard mixture model to quantify performance. As a result, the purpose of the study was two-fold. First, we asked whether the standard mixture model is a good choice for quantifying orientation perception task performance by comparing the fits of other appropriate working memory models to the data. All the working memory models we tested made the same assumption that the distribution of errors could be separated in a uniform distribution representing guesses and a normal distribution of seen or remembered targets. The main difference between models was how the variability of the normal distribution got defined. This means that regardless of the model, there would be a standard deviation parameter (the standard deviation parameter could be defined by one value or two depending on the model). The uniform distribution quantified by a guess rate parameter may or may not be included depending on the model. Therefore, our second purpose was to test the relationship between EEG activity and the model parameters. We hypothesized that alpha activity prior to the target onset would be related to whether the target was later perceived or not which would be reflected as a modulation of the guess rate parameter or modulation of the mean SD/mode precision if there is no guess rate parameter. We also hypothesized that the precision of perceptual representations was a fixed range (*i.e.*, based on the same distribution across trials) and that it would be related to post-target activity in the lower frequency ranges (4-7 Hz) which would be reflected as modulation of the standard deviation parameter. To address these questions and test our hypotheses, we modified an orientation

memory task from Bae and Luck's (2018) so that it probed participants' perception of the target's orientation rather than their ability to remember it. We then recorded EEG activity as participants performed the adapted task so we can see how brain activity varies with their perceptual performance.

2.2 Materials and Methods

Participants

Twenty-eight participants from the University of Alberta community participated in the study (age range = 17-35 years). Two participants were not included in the analysis due to excessive movement artifacts (more than 25% of trials rejected due to artifacts). Another two participants were excluded from the analysis due to having extreme outlying performance on the task (see Behavioral Analysis in the Results section for more details). Participants were all right-handed and had normal or corrected normal vision and no history of neurological problems. All participants gave informed written consent, were either compensated at a rate of $10/hr or given research credit for their time. The study was approved by the Internal Ethics Board at the University of Alberta.

Orientation Perception Task

Participants were seated 57 cm away from a 1920 x 1080 pixel^2 ViewPixx/EEG LCD monitor (VPixx Technologies, Quebec, Canada) with a refresh rate of 120 Hz, simulating a CRT display with LED backlight rastering. The rastering, along with 8-bit digital TTL output triggers yoked to the onset and value of the top left pixel, allowed for submillisecond accuracy in pixel illumination times, which were confirmed with a photocell prior to the experiment. Stimuli were presented using a Windows 7 PC running MATLAB R2012b with the Psychophysics toolbox (Version 3; Brainard, 1997; Pelli, 1997). The code running the task was a modified version of the

ColorWorkingMemoryExperiment.m code from MemToolbox (Suchow *et al.*, 2013; memtoolbox.org). The modified version of color working memory experiment can be found here: https://github.com/APPLabUofA/OrientTask_paper/tree/master/OrientationTask. Video output was sent to the ViewPixx/EEG with an Asus Striker GTX760 (Fremont, CA) graphics processing unit.

Each trial began with a white fixation dot presented at the center of the monitor for 742, 783, 825, or 867 ms (target stimulus onset asynchrony; tSOA) after which the target appeared for 8.33 ms (one monitor refresh). The target was in the shape of a needle and was pointing toward one of 24 predefined evenly spaced directions so that all the orientations covered 360 degrees. The direction of the target was randomly selected on each trial. Of all the trials, 20% were randomly chosen not to have a target. All aspects of the target-present and target-absent trials were identical except that for the target-absent condition a blank interval replaced target presentation. A backward mask lasting for 8.33 ms with a constant 41.7 ms target-mask stimulus onset asynchrony (mSOA) appeared centrally. The mask was created by overlaying the target orientated in all 24 directions which created a star shape seen in Figure 2.1A. Following the mask offset, a 500 ms blank interval period occurred.

After the blank interval, a response screen appeared with the needle in the center of the screen. Using the computer mouse, participants were asked to rotate the needle so that it was pointed in the same direction as the previous target. If participants detected a target but could not remember its orientation, they were asked to guess the orientation of the target. Participants could provide their response at their own pace so that they could prioritize response accuracy over speed. No feedback was given to participants. The next trial began immediately after a

needle's orientation was selected. See Figure 2.1A for a summary of the task sequence and the stimulus dimensions.

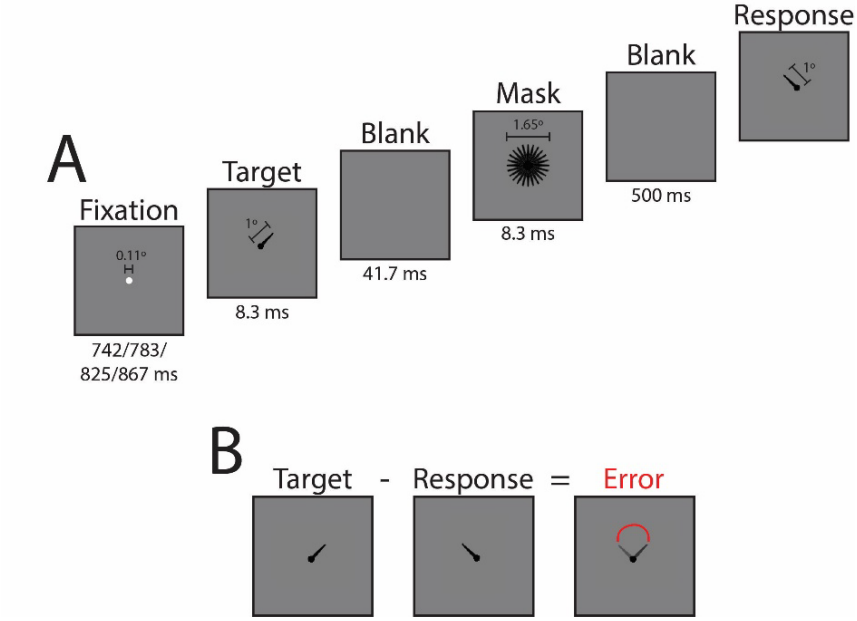

Figure 2.1. ***Orientation perception task***

A) Sequence of task events with duration of each screen presentation and sizes of fixation, target, mask, and response stimuli. Sizes are in degrees of visual angle. **B)** Example of response error calculation. Response errors are reported in degrees.

Participants completed seven blocks consisting of 48 trials each, along with 20 practice trials at the beginning of the experiment. Participants could rest at their own pace every 48 trials. Extensive written and verbal instructions were presented to participants prior to the practice trials. Instructions thoroughly explained and demonstrated each component that would compose a single trial.

Before the orientation perception task, participants performed a staircased target detection task that had the same parameters as the orientation perception task except that participants only

reported whether they saw the target or not using the keyboard. The target color was a gray determined by a scalar value passed to the functions in Psychtoolbox (Version 3; Brainard, 1997; Pelli, 1997). In the staircased target detection task, the target color value could range from the background color (making it not visible; corresponding value of 256) to black (making it the most visible; corresponding value of 0). This target gray value was adjusted throughout the task based on a 1-up/2-down staircasing procedure targeting a 0.6 target detection rate for each individual (García-Pérez, 1998; Kingdom and Prins, 2016). The staircased task consisted of three blocks of 32 trials. The target gray value was determined for each participant by taking the average target gray value across the last two blocks of trials. These final average values ranged from 70 to 112 and were used as the target gray value in the orientation perception task.

The MATLAB code for the a staircased target detection task and the orientation perception task are available at https://osf.io/cw7ux/ and https://github.com/APPLabUofA/OrientTask_paper.

EEG Recording

During the experiment, EEG data was recorded from each participant with a Brain-Amp 32-channel amplifier (BrainVision) using gelled low-impedance electrodes (actiCAP passive electrodes kept below 5 kΩ). Inter-electrode impedances were measured at the start of each experiment. All electrodes were arranged in the same 10-20 positions (Fp2, Fp1, F4, F3, F8, F7, FC2, FC1, FC6, FC5, C4, C3, CP2, CP1, CP6 CP5, P4, P3 P6, P5, P8, P7, PO4, PO3, O2, O1, Fz, FCz, Cz, Pz, and Oz). In addition to the 31 EEG sensors, a ground electrode was used, positioned at AFz. Two reference electrodes and the vertical and horizontal bipolar EOG were recorded from passive Ag/AgCl easycap disk electrodes affixed on the mastoids, above and below the left eye, and 1 cm lateral from the outer canthus of each eye. The bipolar channels

were recorded using the AUX ports of the Brain-Amp amplifier. SuperVisc electrolyte gel and mild abrasion with a blunted syringe tip were used to lower impedances. Gel was applied and inter-electrode impedances were lowered to less than 5 kΩ for all electrode sites. EEG data was recorded online referenced to an electrode attached to the left mastoid. Offline, the data were re-referenced to the arithmetically derived average of the left and right mastoid electrodes.

Data were digitized at 1000 Hz with a resolution of 24 bits. Data were filtered with an online bandpass with cutoffs of 0.1 Hz and 250 Hz. The experiment was run in a dimly lit, sound and radio frequency-attenuated chamber from Electromedical Instruments, with copper mesh covering the window. The only electrical devices in the chamber were an amplifier, speakers, keyboard, mouse, and monitor. The monitor ran on DC power from outside the chamber, the keyboard and mouse were plugged into USB outside the chamber, and the speakers and amplifier were both powered from outside the chamber, and nothing was plugged into the internal power outlets. Any devices transmitting or receiving radio waves (*e.g.*, cell phones) were removed from the chamber for the duration of the experiment.

EEG Preprocessing

All analyses were completed using Matlab R2018b with the EEGLAB 13.6.5b (Delorme and Makeig, 2004) and CircStat (Berens, 2009) toolboxes, as well as custom scripts. After the data had been re-referenced offline, the bandpass FIR filter from EEGLAB was applied with lower and upper cut-offs of 0.1 Hz and 50 Hz. Data was segmented into 3000 ms epochs aligned to target onset (-1500 ms pre-target onset to 1500 ms post-target onset). The average voltage in the 200 ms baseline prior to the target was subtracted on each trial for every electrode, and trials with absolute voltage fluctuations on any channel greater than 1000 μV were discarded. Eye movements were then corrected with a regression-based procedure developed by Gratton, Coles,

and Donchin (1983). After a second baseline subtraction with 200 ms pre-target, trials with remaining absolute voltage fluctuations on any channel greater than 500 μV were removed from further analysis. Data was then subjected to visual inspection and manual rejection of trials contaminated by artifacts. On average, 3% of trials were rejected during visual inspection. Other than the two participants mentioned earlier, none of the remaining participants had more than 20% of trials rejected in this manner.

Data Analyses

Data analysis was performed using MATLAB R2018b (The MathWorks Inc, Natick, MA, USA) and EEGLAB 13.6.5b (Delorme and Makeig, 2004). All statistical analyses were conducted using MATLAB R2018b. Red-white-blue colormaps were created using the redblue.m function by Auton (2009) found here: https://www.mathworks.com/matlabcentral/fileexchange/25536-red-blue-colormap. The MATLAB code for data analysis is available at the GitHub repository https://github.com/APPLabUofA/OrientTask_paper and the raw data files are available at https://osf.io/cw7ux/.

Behavioral Data

Response errors on each trial were calculated by subtracting the orientation of the response stimulus, as reported by the participant, from the orientation of the target stimulus (see Figure 2.1B).

Comparing Model Fits. In addition to the standard mixture model proposed by Zhang and Luck (2008), the working memory literature has several other models similar to the standard mixture model but makes different assumptions about some of the parameters. Some of the working memory models are not appropriate for the current visual orientation perception task

such as those that have an additional Von Mises distributions to account for "swapping" errors or errors where the participant report a distractor item rather than the target (Bays, Catalao and Husain, 2009). On the other hand, the variable precision models were ones that could be appropriate for the current study. The original idea behind to model was that the precision of memory varies from trial-to-trial rather than being fixed as it is in the standard mixture model. This is done by Fougnie and colleagues (2012) by having the standard deviation parameter be distributed according to a higher-order distribution, we chose a Gaussian distribution in this case. The variable precision model proposed by van den Berg and colleagues (2012) has a precision (*i.e.*, the inverse of variance) parameter drawn from a gamma distribution. Neither paper presented clear justification for choosing one distribution over another, especially when the set size is always one, so we tested both distributions. In addition, we tested whether the variable precision models fit better to the response error data when they did not have the guess rate parameter compared to the standard mixture model and the variable precision models with a guess rate parameter. According to the variable precision models, what seems to be guessing is just low precision on that trial (van den Berg *et al.*, 2012). If this were the case, the variable precision models without a guess rate parameter would fit the data better than the standard mixture models. On the other hand, the variable precision models do not, necessarily, preclude guessing. Fougnie *et al* (2012) found that the models with a guess rate parameter described their data better than those without. To determine whether their findings extend to orientation perception data, variable precision models with a guess rate parameter were also tested.

We determined which model better fit the response errors using the model comparison routine in the MemToolbox (Suchow *et al.*, 2013). We included the standard mixture model with the bias parameter in addition to the two variable precision models with and without the guess

rate parameter. The goodness-of-fit measures used were the log likelihood and the Bayesian information criterion (BIC).

Standard Mixture Model. After determining the standard mixture model proposed by Zhang and Luck (2008) was the best fit to the current data set, the model was fit to each participant's response errors using the maximum likelihood estimation routine in the MemToolbox (Suchow *et al.*, 2013). According to the standard mixture model, response deviations from the actual target orientation reflect a mixture of trials where the target's orientation was detected and trials where participants did not detect the target so guessed randomly. Therefore, the distribution of response errors consists of a mixture of a von Mises distribution (representing the trials where the target's orientation was detected) and a uniform distribution (random guesses (g)). Parameter sigma (σ) is the standard deviation of the von Mises distribution, which represents the width of the response error distribution of trials that the target's orientation was detected. Parameter g is the height of the uniform distribution representing the guessing probability. A third parameter, mu (μ), which is the mean of the von Mises distribution and represents systematic bias of the response error distribution was included in the standard mixture model of two participants because the Bayesian information criterion (BIC), calculated with the model comparison functions provided by MemToolbox (Suchow *et al.*, 2013), indicated that the three-parameter standard mixture model provided better fits for those two participants (see Table 2.1). Although the three-parameter model was used for all analysis of those two participants, the systematic bias was much smaller than the spacing between adjacent target orientations (spacing was 15° whereas the two participants' μ was -4.2° and 2.7°) indicating that those two participants had a slight clockwise and counterclockwise bias, respectively. The two-

parameter standard mixture model was used for all analysis of the remaining 22 participants because it provided a better fit according to the BIC.

Time-Frequency Analyses

To calculate the phase angle and power for each trial, we used Morlet wavelet transform of single trials using the newtimef() function of EEGLAB. A Morlet wavelet is a tapered sinusoid, constructed by modulating a sine wave with a Gaussian envelope. Wavelet transformation was created with 1.027 Hz linear steps and cycles starting from 2 cycles at 2 Hz to 12 cycles at 40 Hz. The output of this function was a matrix of complex values. The abs() function from MATLAB was used to get the instantaneous amplitude and the instantaneous phase angle of each trial was calculated using the angle() function from MATLAB.

EEG power data was converted to *Z* scores by applying a single-trial normalization procedure to the data from each participant at each electrode and frequency separately. This was done because it helps disentangle background from task-related dynamics, allows for comparison across different frequency bands and electrodes, and facilitates group-level analysis (Cohen, 2014). Each trial's entire epoch (-700 ms to 800 ms relative to target onset) was used for the baseline during normalization because it has been shown to be robust to the effects of noisy trials (Grandchamp and Delorme, 2011). The downside to using the entire epoch for the baseline normalization is that sustained changes throughout the trial period become difficult to detect (Cohen, 2014). Ultimately, we considered this an acceptable trade-off for being able to compare effects in power and behavioral measures across participants without having to make as many assumptions about frequency bands and time-windows. Plots of mean normalized power at select electrodes can be seen in Figure 2.2.

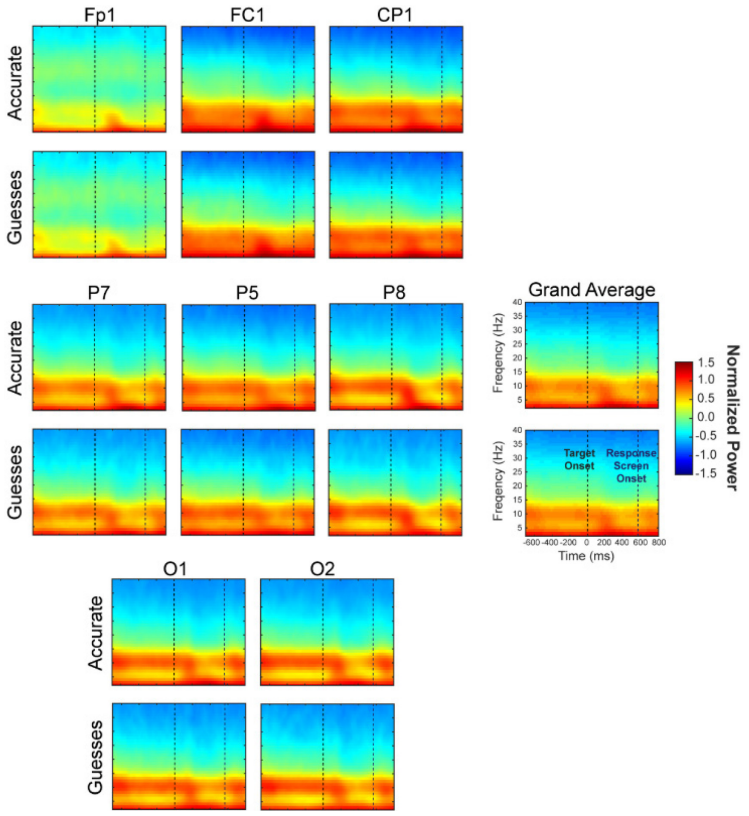

Figure 2.2. ***Time-frequency plots of mean normalized power***

Time-frequency plots showing the mean normalized power of trials categorized as accurate and guesses at selected electrodes and the average of all electrodes (Grand Average).

Another possible limitation of using the entire epoch for the baseline during normalization is that changes in pre-target power may be obscured by post-target activity. However, comparing effects across participants using raw EEG power is difficult due to individual differences caused by factors independent of the experimental manipulations (*e.g.*, skull thickness) (Cohen, 2014). Therefore, when possible, the logarithmically transformed power was used. EEG power data was logarithmically transformed by applying a single-trial log10 transformation procedure to the data from each participant at each electrode and frequency

separately. When the raw log transformed power is used, it is referred to as log power. EEG power that was converted to *z*-scores is called baseline normalized power.

Accurate vs Guess Trials

To test for significant differences in brain activity on trials where participants had small response errors compared to large response errors, we separated each participant's trials based on the sigma value from the fits of their individual response errors to the standard mixture model. This was done by defining each participant's trials with response errors between -0.75σ and +0.75σ as "accurate," and trials with response errors less than -1.5σ and greater than +1.5σ as "guesses" (Figure 2.3A). Trials where the participant clearly perceives the target are likely trials with a response error less than the participant's overall response standard deviation, and trials the participant has little to no perception of the target are likely trials with a response error greater than just the participant's response standard deviation. It should be noted that there are various reasons for participants to be accurate when they are guessing or have a large response error when they accurately perceived the target. However, such events are thought to be rare enough, or at least not systematic, that they will not unduly affect the overall distribution.

The main reason we separated trials into "accurate" or "guess" was to see if the standard mixture model parameters could be used to categorize trials in a meaningful way. Though this method resulted in excluding some trials, namely ones that fell between the cutoffs for accurate and guess, the outcome provided insight into how brain activity differs between different levels of objective perceptual performance. Overall, the mean proportion of trials excluded by falling between the cutoffs was $M = 0.25$, $SD = 0.05$.

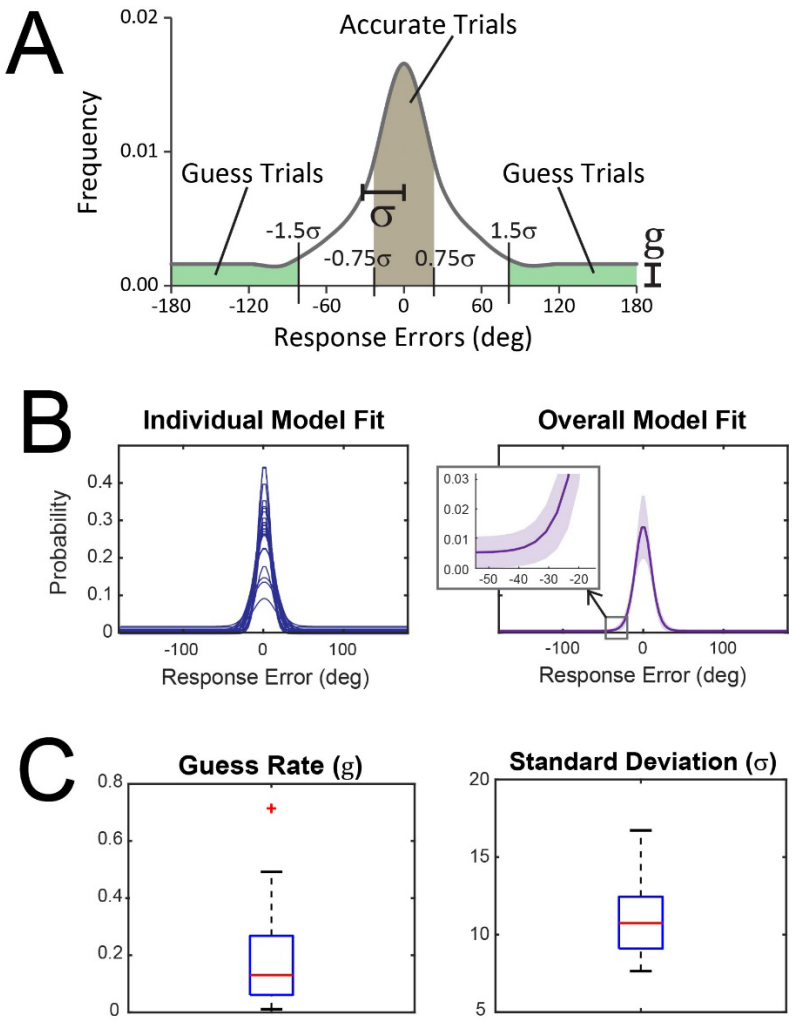

Figure 2.3. Accurate and Guess trial categories and fitted standard mixture model

A) Representation of how trials were split into the two categories, Accurate and Guess. This was done by defining each participant's trials with response errors between -0.75σ and +0.75σ as "accurate" (shaded brown region), and trials with response errors less than -1.5σ and greater than +1.5σ as "guesses" (shaded green regions). Trials that did not fall in either category were discarded from this analysis between the two trial categories. **B)** *Left*, model fit of each participant. *Right*, solid purple line is the average of participants' model fit. Light purple area represents $\pm$*SEM*. Zoomed in window shows

upward shift of the averaged model fit showing a non-zero guess rate. **C)** Boxplots of parameter values (*left*) guess rate and (*right*) standard deviation estimated from model fits of participants' response errors.

ERP Analyses. To remove the activity elicited by the mask without removing activity resulting from the interaction of mask and target, the catch trials (mask-only) average was subtracted from the orientation detection trials (target-plus-mask) average. ERP data was submitted to a repeated-measures, two-tailed permutation test based on the *tmax* statistic (Blair and Karniski, 1993) using the mxt_perm1() function from the Mass Univariate ERP Toolbox (Groppe, Urbach and Kutas, 2011). The time windows of interest were the P1 (80-140 ms), N1 (140-200 ms), P2 (200-255 ms), N2 (255-360 ms), and P3 (360-500 ms) components. The ERP component time windows were selected based on previous literature (Koivisto and Revonsuo, 2003, 2010). All 31 brain electrodes were included in the test. 100,000 random within-participant permutations were used to estimate the distribution of the null hypothesis and the familywise alpha (α) was set to 0.05. Based on this estimate, critical *t*-scores of +/-3.68 ($df = 23$) were derived. Any *t*-scores that exceeded the critical *t*-score were considered statistically significant.

Baseline Normalized EEG Power Analysis. To analyze differences in EEG baseline normalized power between guess and accurate trials, nonparametric permutation testing with a pixel-based multiple-comparison correction procedure (Cohen, 2014) was used to analyze differences in EEG band power between guess and accurate trials. The pixel-based multiple-comparison correction method involves creating one distribution of the largest positive pixel value and another distribution of the largest negative pixel value from each iteration of the permutation testing. After all iterations, the statistical threshold is defined as the value

corresponding to the 2.5th percentile of the smallest values and the value corresponding to the 97.5th percentile of the largest values which are the thresholds corresponding to an α of 0.05. Any pixel that has a value exceeding the upper or lower value is considered significant. The pixel-based method corrects for multiple comparisons by creating two distributions based on map-level information instead of pixel-level information. In other words, this method results in two distributions of the most extreme null-hypothesis test statistical values across all pixels rather than calculating null-hypothesis distributions for each pixel (see Cohen (2014) for further details about pixel-based multiple-comparison correction method). All analysis using nonparametric permutation testing with pixel-based multiple-comparison correction performed 10,000 iterations per test. To obtain more stable estimates from permutation testing, we ran a "meta-permutation test" by repeating the pixel-level permutation procedure 10 times and then averaging the results (Cohen, 2014). It needs to be pointed out that a "significant effect" determined by pixel-based permutation testing should not be considered a precise estimate in the temporal and frequency domains. Although pixel-based permutation testing is more stringent than cluster-based permutation tests (Cohen, 2014), caution should still be used when interpreting "significant" differences, especially if the temporal and frequency range of each pixel is relatively small.

EEG Phase Analysis. To determine whether the mean phase values significantly differ between accurate and guess trials, we used the circular Watson–Williams (W-W) test which was calculated using the PhaseOpposition.m function by VanRullen (2016a). We chose the parametric circular W-W test because it has shown to be equivalent to the non-parametric phase opposition sum (POS) measures under most conditions and performed better in situations where either the relative trial number or the ERP amplitude differed between the two trial groups (VanRullen, 2016a). The statistical significance of the W-W test across participants was determined by

combining the individual-level *p*-value time-frequency map at each electrode across participants using Stouffer's method (Stouffer *et al.*, 1949; VanRullen, 2016a), transforms individual *p*-values into *z*-scores, combines them across participants, and converts the resulting *z*-score to a combined probability. *P*-values were then corrected for multiple comparisons across time points and frequencies at each electrode using the false discovery rate (FDR) procedure described in Benjamini and Yekutieli (2001). Effects that satisfied a 5% FDR criterion were considered significant.

Single-Trial EEG Activity and Response Errors

To test the correlation between time-frequency log power and degree of response error, Spearman's rho (r_s) correlation coefficients were calculated using a nonparametric permutation testing approach with the pixel-based multiple-comparison correction procedure described above. The null-hypothesis distribution was created by shuffling power values and response errors on each trial with respect to each other. This provided a data-driven test of the null hypothesis that there is no consistent relationship between degree of response error and EEG power.

To look at whether task performance is related to oscillatory phase, and if yes, at what frequency, we used the weighted inter-trial phase clustering (wITPC) (Cohen and Voytek, 2013; Cohen, 2014). The logic behind the inter-trial phase coherence (ITPC) is that a systematic relation between EEG phase and behavioral outcome should result in a higher-than-chance ITPC in each of the trial subgroups. However, if the phase of the EEG signal is randomized and unpredictable, the distribution of phases at a given time period should follow a uniform distribution over all trials. The problem with ITPC is that it assumes EEG phase is relevant to experimental measures only when phase values are similar across trials (van Diepen and

Mazaheri, 2018). Unlike ITPC, wITPC is sensitive to modulations of phase values even if those phases are randomly distributed across trials as would be expected if response errors (which differs from trial to trial) were modulated by oscillatory phase (Cohen and Voytek, 2013; Cohen, 2014).

The wITPC was computed for each participant as the resultant vector length, or ITPC, of phase angles across trials once the length of each vector has been weighted by a variable of interest (in this case, each trial's phase vector is weighted by the degree of response error on that trial; see Figure 2.7A for example of computation) (Cohen and Voytek, 2013; Cohen, 2014). For statistical testing, a null-hypothesis distribution was created by shuffling the phase values relative to trial response error 10,000 times (see Figure 2.7A middle and bottom left). The wITPCz was calculated as the wITPC standardized relative to the null-hypothesis distribution, providing a *z*-value corresponding to the probability of finding the observed response error–phase modulation by chance, given the measured data. As was done for the parametric circular W-W test, statistical significance of the wITPCz across participants was evaluated by combining the individual-level *p*-value, calculated from the *z*-values, time-frequency map at each electrode across participants using Stouffer's method (Stouffer *et al.*, 1949; VanRullen, 2016a). *P*-values were then corrected for multiple comparisons across time points and frequencies at each electrode using the false discovery rate (FDR) procedure described in Benjamini and Yekutieli (2001). Effects that satisfied a 5% FDR criterion were considered significant.

We chose to use the phase opposition measure and the wITPCz even though they are both quantifying phase coherence because they provide slightly different but complementary information about the effects of phase. The phase opposition measure provides insight into whether there is an overall consistent difference in mean phase values between trials separated

by model parameter defined categories (*i.e.*, “accurate” and “guess”). On the other hand, the weighted single-trial phase modulation metric (*i.e.*, wITPCz) provides information about response error-specific modulations of phase values irrespective of the model. In other words, the circular W-W test reflects differences between the mean phase of the binned trials while wITPCz reflects differences in phase as it relates to the continuous measure of response errors. Also, the wITPCz does not rely on phase values being consistent over trials, they only need to be consistently related to response errors (Cohen and Cavanagh, 2011). This is an important distinction when trying to determine how much of the phase modulation is an artifact of the stimulus-evoked activity and how much is related to the difference in task performance.

Relationship Between Log Power and Standard Mixed Model Parameters

To determine how mixture model parameters standard deviation and guess rate varied as power varied, a median split of trials according to raw power at each time and frequency point was done for each participant at each electrode separately. EEG power from the Morlet Wavelet transformation was logarithmically transformed by applying a single-trial log10 transformation then trials were split by whether they were above or below the median power at each time point and frequency. This was done separately for each participant at each electrode. The standard mixture model was then fit to each set of response errors on the high power and low power trials to get model parameter values. This meant that every time-frequency point had a standard deviation and guess rate from trials with high power and low power. The “high power” and “low power” parameters were then averaged across a frequency band (2-3 Hz, 4-7 Hz, 8-14 Hz, 15-29 Hz or 30-40 Hz) and then tested statistically with the same procedure as the ERP analysis except each time point was tested rather than averaging across a time window and the alpha level was set to 0.01 to control for the familywise error rate (Bonferroni corrected alpha level $\alpha_{corr} = 0.05/5$

to account for the five frequency bands). Figure 2.4 gives a visual overview of each step in this analysis.

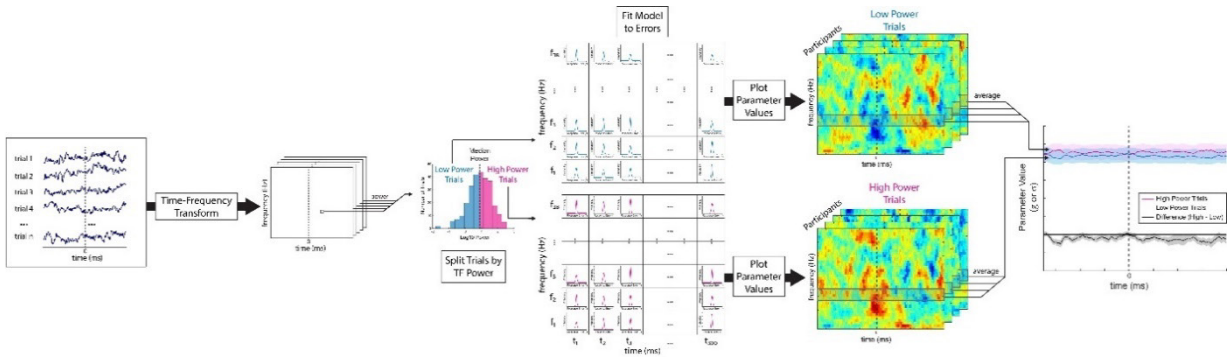

Figure 2.4. Illustration of parameter values derived from high/low power trials

Illustration of the analysis looking at how the estimated parameter values from the standard mixture model varied across an epoch when trials were separated by the power within a frequency band at each time point. First, time-frequency transformation (e.g., Morlet wavelet transformation) of single-trial data was used to calculate raw power of every time and frequency point for each trial. Trials were split by median power at each time and frequency point then the standard mixture model was fit to the trials' response errors. This was done for each participant and electrode separately. An average of the parameter values (*i.e.,* standard deviation and guess rate) from the "high power" and "low power" trials were calculated across the five frequency bands (2-3 Hz, 4-7 Hz, 8-14 Hz, 15-29 Hz or 30-40 Hz) at each time point and then were compared statistically using a repeated measures, two-tailed permutation test based on the *tmax* statistic (Blair and Karniski, 1993).

Considering the timing and frequency of these significant effects, it is likely they reflect the same processes measured by the ERP components. To test this idea, a procedure like the one described above was applied to the ERP data so that trials were split by the average amplitude of each ERP component rather than at each time point. The "high amplitude" and "low amplitude" fitted model parameters were tested statistically with the same procedure as the accurate vs guess ERP analysis.

For comparison with the ERP results, the guess rate and standard deviation parameters from high and low 2-3 Hz and 4-7 Hz log power trials were averaged across the time windows used for each ERP component: 80-140 ms (P1), 140-200 ms (N1), 200-255 ms (P2), 255-360 ms (N2), and 360-500 ms (P3). These were submitted to the same statistical procedure as the ERP components except the alpha level was Bonferroni corrected to 0.025 to account for testing two frequency bands. The two frequency bands were chosen because they are the only ones that have shown significant effects across all previous analyses.

Stepwise multiple regression analyses were performed for the standard mixture model parameters. Details about the methods and results can be found in Supporting Information.

2.3 RESULTS

Comparing Model Fits

We tested the best fitting model using the goodness-of-fit measures log likelihood and the Bayesian information criterion (BIC). The results are presented in Figure 2.5 and the *mean* ± *SEM* of the fitted parameters for all the tested models are in Table 2.1. Overall, the BIC indicates the standard mixture model fits the data better than any of the variable precision models and the standard mixture model with a bias parameter. As Fougnie and colleagues (2012) found, the models also performed better when they included a guess rate parameter. The log likelihood indicates the standard mixture model with a bias parameter is better than the standard mixture model and the variable precision models. The differences between the BIC and log likelihood metrics can be attributed to the BIC having a penalty for model complexity whereas the log likelihood does not control for those factors.

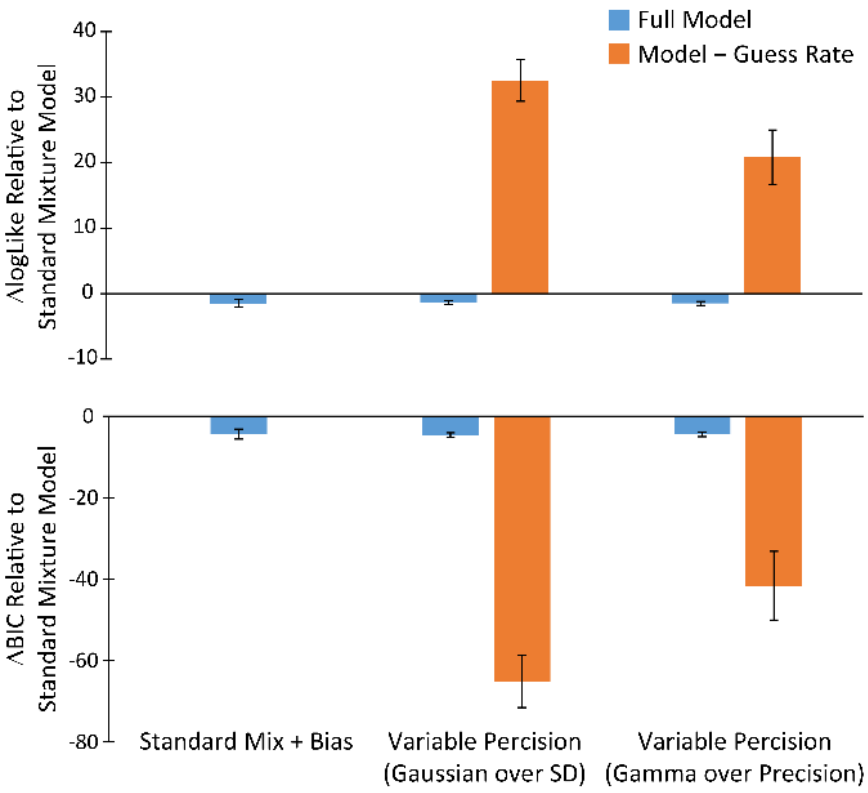

Figure 2.5. ***Goodness-of-fit measures***

Goodness-of-fit measures relative to the standard mixture model. The models compared to the standard mixture model were the standard mixture model with a bias parameter and the two variable precision models with and without a guess rate parameter (Model – Guess Rate). Top, the difference in log likelihood values compared to the standard mixture model with positive values favoring the standard mixture model. Bottom, the difference in Bayesian Information Criterion (BIC) values compared to the standard mixture model with negative values favoring the standard mixture model. Log likelihood favors the standard mixture model with a bias parameter (μ) over the standard mixture model and both variable precision models. The BIC favors the standard mixture model over the other three models. Plots are the means and error bars are $\pm SEM$.

Table 2.1. *List of goodness-of-fit measures comparing the standard mixture model to the standard mixture model with a bias parameter (μ) for each participant.*

	Log Likelihood			Bayesian Information Criterion (BIC)		
	Standard Model	Model + Bias	Difference	Standard Model	Model + Bias	Difference
Participant 1	-1255.82	-1255.33	-0.49	2526.45	2532.88	-6.44
Participant 2	-1213.93	-1212.78	-1.15	2442.77	2447.92	-5.15
Participant 3	-1095.28	-1094.58	-0.70	2205.45	2211.50	-6.05
Participant 4	-1093.29	-1093.24	-0.05	2201.25	2208.50	-7.24
Participant 5	-1191.23	-1190.92	-0.31	2397.23	2404.01	-6.77
Participant 6	-1113.21	-1111.14	-2.07	2241.28	2244.57	-3.29
Participant 7	-965.54	-964.92	-0.62	1945.90	1952.06	-6.16
Participant 8	-1022.30	-1021.07	-1.23	2059.48	2064.47	-4.99
Participant 9	-1109.18	-1109.12	-0.06	2233.12	2240.39	-7.27
Participant 10	-1422.57	-1422.42	-0.15	2859.94	2867.05	-7.11
Participant 11	-1384.47	-1384.46	-0.00	2783.78	2791.20	-7.42
Participant 12	-1017.58	-1015.52	-2.06	2049.58	2052.67	-3.09
Participant 13	-1498.89	-1498.55	-0.34	3012.59	3019.32	-6.73
Participant 14	-1071.57	-1071.55	-0.02	2157.98	2165.36	-7.38
Participant 15	-1124.71	-1123.84	-0.87	2264.26	2269.94	-5.68
Participant 16	-985.46	-985.17	-0.29	1985.36	1991.99	-6.63
Participant 17	-1149.36	-1149.26	-0.11	2313.61	2320.84	-7.23
Participant 18	-1136.58	-1136.50	-0.09	2287.86	2295.02	-7.17
Participant 19	-1133.03	-1132.91	-0.12	2280.88	2288.04	-7.16
Participant 20	-1276.89	-1275.81	-1.08	2568.44	2573.61	-5.17
Participant 21	-1138.27	-1133.04	-5.23	2291.40	2288.37	3.03[a]
Participant 22	-1003.69	-988.80	-14.89	2022.10	1999.69	22.41[a]
Participant 23	-1011.18	-1010.68	-0.50	2037.17	2043.57	-6.40
Participant 24	-1166.38	-1162.88	-3.49	2347.60	2348.04	-0.44

Note. Difference is calculated as the goodness-of-fit measure of the standard mixture model with a bias model subtracted from the goodness-of-fit measure of the standard mixture model.
[a] Positive difference indicates the standard mixture model with a bias parameter (μ) fits better to the participants' response errors (*i.e.*, has a smaller BIC) than the standard mixture model.

Accurate vs Guess Trials

Two participants were excluded before further analysis because one had a guess rate more than three *IQR*s from the median and the other had a guess rate of 3.9e-15 indicating that the staircasing procedure did not work properly for this individual. These participants were not included in further analysis. Figure 2.3B shows the fit of the standard mixture model (or standard

mixture model with a bias parameter for the participants mentioned in the Methods section) to each participant's response errors as well as the average fit of response errors across participants. The remaining 24 participants had a mean guess rate of 0.19 (*SD* = 0.18) and mean standard deviation (σ) parameter of 11.1 (*SD* = 2.5). The boxplots in Figure 2.3C summarizes the distributions.

ERP Analysis

The ERPs from accurate and guess trials (Figure 2.6A) showed no statistical difference for the first 200 ms following target onset across all electrodes. A divergence in the waveforms can be seen in the P2 (200-300 ms) component for the frontal, central, and centroparietal electrodes (Figure 2.6B left) in that the voltage of the guess trial ERPs was attenuated compared to the accurate trial ERPs. On the other hand, the voltage of the N2 (255-360 ms) component was more negative in the guess trials than accurate trials (Figure 2.6A) and this difference was only significant in the right frontocentral, central, centroparietal and parietal electrodes (Figure 2.6B middle). Finally, the P3 (360-500 ms) component from the guess trials had a similar attenuation as was seen in the P2 component (Figure 2.6A), but the distribution was more posterior with significant effects seen in the right central, centroparietal and parietal electrodes as well as bilateral parietooccipital and occipital electrodes (Figure 2.6B right).

EEG Power Analysis

Pixel-based permutation test indicated significant differences between accurate and guess trials within the 2-4 Hz frequency range which was observed to start around 310 ms post-target onset in P8 with a duration of about 70 ms and 350 ms post-target onset in P7 with a duration of around 120 ms (Figure 2.6C).

Overall, there was a trend for increased 4-7 Hz power in accurate trials compared to guess trials, especially in left frontal and right parietal areas, though this difference was not significant. This lack of significance might be due to too much variability in when the 4-7 Hz power changed during the trial. It is also possible that 4-7 Hz activity reflects a perceptual process that could occur in both accurate and guess trials, though more often or to a greater degree in one type of trial compared to the other.

Finally, there were a brief period (20-30 ms) where guess trials had significantly more baseline normalized power than accurate trials at around 2 Hz right before target onset in FC2 (around -50 ms; Figure 2.6C) and Cz (around -70 ms; not shown). However, because of the wavelet parameters used and the timing being around a large evoked response, the timing of the difference is likely smeared backward so that the effect probably occurred after the target had been presented (VanRullen, 2011; Herrmann *et al.*, 2014; Brüers and VanRullen, 2017). It should be noted that no other analysis yielded a significant effect immediately before or after target onset suggesting that these results are false positives, or the other analyses lacks the power to detect the effect. The very short duration of an effect at such a low frequency suggests the former is more likely. If it is the latter, the timing suggests it might have something to do with the mask onset (*e.g.*, anticipation of the mask stimuli) rather than the target. However, the current study was not designed to investigate the masking stimulus making it difficult to determine the truth behind the observed effect.

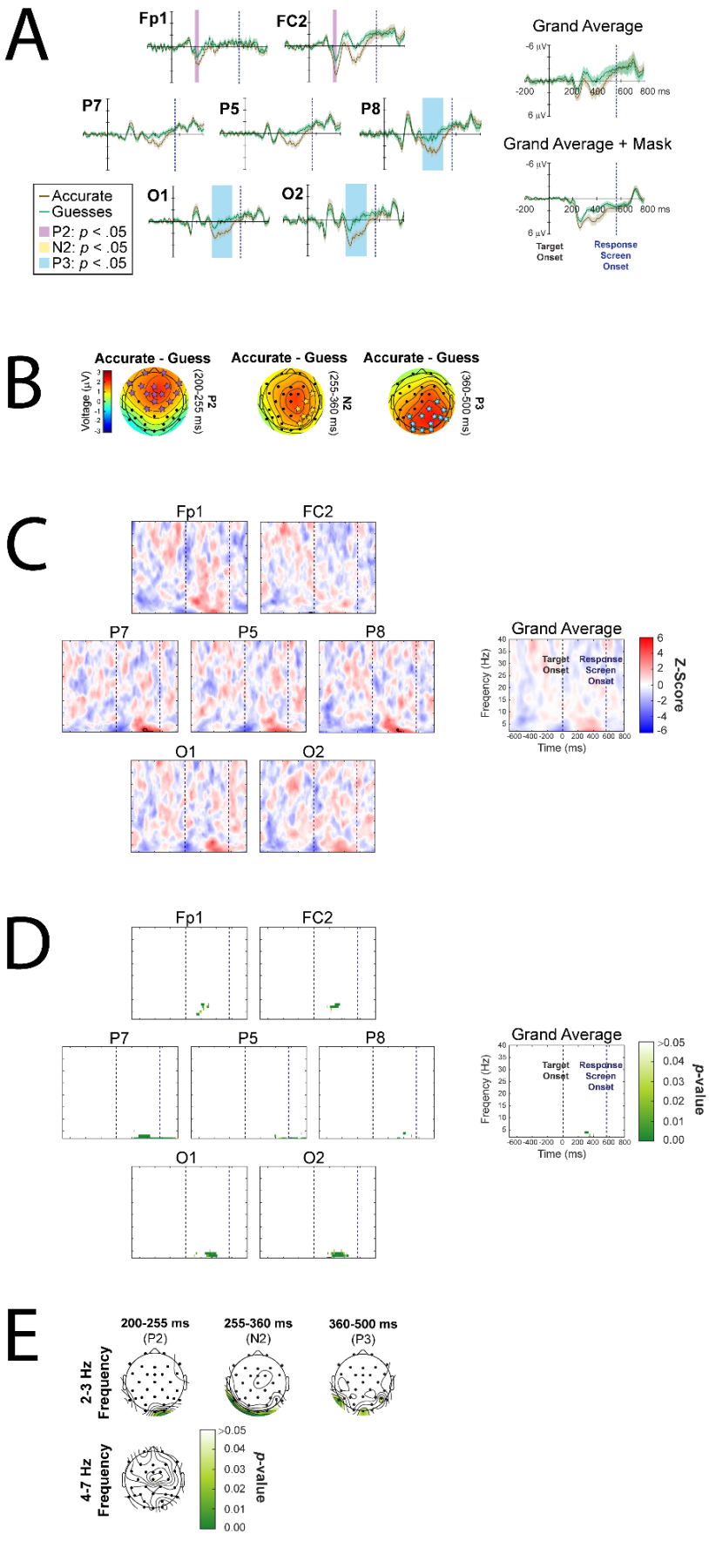
A
Fp1
FC2
P7
P5
P8
O1
O2
Accurate
Guesses
P2: p < .05
N2: p < .05
P3: p < .05
Grand Average
Grand Average + Mask
Target Onset
Response Screen Onset
B
Accurate - Guess
Voltage (μV)
P2 (200-255 ms)
N2 (255-360 ms)
P3 (360-500 ms)
C
Grand Average
Frequency (Hz)
Time (ms)
Z-Score
D
p-value
E
200-255 ms (P2)
255-360 ms (N2)
360-500 ms (P3)
2-3 Hz Frequency
4-7 Hz Frequency
p-value

Figure 2.6. ***Summary of accurate vs guess trial analysis***

A) ERPs of accurate trials and guess trials aligned to target onset at selected electrodes and averaged across all electrodes (Grand Average). Light brown and light green shaded areas around waveforms represent $\pm SEM$ of accurate trials and guess trials, respectively. Mask trial EPRs have been subtracted out of the ERPs to remove mask-related brain activity except for the Grand Average + Mask ERPs plot. Time period shaded in purple indicates significant difference between accurate and guess trials 200-255 ms (P2) post-target. Blue shaded time period indicates significant difference between accurate and guess trials 360-500 ms (P3) post-target. **B)** Topographies of the voltage distribution difference between accurate and guess trials. The time periods in each topography are as follows: 200-255 ms (P2), 255-360 ms (N2), and 360-500 ms (P3) post-target. Stars indicate electrodes with significant differences between accurate and guess ERPs. Mask trial activity has been subtracted out of the ERPs to remove mask-related brain activity. **C)** Analysis results from comparing the baseline normalized power of accurate vs guess trials. Time-frequency plots showing the results of the statistical analysis of the difference in power between accurate vs guess trials at each time-frequency point at selected electrodes and the average of all electrodes (Grand Average). Black contour denotes statistically significant differences (after applying the pixel-based multiple-comparison correction procedure) at $p < .05$. **D)** Phase analysis of accurate vs guess trials. Time-frequency plots showing the *p*-values (after applying FDR correction) from the statistical analysis testing differences in the mean phase of accurate trials vs guess trials. Plots are from selected electrodes and the average of all electrodes (Grand Average). Time-frequency points with *p*-values above the threshold of FDR correction for multiple comparisons were set to 1. **E)** Topographies of the *p*-value distribution averaged across the 2-3 Hz frequency (top) and 4-7 Hz frequency (bottom) indicating significant differences in the mean phase of accurate trials vs guess trials. Time-frequency points with *p*-values above the threshold of FDR correction for multiple comparisons were set to 1. The time periods in each topography are the same as used for the ERP analysis: 200-255 ms (P2), 255-360 ms (N2), and 360-500 ms (P3) post-target. Only the time periods and frequency bands that had significant effects after averaging over the time window are shown.

EEG Phase Analysis

Similar to the baseline normalized power results, significant differences in mean phase between accurate and guess trials were found in the 2-7 Hz frequency ranges following target onset (Figure 2.6D). Central and bilateral frontal, frontocentral, and central electrodes show significant phase differences in 4-7 Hz starting between 150-200 ms and terminating before 350 ms post-target (not shown). The duration of this effect varies so that the more central electrodes tended to have longer durations than those placed more laterally on the head. This effect was more prevalent in the right hemisphere in the early period.

The most lateral parietal and centroparietal electrodes on the left side of the head show significant phase differences within 2-3 Hz after the response screen onset (Figure 2.6E). On the other hand, Pz, P3 (Figure 2.6D), P4, and PO3 electrodes had no significant effects in phase while P6 and P8 had brief periods of significant phase differences starting a little after 300 ms until 500 ms post-target in the 2-3 Hz frequency range. P7 showed a similar significant difference in mean phase at 2 Hz starting around 225 ms and continuing until more than 200 ms after the response screen had been presented (about 770 ms post-target; Figure 2.6D). The occipital electrodes had significant phase effects primarily in the 3-5 Hz range starting a little after 100 ms on the left (not shown) and 150 ms on the right but were brief time periods until 200 ms post-target which then had significant differences lasting for about 200 ms (Figure 2.6D). PO4 electrode showed a similar difference, but the effect was less continuous and had larger *p*-values (*i.e.*, smaller phase difference between accurate and guess trials) than the occipital electrodes; however, PO4 also had significant differences within 2-3 Hz frequency between 400 and 500 ms (Figure 2.6D).

It should be noted that the time window of significant phase opposition overlaps with the significant differences in ERP amplitudes. ERP amplitudes have been shown to have a "masking" effect on phase opposition measures resulting in a decrease in their statistical power (VanRullen, 2016a) while at the same time the stimulus-evoked activity results in temporal distortion of oscillatory activity towards earlier latencies (Brüers and VanRullen, 2017). While the circular W-W test is relatively robust against the detrimental effect of ERPs, it does not negate their influence entirely (VanRullen, 2016a). Therefore, it is important to be aware that the significant effects of phase are affected by the stimulus evoked activity and the different ERP amplitudes between accurate and guess trials.

Single-Trial EEG Activity and Response Errors

To see whether response errors were related to trial-by-trial changes in pre-target alpha power, the Spearman's rho correlations were calculated between log power and degree of response error on each trial. Our results did not allow us to reject the null hypothesis. Follow-up analysis on the entire time-frequency space also yielded no significant results (not shown).

To examine the relationship between response errors and the distribution of phase values, we used the wITPCz. As can be seen in Figure 2.7B, phase was primarily modulated by degree of response errors in the 2-3 Hz frequency range in the posterior electrodes starting at around 200 ms post-target and lasting until response screen onset. PO3 was similar except the effect started at around 250 ms (not shown), but PO4 showed an effect starting at 350 ms and lasting until almost 100 ms after the response screen onset (not shown). Parietal electrodes show a significant effect in the low frequency bands starting at around 200 ms until about 800 ms post-target (Figure 2.7B, top and bottom rows). Centroparietal and central electrodes had a significant relationship between phase at 2-3 Hz and response errors at around 300-400 ms post-target and

lasted until after response screen onset. All frontocentral electrodes had response errors significantly related to 2-3 Hz phase starting between 200 ms and 300 ms post-target and lasting until shortly after response screen onset. Out of all the frontal electrodes, only Fz and F3 had a significant 2-7 Hz phase relationship to response errors (not shown).

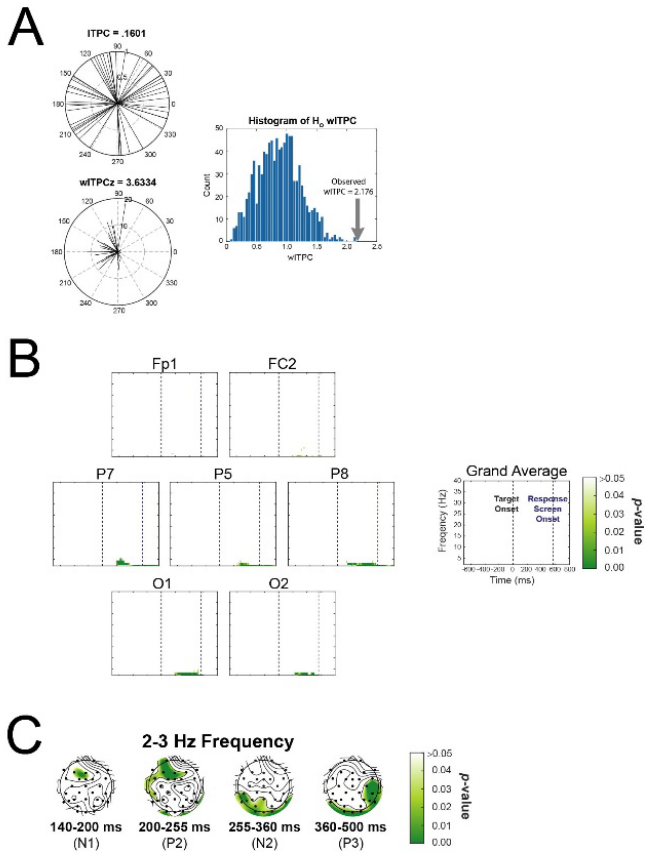

Figure 2.7. ***Summary of wITPCz analysis and results***

A) Example computation of weighted inter-trial phase clustering (wITPC) to relate single-trial phase to degree of response error. Top left, single-trial prestimulus phase vectors are shown as black lines and are not clustered across trials due to the randomization of the fixation length, leading to a low resultant vector length (i.e., low ITPC). Right, histogram of null-hypothesis vector lengths created by shuffling the mapping of the trial response error values to the trial phase values. The observed vector length (large arrow) is calculated from the distribution shown in bottom left panel. Bottom left shows how the length each trial's phase vector is scaled by that trial's degree response error and a weighted ITPC is computed,

reflecting the relationship between the distribution of phase angles and degree of response error even though the distribution of the phase angles themselves is uniform (as seen in the top left plot). The wITPCz value is the wITPC standardized relative to the null-hypothesis distribution seen in the histogram plot. Example based on figure by Cohen (2014). **B)** Time-frequency plots of analysis relating single-trial phase activity and response errors. Significant *p*-values indicating that the normalized distance of the observed wITPC (i.e., wITPCz) is significantly different from the distribution of null hypothesis wITPC values. This measure represents the relationship between the distribution of phase angles and the degree of response error on each trial. Plots are only of selected electrodes and the average of all electrodes (Grand Average). Time-frequency points with *p*-values at or above .05 were set to 1. **C)** Topographies of the *p*-value distribution (after applying FDR correction) averaged across the 2-3 Hz frequency indicating that the normalized distance of the observed wITPC (i.e., wITPCz) is significantly different from the distribution of null hypothesis wITPC values. This measure represents the relationship between the distribution of phase angles and the degree of response error on each trial. Time-frequency points with *p*-values above the threshold of FDR correction for multiple comparisons were set to 1. The time periods in each topography are the same as used for the ERP analysis: 120-200 ms (N1), 200-255 ms (P2), 255-360 ms (N2), and 360-500 ms (P3) post-target. Only showing time periods and frequency bands that had significant effects after averaging over the time window.

Relationship Between Log Power and Standard Mixed Model Parameters

A repeated measure, two-tailed permutation test indicated that significant differences in parameter values between high and low power trials were within the 2-3 Hz frequency band following target onset. Figure 2.8A shows the electrodes that had significant differences in guess rate and Figure 2.8B shows the electrodes that significant differences in the standard deviation (σ) parameter. No other electrodes had significant parameter value differences. Most of the effects are seen in the occipital and parietal electrodes except for the left frontal electrode which had a significant difference in guess rate at the later time points than observed in the other

electrodes. The left parietal and occipital electrodes showing significant effects in standard deviation were not the same electrodes showing significant effects in guess rate. Interestingly, both the guess rate and standard deviation were higher in trials with low 2-3 Hz log power than high. No significant differences were seen in the 2-3 Hz frequency band prior to 250 ms post-target onset and did not occur later than 100 ms before the response screen appeared. It should be noted that, unlike the accurate vs. guess analysis, these results are based on the log power so the lack of pre-target effects cannot be an artifact of the normalization process.

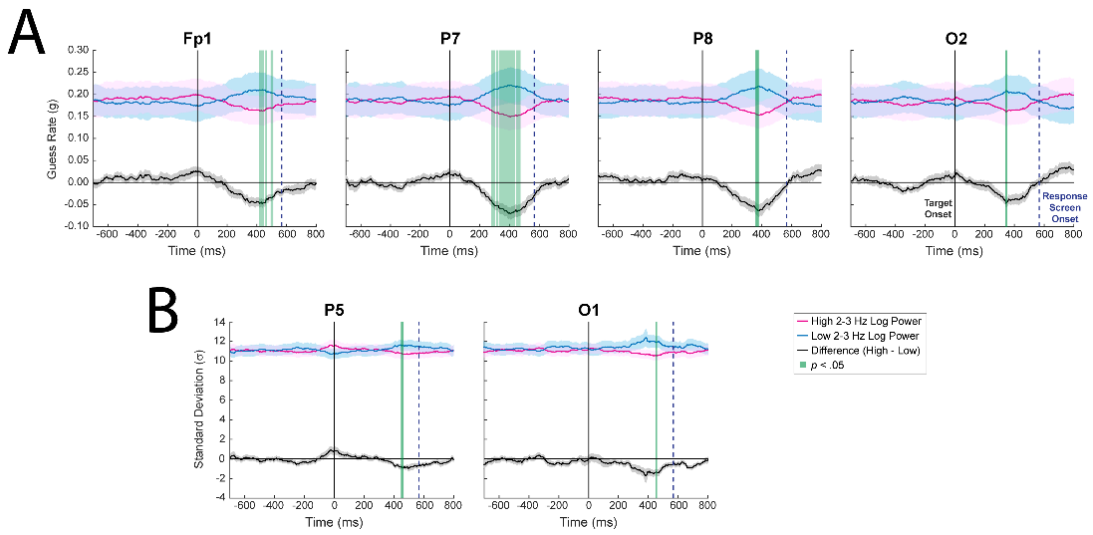

Figure 2.8. ***Relationship between log power and model parameter values***

A) Plots of the fluctuations in the guess rate parameter across time in trials with high and low log power in the 2-3 Hz frequency band. No other frequency band had significant differences in guess rate between high and low power trials. Only electrodes with significant effects are shown. Green shaded regions indicate time points where guess rate in high and low power trials significantly differed. Shaded regions around waveforms are $\pm SEM$. **B)** Plots of the fluctuations in the standard deviation (σ) parameter across time in trials with high and low log power in the 2-3 Hz frequency band. No other frequency band had significant differences in standard deviation between high and low power trials. Only electrodes with significant effects are shown. Green shaded regions indicate time points where the standard deviation

parameter in high and low power trials significantly differed. Shaded regions around waveforms are ±*SEM*.

When the parameter values on high and low log power trials were averaged over the ERP time windows, a similar pattern of effects were seen in the 2-3 Hz frequency band. There was an overall trend for higher guess rates (Figure 2.9A) and larger standard deviations (Figure 2.9B) on trials with lower log power. The most notable difference was a significant difference in guess rate on trials with high and low 4-7 Hz log power at Pz in the 200-255 ms time window. Interestingly, when compared to the guess rates on trials with high and low P2 amplitudes, the ERP component during that time period, the significant differences are concentrated in the frontal and central electrodes. Based on visual inspection, the 4-7 Hz log power seems to contribute to P2 differences, but only weakly.

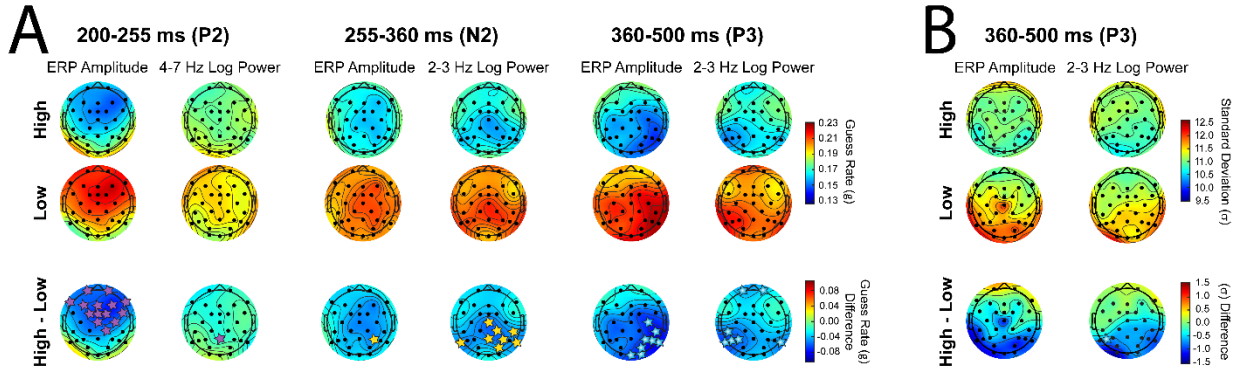

Figure 2.9. Topographies comparing the relationship between ERP amplitudes and parameter values and the relationship between log power and parameter values
Topographies of the **A**) guess rate (g) and **B**) standard deviation (σ) parameters from fitting the standard mixture model to trials categorized as having high (top row) or low (middle row) ERP amplitude compared to the trials categorized as having high (top row) or low (middle row) log power in the specified frequency band. The bottom row shows the differences in the parameter values between high and low trials. The time period in each topography are the windows over which the mean amplitude was calculated for the ERP analysis and the windows over which

the guess rate (g) or standard deviation (σ) parameters were averaged for the log power analysis (see Figure 2.4 for more details). All time periods are relative to target onset. On the bottom row, stars indicate electrodes with significant differences between parameter values. The alpha level for the ERP amplitude and log power statistical comparisons was 0.05 and 0.025, respectively. Only the time periods and frequency bands with significant effects are shown except for the standard deviation (σ) parameters from fitting the ERP amplitude (**B**, left column) which were included for comparison.

In contrast, the significant effects for the 2-3 Hz frequency band activity during the N2 ERP (255-360 ms) is obscured for the ERP component itself. Only P6 had a significant difference in guess rate based on differences in N2 amplitude where most right centroparietal, parietal, and parietooccipital electrodes exhibited significant guess rate differences as well as the left parietal electrode P7.

Finally, the large P3 ERP showed a significant difference in guess rates at the more posterior electrodes though these differences were primarily on the right side. In comparison, during the P3 time window (360-500 ms) the more lateral parietal and centroparietal electrodes on the left side and the most lateral parietal electrode on the right side (P8) showed a different difference in guess rate on trials with high vs low 2-3 Hz log power. Interestingly, Fp1 and Fp2 also showed a significant difference in guess rates at 2-3 Hz frequency. Consistent with the time courses shown in Figure 2.8B, it was only during this late time period that a significant difference was seen in the standard deviation (σ) parameter values. Like the guess rate parameter, trials with high 2-3 Hz log power had greater standard deviations (σ) than trials with low log power. This significant difference was only observed at the left posterior electrode, P5, though there was a trend for the bilateral occipital and parietal electrodes to have a relatively large standard deviation (σ) on the low 2-3 Hz power trials (Figure 2.9B, middle row). In comparison,

there were no ERP amplitudes showing a significant difference in the standard deviation (σ) parameter.

2.4 Discussion

There were two goals for the present study. First, we asked what working memory model best fit to continuous response measures on an orientation perception task? The second goal of the study was to ask what might the relationship be between the parameters of the best-fitting model and EEG activity?

Comparing Model Fits

Since perceiving the visual stimuli usually precedes remembering those same stimuli, some of the assumptions built into the visual working memory models are applicable to visual perception. Namely, the assumption that there are a set of targets that are remembered and a set of targets that are not remembered and they can be represented by two distributions which would translate to the current task as a set of targets that are seen and another set of targets not seen. For this reason, the first question addressed was what working memory model and their associated assumption could be extended to the current study's orientation perception task? Based on goodness-of-fit metrics, we found that the standard mixture model fit the current data set better than the models that assumed a varying distribution for the standard deviation parameter. In other words, we did not find evidence supporting the idea that precision can be described by a variable distribution during orientation perception. This result is consistent with Shen and Ma (2019) who also found little evidence for variable precision during visual perception. Furthermore, we found that the models that included a guess rate parameter performed better than the variable precision models that did not. This indicates that the existence of guessing cannot only be attributed to the low perceptual quality that was drawn, by chance, from a stochastic distribution. It is important

to point out that this does not mean there is no variability in performance over the course of an experiment. It has been noted by many authors that performance changes as participants get better at the task or when they get tired towards the end of the experiment. Rather, these results suggest that a model with a fixed standard deviation fits better to orientation perception task performance than one that varies from trial to trial according to some underlying distribution.

EEG Activity, Model Parameters and Perceptual Behavior

The second goal was to try to answer the question of how brain activity modulates perceptual representation as it is quantified by the guess rate and standard deviation parameters. Specifically, we wanted to see if brain activity prior to the target onset in the 8-14 Hz frequency range (alpha band) modulated whether a target is perceived (*i.e.*, guess rate); and, we tested whether the quality of target's perceptual representation (*i.e.*, standard deviation parameter) was related to post-target brain activity in the 4-7 Hz frequency range (theta band). To this end, trials were categorized as accurate or guesses based on model parameter values. The EEG activity on accurate and guess trials were then compared across participants. Then, a complementary approach was used that did a median split of trials based on EEG power. The model was fit to the high power and low power trials and the resulting parameter values were compared across time within different frequency bands. Despite our original hypothesis that alpha activity (8-14 Hz) would be related to guess rate or the standard deviation parameter, the evidence did not support this idea. Instead, the model-based and power-based approaches both found that 2-7 Hz activity after target onset modulated perceptual representation as it was quantified by the guess rate and standard deviation parameters.

Accurate vs Guess Trials: ERP Activity

Significant differences in ERP waveforms of the accurate and guess trials started at around 200 ms post-target onset in the anterior locations on the head (Figure 2.4B) which corresponds to the P2 component (Potts and Tucker, 2001; Key, Dove and Maguire, 2005; Di Russo *et al.*, 2019). The greater amplitude of the P2 for accurate guess trials fits with the P2 being related to the salience of stimuli (Potts and Tucker, 2001) or stimulus recognition (Harel *et al.*, 2016).

We also observed a more negative N2 for guess trials, that seems to go against current literature which suggests that the onset of visual consciousness can be marked by a greater negativity in the N2 time range due to an overlapping posterior negative component called the visual awareness negativity (VAN) (Koivisto and Revonsuo, 2003, 2010; Förster, Koivisto and Revonsuo, 2020). However, the separation of trials based on response performance rather than awareness (according to Koivisto and Revonsuo (2010), the VAN can only be reliably detected by comparing aware and unaware conditions), would explain why we would not expect greater negativity in the N2 time range for accurate ERPs compared to guess ERPs. Furthermore, the distribution of the observed N2 component (mostly right central electrodes) does not match the typical posterior VAN distribution (Förster, Koivisto and Revonsuo, 2020). In fact, the N2 distribution points towards the presence of the much larger P3 component. The most likely explanation is that the attenuated guess trial ERPs (compared to accurate trials) results in a smaller or later positive voltage from the much larger P3 overlapping the negative deflection at the N2 time period (Koivisto and Revonsuo, 2010; Förster, Koivisto and Revonsuo, 2020) so that the N2 appears more negative in guess trials when it is actually due to the P3 being smaller. The voltage increase of accurate compared to guess ERPs during the P3 time window follow previous

findings on attention and visual perception (Key, Dove and Maguire, 2005; Salti, Bar-Haim and Lamy, 2012). In the current study the P3 is likely related to processes such as stimulus classification and saliency evaluation (Salti, Bar-Haim and Lamy, 2012; Helfrich and Knight, 2019; Doradzińska *et al.*, 2020; Förster, Koivisto and Revonsuo, 2020) and that these processes are overwhelmingly more relevant to accurate orientation perception than processes for conscious perception as reflected by the relatively smaller N2 ERP. Furthermore, the difference in ERPs between accurate trials and guess trials during the N2 time period (see middle topographic plot of Figure 2.4B) indicates that the processes reflected by the N2 likely occur in both types of trials though to differing degrees. Instead, it appears that the main difference between accurate and guess trials is the extent that the target can be classified or evaluated by the brain regardless of consciously perceiving the target.

Accurate vs Guess Trials: EEG Activity

We had originally hypothesized activity within the alpha frequency band (8-14 Hz range), especially prior to target onset, mediating task performance. However, the results did not support this hypothesis. It is possible a null effect could be attributed to using both pre- and post-target activity in the pixel-based multiple correction procedure. Relative to post-target activity, pre-stimulus power would be very small since the only thing for participants to do was fixate on a white circle. As a result, differences in pre-target activity might not exceed significance thresholds when those thresholds were based on the background spectra of the combined pre- and post-target activity. However, we tested this possibility by analyzing power in the 8-14 Hz frequency range during just the pre-target time period and found no significant differences between accurate and guess trials (data not shown). Therefore, it is unlikely that a lack of

significant difference in pre-target 8-14 Hz range is due to an exceedingly high statistical threshold set by the post-target activity.

Another possibility is that the short intertrial interval (ITI) between participants' response and fixation onset starting the next trial meant alpha desynchronization carried over to the next trial so that it masked any true effects of spontaneous alpha. While this is a possibility, alpha activity following the end of a trial is also affected by evaluating their response, task load, and motivational state (Compton *et al.*, 2011; Compton, Bissey and Worby-Selim, 2014; Compton, Heaton and Ozer, 2017). While the short ITI is problematic for alpha analysis in some regards, it is beneficial in other ways such as discouraging participants from strategizing or reflecting back on the previous trial.

Similarly, the interstimulus interval (ISI) between fixation onset and target onset is possibly too short to let event-related desynchronization (ERD) of alpha to recover, thus masking the effects of spontaneous alpha during the pre-target period. Although potentially problematic, this should not adversely affect results because the ERD should be equal across all conditions since fixation is the same on all trials. Therefore, the activity related to the target perception is equally affected so relative differences can still be detected if they are present.

The most likely reason for not finding a pre-target effect of 8-14 Hz activity is that there was no information for the participant to use before a target was presented, so there would be no attention-related changes or task-based preparation prior to the target. This means that the only activity present during fixation are the spontaneous fluctuations of normal neural activity. Recent work by Samaha *et al* (2020) propose that spontaneous alpha activity modulates neural activity in a non-specific manner, thus neither facilitating nor inhibiting perceptual activity. The net effect

would be no change to performance which is line with what the model proposed by Samaha and colleagues (2020) would predict.

The absence of significant effects in post-target 8-14 Hz (alpha band) activity suggests that alpha activity is not related to the processes responsible for differences between accurate and guess trials. The fact that post-target 8-14 Hz activity was also unrelated to response errors on a trial-by-trial basis suggests that 8-14 Hz activity is not related to perception of a target's orientation. This is consistent with Bae and Luck (2018) who found that alpha activity did not encode a target's orientation when the target's spatial location was controlled for. An absence of a relationship between 8-14 Hz power and performance measures has been noted in other studies though they were not able to rule out changes in detection bias which can be ruled out in the current study since guess rate was not related to alpha activity (Benwell *et al.*, 2017; Keitel *et al.*, 2018). However, awareness bias might be a possibility assuming orientation perception can proceed in the absence of conscious awareness which seems likely based on previous research (Benwell *et al.*, 2017; Koenig and Ro, 2019; Doradzińska *et al.*, 2020). In sum, it is likely that 8-14 Hz (alpha band) activity is more related to a global process that is not dependent on conscious awareness and would not change across trials such as feature-independent stimulus processing.

The most significant differences between accurate and guess trials were in the 2-4 Hz frequency ranges, particularly in the parietal and parietooccipital electrodes during the latter half of the post-stimulus epoch (Karakaş, 2020). A significant increase of delta and low theta power in accurate compared to guess trials could be seen at around 300 ms though their differences in mean phase, especially for theta, started earlier (200 ms post-target). Although there was a trend in our data for increased theta power in accurate trials compared to guess trials, this difference was not reliable.

The significant differences in theta and delta seem to correspond to changes in the N2 and P3 ERP components observed in the time domain. Many studies have shown that delta and theta are the primary contributors to the formation of the N2 and P3 (Karakaş, Ömer Utku Erzengin and Başar, 2000; Harmony, 2013; Harper, Malone and Bernat, 2014). It has been proposed that activity in the 2-3 Hz range contributes continuous positivity throughout the ERP response while theta activity corresponds to the polarity change as the negative deflection during the N2 shifts to the positive deflection during the P3 (Harper, Malone and Bernat, 2014). This fits with the observed EEG activity of accurate and guess trials (Figure 2.4C and Figure 2.4D). Furthermore, the interplay between theta and delta activity would explain the indistinct N2 but large P3 waveforms (Karakaş, Ö U. Erzengin and Başar, 2000).

The increase in baseline normalized 4-7 Hz power during accurate trials relative to guess trials has the earliest onset in left frontal and right parietal electrodes. Prolonged theta in right posterior electrodes is accompanied by significant differences in mean (low) theta phase between accurate and guess trials. Theta has been interpreted as being correlated with selective attentional processing (Karakaş, Ö U. Erzengin and Başar, 2000; Başar *et al.*, 2001; Karakaş, 2020) and an increase in theta synchronization and power has been associated with successful memory encoding (Klimesch, 1999) and right hemispheric theta is greater than left when encoding visuospatial information (Sauseng *et al.*, 2004). Although the task in this study was not a memory task, encoding information is still a viable way of looking at how the brain transforms the visual sensory information into perceptual representations. In fact, theta has been shown to be sensitive to target and non-target stimuli regardless of memory load (Palomäki *et al.*, 2012). Therefore, it is probable that theta activity might be related to the “encoding” of the target’s orientation or just the detectability of target itself. Both functions could occur in accurate and

guess trials, though more often or to a greater degree in accurate trials compared to guess trials. This would explain why 4-7 Hz activity showed a trend for increased power in accurate trials compared to guess trials though this difference was usually not significant.

In contrast to the 4-7 Hz activity, activity within 2-3 Hz showed a more spatially diffuse increase in power in accurate vs guess trials with maxima over the lateral parietal areas. Delta phase differed significantly between accurate and guess trials over the occipital and lateral parietal areas with the most robust phase differences at around 350 ms post-target. Several experiments that showed increases in delta activity during the performance of different mental tasks and conflict-monitoring paradigms have led investigators to associate delta with modulation of networks that should be inactive to accomplish the task (Harmony, 2013; Rawls, Miskovic and Lamm, 2020). Investigators have also noted a close association between delta activity and the P3 ERP waveform (Schürmann *et al.*, 1995, 2001; Harper, Malone and Bernat, 2014; Rawls, Miskovic and Lamm, 2020). If the P3 reflects post-perceptual processes, then it is likely 2-3 Hz activity is also involved. Whether that role is as an inhibitory mechanism or not remains unknown. Overall, when considering the time and frequency at which reliable differences were observed between accurate and guess trials, it seems likely that this post-target activity reflects differences in the level of perceptual encoding of the target orientation and the subsequent precision of responses on the task.

Single-Trial EEG Activity and Response Errors

We were surprised to find no significant correlation between response error and oscillatory power in any of the measured frequencies, but this could also be attributed to the lack of sensitivity of the analysis method. Since we failed to find support for our hypothesis regarding alpha oscillations, we chose to take a conservative approach when analyzing the rest of the time-

frequency space. Using a less conservative method might help answer the question but that would increase the risk of finding false positives which could be more harmful than accepting false negatives.

Interestingly, we did find a relationship between response error and phase values in the 2-7 Hz frequencies similar to the significant differences in mean phase of accurate trials compared to guess trials. In fact, phase modulation by response errors is even more pronounced than the differences in phase between accurate and guess trials. This strongly suggests 2-7 Hz phase activity plays an important role in the amount of participants' response error on a trial-by-trial bases. Delta (2-3 Hz) and theta (4-7 Hz) frequencies are usually associated with working memory and cognitive control, but these results imply that they have an important role in visual perceptual processes as well.

Relationship Between Log Power and Standard Mixed Model Parameters

There were significant differences in the guess rate and standard deviation parameter values from trials with high compared to low log power at 2-3 Hz starting at around 255 ms post-target onset. The trend was for trials with low power to have higher guess rate and standard deviation parameter values than trials with high power. The same trend was found for the guess rates on trials with high vs low 4-7 Hz log power though those effects started a little earlier (around 200 ms post-target onset) than those at 2-3 Hz frequency range. These results are in line with the accurate vs guess analysis performed on baseline normalized power data. Specifically, trials categorized as "accurate" had more power and a different preferred phase in the 2-7 Hz frequency range than trials considered "guesses." There were no significant effects prior to the target onset which fits with the baseline sensory excitability model proposed by Samaha and colleagues (2020).

Interestingly, Fp1 electrode showed significant difference in guess rate between high and low power trials prior to the onset of the response screen. Accumulation of evidence has led investigators to associate frontal delta (2-3 Hz) activity with top-down control and response inhibition (Harmony, 2013; Helfrich *et al.*, 2017; De Vries *et al.*, 2018; Rawls, Miskovic and Lamm, 2020). Considering that these late significant effects in the frontal area are almost entirely after those in the parietal and occipital electrodes and are only for guess rate, it is likely top-down control has to do with maintaining the perceptual representation or inhibiting distracting information during the delay period. In this way, an increase in 2-3 Hz brain activity would help maintain a target's "perceived" state rather than the target becoming part of the "unseen" distribution that the guess rate represents.

Considering the timing and frequency of these significant effects, it seems likely that they reflect the same processes measured by the ERP components in the accurate vs guess analysis. However, as others have found (and can be seen in Figure 2.9 and Appendix Table B.1 and Appendix Table B.2), an ERP component's amplitude is usually determined by a combination of different underlying brain potentials which often represent separable functional processes (Karakaş, Ömer Utku Erzengin and Başar, 2000; Woodman, 2010; Harper, Malone and Bernat, 2014). In the current study, it is likely that the activity at 2-3 Hz and 4-7 Hz interact dynamically to contribute to the measured ERP components morphology.

Conclusion and Future Directions

Overall, we have shown that the standard mixture model can be extended to a visual perception task and that doing so provides important insight into how brain activity shapes visual perception. Our results point towards a perceptual representation that has a fixed precision meaning that while response errors vary with the level of neural activity after stimulus onset,

their variability is according to the same distribution across trials. Whether this is true across different levels of target visibility is not known but would be an interesting question for future research.

It is important to note that our results are not suggesting pre-target EEG activity has no effect on visual perception. There is a lot of evidence to contrary. It has been proposed that pre-target alpha activity alters participants' confidence rather than performance on visual perception tasks (Samaha, Iemi and Postle, 2017; Samaha *et al.*, 2020), a distinction the current study was not designed to test. It is possible the analysis methods were not sensitive enough to pick up changes in pre-target activity though there were no significant effects in a follow-up analysis analyzing just the pre-target time period making a lack of statistical power unlikely. The most likely explanation for an absence of pre-target effects is that participants did not have information about an upcoming trial so there was no reason to prepare prior to the target. A follow-up study that directly manipulates attention or detectability of the target and measures participants' confidence along with the objective measures of response error, might be able to better test how differences in brain activity prior to target onset affect visual perception and subsequent task performance.

References

Auton, A. (2009) 'Red Blue Colormap'. MATLAB Central File Exchange. Available at: https://www.mathworks.com/matlabcentral/fileexchange/25536-red-blue-colormap.

Bae, G.-Y. and Luck, S. J. (2018) 'Dissociable decoding of spatial attention and working memory from EEG oscillations and sustained potentials', *Journal of Neuroscience*. Society for Neuroscience, 38(2), pp. 409–422. doi: 10.1523/JNEUROSCI.2860-17.2017.

Başar, E. *et al.* (2001) 'Gamma, alpha, delta, and theta oscillations govern cognitive processes', *International Journal of Psychophysiology*. Elsevier, 39(2–3), pp. 241–248. doi: 10.1016/S0167-8760(00)00145-8.

Bays, P. M. (2016) 'A signature of neural coding at human perceptual limits', *Journal of Vision*. Association for Research in Vision and Ophthalmology Inc., 16(11), p. Article 4. doi: 10.1167/16.11.4.

Bays, P. M., Catalao, R. F. G. and Husain, M. (2009) 'The precision of visual working memory is set by allocation of a shared resource', *Journal of Vision*. The Association for Research in Vision and Ophthalmology, 9(10), pp. 7–7. doi: 10.1167/9.10.7.

Benjamini, Y. and Yekutieli, D. (2001) 'The control of the false discovery rate in multiple testing under dependency', *Annals of Statistics*, 29(4), pp. 1165–1188. doi: 10.1214/aos/1013699998.

Benwell, C. S. Y. *et al.* (2017) 'Prestimulus EEG Power Predicts Conscious Awareness But Not Objective Visual Performance.', *eNeuro*. Society for Neuroscience, 4(6). doi: 10.1523/ENEURO.0182-17.2017.

Berens, P. (2009) 'CircStat: a MATLAB toolbox for circular statistics', *Journal of Statistical Software*, 31(10), pp. 679–685. doi: 10.1016/j.amp.2012.05.023.

van den Berg, R. *et al.* (2012) 'Variability in encoding precision accounts for visual short-term memory limitations', *Proceedings of the National Academy of Sciences of the United States of America*. National Academy of Sciences, 109(22), pp. 8780–8785. doi: 10.1073/pnas.1117465109.

Blair, R. C. and Karniski, W. (1993) 'An alternative method for significance testing of waveform difference potentials', *Psychophysiology*. John Wiley & Sons, Ltd, 30(5), pp. 518–524. doi: 10.1111/j.1469-8986.1993.tb02075.x.

Brainard, D. H. (1997) 'The Psychophysics Toolbox.', *Spatial vision*, 10(4), pp. 433–436. Available at: http://www.ncbi.nlm.nih.gov/pubmed/9176952 (Accessed: 5 October 2017).

Brüers, S. and VanRullen, R. (2017) 'At what latency does the phase of brain oscillations influence perception?', *eNeuro*. Society for Neuroscience, 4(3). doi: 10.1523/ENEURO.0078-17.2017.

Chaumon, M. and Busch, N. A. (2014) 'Prestimulus neural oscillations inhibit visual perception via modulation of response gain', *Journal of Cognitive Neuroscience*. MIT Press Journals, 26(11), pp. 2514–2529. doi: 10.1162/jocn_a_00653.

Cohen, M. X. (2014) *Analyzing neural time series data: theory and practice*. Cambridge, Massachusetts: MIT Press.

Cohen, M. X. and Cavanagh, J. F. (2011) 'Single-trial regression elucidates the role of prefrontal theta oscillations in response conflict', *Frontiers in Psychology*, 2. doi: 10.3389/fpsyg.2011.00030.

Cohen, M. X. and Voytek, B. (2013) 'Linking nonlinear neural dynamics to single-trial human behavior', in Pesenson, M. (Meyer) Z. (ed.) *Multiscale Analysis and Nonlinear Dynamics*. Wiley-VCH Verlag GmbH & Co. KGaA., pp. 217–232. doi:

10.1002/9783527671632.

Compton, R. J. *et al.* (2011) 'Cognitive control in the intertrial interval: Evidence from EEG alpha power', *Psychophysiology*. Blackwell Publishing Inc., 48(5), pp. 583–590. doi: 10.1111/j.1469-8986.2010.01124.x.

Compton, R. J., Bissey, B. and Worby-Selim, S. (2014) 'Task motivation influences alpha suppression following errors', *Psychophysiology*. Blackwell Publishing Inc., 51(7), pp. 585–595. doi: 10.1111/psyp.12212.

Compton, R. J., Heaton, E. and Ozer, E. (2017) 'Intertrial interval duration affects error monitoring', *Psychophysiology*. Blackwell Publishing Inc., 54(8), pp. 1151–1162. doi: 10.1111/psyp.12877.

Delorme, A. and Makeig, S. (2004) 'EEGLAB: An open source toolbox for analysis of single-trial EEG dynamics including independent component analysis', *Journal of Neuroscience Methods*. Elsevier, 134(1), pp. 9–21. doi: 10.1016/J.JNEUMETH.2003.10.009.

van Diepen, R. M. and Mazaheri, A. (2018) 'The Caveats of observing Inter-Trial Phase-Coherence in Cognitive Neuroscience', *Scientific Reports*. Nature Publishing Group, 8(1), p. 2990. doi: 10.1038/s41598-018-20423-z.

Doradzińska, Ł. *et al.* (2020) 'Unconscious perception of one's own name modulates amplitude of the P3B ERP component', *Neuropsychologia*. Elsevier Ltd, 147, p. 107564. doi: 10.1016/j.neuropsychologia.2020.107564.

Fischer, J. and Whitney, D. (2014) 'Serial dependence in visual perception', *Nature Neuroscience*. Nature Publishing Group, 17(5), pp. 738–743. doi: 10.1038/nn.3689.

Förster, J., Koivisto, M. and Revonsuo, A. (2020) 'ERP and MEG correlates of visual consciousness: The second decade', *Consciousness and Cognition*. Academic Press Inc.,

80, p. Article 102917. doi: 10.1016/j.concog.2020.102917.

Fougnie, D., Suchow, J. W. and Alvarez, G. A. (2012) 'Variability in the quality of visual working memory', *Nature Communications*. NIH Public Access, 3, p. 1229. doi: 10.1038/ncomms2237.

García-Pérez, M. A. (1998) 'Forced-choice staircases with fixed step sizes: asymptotic and small-sample properties', *Vision Research*, 38(12), pp. 1861–1881. doi: 10.1016/S0042-6989(97)00340-4.

Grandchamp, R. and Delorme, A. (2011) 'Single-trial normalization for event-related spectral decomposition reduces sensitivity to noisy trials.', *Frontiers in psychology*. Frontiers Media SA, 2, p. 236. doi: 10.3389/fpsyg.2011.00236.

Gratton, G., Coles, M. G. . and Donchin, E. (1983) 'A new method for off-line removal of ocular artifact', *Electroencephalography and Clinical Neurophysiology*, 55(4), pp. 468–484. doi: 10.1016/0013-4694(83)90135-9.

Groppe, D. M., Urbach, T. P. and Kutas, M. (2011) 'Mass univariate analysis of event-related brain potentials/fields I: A critical tutorial review', *Psychophysiology*. John Wiley & Sons, Ltd (10.1111), 48(12), pp. 1711–1725. doi: 10.1111/j.1469-8986.2011.01273.x.

Harel, A. *et al.* (2016) 'The temporal dynamics of scene processing: A multifaceted EEG investigation', *eNeuro*. Society for Neuroscience, 3(5), p. Article e0139-16.2016. doi: 10.1523/ENEURO.0139-16.2016.

Harmony, T. (2013) 'The functional significance of delta oscillations in cognitive processing', *Frontiers in Integrative Neuroscience*. Frontiers, 7, p. Article 83. doi: 10.3389/fnint.2013.00083.

Harper, J., Malone, S. M. and Bernat, E. M. (2014) 'Theta and delta band activity explain N2 and

P3 ERP component activity in a go/no-go task', *Clinical Neurophysiology*. Elsevier, 125(1), pp. 124–132. doi: 10.1016/j.clinph.2013.06.025.

Helfrich, R. F. *et al.* (2017) 'Prefrontal cortex modulates posterior alpha oscillations during top-down guided visual perception', *Proceedings of the National Academy of Sciences of the United States of America*. National Academy of Sciences, 114(35), pp. 9457–9462. doi: 10.1073/pnas.1705965114.

Helfrich, R. F. and Knight, R. T. (2019) 'Cognitive neurophysiology: Event-related potentials', in *Handbook of Clinical Neurology*. Elsevier B.V., pp. 543–558. doi: 10.1016/B978-0-444-64032-1.00036-9.

Herrmann, C. S. *et al.* (2014) 'Time–frequency analysis of event-related potentials: A brief tutorial', *Brain Topography*. Springer US, 27(4), pp. 438–450. doi: 10.1007/s10548-013-0327-5.

Kader, G. D. and Perry, M. (2007) 'Variability for Categorical Variables', *Journal of Statistics Education*, 15(2). Available at: https://eric.ed.gov/?id=EJ842705 (Accessed: 16 March 2021).

Karakaş, S. (2020) 'A review of theta oscillation and its functional correlates', *International Journal of Psychophysiology*. Elsevier B.V. doi: 10.1016/j.ijpsycho.2020.04.008.

Karakaş, S., Erzengin, Ö U. and Başar, E. (2000) 'A new strategy involving multiple cognitive paradigms demonstrates that ERP components are determined by the superposition of oscillatory responses', *Clinical Neurophysiology*. Elsevier, 111(10), pp. 1719–1732. doi: 10.1016/S1388-2457(00)00418-1.

Karakaş, S., Erzengin, Ömer Utku and Başar, E. (2000) 'The genesis of human event-related responses explained through the theory of oscillatory neural assemblies', *Neuroscience*

Letters. Elsevier, 285(1), pp. 45–48. doi: 10.1016/S0304-3940(00)01022-3.

Keitel, C. *et al.* (2018) 'No changes in parieto-occipital alpha during neural phase locking to visual quasi-periodic theta-, alpha-, and beta-band stimulation', *European Journal of Neuroscience*, pp. 1–15. doi: 10.1111/ejn.13935.

Key, A. P. F., Dove, G. O. and Maguire, M. J. (2005) 'Linking brainwaves to the brain: An ERP primer', *Developmental Neuropsychology*, 27(2), pp. 183–215. doi: 10.1207/s15326942dn2702_1.

Kingdom, F. A. A. and Prins, N. (2016) 'Chapter 5 – Adaptive Methods', in *Psychophysics*. Second Edi. San Diego: Academic Press, pp. 119–148. doi: 10.1016/B978-0-12-407156-8.00005-0.

Klimesch, W. (1999) 'EEG alpha and theta oscillations reflect cognitive and memory performance: a review and analysis', *Brain Research Reviews*. Elsevier, 29(2–3), pp. 169–195. doi: 10.1016/S0165-0173(98)00056-3.

Koenig, L. and Ro, T. (2019) 'Dissociations of conscious and unconscious perception in TMS-induced blindsight', *Neuropsychologia*. Elsevier Ltd, 128, pp. 215–222. doi: 10.1016/j.neuropsychologia.2018.03.028.

Koivisto, M. and Revonsuo, A. (2003) 'An ERP study of change detection, change blindness, and visual awareness', *Psychophysiology*. Society for Psychophysiological Research, 40(3), pp. 423–429. doi: 10.1111/1469-8986.00044.

Koivisto, M. and Revonsuo, A. (2010) 'Event-related brain potential correlates of visual awareness', *Neuroscience & Biobehavioral Reviews*. Pergamon, 34(6), pp. 922–934. doi: 10.1016/j.neubiorev.2009.12.002.

Mathewson, K. E. *et al.* (2011) 'Pulsed out of awareness: EEG alpha oscillations represent a

pulsed-inhibition of ongoing cortical processing.', *Frontiers in Psychology*, 2, p. Article 99. doi: 10.3389/fpsyg.2011.00099.

Palomäki, J. *et al.* (2012) 'Brain oscillatory 4-35 Hz EEG responses during an n-back task with complex visual stimuli', *Neuroscience Letters*. Elsevier, 516(1), pp. 141–145. doi: 10.1016/j.neulet.2012.03.076.

Pelli, D. G. (1997) 'The VideoToolbox software for visual psychophysics: transforming numbers into movies.', *Spatial vision*, 10(4), pp. 437–442. Available at: http://www.ncbi.nlm.nih.gov/pubmed/9176953 (Accessed: 5 October 2017).

Potts, G. F. and Tucker, D. M. (2001) 'Frontal evaluation and posterior representation in target detection', *Cognitive Brain Research*. Elsevier, 11(1), pp. 147–156. doi: 10.1016/S0926-6410(00)00075-6.

Rawls, E., Miskovic, V. and Lamm, C. (2020) 'Delta phase reset predicts conflict-related changes in P3 amplitude and behavior', *Brain Research*. Elsevier B.V., 1730, p. 146662. doi: 10.1016/j.brainres.2020.146662.

Di Russo, F. *et al.* (2019) 'Normative event-related potentials from sensory and cognitive tasks reveal occipital and frontal activities prior and following visual events', *NeuroImage*. Academic Press Inc., 196, pp. 173–187. doi: 10.1016/j.neuroimage.2019.04.033.

Salti, M., Bar-Haim, Y. and Lamy, D. (2012) 'The P3 component of the ERP reflects conscious perception, not confidence', *Consciousness and Cognition*. Academic Press, 21(2), pp. 961–968. doi: 10.1016/j.concog.2012.01.012.

Samaha, J. *et al.* (2020) 'Spontaneous Brain Oscillations and Perceptual Decision-Making', *Trends in Cognitive Sciences*. Elsevier Ltd, 24(8), pp. 639–653. doi: 10.1016/j.tics.2020.05.004.

Samaha, J., Iemi, L. and Postle, B. R. (2017) 'Prestimulus alpha-band power biases visual discrimination confidence, but not accuracy', *Consciousness and Cognition*. Academic Press, 54, pp. 47–55. doi: 10.1016/J.CONCOG.2017.02.005.

Samaha, J., Switzky, M. and Postle, B. R. (2019) 'Confidence boosts serial dependence in orientation estimation', *Journal of Vision*. Association for Research in Vision and Ophthalmology Inc., 19(4). doi: 10.1167/19.4.25.

Sauseng, P. *et al.* (2004) 'Theta coupling in the human electroencephalogram during a working memory task', *Neuroscience Letters*. Elsevier Ireland Ltd, 354(2), pp. 123–126. doi: 10.1016/j.neulet.2003.10.002.

Schürmann, M. *et al.* (1995) 'A new metric for analyzing single-trial event-related potentials (ERPs): application to human visual P300 delta response', *Neuroscience Letters*. Elsevier, 197(3), pp. 167–170. doi: 10.1016/0304-3940(95)11912-G.

Schürmann, M. *et al.* (2001) 'Delta responses and cognitive processing: Single-trial evaluations of human visual P300', *International Journal of Psychophysiology*. Elsevier, 39(2–3), pp. 229–239. doi: 10.1016/S0167-8760(00)00144-6.

Shen, S. and Ma, W. J. (2019) 'Variable precision in visual perception', *Psychological Review*, 126(1), pp. 89–132. doi: 10.1037/rev0000128.

Stouffer, S. A. *et al.* (1949) 'Studies in social psychology in World War II: the American soldier', in *Adjustment During Army Life*. Vol. 1. Princeton, NJ.: Princeton University Press. Available at: https://psycnet.apa.org/record/1950-00790-000.

Suchow, J. W. *et al.* (2013) 'Modeling visual working memory with the MemToolbox.', *Journal of Vision*. Association for Research in Vision and Ophthalmology, 13(10), pp. 1–8. doi: 10.1167/13.10.9.

VanRullen, R. (2011) ‘Four common conceptual fallacies in mapping the time course of recognition.’, *Frontiers in Psychology*. Frontiers Media SA, 2, p. Article 365. doi: 10.3389/fpsyg.2011.00365.

VanRullen, R. (2016) ‘How to Evaluate Phase Differences between Trial Groups in Ongoing Electrophysiological Signals’, *Frontiers in Neuroscience*. Frontiers, 10, p. 426. doi: 10.3389/fnins.2016.00426.

De Vries, I. E. J. *et al.* (2018) ‘Priority switches in visual working memory are supported by frontal delta and posterior alpha interactions’, *Cerebral Cortex*. Oxford University Press, 28(11), pp. 4090–4104. doi: 10.1093/cercor/bhy223.

Woodman, G. F. (2010) ‘A brief introduction to the use of event-related potentials in studies of perception and attention’, *Attention, Perception, & Psychophysics*. Springer-Verlag, 72(8), pp. 2031–2046. doi: 10.3758/BF03196680.

Zhang, W. and Luck, S. J. (2008) ‘Discrete fixed-resolution representations in visual working memory.’, *Nature*. NIH Public Access, 453(7192), pp. 233–235. doi: 10.1038/nature06860.

3

THE EFFECT OF COVERT SPATIAL ATTENTION ON THE RELATIONSHIP BETWEEN PERCEPTUAL QUALITY AND 1/F AND PERIODIC ELECTROENCEPHALOGRAPHY ACTIVITY IN A CUED ORIENTATION PERCEPTION TASK

3.1 INTRODUCTION

Our brain must deal with a large amount of incoming visual information in a way that is energy efficient, fast, and accurate. To satisfy all three criteria, attention is used to selectively improve processing of visual input relevant to our behavioral goals. In this way, our brain can conserve energy by processing only a subset of sensory information while still being able to respond to the environment in a timely manner. Our brain accomplishes this by using attention to selectively focus on those things in the environment that are salient or goal-related. Attention is a neuro-cognitive process that enables relative improvement in task-related sensory processing and subsequent performance (Desimone, 1995; Carrasco, 2011; Nobre and Kastner, 2014). Although this selective attention-related processing has been found across different sensory modalities and at multiple levels of the information processing hierarchy, how these mechanisms work and the details of their underlying neural circuity is still debated.

Orientation estimation tasks are common in the visual perception literature (Fischer & Whitney, 2014) and the application of the standard mixture model to orientation perception (Bays, 2016; Samaha, Switzky and Postle, 2019) and attention (Michel, Dugué and Busch, 2021)

has been previously studied. In previous work, we have shown that performance on a visual orientation perception task can be quantified using the standard mixture model originally developed by Zhang and Luck (2008) to investigate visual working memory (Sheldon and Mathewson, 2021). Furthermore, we were able to associate task performance to changes in EEG activity. Now, our aim is to extend this previous study to investigate whether visual working memory models can quantify the effect of covert spatial attention on the visual orientation perception task and how EEG brain activity varies as a function of attention, perception, and task performance.

To study attention, a spatial cueing component has been added to the original orientation perception task. Specifically, targets now appeared in the left or right visual field instead of centrally. Participants receive a cue about the side the target will appear on and are instructed to pay attention to that side without moving their eyes. In the control condition, participants still receive a cue, but the cue does not indicate which side the target will be presented. This is a common paradigm used in the visuospatial literature with well documented effects of hemifield-selective attention on the lateralization of alpha oscillations and various ERP components (Carrasco, 2011, Di Russo et al., 2021, Foxe and Snyder, 2011, Kelly et al., 2009, Kelly et al., 2006, Luck et al., 2000, Slagter et al., 2016). In other words, it provides a good basis for the current research study.

There has been a great deal of research on alpha-related (8-14 Hz) neural mechanisms underlying visuospatial attention. While the relationship between alpha-band activity and visuospatial has been reported numerous times, it is unclear how this process unfolds. Some evidence has pointed towards alpha activity having a role in visuospatial attention by selectively *suppressing* distracting or irrelevant information (Kelly *et al.*, 2006; Jensen and Mazaheri, 2010;

Klimesch, 2012). Others have found support for alpha activity *facilitating* relevant information processing by modulating cortical excitability of task-related sensory regions (Gould, Rushworth and Nobre, 2011; Foster and Awh, 2019). Yet still, there is evidence for alpha being involved in both attentional mechanisms (Rihs, Michel and Thut, 2009; Sokoliuk *et al.*, 2019). These mixed results could be attributed to a heterogeneity in alpha generation where thalamic and cortical brain areas give rise to alpha oscillations with the same frequency spectra but serve different functional roles (Başar, 2012; Halgren *et al.*, 2019; Bourgeois *et al.*, 2020). Another possibility is that results have been confounded by the contributions of aperiodic activity that may underlie apparent differences in oscillatory power if not controlled for (Donoghue *et al.*, 2020; Donoghue, Dominguez and Voytek, 2020; Gyurkovics *et al.*, 2021).

Recent studies have started to raise concerns about evidence found using the standard analytic approaches that focus only on the periodic oscillatory activity of electrophysiological signals, including evidence related to alpha activity (Iemi *et al.*, 2019; Donoghue *et al.*, 2020; Gyurkovics *et al.*, 2021; Waschke *et al.*, 2021). Most time-frequency analysis focuses on measures of the periodic or oscillatory activity even though electrophysiological brain activity contains 1/f-like aperiodic activity (*i.e.,* power decreases with increasing frequency) that can confound results (Donoghue *et al.*, 2020; Donoghue, Dominguez and Voytek, 2020). Traditionally, researchers ignored or discarded a spectra's aperiodic activity, considering it to be neural noise.

Recently, interest in the 1/f aperiodic activity has gained momentum as more studies have shown it to have biological importance. For example, a lower (flatter) 1/f exponent has been associated with age-related decline in working memory performance (Voytek *et al.*, 2015; Donoghue *et al.*, 2020) while an increase has been correlated with performance on various

cognitive tasks including successful lexical predication (Dave, Brothers and Swaab, 2018) and reaction time on a visual short-term memory task (Thuwal, Banerjee and Roy, 2021). Evidence from computational models and invasive neural recordings have demonstrated that 1/f exponent of electrophysiological spectra reflects the balance between excitation (E) and inhibition (I) neural activity (Gao, Peterson and Voytek, 2017) while optogenetics has shown that a lower 1/f exponent is causally linked to increased E:I balance (Chini, Pfeffer and Hanganu-Opatz, 2021). In addition, induced changes in E:I balance by ketamine and propofol were well approximated by the EEG spectral 1/f exponent (Waschke *et al.*, 2021). A recent study by Waschke et al (2021) found that selective attention to sensory input from different modalities resulted in a reduction of the 1/f exponent in the corresponding modality-specific brain areas. Interestingly, the authors found that the attention-related decrease in EEG aperiodic exponents exceeded the changes observed in alpha oscillations (Waschke *et al.*, 2021).

In the current study, we predict that cues informative about the location of the upcoming target will improve the probability of the participant perceiving the target thereby decreasing guess rate relative to when the cue is non-informative. If the 1/f aperiodic exponent reflects changes in the E:I ratio, and covert spatial attention improves the quality of the stimulus representation by increasing the gain on the signal (Sokoliuk *et al.*, 2019), then we hypothesize that there will be a decrease in the response variability as a function of a decreasing 1/f exponent. Furthermore, if the 1/f aperiodic exponent is a better indicator of these attention-related shifts in the E:I balance that are thought to reflect local desynchronization and the corresponding changes to the efficacy of information processing (Harris and Thiele, 2011; Gao, Peterson and Voytek, 2017; Waschke *et al.*, 2021), then the 1/f aperiodic exponent should better capture the dynamics of the task performance measures than alpha oscillatory activity.

3.1 Materials and Methods

Participants

Thirty-five participants from the University of Alberta community participated in the study (age range = 17-34 years). Seven participants were not included in the analysis due to 30% or more trials containing eye movement artifacts (*i.e.*, overt attention; see the EEG Preprocessing section for more details). One other participant was excluded from the analysis due to having extreme outlying performance on the task (see Behavioral Analysis in the Results section for more details). Participants were all right-handed and had normal or corrected normal vision and no history of neurological problems. All participants gave informed written consent, were either compensated at a rate of $10/hr or given research credit for their time. The study adhered to the tenets of the Declaration of Helsinki and was approved by the Internal Ethics Board at the University of Alberta.

Cued Orientation Perception Task

Participants were seated 57 cm away from a 1920 x 1080 pixel^2 ViewPixx/EEG LCD monitor (VPixx Technologies, Quebec, Canada) with a refresh rate of 120 Hz, simulating a CRT display with LED backlight rastering. The rastering, along with 8-bit digital TTL output triggers yoked to the onset and value of the top left pixel, allowed for submillisecond accuracy in pixel illumination times, which were confirmed with a photocell prior to the experiment. Stimuli were presented using a Windows 7 PC running MATLAB R2012b with the Psychophysics toolbox (Version 3; Brainard, 1997; Pelli, 1997). The code running the task was a modified version of the Orientation Perception Task code from Sheldon and Mathewson (2021). The original version of the code can be found here: https://github.com/APPLabUofA/OrientTask_paper. Video output

was sent to the ViewPixx/EEG with an Asus Striker GTX760 (Fremont, CA) graphics processing unit.

Each trial began with a white fixation dot presented at the center of the monitor and two dark gray circles to the left and right of the fixation dot for 700 ms after which one of three possible cues appeared above the central fixation dot, vertically aligned to the top of the circles (Figure 3.1A). Two cues were black triangles pointing towards the left or right, indicating the side the target will appear (*i.e.,* informative cues). The third cue was both black triangles pointed toward each other indicating that the target will appear to the left or right (*i.e.,* non-informative cue). The cues remained on screen for 1242, 1284, 1325, or 1367 ms. After the cue, the target appeared for 8.33 ms (one monitor refresh) in the center of the left or right circle. The target always appeared to the side indicated by the informative cue. For non-informative cues, the target could appear on the left or right with equal probability. The target was in the shape of a needle and was pointing toward one of 24 predefined evenly spaced directions so that all the orientations covered 360 degrees. The direction of the target was randomly selected on each trial. A backward mask lasting for 8.33 ms with a constant 41.7 ms target-mask stimulus-onset asynchrony appeared in the center of both circles regardless of the side the target appeared. The mask was created by overlaying the target orientated in all 24 directions which created a star shape seen in Figure 3.1A. Following the mask offset, a 516.6 ms blank interval period occurred identical to the fixation.

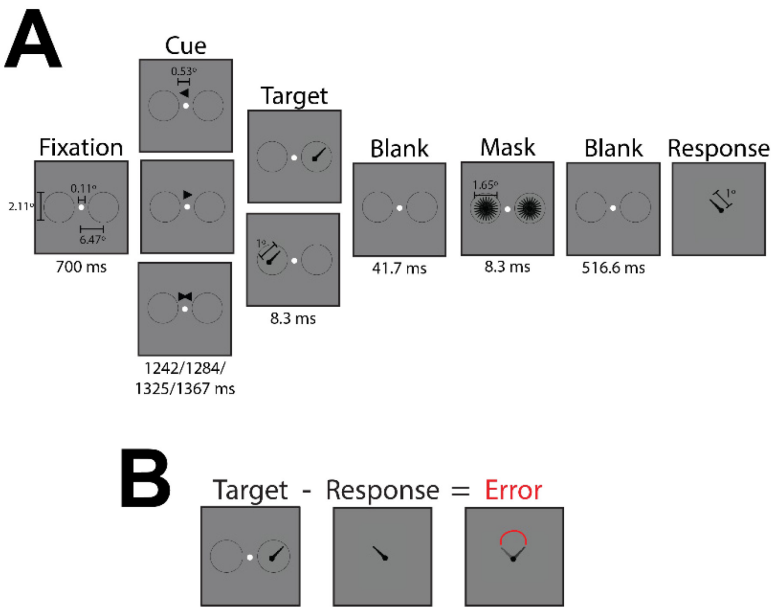

Figure 3.1. *Cued orientation perception task*

A) Sequence of task events with duration of each screen presentation and sizes of fixation, cues, target, mask, and response stimuli. Sizes are in degrees of visual angle. **B)** Example of response error calculation. Response errors are reported in degrees.

After the blank interval, a response screen appeared with the needle in the center of the screen. Using the computer mouse, participants were asked to rotate the needle so that it was pointed in the same direction as the previous target. If participants detected a target but could not remember its orientation, they were asked to guess the orientation of the target. Participants could provide their response at their own pace. No feedback was given to participants. The next trial began immediately after a needle's orientation was selected. See Figure 3.1A for a summary of the task sequence and the stimulus dimensions.

Participants completed eight blocks consisting of 48 trials each, along with 20 practice trials at the beginning of the experiment. Participants completed a total of 404 trials with 33% of

trials having a non-informative cue and about equal left and right targets, 33% of trials having a right target and informative cue, and 33% of trials having a left target and informative cue. Participants could rest at their own pace every 48 trials. Extensive written and verbal instructions were presented to participants prior to the practice trials. Instructions thoroughly explained and demonstrated each component that would compose a single trial.

Before the cued orientation perception task, participants performed a staircased cued target detection task that had the same parameters as the cued orientation perception task except that participants only reported whether they saw the target or not using the keyboard. The target color was a gray determined by a scalar value passed to the functions in Psychtoolbox (Version 3; Brainard, 1997, Pelli, 1997). In the staircased cued target detection task, the target color value could range from the background color (making it not visible; corresponding value of 256) to black (making it the most visible; corresponding value of 0). This target gray value was adjusted throughout the task based on a 1-up/2-down staircasing procedure targeting a 0.65 target detection rate for each individual (García-Pérez, 1998; Kingdom and Prins, 2016). The staircased task consisted of three blocks of 48 trials. The target gray value was determined for each participant by taking the average target gray value across the last two blocks of trials. These final values came to be 56 on average (SD = 20) and were used as the target gray value in the cued orientation perception task.

The MATLAB code for the cued staircased target detection task and the cued orientation perception task are available at https://github.com/APPLabUofA/CuedOrientTask_paper.

Behavioral Data Analyses

Response errors on each trial were calculated by subtracting the orientation of the response stimulus, as reported by the participant, from the orientation of the target stimulus (see

Figure 3.1B).

Comparing Model Fits

In addition to the standard mixture model proposed by Zhang and Luck (2008), the working memory literature has several other models similar to the standard mixture model but makes different assumptions about some of the parameters. For example, the variable precision models are based on the idea that the precision of memory varies from trial-to-trial rather than being fixed as it is in the standard mixture model. This is done by Fougnie and colleagues (2012) by having the standard deviation parameter be distributed according to a higher-order distribution, we chose a Gaussian distribution in this case. The variable precision model proposed by van den Berg and colleagues (2012) has a precision (*i.e.*, the inverse of variance) parameter drawn from a gamma distribution. Neither paper presented clear justification for choosing one distribution over another, especially when the set size is always one, so we tested both distributions.

Due to the targets' location being left or right of fixation, all the models were tested with and without a third parameter, referred to as the bias or mu (μ), which is the mean of the von Mises distribution and represents systematic bias of the response error distribution. It was included in case there were any clockwise or counterclockwise biases in the perceived target's orientation due to its lateral locations.

After finding that the models had a significantly worse fit when there were informative cues than non-informative cues (see Results section), we tested whether foreknowledge of the target eliminated guessing. Since target detection rates were determined using the average threshold across trials with informative and non-informative cues, there could be two possible explanations. First, having an informative cue eliminates the need for guessing so removing the

guess rate parameter would result in improved model fitting for the trials with an informative cue. Or, second, there is something else about having prior information about the target's upcoming location that the models are not able to account for other than an absence in guessing. we tested whether the variable precision models fit better to the response error data when they did not have the guess rate parameter compared to the standard mixture model and the variable precision models with a guess rate parameter. Furthermore, according to the variable precision models, what seems to be guessing is just low precision on that trial (van den Berg *et al.*, 2012). If this were the case, the variable precision models without a guess rate parameter would fit the data better than the standard mixture models. To determine whether this extends to orientation perception data, variable precision models without a guess rate parameter were also tested.

We determined which model better fit the response errors using the model comparison routine in the MemToolbox (Suchow *et al.*, 2013). In the first test, we included the standard mixture model with the bias parameter in addition to the two variable precision models with and without a bias parameter. In the second test, we wanted to see if there was an absence in guessing or another alternative reason for the models fitting worse when the cues were informative compared to non-informative. To this end, we selected the two best fitting models and compared them to versions without their guess rate parameter and included a new model called the stochastic sampling model which is based on neural population coding principles that has been successful at explaining performance across different visual working memory tasks (Bays, 2014, 2016; Schneegans, Taylor and Bays, 2020). All the models had a bias parameter since they performed equally well as models without (see Results section) and might be useful due to the spatial component of the task. Therefore, the second test compared the stochastic sampling model with and without a bias (μ) parameter, the standard mixture model and variable precision

model with the bias (μ) parameter and the guess rate parameter, and the standard mixture model and variable precision model with the bias (μ) parameter and without the guess rate parameter.

The goodness-of-fit measure used for the comparisons between models was the corrected Akaike information criterion (AICc) which includes a penalty for each additional model parameter and a correction for finite data (Suchow *et al.*, 2013). The smaller the AICc value, the better the fit of the model. The AICc values were submitted to a repeated-measures factorial ANOVA (target side and cue type the within-subject factors) using the permutation-based *Fmax* statistic (first described by Blair & Karniski, 1993) which is a mass univariate approach for factorial ANOVAs. The *Fmax* statistic has the advantages of permutation testing in there are less assumptions about the data than traditional statistical approaches, and has been shown to be very good at controlling Type I errors (Fields and Kuperberg, 2019). The implementation of the *Fmax* test was done with code modified from the Factorial Mass Univariate Toolbox (FMUT; Fields, 2017). The original code can be found here: https://github.com/ericcfields/FMUT/releases.

Follow-up pairwise comparisons of significant interactions and main effects was done with a repeated-measures, two-tailed permutation test based on the *tmax* statistic (Blair and Karniski, 1993) using the mxt_perm1() function from the Mass Univariate ERP Toolbox (Groppe, Urbach and Kutas, 2011). *P*-values were then corrected for multiple comparisons using the false discovery rate (FDR) procedure described in Benjamini and Yekutieli (2001). Effects that satisfied a 5% FDR criterion were considered significant. 10,000 random within-participant permutations were used to estimate the distribution of the null hypothesis for all permutation-based tests (*i.e., Fmax* and *tmax*) and the familywise alpha (α) was set to 0.05.

Model Parameter Analysis

According to the first test comparing models' goodness-of-fit, the standard mixture

model + bias (μ) was the best fit to the current data set. The model was fit to each participant's response errors using the maximum likelihood estimation routine in the MemToolbox (Suchow *et al.*, 2013). According to the standard mixture model, response deviations from the actual target orientation reflect a mixture of trials where the target's orientation was detected and trials where participants did not detect the target so guessed randomly. Therefore, the distribution of response errors consists of a mixture of a von Mises distribution (representing the trials where the target's orientation was detected) and a uniform distribution (random guesses (g)). Parameter sigma (σ) is the standard deviation of the von Mises distribution, which represents the width of the response error distribution of trials that the target's orientation was detected. Parameter *g* is the height of the uniform distribution representing the guessing probability. A third parameter, mu (μ), which is the mean of the von Mises distribution and represents systematic bias of the response error distribution was included to account for any influences by the lateralized target locations in the task. The three parameters standard mixture model was fit to all participants' response errors from the four different trial conditions (informative cue + left target, informative cue + right target, non-informative cue + left target, non-informative cue + right target) separately. This means that each participant had a total of 12 parameters calculated from their behavioral data. In addition, the probability of a trial being from the uniform distribution (*i.e.,* a guess trial) was calculated for each trial condition using code modified from the mixture model methods code (Bays, Catalao and Husain, 2009; Schneegans and Bays, 2016) in the Bayslab's Analogue Report Toolbox found here: https://www.paulbays.com/toolbox/index.php. The same statistical procedure used to test the goodness-of-fit values was applied to the model parameters except the alpha level was set to 0.0167 to control for the familywise error rate (Bonferroni corrected alpha level $\alpha_{corr} = 0.05/3$ to account for the three parameters).

To further investigate why model fits were significantly better on non-informative cued trials than informative cued trials, we performed a second test comparing models' goodness-of-fit. The second test found that the stochastic model + bias (μ) was the best fit to the current data set. The model was fit to each participant's response errors using the maximum likelihood estimation routine in the MemToolbox (Suchow *et al.*, 2013). The code for the probability density function (pdf) of the stochastic model came from the Bayslab's Analogue Report Toolbox found here: https://www.paulbays.com/toolbox/index.php. The stochastic model was originally developed to account for short-term working memory errors (Bays, 2014; Schneegans, Taylor and Bays, 2020) and is based on a simple sensory neural population coding model (Pouget, Dayan and Zemel, 2000). The idea is that a large number of neurons tuned to respond to a basic visual feature (*i.e.,* orientation), but vary in their preferred value so that their tuning curve, which can be described by Gaussian function, evenly covers the space of possible feature values. These neurons generate discrete spikes through a Poisson process where each spike is associated with the preferred value of the neuron that generated it. The number of spikes or samples that contribute to the feature representation of each item is drawn independently from a Poisson distribution. The more spikes, or samples, that are drawn, the more precisely the true stimulus feature can be estimated. Because the tuning curves are Gaussian, the distribution from which samples are drawn are Gaussian and the distribution of decoding errors is likewise Gaussian. Therefore, the distribution of response errors can be described as a mixture of Gaussian distributions with different precisions, each corresponding to a certain number of samples and weighted with the probability of obtaining that sample count which follows a Poisson distribution. The neural population generating this distribution can be described by the tuning width or precision (kappa, κ) of the Gaussian tuning curve, and the mean number of

spikes generated in a fixed decoding interval (referred to as γ). Same as the standard mixture model, a third parameter, mu (μ), which is the mean of the Gaussian distributions represents systematic bias in the response error distribution (which could be attributed to a bias in the preferred values of the tuned neurons, a bias in the decision criteria, or a bias in response generation) was included to account for any influences by the lateralized target locations in the task. The model fitting and statistical testing were the same as the standard mixture model parameter analyses.

Follow-up analysis to investigate the effects of each target's orientation on model parameters was conducted on the combined data of all participants. Since this was an unexpected effect, the experiment was not designed for a sufficient number of trials with each target orientation in each condition to conduct statistical analysis, so all results reported are based on descriptive statistics.

EEG Recording

During the experiment, EEG data was recorded from each participant with a Brain-Amp 32-channel amplifier (BrainVision) using gelled low-impedance electrodes (actiCAP passive electrodes kept below 5 kΩ). Inter-electrode impedances were measured at the start of each experiment. All electrodes were arranged in the same 10-20 positions (Fp2, Fp1, F4, F3, F8, F7, FC2, FC1, FC6, FC5, C4, C3, CP2, CP1, CP6 CP5, P4, P3 P6, P5, P8, P7, PO4, PO3, O2, O1, Fz, FCz, Cz, Pz, and Oz). In addition to the 31 EEG sensors, a ground electrode was used, positioned at AFz. Two reference electrodes and the vertical and horizontal bipolar EOG were recorded from passive Ag/AgCl easycap disk electrodes affixed on the mastoids, above and below the left eye, and 1 cm lateral from the outer canthus of each eye. The bipolar channels were recorded using the AUX ports of the Brain-Amp amplifier. SuperVisc electrolyte gel and

mild abrasion with a blunted syringe tip were used to lower impedances. Gel was applied and inter-electrode impedances were lowered to less than 5 kΩ for all electrode sites. EEG data was recorded online referenced to an electrode attached to the left mastoid. Offline, the data were re-referenced to the arithmetically derived average of the left and right mastoid electrodes.

Data were digitized at 1000 Hz with a resolution of 24 bits. Data were filtered with an online bandpass with cutoffs of 0.1 Hz and 250 Hz. The experiment was run in a dimly lit, sound and radio frequency-attenuated chamber from Electromedical Instruments, with copper mesh covering the window. The only electrical devices in the chamber were an amplifier, speakers, keyboard, mouse, and monitor. The monitor ran on DC power from outside the chamber, the keyboard and mouse were plugged into USB outside the chamber, and the speakers and amplifier were both powered from outside the chamber, and nothing was plugged into the internal power outlets. Any devices transmitting or receiving radio waves (*e.g.*, cell phones) were removed from the chamber for the duration of the experiment.

EEG Preprocessing

All analyses were completed using Matlab R2021a with the EEGLAB 13.6.5b (Delorme and Makeig, 2004) and CircStat (Berens, 2009) toolboxes, as well as custom scripts. After the data had been re-referenced offline, the bandpass FIR filter from EEGLAB was applied with lower and upper cut-offs of 0.1 Hz and 50 Hz. Data was segmented into 3000 ms epochs aligned to target onset (-2400 ms pre-target onset to 1400 ms post-target onset). The average voltage in the 200 ms baseline following fixation onset was subtracted on each trial for every electrode, and trials with absolute voltage fluctuations on any channel greater than 1000 μV were discarded. Eye movements were then corrected with a regression-based procedure developed by Gratton, Coles, and Donchin (1983). After a second baseline subtraction with 200 ms following fixation

onset, trials with remaining absolute voltage fluctuations on any channel greater than 500 μV were removed from further analysis.

To ensure there were no horizontal eye movements during the trial, we use a split-half sliding window approach on the HEOG signal. We slid a 100 ms time window in steps of 10 ms from 1600 ms prior to target onset (at least 200 ms before the first cue appears) to the response screen onset 600 ms after target onset. If the change in voltage from the first half to the second half of the window was greater than 25 μV, it was marked as an eye movement and rejected (Hong *et al.*, 2015; Hakim *et al.*, 2019). Seven participants had to be removed from further analysis after this procedure because more than 30% of trials got rejected indicating that they did not use covert attention as instructed. The resulting data set was then analyzed in the time and frequency domains (details provided below).

EEG Data Analyses

Data analysis was performed using MATLAB R2019b (The MathWorks Inc, Natick, MA, USA) and EEGLAB 13.6.5b (Delorme and Makeig, 2004). All statistical analyses were conducted using MATLAB R2019b and R version 3.6.2 (R Core Team, 2021). The MATLAB code for data analysis is available at the GitHub repository https://github.com/APPLabUofA/CuedOrientTask_paper and the raw data files are available at https://osf.io/dexm2/.

ERP Analysis

Event-related potential (ERP) data was submitted to a repeated-measures factorial ANOVA (hemisphere, target side and cue type the within-subject factors) using the permutation-based *Fmax* statistic. The implementation of the *Fmax* test was done with code modified from the Factorial Mass Univariate Toolbox (FMUT; Fields, 2017). The original code can be found

here: https://github.com/ericcfields/FMUT/releases. The time windows of interest were the CNV 1 (-1000 to -500 ms), CNV 2 (-500 to 0 ms), P1 (80-140 ms), N1 (140-200 ms), P2 (200-255 ms), N2 (255-360 ms), and P3 (360-500 ms) components. The ERP component time windows were selected based on previous literature (Luck, Woodman and Vogel, 2000; Nobre, Sebestyen and Miniussi, 2000; Koivisto and Revonsuo, 2010; Luck, 2014; Di Russo *et al.*, 2021). Thirteen brain electrode pairs were included in the test. The left hemisphere-right hemisphere electrode pairings were O1-O2, PO3-PO4, P7-P8, P5-P6, P3-P4, CP5-CP6, CP1-CP2, C3-C4, FC5-FC6, FC1-FC2, F7-F8, F3-F4, Fp1-Fp2. 10,000 random within-participant permutations were used to estimate the distribution of the null hypothesis and the familywise alpha (α) was set to 0.05. This analysis was repeated on the mean difference between contralateral and ipsilateral electrodes relative to the target's location. The procedure was identical except that there was no hemisphere factor since this was investigating mean lateralized activity relative to the target side.

ERP traces from -1000 to 0 relative to target onset was submitted to a repeated-measures factorial ANOVA (hemisphere, trial type the within-subject factors) using the permutation-based *Fmax* statistic. The time period was parsed and averaged into 20 ms non-overlapping windows giving a total of 50 time points being tested. Because this time period is prior to target onset, non-informative cued trials were collapsed across left and right targets. This gave the following three trial types as the levels for the within-subject factor: cued left, cued right, and non-informative cue.

It is important to note that because the ERP component names in this study have pre-selected time windows instead of time windows based on the peaks in the data, the ERP labels in the current experiment will not necessarily be the ERP waveforms normally associated with that particular label. Instead, the label refers to the time window previous studies used when

calculating that ERP component (*e.g.*, the P1 will not always be the first positive peak following stimulus onset but will be the mean voltage between 80-140 ms post-target).

Spearman rank correlations were calculated between ERP values and the three parameters from the standard mixture model and the stochastic model. This was done for each ERP component at each electrode and trial condition separately and each contralateral minus ipsilateral electrode pairs relative to the target locations and by informative and non-informative cues. *P*-values were then corrected for multiple comparisons across ERPs and trial conditions at each electrode using the false discovery rate (FDR) procedure described in Benjamini and Yekutieli (2001). Effects that satisfied a 1.67% FDR criterion ($\alpha = 0.05/3$ to account for the three parameters) were considered significant.

Periodic and Aperiodic Components

Because neural power spectra consist of overlapping periodic and aperiodic components, it is important to consider the aperiodic activity when measuring a signal's oscillatory properties. For this reason, the FOOOF toolbox (version 1.0.0; Donoghue et al., 2020) was used to identify peaks within the alpha (8-14 Hz) and low beta (15-22 Hz) frequency ranges after adjusting for the aperiodic component. FOOOF is a spectral parameterization algorithm which decomposes the power spectrum into periodic and aperiodic components via an iterative process of model fitting (see Donoghue et al., (2020) for detailed description). The FOOOF toolbox is available on https://github.com/fooof-tools/fooof.

Before FOOOF, the power spectral density (PSD) was estimated using the mean Welch's method by applying the compute_spectrum() function from the NeuroDSP package (version 2.1.0; Cole et al., 2019) in python. The PSD was calculated from 1 to 40 Hz at four different time windows for each participant, electrode, and trial separately. The four time windows were target-

aligned and as follows: fix (-1760 to -1360 ms) which is 180 ms after fixation onset to earliest cue onset; early (-1000 to -500 ms) which corresponds to the CNV-1 ERP component; late (-500 to 0 ms) which corresponds to the CNV-2 ERP component; and, post (80 500 ms) which is post-target starting from the P1 ERP component to the end of the P3 ERP components right before response screen onset. The shorter time windows meant that changes in the oscillatory and broadband power could be analyzed for temporal changes within the trial, but the trade-off was that frequencies slower than alpha would be invisible. After the PSDs were calculated, these PSDs were then submitted to FOOOF in Python for fitting.

Settings for the FOOOF algorithm were set as: peak width limits: [1,5]; max number of peaks: 8; and aperiodic mode: fixed. These settings were chosen because they resulted in better fits overall. Power spectra were parameterized across the frequency range 1 to 40 Hz with a frequency resolution of 2.49 Hz for the fixation, 2.00 Hz for the mid and late time windows and 2.38 Hz for the post time window. Alpha and beta peaks and the aperiodic component were identified on a trial-by-trial basis for each electrode and participant separately. The algorithm returns the power at the oscillatory peaks adjusted for the aperiodic component (i.e., the magnitude of the peak above the aperiodic component; see Donoghue et al (2020) for more details) and aperiodic component measures, offset and exponent. The values from the fixation time window were subtracted from the other three time windows so that the measures were relative to the fixation time period. These relative values were used in subsequent permutation-based statistical analyses were submitted to a repeated-measures factorial ANOVA (electrode hemisphere, target side and cue type the within-subject factors) using the permutation-based Fmax statistic. The implementation of the Fmax test was done with code modified from the Factorial Mass Univariate Toolbox (FMUT; Fields, 2017). 10,000 random within-participant

permutations were used to estimate the distribution of the null hypothesis for all permutation-based tests and the familywise alpha (α) was set to 0.05.

After subtracting the fixation time window values, alpha and beta peaks and the two measures of the aperiodic component were tested statistically with the same procedure as the ERP analysis except the three time windows early, late, and post were tested and the alpha level was set to 0.025 to control for the familywise error rate (Bonferroni corrected alpha level α_{corr} = 0.05/2 to account for the two peak frequencies and again to account for the two aperiodic component measures).

Spearman rank correlations were calculated between all the measures (after subtracting the fixation values) and the three parameters from the standard mixture model and the stochastic model. This was done at each time window, electrode, and trial condition separately. *P*-values were then corrected for multiple comparisons across time windows and trial conditions at each electrode using the false discovery rate (FDR) procedure described in Benjamini and Yekutieli (2001). Effects that satisfied a 1.67% FDR criterion (α = 0.05/3 to account for the three parameters) were considered significant.

Time-Frequency Analysis

To investigate the relationship between how EEG brain activity varies as a function of attention, perception, and task performance the phase angle and power on each trial was calculated using the fast Fourier transform (FFT) on each trial's 3000 ms epochs (-2400 ms pre-target onset to 1400 ms post-target onset) using the newtimef() function of EEGLAB. The FFT yielded complex values for 81 frequencies ranging from 0.98 to 40 Hz with a frequency resolution of 0.49 Hz. The abs() function from MATLAB was used to get the instantaneous amplitude and the instantaneous phase angle of each trial was calculated using the angle()

function from MATLAB. The power calculated using the FFT, a traditional time-frequency decomposition method, was also used for comparison to aperiodic-adjusted results from FOOOF.

EEG Power Analysis. EEG power data was converted to a decibel (dB) scale using the same baseline time window as the ERPs (-1600 to -1400 ms relative to target onset). This was done to the data from each participant at each electrode and frequency separately. EEG power data was then averaged across pre-determined frequency bands (1-3 Hz, 4-7 Hz, 8-14 Hz, and 15-22 Hz) and then tested statistically with the same procedure as the ERP analysis except each time point was tested rather than averaging across a time window and the alpha level was set to 0.0125 to control for the familywise error rate (Bonferroni corrected alpha level $\alpha_{corr} = 0.05/4$ to account for the four frequency bands).

To test for a relationship between mean power relative to fixation in each frequency band and the fitted parameters from the standard mixture model (*i.e.,* bias, variability, and guess rate) and stochastic model (*i.e.,* bias, precision, and mean spikes), a nonparametric permutation version of the Spearman's rank correlation test was used with a pixel-based multiple-comparison correction procedure (Cohen, 2014). The pixel-based multiple-comparison correction method involves creating one distribution of the largest positive pixel value and another distribution of the largest negative pixel value from each iteration of the permutation testing. After all iterations, the statistical threshold is defined as the value corresponding to the 2.5^{th} percentile of the smallest values and the value corresponding to the 97.5^{th} percentile of the largest values which are the thresholds corresponding to an α of 0.0125 ($\alpha = 0.05/4$ to account for the four trial conditions). Any pixel that has a value exceeding the upper or lower value is considered significant. The pixel-based method corrects for multiple comparisons by creating two distributions based on map-level information instead of pixel-level information. In other words,

this method results in two distributions of the most extreme null-hypothesis test statistical values across all pixels rather than calculating null-hypothesis distributions for each pixel (see Cohen (2014) for further details about pixel-based multiple-comparison correction method). All analysis using nonparametric permutation testing with pixel-based multiple-comparison correction performed 10,000 iterations per test. To obtain more stable estimates from permutation testing, we ran a "meta-permutation test" by repeating the pixel-level permutation procedure 10 times and then averaging the results (Cohen, 2014). It needs to be pointed out that a "significant effect" determined by pixel-based permutation testing should not be considered a precise estimate in the temporal domain. Although pixel-based permutation testing is more stringent than cluster-based permutation tests (Cohen, 2014), caution should still be used when interpreting "significant" effects, especially if the temporal range of each pixel is relatively small.

EEG Phase Analysis. To look at whether task performance is related to oscillatory phase, and if yes, at what frequency, we used the weighted inter-trial phase clustering (wITPC) (Cohen and Voytek, 2013; Cohen, 2014). The logic behind the inter-trial phase coherence (ITPC) is that a systematic relation between EEG phase and behavioral outcome should result in a higher-than-chance ITPC in each of the trial subgroups. However, if the phase of the EEG signal is randomized and unpredictable, the distribution of phases at a given time period should follow a uniform distribution over all trials. The problem with ITPC is that it assumes EEG phase is relevant to experimental measures only when phase values are similar across trials (van Diepen and Mazaheri, 2018). Unlike ITPC, wITPC is sensitive to modulations of phase values even if those phases are randomly distributed across trials as would be expected if performance (which differs from trial to trial) were modulated by oscillatory phase (Cohen and Voytek, 2013; Cohen, 2014).

We chose to use the wITPCz because it provides information about performance-specific modulations of phase values irrespective of the model. Also, the wITPCz does not rely on phase values being consistent over trials, they only need to be consistently related to response errors (Cohen and Cavanagh, 2011). This is important for determining how much of the phase modulation is an artifact of the stimulus-evoked activity and how much is related to the differences in task performance.

The wITPC was computed for each participant as the resultant vector length, or ITPC, of phase angles across trials once the length of each vector has been weighted by a variable of interest (in this case, each trial's phase vector is weighted by the absolute degree of response error on that trial or the probability the trial was from the uniform/guess distribution (Cohen and Voytek, 2013; Cohen, 2014). For statistical testing, a null-hypothesis distribution was created by shuffling the phase values relative to trial response error 1,000 times. The wITPCz was calculated as the wITPC standardized relative to the null-hypothesis distribution, providing a *z*-value corresponding to the probability of finding the observed behavior measure–phase modulation by chance, given the data. Statistical significance of the wITPCz across participants was evaluated by combining the individual-level *p*-value, calculated from the *z*-values, time-frequency map at each electrode across participants using Stouffer's method (Stouffer *et al.*, 1949; VanRullen, 2016a). *P*-values were then corrected for multiple comparisons across time points and frequencies at each electrode using the false discovery rate (FDR) procedure described in Benjamini and Yekutieli (2001). Effects that satisfied a 1.25% FDR criterion (α = 0.05/4 to account for the four trial conditions) were considered significant. The cue-target interval (-1000 to 0 ms relative to target onset) and post-target time period (0 to 500 ms relative to target onset) were calculated separately in case larger effects due to target onset created a

threshold too high for any smaller pre-target phase effects to be detectable. The results from both time periods were combined before applying Stouffer's method and the FDR procedure so that statistical significance across participants could be evaluated as one time window.

3.1 RESULTS

Comparing Model Fits

We first tested whether the best fitting model was a standard mixture model or the variable precision models and whether a bias parameter affected the fits. The goodness-of-fit measure was the corrected Akaike information criterion (AICc). Overall, the three-way interaction was not significant ($Fmax(5,130) = 1.26$ (critical $Fmax = \pm 2.26$), $p = 0.29$) nor was the model x cue type interaction ($Fmax(5,130) = 1.58$ (critical $Fmax = \pm 2.22$), $p = 0.17$) and the target side x cue type interaction ($Fmax(1,26) < 1$). The model x target side interaction was significant ($Fmax(5,130) = 4.29$ (critical $Fmax = \pm 2.28$), $p < 0.001$) as well as the model main effect ($Fmax(5,130) = 28.46$ (critical $Fmax = \pm 2.29$), $p < 0.001$) and cue type main effect ($Fmax(1,26) = 895.48$ (critical $Fmax = \pm 4.25$), $p < 0.001$). The target side main effect was not significant: $Fmax(1,26) = 2.25$ (critical $Fmax = \pm 4.22$), $p = 0.15$. The cue type main effect indicated that the models fit the data from trials with non-informative cues significantly better than trials with informative cues: $M = 518.1$, $SD = 67.0$; $M = 999.4$, $SD = 135.5$, respectively. As can be seen in Figure 3.2A and Table 3.1, the AICc indicates that both standard mixture models fit the data better than any of the variable precision models. Furthermore, adding the bias parameter did not significantly change any of the models' goodness-of-fit values. With regards to the target side and model interaction, most significant differences were between models fitted to trials that had their target on the same side. Comparisons between models fit to trials with different target locations (*i.e.,* targets on right vs left) showed no significant differences.

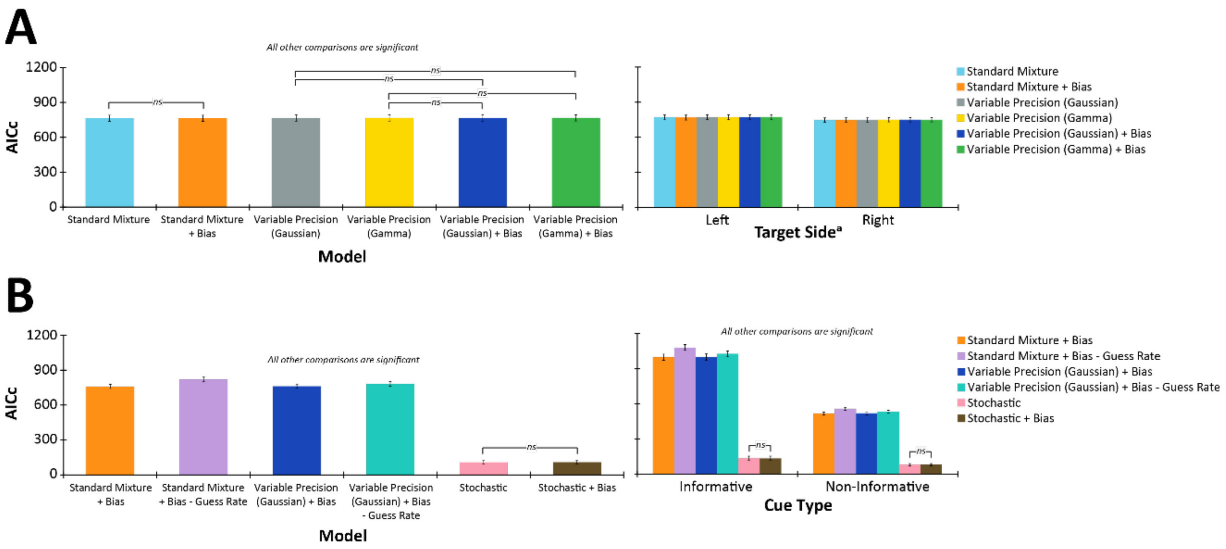

Figure 3.2. *Goodness-of-fit results*

Summary of results comparing the goodness-of-fit metric AICc of different model fits. **A)** Results from the first test comparing the standard mixture model and two variations of the variable precision model with and without a bias (μ) parameter. *Left* shows AICc values and pairwise comparisons between each model. All comparisons are significant except where noted on plot. *Right* plots the AICc values for each model fitted to data with left and right targets separately. Summary of statistical results can be found in Table 3.1. **B)** Results from the second test investigating the significantly worse fits to informative cued trials than non-informative cued trials found in the first test. Comparison was between the standard mixture model, the variable precision model with the standard deviation parameter (σ) described by a Gaussian distribution, and the stochastic model. The standard mixture model and variable precision model are compared with and without their guess rate parameter. All models include a bias parameter (μ) except for the stochastic model which is tested with and without the third parameter. *Left* shows AICc values and pairwise comparisons between each model. All comparisons are significant except between the stochastic model and the stochastic model with a bias parameter (μ). *Right* plots the AICc values for each model fitted to data with informative and non-informative cues separately. All comparisons are significant except between the stochastic model and the stochastic model with a bias parameter (μ).

[a]See Table 3.1 for results from pairwise comparison of the interaction effect.

Table 3.1. *P-values from pairwise comparisons between target side x models with and without bias (μ) parameter*

Target Side	Model	Right Targets						Left Targets				
		Standard Mixture + μ	Standard Mixture	VP (Gaussian)	VP (Gamma)	VP (Gaussian) + μ	VP (Gamma) + μ	Standard Mixture	Standard Mixture + μ	VP (Gaussian)	VP (Gamma)	VP (Gaussian) + μ
Right Targets	Standard Mixture	0.074	-									
	VP (Gaussian)	0.203	**0.001**	-								
	VP (Gamma)	**0.002**	**0.000**	**0.000**	-							
	VP (Gaussian) + μ	**0.000**	**0.001**	**0.039**	0.295	-						
	VP (Gamma) + μ	**0.000**	**0.000**	**0.002**	**0.034**	**0.000**	-					
Left Targets	Standard Mixture	0.203	0.203	0.203	0.203	0.206	0.206	-				
	Standard Mixture + μ	0.203	0.203	0.206	0.206	0.213	0.234	0.203	-			
	VP (Gaussian)	0.203	0.203	0.203	0.203	0.203	0.203	**0.000**	**0.000**	-		
	VP (Gamma)	0.203	0.203	0.203	0.203	0.203	0.203	**0.000**	**0.000**	**0.000**	-	
	VP (Gaussian) + μ	0.203	0.203	0.203	0.203	0.203	0.203	0.203	**0.000**	0.234	0.198	-
	VP (Gamma) + μ	0.203	0.203	0.203	0.203	0.203	0.203	0.079	**0.000**	0.614	0.234	**0.000**

Note. VP = Variable Precision; μ = bias parameter. Bold numbers indicate significant *p*-values

The second test was to see if the models fit better when they did not include a guess rate parameter. As others have found (Fougnie, Suchow and Alvarez, 2012; Sheldon and Mathewson, 2021), all the models performed better when they included a guess rate parameter regardless of other variables. There was a significant main effect for model type which can be seen in Figure 3.2B ($Fmax(5,130) = 3005.3$ (critical $Fmax = \pm 2.30$), $p < 0.001$). The surprising result was that the stochastic model fit the data better than any other model. The purpose for including the stochastic model was to see if a model based on neural population coding could better account for the significant difference in goodness-of-fit between informative cued trial and non-informative cued trials. While this was not the case (see Figure 3.2B), the difference in AICc value between the stochastic model and other tested models was surprising. While there was a significant interaction between model and cue type ($Fmax(5,130) = 1889.5$ (critical $Fmax = \pm 2.27$), $p < 0.001$), this was only because the two-parameter stochastic model did not significantly differ from the three-parameter stochastic model within the same cue type condition (see Figure 3.2B). The models still fit significantly better to trials with a non-informative cue

than informative cue ($Fmax(1,26) = 640.93$ (critical $Fmax = \pm 4.14$), $p < 0.001$; non-informative cue: $M = 380.5$, $SD = 58.0$; informative cue: $M = 729.0$, $SD = 118.3$). In addition, there was significant effect for target side ($Fmax(1,26) = 4.31$ (critical $Fmax = \pm 4.14$), $p < 0.05$) with the models fitting better to trials with the targets on the right than the left ($M = 541.9$, $SD = 86.2$; $M = 567.5$, $SD = 97.1$, respectively). Like the first test, the three-way interaction and the target side x cue type interaction were not significant ($Fmax(5,130) < 1$ and $Fmax(1,26) < 1$, respectively). The model x target side interaction also not significant ($Fmax(5,130) = 1.35$ (critical $Fmax = \pm 2.23$), $p = 0.25$).

Model Parameter Analysis

Based on the first test, the standard mixture model tended to fit better than the variable precision models and the addition of the bias parameter resulted in a slightly better mean AICc value (757.65 vs 757.57), the three-parameter standard mixture model was used to quantify performance on the visual orientation perception task. The variability (σ) parameter showed no significant main effects (target side: $Fmax(1,26) < 1$; cue type: $Fmax(1,26) = 1.52$ (critical $Fmax = \pm 5.93$), $p = 0.23$) or interactions ($Fmax(1,26) < 1$). In contrast, the guess rate (g) parameter had a significant main effect for target side ($Fmax(1,26) = 13.54$ (critical $Fmax = \pm 6.29$), $p < 0.001$), cue type ($Fmax(1,26) = 8.65$ (critical $Fmax = \pm 6.50$), $p < 0.01$), and a significant interaction between target side and cue type ($Fmax(1,26) = 12.22$ (critical $Fmax = \pm 6.64$), $p < 0.01$). As can be seen in Figure 3.3B, all pairwise comparisons were significant except between the informative vs non-informative cues when the target was on the right side. Otherwise, the guess rate parameter was significantly larger when the target was on the left side than the right side, and the non-informative cues had larger guess rate parameters than informative cues when targets where on the left.

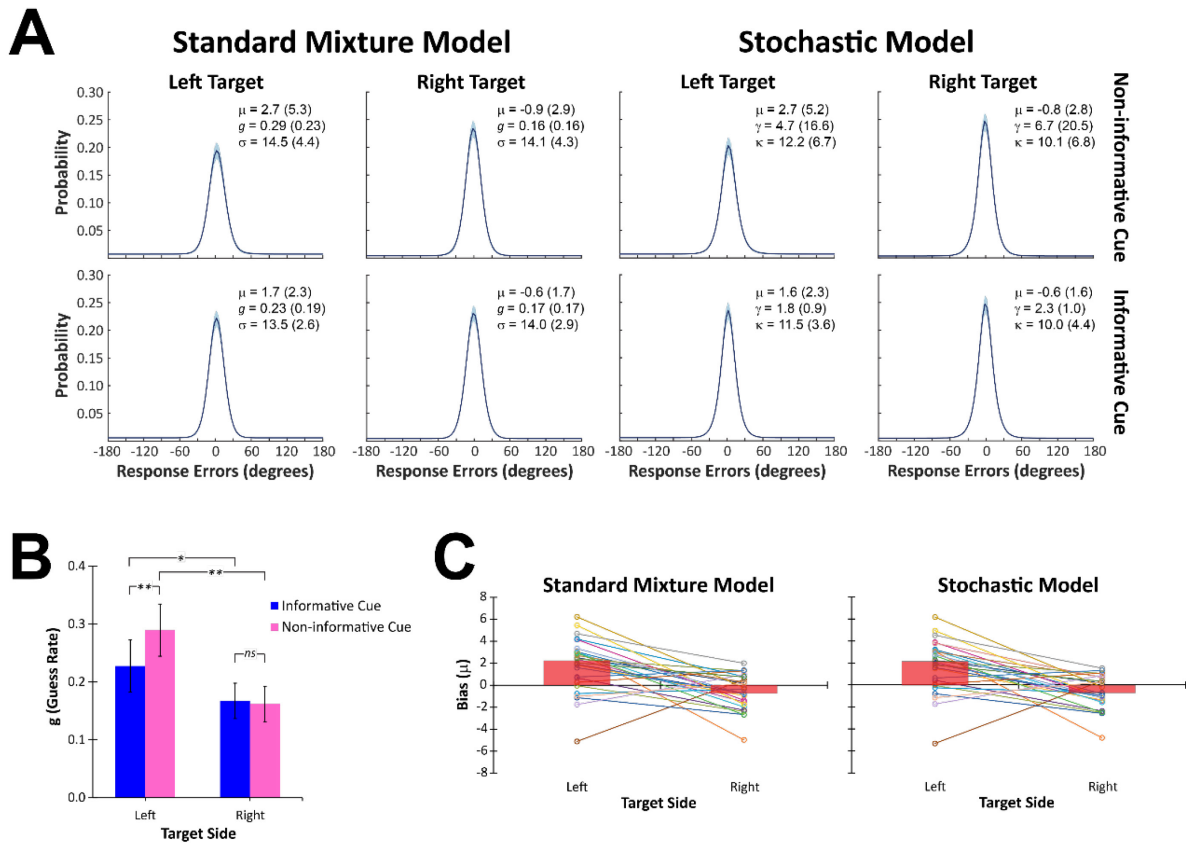

Figure 3.3. *Summary of model fits and parameter value analysis*

A) Standard mixture model and stochastic model fits to the data separated by cue type and target side. The main difference between the models is that the stochastic model tends to have higher peaks than the standard mixture model. Shaded region around the lines are ± *SEM.* **B)** Significant effects of experimental conditions on the fitted parameter guess rate (g) from the standard mixture model. Error bars are the ±*SEM.* **C)** Significant effects of the experimental condition target side on the fitted parameter bias (m) from the standard mixture model and stochastic model. Red bars are the means at each target location. The bias values at each target location are represented for all the participants. A continuous line joins each participant's bias parameter values derived for each target location.

Interestingly, the bias parameter (μ) had a significant main effect for target side ($Fmax(1,26) = 16.99$ (critical $Fmax = \pm 5.98$), $p < 0.001$), where the target's orientation was perceived, on average, more clockwise than its true orientation when it was located on the left (*M*

= 2.2, *SD* = 3.1), and more counterclockwise when the target was located on the right (*M* = -0.7, *SD* = 1.8). Visual inspect indicates the variability of the bias parameter was also greater for targets located on the left than right. There was no significant main effect for cue type (*Fmax*(1,26) < 1) nor for the interaction between target side and cue type (*Fmax*(1,26) = 1.50 (critical *Fmax* = ±5.98), *p* = 0.24).

Based on the second test, the stochastic model fit better than any other model so analysis was conducted on the fitted parameter values of the three-parameter stochastic model. The three-parameter model was used because the model had a slightly better AICc value when the bias parameter (μ) was included (without μ: *M* = 106.56; with μ: *M* = 106.55). After fitting the models to each participants' data separated by trial condition and statistical testing, the only significant effect was for the bias parameter (μ) in that there was a significant systematic difference in the target's perceived orientation when they were located on right then the left (*Fmax*(1,26) = 16.90 (critical *Fmax* = ±6.81), *p* < 0.001). Notably, this is the same effect found in the bias parameter (μ) of the standard mixture model. Their similarity can be seen in Figure 3.3C showing the individual and mean bias parameter values for left and right targets.

ERP Analysis

The three-way interaction was not significant (critical *Fmax*(1,26) = +/-13.44), nor the hemisphere x cue type interaction (critical *Fmax*(1,26) = +/-13.39) and the cue type x target side interaction (critical *Fmax*(1,26) = +/-12.21). The hemisphere x target side interaction (critical *Fmax*(1,26) = +/-13.41) was significant for the CNV-2 (-500-0 ms), P1 (80-140 ms), P2 (200-300 ms), and P3 (300-500 ms) components. The significant interaction for the CNV-2 was in the occipital electrodes. Pairwise comparisons showed that this was mostly between the O1 and O2 when targets were going to appear on the right (O2 had a more negative voltage deflection). The

P1 was significant in the F3-F4 pair though none of pairwise comparisons were significant. The O1-O2 pair also showed a significant P1 interaction that can be seen in Figure 3.4A. The P2 significant interaction was seen in the occipital, parietooccipital, the two most lateral parietal electrodes and both centroparietal electrode pairs. However, as can be seen in Figure 3.4A, it is likely the P2 and much larger P3 overlapped so what is seen as a significant interaction in the P2 component is likely a significant interaction in the early part the P3. In fact, the differences in the P3 ERP were for the same electrodes as the P2 ERP interaction effects the exception being the centroparietal electrodes. The interaction in the P3 component was strongly driven by the difference between the left and right electrodes when targets were on the left and the difference between targets on the left and right in the electrodes located in the right hemisphere, though electrode P7 (left electrode) also showed a significant difference between left and right targets.

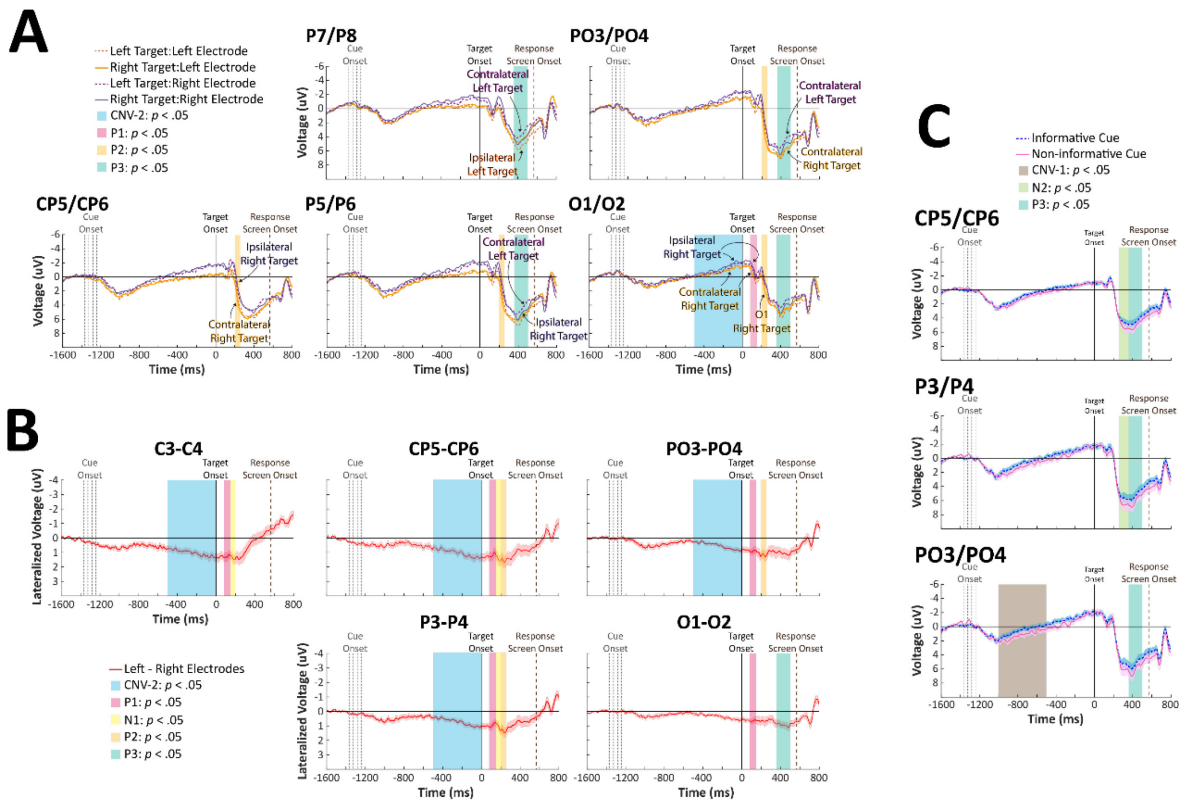

Figure 3.4. *Summary of ERP analysis results*

A) ERPs of left (orange lines) and right (purple lines) electrodes when targets were on the left (dashed lines) and right (solid lines). Labels indicate comparisons of interest. Note the waveforms do not contain $\pm SEM$ to aide visualization. **B)** ERPs of the difference between left and right electrodes. Light red shaded area around waveforms represents $\pm SEM$ of difference between left and right electrodes. **C)** ERPs from trial with informative (blue dashed line) and non-informative (pink solid line) cues. Light blue and pink shaded areas around waveforms represent $\pm SEM$ of the informative cues and non-informative ERPs, respectively. In all plots, time period shaded in brown and blue indicates significant effect prior to target onset at -1000 to -500 ms (CNV-1) and -500-0 ms (CNV-2), respectively. Rose shaded time period indicates significant effect at 80-140 ms (P1) post-target. Yellow shaded time period indicates significant effect at 140-200 ms (N1) post-target. Orange shaded time period indicates significant effect at 200-255 ms (P2) post-target. Yellow-green shaded time period indicates significant effect at 255-360 ms (N2) post-target. Turquoise

shaded time period indicates significant effect at 300-500 ms (P3) post-target. All ERPs are aligned to target onset.

With regards to the main effects, while target side was not significant (critical *Fmax*(1,26) = +/-12.72), both hemisphere and cue type were statistically significant (critical *Fmax*(1,26) = +/-12.58 and critical *Fmax*(1,26) = +/-14.42, respectively). As can be seen in Figure 3.4B, the main effect of hemisphere was largest during the CNV-2 component with the right electrodes having a more negative deflection than the left electrodes. This difference was seen across all central, centroparietal, parietal, and parietooccipital electrodes. The more medial of the frontocentral electrode pairs also had a significant difference between left and right electrodes at the CNV-2. The P1 and N1 (140-200 ms) ERP components were also significantly different between the left and right central, centroparietal, and medial parietal electrodes. In addition, the P1 was significantly different between the occipital and parietooccipital left and right electrodes. The P2 component was also significantly different between the left and right parietooccipital, medial parietal, and both centroparietal electrodes. All three early ERP components showed greater negativity in the right hemisphere than the left. Finally, the P3 ERP component was significantly different between left and right electrodes at the occipital, medial frontocentral, and medial frontal electrodes. While the occipital electrode had the same trend as the earlier ERP components in that the right electrode, O2, was less positive (*i.e.,* more negative) than the left electrode, O1, the frontocentral and frontal electrodes were the opposite with the right electrodes, F4 and FC2, more positive than the left electrodes, F3 and FC1. The increasing negativity starting at around 400 ms post-target until response screen onset can likely be attributed to the SPCN (sustained posterior contralateral negativity) which is thought to reflect neural activity associated with retention in visual short-term memory (Jolicœur, Brisson and

Robitaille, 2008) or the LPN (lateralized readiness potential) for the central and frontal electrodes (Woodman, 2010).

With regards to the cue type main effect, the parietooccipital electrode pairs had a CNV-1 (-1000 to -500 ms) that showed a more negative voltage deflection (*i.e.,* closer to baseline) when the cues were informative compared to non-informative. The voltage of the N2 (255-360 ms) component was more positive in the trials with a non-informative cue than informative (Figure 3.4C) and this difference was in the pair of central electrodes, both pairs of centroparietal electrodes and the more medial pair of parietal electrodes. However, the N2 likely overlaps with the much larger positive P3 component though the N2 and P3 components are more attenuated for informative cues than non-informative suggesting that the N2 is larger for informative cues resulting in an overall less positive deflection in the P3 ERP. The P3 ERP showed significant differences or near significant differences in some of the same electrodes as the N2 except for the more medial pair of centroparietal electrodes showing no significant effect in the P3. In addition, the parietooccipital pair also had a significant difference in the P3 voltage with a less positive P3 in the informative cued condition compared to the non-informative cued.

The analysis of the -1000 ms time period prior to target onset yielded a significant interaction between hemisphere and trial type (critical $Fmax(2,52) = +/-11.34$) at electrode pairs O2/O1, PO4/PO3, and P8/P7 (Figure 3.5A and Figure 3.5B). The time range for O2/O1 was between -250 to -90 ms pre-target which pairwise comparisons indicate the interaction being mostly due to the relative decrease in mean voltage of the right hemisphere compared to the left, especially when cued towards the right hemifield or when the cue was non-informative. PO4/PO3 electrode pair showed a significant interaction between -190 to -150 ms pre-target also mostly due to a large negativity in the right electrode for cues towards the right and non-

informative cues except there was no significant difference between being cued towards the left (contralaterally) compared to right (ipsilaterally) in the right electrode. The P8/P7 electrodes showed a significant interaction between -660 and -620 ms with cued right showing a large decrease in the right electrode and an increase in the left electrode. The left electrode also remained close to the fixation baseline when cued to the left. Finally, the P8/P7 electrodes had a significant interaction effect between -330 to -90 ms pre-target. The pairwise comparisons indicate that the right electrode significantly decreased in voltage relative to fixation when cued to the right and when the cue was non-informative. Being cued to the left yielded no significant difference between the right and left electrodes. In fact, the left electrode, P7, showed a small amount of significance in the difference between cue left and cue right trials at both significant time ranges.

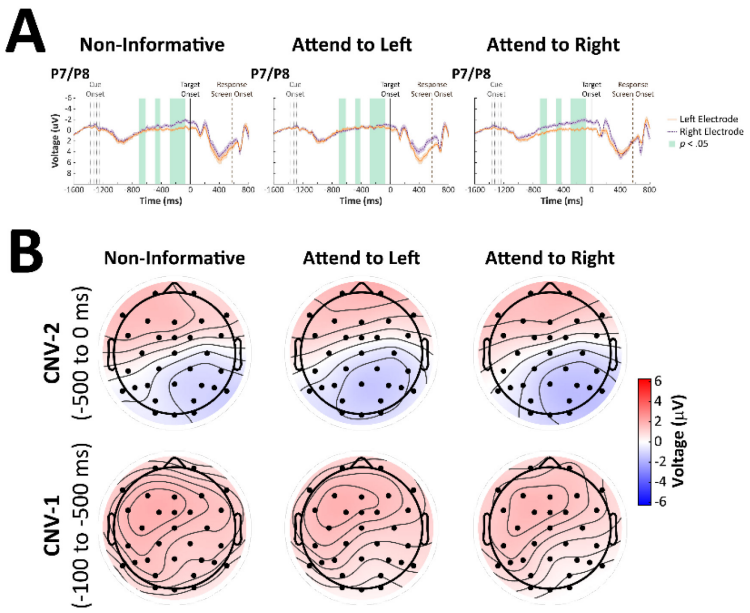

Figure 3.5. *ERP analysis of the activity prior to target onset*

A) ERPs at P7 and P8 of pre-target activity when the cue was non-informative (*left*), and when the cue was

informative indicating the target will appear on the left (*middle*) and right (*right*). Solid orange line is the ERP of the left electrode and dashed purple is the ERP of the right electrode. Time points in green indicate a significant hemisphere x trial type interaction. Analysis did not include time points after the target onset. Light orange and light green shaded areas around waveforms represent ±*SEM* of mean activity at the left electrode and right electrode, respectively. All ERPs are aligned to target onset. **B)** Topographic plots of the voltage distributions during the CNV-1 *(bottom)* and the CNV-2 *(top)* in trials with non-informative cue *(left),* cues to the left *(middle*) and cues to the right (*right*).

The hemisphere comparison was found to be significant between -1000 and -900 ms relative to target onset between the electrodes CP2 and CP1 and C4 and C3. After that, the most medial parietal electrode and all the centroparietal and central electrodes differed between the left and right hemisphere starting at around -400 ms until target onset. The two most lateral parietal electrodes and the parietooccipital electrodes had the same significant difference starting at around -170 ms until target onset. The occipital electrodes showed a small amount of significance at -120 ms for about 100 ms. The only significant main effect for trial type was at the P8/P7 electrode pair around -910 ms pre-target where the cued right trials showed a larger decrease from fixation compared to the cued left and non-informative cued trials.

The analysis on contralateral minus ipsilateral waveforms yielded no significant interaction between cue type and target side nor a significant main effect for cue type (critical *Fmax*(1,26) = +/-13.45 and critical *Fmax*(1,26) = +/-13.67, respectively). As can be seen in Figure 3.6B significant main effect for target side was found in the CNV-2, P1, N1, P2, and P3

ERP components (critical *Fmax*(1,26) = +/-12.21). The difference between contralateral and ipsilateral electrodes relative to the right target was more positive than the left target during the CNV-2 at the parietooccipital area, medial and lateral parietal and centroparietal areas, central area, and most lateral frontocentral and frontal areas. The trend for the waveform difference to be more positive for right targets continued into the P1, N1, and P2 ERPs. This difference was observed between the most medial parietal electrodes, both centroparietal electrode pairs, and central electrodes across all three ERP components. The parietooccipital electrodes had the significant effect in the P1 and P2 while the occipital electrodes were in the P1. The occipital electrodes in the P3 also showed the same difference with right targets having a more negative difference waveform than the left. However, the medial frontocentral and frontal electrodes showed the reverse in the P3 component with the difference wave being more positive for right targets than left.

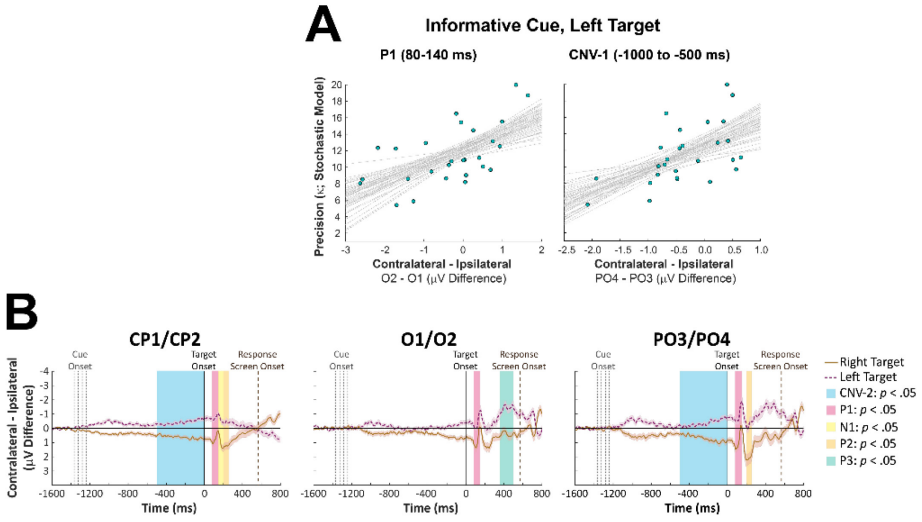

Figure 3.6. *Summary of contralateral minus ipsilateral difference waveforms analysis*

A) Scatterplots of the relationship between ERP contralateral – ipsilateral difference waveforms and the precision (κ) parameter from the stochastic model when cues were informative, and the target was on

the left. Gray lines are bootstrapped least-squares correlation lines fit to 1000 bootstrap samples. **B**) ERPs of the contralateral – ipsilateral difference waves from trials with right targets (brown solid line) and left targets (purple dashed line). Light brown and purple shaded areas around waveforms represent $\pm SEM$ of the right and left difference waves, respectively. In all plots, time period shaded in blue indicates significant effect prior to target onset at -500-0 ms (CNV-2). Rose shaded time period indicates significant effect at 80-140 ms (P1) post-target. Yellow shaded time period indicates significant effect at 140-200 ms (N1) post-target. Orange shaded time period indicates significant effect at 200-255 ms (P2) post-target. Turquoise shaded time period indicates significant effect at 300-500 ms (P3) post-target. All ERPs are aligned to target onset.

Spearman rank correlations yielded a significant relationship between the contralateral minus ipsilateral difference in mean voltage of the CNV-1 and P1 at the electrode pair PO4/PO3 and the P1 ERP at the electrode pairs O2/O1 and P4/P3 and the fitted parameter values precision (κ) from the stochastic model for informative cued left targets (Figure 3.6A). All the correlations were positive indicating that precision (κ) increased as the difference between the contralateral and ipsilateral electrodes shifted from negative to positive when there was an informative cue about a left target. No other significant correlations were found.

Periodic and Aperiodic Components

The aperiodic offset and exponent showed no significant main effects (mean critical *Fmax*(1,26) = +/-14.44 and mean critical *Fmax*(1,26) = +/-14.60, respectively). The offset also showed no significant three-way interaction (critical *Fmax*(1,26) = +/-14.92) nor a significant interaction for hemisphere x target side (critical *Fmax*(1,26) = +/-14.98) and cue type x target side (critical *Fmax*(1,26) = +/-14.81). The aperiodic offset had a significant interaction between

hemisphere and cue type at the electrode pair P8/P7 during the post time period (critical *Fmax*(1,26) = +/-15.03). Pairwise comparisons indicate that the right electrode had a significantly larger offset relative to fixation when the cue was non-informative (*M* = 0.36, *SD* = 0.20) than informative (*M* = 0.21, *SD* = 0.20) as well as significantly larger than the left electrode when the cue was non-informative (*M* = 0.23, *SD* = 0.12). The aperiodic exponent had no significant interaction between hemisphere and target side and cue type (critical *Fmax*(1,26) = +/-15.16) and target side (critical *Fmax*(1,26) = +/-14.31). There was a significant three-way interaction (critical *Fmax*(1,26) = +/-14.92) and a significant two-way interaction between hemisphere and cue type (critical *Fmax*(1,26) = +/-14.97), both in the post time window. Like the offset, the aperiodic exponent had the hemisphere x cue type interaction at the electrode pair P8/P7 with the non-informative cue generating a larger exponent in the right electrode (*M* = 0.29, *SD* = 0.15) than the left (*M* = 0.20, *SD* = 0.11) and larger than the right electrode when the cue was informative (*M* = 0.18, *SD* = 0.16). As can be seen in Figure 3.7A, a pairwise comparison of the three-way interaction found that significant differences were only for left targets where the non-informative cued trials had an increased exponent compared to informative cued trials in the right electrode and the reverse in the left electrode. The non-informative and informative cued trials in the right electrode also significantly differed from the values in the left electrode.

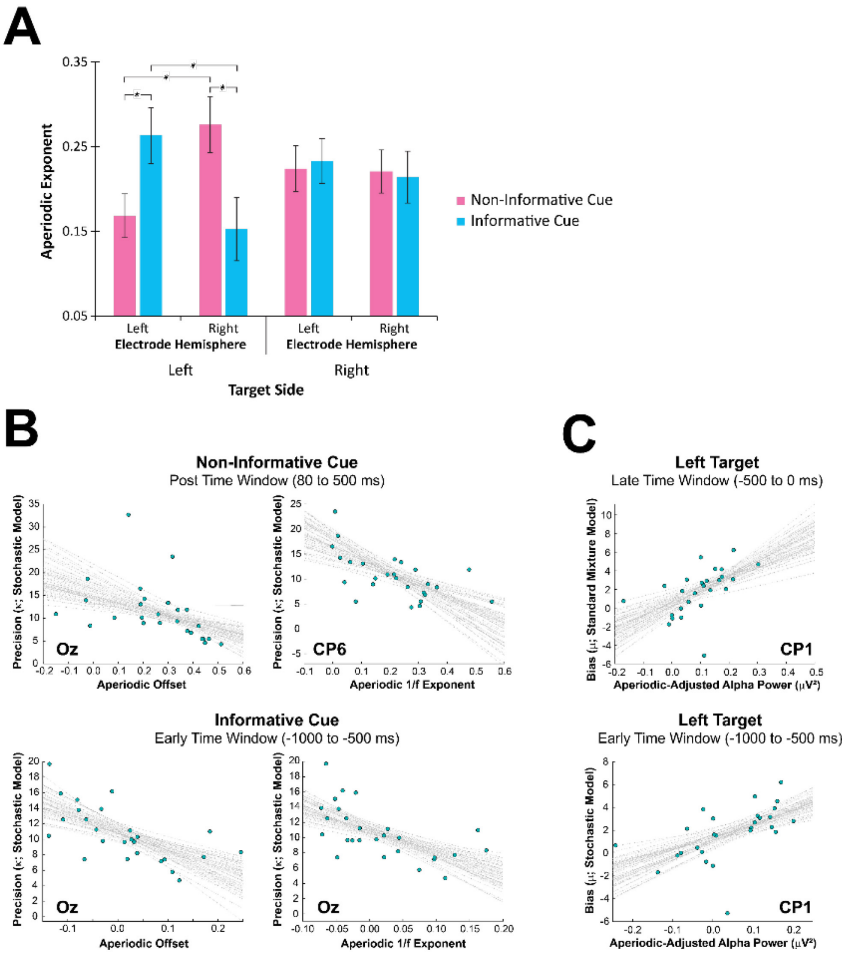

Figure 3.7. *Summary of analysis on 1/f aperiodic activity*

A) Plot of the three-way interaction between electrode hemisphere, target side and cue type for the 1/f aperiodic exponent values in the post time window (80-500 ms post-target) relative to fixation at electrodes P5 and P6. Error bars are the ±*SEM.* Stars indicate significant pairwise comparisons. **B)** Scatterplots of the relationship between the aperiodic activity measures offset (*left*) and 1/f exponent (*right*) and the precision (κ) parameter from the stochastic model. *Top*, aperiodic activity measured during the post-target time window (80-500 ms) when cues were non-informative. *Bottom*, aperiodic activity measured during the pre-target early time window (-1000 to -500 ms) when cues were informative. Gray lines are bootstrapped least-squares correlation lines fit to 1000 bootstrap

samples. **C)** Scatterplots of the relationship between the aperiodic-adjusted power of the peak frequencies in the alpha band in trials with left targets (*top*) during the pre-target late time window (-500 to 0 ms) and the bias (μ) parameter from the standard mixture model and (*bottom*) during the pre-target early time window (-1000 to -500 ms) and the bias (μ) parameter from the stochastic model. Gray lines are bootstrapped least-squares correlation lines fit to 1000 bootstrap samples.

The power above the aperiodic component was measured at the median peak frequencies within the alpha (8-14 Hz) and low beta (15-22 Hz) frequency ranges. There were no significant interactions or main effects for low beta power (mean critical $Fmax(1,26) = +/-14.81$). Alpha power showed a significant main effect for electrode hemisphere at the electrode pair P7/P8 in the post-target time window (critical $Fmax(1,26) = \pm 14.08$). The right electrode, P8, had a greater decrease in power than the left electrode, P7, relative to fixation (electrode P8: $M = -0.12$, $SD = 0.09$; electrode P7: $M = -0.07$, $SD = 0.09$). No other significant interactions or main effects were found (mean critical $Fmax(1,26) = +/-14.93$).

Spearman rank correlations yielded no significant relationships between the periodic and aperiodic measures and the parameter values from both models when separated by cue type and trial side. When trials were collapsed across target side, a significant relationship was found between peak alpha power and the bias (μ) parameters from both models at electrode CP1 (Figure 3.7C). This association was significant at the early and late time periods for the standard mixture model parameter ($\rho(25) = 0.70$, $p < 0.05$; and ($\rho(25) = 0.67$, $p < 0.05$, respectively) and just the early time period for the stochastic model parameter ($\rho(25) = 0.68$, $p < 0.05$). As can be seen in Figure 3.7B, when trials were collapsed across cue type, a significant relationship was

found between the aperiodic exponent and the precision parameter (κ) from the stochastic model at electrode Oz during the early period of the cue-target interval for informative cues ($\rho(25) = -0.65$, $p < 0.05$). It was also found that κ and the aperiodic exponent at Oz and CP6 for non-informative cues except it was during the post-target time period ($\rho(25) = -0.65$, $p < 0.05$; and ($\rho(25) = -0.66$, $p < 0.05$, respectively). A similar relationship was found between κ and the aperiodic offset in electrode Oz when the cue was informative and it was the early part time window ($\rho(25) = -0.68$, $p < 0.05$), and when the cue was non-informative during the post-target time window ($\rho(25) = -0.67$, $p < 0.05$). No other significant correlations were found.

EEG Power Analysis

In addition to the periodic and aperiodic component analysis, power relative to fixation was analyzed in the following four frequency bands: 1-3 Hz, 4-7 Hz, 8-14 Hz, and 15-22 Hz. This was done so that the slower frequencies could be investigated, and the faster frequencies could be tested on a more precise time scale. The downside is that it is unknown whether activity in these bands represent oscillatory activity or are mostly comprised of aperiodic activity found across all frequencies.

None of the frequency bands showed a significant three-way interaction (critical *Fmax*(1,26) = +/-26.17 (delta, 1-3 Hz), +/-25.61 (theta, 4-7 Hz), +/-25.62 (alpha, 8-14 Hz), and +/-25.20 (low beta, 15-22 Hz)), hemisphere x cue type interaction (critical *Fmax*(1,26) = +/-26.08 (delta, 1-3 Hz), +/-24.87 (theta, 4-7 Hz), +/-24.84 (alpha, 8-14 Hz), and +/-25.78 (low beta, 15-22 Hz)), nor a cue type x target side interaction (critical *Fmax*(1,26) = +/-23.09 (delta, 1-3 Hz), +/-22.94 (theta, 4-7 Hz), +/-23.37 (alpha, 8-14 Hz), and +/-23.01 (low beta, 15-22 Hz)). Cue type (critical *Fmax*(1,26) = +/-23.12 (delta, 1-3 Hz), +/-23.84 (theta, 4-7 Hz), +/-23.47 (alpha, 8-14 Hz), and +/-22.76 (low beta, 15-22 Hz)) and target side (critical *Fmax*(1,26) = +/-

23.92 (delta, 1-3 Hz), +/-23.06 (theta, 4-7 Hz), +/-21.38 (alpha, 8-14 Hz), and +/-22.94 (low beta, 15-22 Hz)) main effects were also not significant in any frequency band.

Two frequency bands had a significant interaction between hemisphere and target side (critical *Fmax*(1,26) = +/-25.36 (delta, 1-3 Hz) and +/-24.62 (alpha, 8-14 Hz)) and one had a significant main effect for hemisphere (critical *Fmax*(1,26) = +/-23.65 (low beta, 15-22 Hz)). The significant interaction, seen in Figure 3.8A for the 1-3 Hz frequency band started close to 100 ms and had a duration of little more than 100 ms at the most medial frontocentral electrode pair. Pairwise comparisons found that the interaction in those electrodes was mostly driven by the difference between right and left electrodes for targets located on the left.

The significant interaction between hemisphere and target side in the 8-14 Hz frequency band in the posterior area of the head. The pairwise comparisons found differences primarily between left and right targets in the left occipital electrode, O1, and between left and right electrodes (O1 and O2) for targets located on the left (see Figure 3.8A). In the left occipital electrode O1, 8-14 power relative to fixation increased for ipsilateral targets (*i.e.,* left targets) and decreased for contralateral targets (*i.e.,* right targets). For targets on the left, the ipsilateral electrode O1 had a significant increase in power relative to fixation while the contralateral electrode O2 had a significant decrease in power relative to fixation.

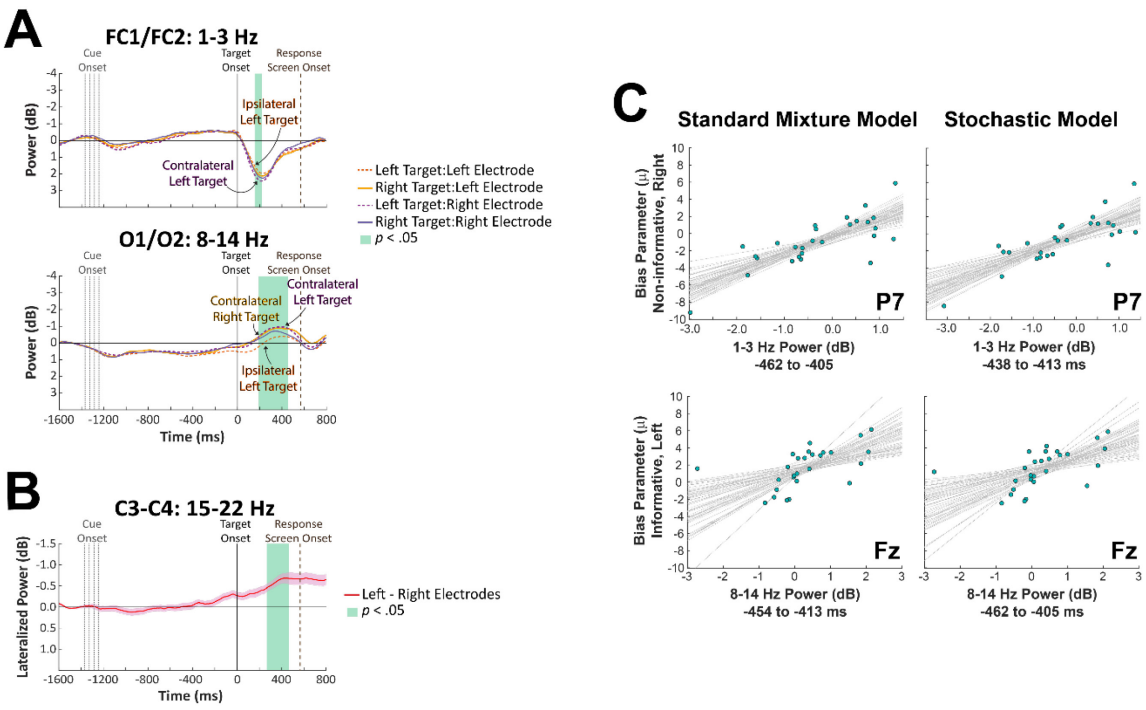

Figure 3.8. *Summary of results from analyzing power within each pre-defined frequency band*

A) Plots are the mean power within the 1-3 Hz and 8-14 Hz frequency bands separated by electrode hemisphere and target location. Left electrodes are orange lines and right electrodes are purple lines. Left targets are the left are dashed lines and right targets are the solid lines. Labels indicate comparisons of interest. The $\pm SEM$ was not included to aide visualization. Time points in green indicate a significant effect. **B**) Plot of the left electrode minus right electrode mean power within 15-22 Hz frequency band. Light red shaded areas around waveform represent $\pm SEM$ of difference between left and right electrodes Negative value indicates the left electrode is more negative than the right. Time points in green indicate a significant effect. **C)** Scatterplots are bootstrap Spearman's rho (r_s) correlation coefficients of mean power across each statistically significant time range and frequency band and bias (μ) from the standard mixture model (*left*) and stochastic model (*right*). Gray lines are bootstrapped least-squares correlation lines fit to 1000 bootstrap samples.

The main effect of electrode hemisphere was observed in the 1-3 Hz frequency band at the medial frontocentral electrodes during the post-target time period at around 120 ms until 250 ms where the right electrode FC2 had a greater increase in power relative to fixation (M = 2.02, SD = 1.21) than the left electrode FC1 (M = 1.73, SD = 1.13). The 8-14 Hz frequency band showed a brief significant difference (about 50 ms) with the left centroparietal electrode CP1 had a greater decrease in power relative to fixation (M = -0.29, SD = 1.38) than the right centroparietal electrode CP2 (M = -0.02, SD = 1.37) at around 150 ms before response screen onset (*i.e.,* 450 ms post-target onset). Finally, the 15-22 Hz frequency range had the most widespread significant difference between electrodes. In the central electrode pair, the left electrode showed a greater decrease in power relative to fixation than the right electrode. The effect started at around 270 ms and ended at about 470 ms after target onset (see Figure 3.8B).

The significance test between hemisphere side and trial type for just the -1000 ms prior to target onset yielded no significant effects in any of the frequency bands: hemisphere x trial type interaction mean critical $Fmax(2,52)$ = +/-12.24, hemisphere main effect mean critical $Fmax(1,26)$ = +/-22.61, and trial type main effect mean critical $Fmax(2,52)$ = +/-11.37.

The significance test on the contralateral minus ipsilateral electrodes relative to the side the target is presented only yielded a significant main effect for target side in the 15-22 Hz frequency band (critical $Fmax(2,52)$ = +/-11.37). This effect was observed at the central electrode pair and started at around 295 ms until 452 ms post-target with the difference in power being negative for left targets (M = -0.67, SD = 0.63) and positive for right targets (M = 0.46, SD = 0.59). No other significant interactions or main effects were found. The correlations between model parameters and the difference between contralateral and ipsilateral electrodes yielded no significant relationships.

Significant correlations between frequency band and model parameters are shown in Figure 3.8C. The power at each frequency band was averaged across significant time points. As can be seen, the bias parameter μ from the standard mixture model and stochastic model was positively correlated with 8-14 Hz power at electrode Fz in the informative cued trials with a left target. Although their time range differed slightly, the bias parameters of both models were correlated with the 8-14 Hz power between -450 ms and -400 ms prior to target onset. The slowest frequency band, 1-3 Hz, also positively correlated with the bias parameter μ from the standard mixture model and stochastic model in the same time range though the electrode was P7 and the trials were non-informative cued with right targets though this effect might be more related to all right targets and just did not reach significance for informative cued trials since the bias parameter was a lot more uniform in the informative cued condition than the non-informative cued (Figure 3.8C). The last correlation was between 4-7 Hz power at electrode C3 and the response variability parameter (σ) from the standard mixture model for trials with non-informative cues and right targets. The correlation was positive in that increasing 4-7 Hz power was associated with increasing response variability (not shown). It should be noted that this correlation was at one time point (468 ms post-target), so any interpretation needs to be done with caution.

EEG Phase Analysis

To examine the relationship between the magnitude of response errors, the probability of a guess response and the distribution of phase values, we used the wITPCz. As can be seen in Figure 3.9, phase during the informative cued trials when targets were located on the left was primarily modulated by the magnitude of response errors in the 1-4 Hz frequency range in the left parietal and centroparietal electrodes P3, P5 and CP5 at around 400 ms until the end of the

analysis time window at 500 ms post-target. It is unknown whether duration of the phase modulation extends beyond 500 ms. Electrode P8 had a brief 35 ms reach significance from 120-155 ms for informative cued trials with right targets at 9 Hz (not shown), but it is difficult to interpret phase modulation lasting such a short time period. It may be that analysis is too conservative to detect the entire duration of the effect.

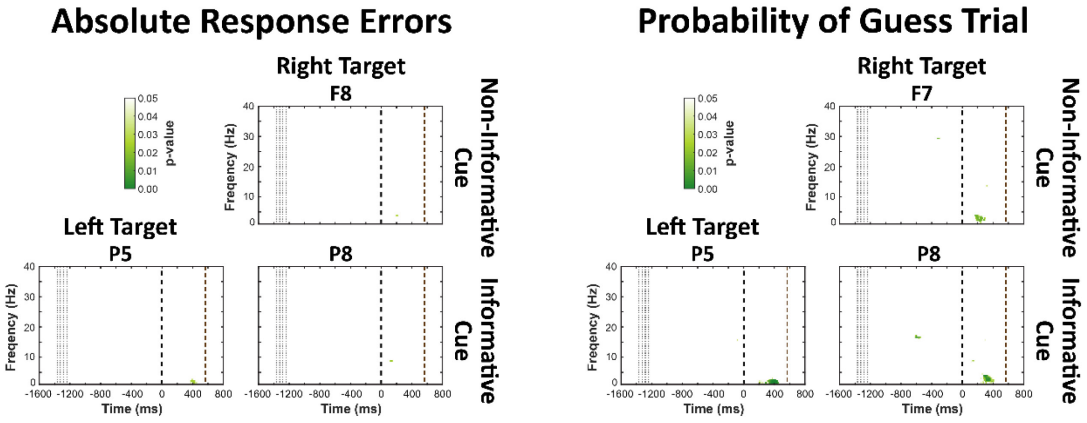

Figure 3.9. *Summary of phase analysis results*

Time-frequency plots of analysis relating single-trial phase activity and response errors *(left*) and probability of the trial being from the guess distribution *(right*). Significant *p*-values indicating that the normalized distance of the observed wITPC (*i.e*., wITPCz) is significantly different from the distribution of null hypothesis wITPC values. This measure represents the relationship between the distribution of phase angles and the magnitude of response error or guess probability on each trial. Plots are only of selected electrodes. Time-frequency points with *p*-values at or above .05 were set to 1.

The relationship between the probability a response is from the guess distribution (*i.e.,* uniform distribution) and the distribution of phase, not surprisingly, followed a similar trend as the magnitude of response errors. As can be seen in Figure 3.9, phase during the informative cued trials when targets were located on the left was modulated by the probability of a guess

response in the 1-4 Hz frequency range in the left parietal electrode P7 in addition to the P3, P5, and CP5 found with phase modulated by response error magnitudes. However, only P3 and P5 had effects extending beyond 400 ms post-target. In addition, the effect seen in P7 was 200-400 ms post-target rather than starting around 400 ms like the other electrodes. In trials with informative cues and right targets, P7 and P8 showed a significant relationship between phase values and guess response probabilities. Unlike for left targets, P7 showed an effect starting after 400 ms until the end of the analysis time window when targets were presented on the right. Electrode P8 showed a significant effect almost -600 ms pre-target at 17 Hz frequency. Then around 200 ms after target onset, phase modulation was seen in the 1-5 Hz frequency range. There was also a brief 120-155 ms time period at 9 Hz with a significant *p*-value, but this too should be interpreted with caution though it is notable this is the same time and frequency seen at P8 for phase modulation by response error magnitude. Finally, for trials with non-informative cues and targets presented on the right, electrode F7 showed significant effects between 150-300 ms post-target in the 2-5 Hz frequency range and electrode FC6 had a similar effect except just between 150 and 200 ms in the same frequency range. For F7, there was also a brief 40 ms window reaching significance starting at around -340 ms pre-target at 30 Hz and again for 20 ms at 300 ms post-target for 14 Hz phase activity. However, these too are difficult to interpret since it is unclear if these are real effects or noise in EEG phase data or behavioral measure.

Phase modulation by response error magnitude and guess trial probability only occurred in the frontal and frontocentral electrodes when the cue was non-informative while informative cues resulted in phase modulation in the parietal and centroparietal electrodes. The frontal phase modulation in non-informative cued trials also tended to occur earlier in the post-target time period and was more strongly modulated by the probability of a guess trial than the magnitude of

response errors. This suggests that there is a relationship between the 2-5 Hz frequency phase values and the detectability of the target likely by mediating attention demands and decision making (Başar *et al.*, 1999; Schürmann *et al.*, 2001; Güntekin and Başar, 2016). Phase modulation during informative cued trials was stronger and more prevalent in the ipsilateral electrodes relative to target location. Considering the parietal location and late post-target time period, the relationship between 1-4 Hz phase values and performance measures are likely indicative of a slower inhibitory process that improves perceptual responses.

3.1 DISCUSSION

Model Fits and Parameter Values

Since perceiving the visual stimuli usually precedes remembering those same stimuli, some of the assumptions built into the visual working memory models are applicable to visual perception. Namely, the assumption that there are a set of targets that are remembered and a set of targets that are not remembered can translate to the current task as a set of targets that are seen, and another set of targets not seen. A natural extension of this assumption is that endogenous, that is, voluntary and goal-driven, attention improves task performance, thereby affecting which targets are seen and which targets are not seen. For this reason, the first question addressed was what working memory model and their associated assumption could be extended to the current study's cued orientation perception task?

Surprisingly, we found that goodness-of-fit was always worse when there were informative cues directing attention to the location the target will appear than non-informative cues that provided no information about the target prior to its presentation. To see if this was due to informative cues eliminating guesses, we compared the goodness-of-fit between models that included and did not include a guess rate parameter. The stochastic model (Bays, 2014;

Schneegans, Taylor and Bays, 2020) was also included as it has been shown to account for visual orientation perception (Bays, 2016) and the use of predictive cues (Bays, 2014). We found that the models that included a guess rate parameter performed better than the models that did not, indicating the existence of guessing in the informative cued trials. In addition, we found that the stochastic model fit the data much better than any other model.

The stochastic model is based on the neural population coding model (Pouget, Dayan and Zemel, 2000) though it is a highly idealized version that assumes the neural population has identical Gaussian tuning functions, no baseline activity, and no interneuronal correlations (Bays, 2016). Even as a simplified version of neural population coding, the stochastic model has been successful at explaining discrepancies between previous working memory models and empirical data (Schneegans, Taylor and Bays, 2020; Taylor and Bays, 2020). However, despite it fitting the data better than the previous models, it still showed a significantly worse fit to trials with informative cues compared to trials with non-informative cues. Perhaps a less idealistic neural population, one with noise in its baseline and correlations between neurons, could better account for the effects of endogenous attention initiated, presumably, by the informative cues. Another possibility that might improve the model's performance on informative cued trials is to include the *attentional gain factor* (α) the author used in one of their first applications of the model though it was used in an experiment that had arrays of at least two items (Bays, 2014).

Although having the best goodness-of-fit values, the fitted parameters κ and γ of the stochastic model showed no differences between trial conditions. This can be taken in one of two ways. First, there is too much noise in the data for the detection of experimental effects. While possible, this first explanation is unlikely since most other measures had detected differences due to the experimental manipulation. Second, the behavior or cognitive state the parameters

represent does not vary or varies unexpectedly as a function of the experimental manipulation. Although more likely, the second explanation is difficult to judge because the stochastic model is an abstract application of neural theory without the grounding in cognitive models that the other working memory models have. Descriptive statistics also supports the latter explanation (see Figure 3.10), though this cannot be adequately investigated since the experimental design was not created to test that hypothesis.

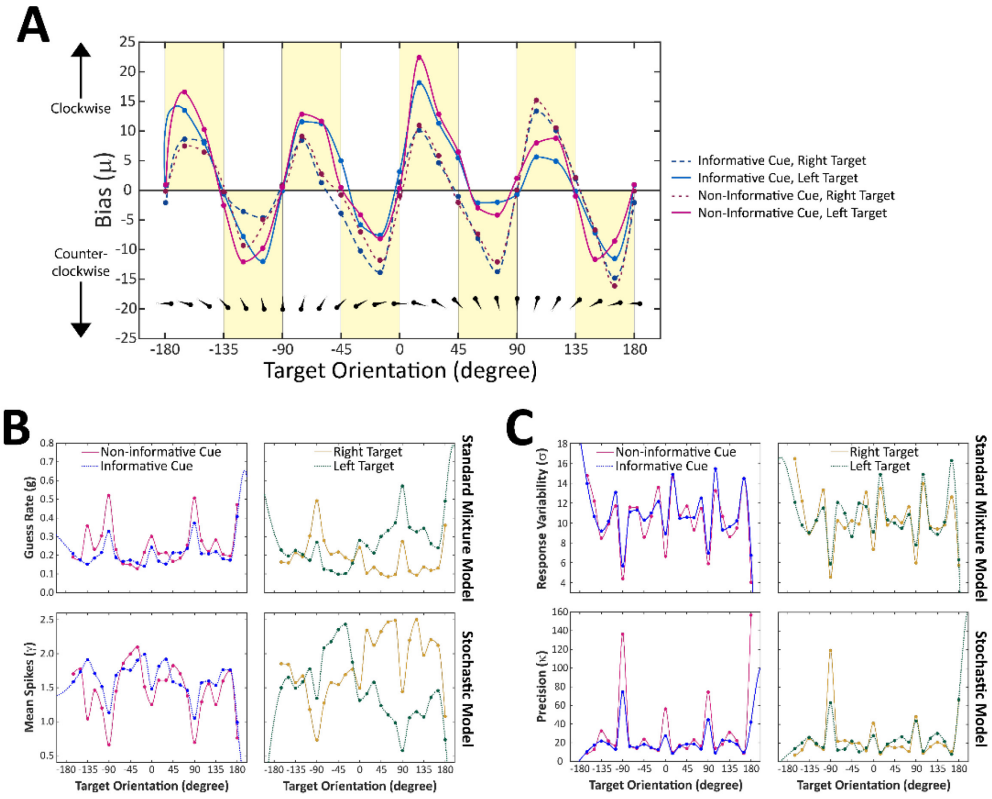

Figure 3.10. *Fitted parameter values by target orientation*

Response errors have been collapsed across participants, standard mixture model and stochastic model were fit to the data from each target orientation separately. All lines are calculated with a shape-preserving interpolation equation and meant to aid visualization. **A)** Plot shows the fitted bias (μ) parameter to the data from each trial condition separated by the orientation of the target on that trial. Solid lines plot biases for left targets and dashed lines plot biases for right targets. Blue lines are biases on informative cued

trials while magenta are biases on non-informative cued trials. Bias parameters from both models were averaged together to illustrate the general trend, which is that most data fall in the shaded regions, indicating response biases away from the closest cardinal axis. The magnitude and rotation direction (*i.e.,* clockwise or counterclockwise) of the perceptual bias varied as a function of the target's hemifield location and orientation. Above the x-axis are images of the targets oriented by the values of the x-axis. **B)** Plots are the fitted guess rate (*g*) parameters from the standard mixture model (*top*) and mean spikes (γ) from the stochastic model (*bottom*) by cue type (*left column*) and target side (*right column*) for each target orientation. **C)** Plots are the response variability (σ) parameters from the standard mixture model (*top*) and precision (κ) from the stochastic model (*bottom*) by cue type (*left column*) and target side (*right column*) for each target orientation.

While the parameters from the standard mixture model and stochastic model might have some surface similarities, their derivations are very different and thus, the concepts they represent are very different. For example, the stochastic model has no parameter comparable to the guess rate parameter. The closest is the γ parameter which describes the mean number of spikes generated in fixed decoding interval and has been interpreted as an indicator of the "strength of evidence" for the true stimulus feature. When γ is 0, then it reasonable to believe the participant will be guessing since there is absolutely no evidence for the true stimulus feature. This is not the same as the guess rate parameter which represents a uniform distribution in the standard mixture model.

The bias parameter in the standard mixture model and stochastic model were significantly different when targets were located on the left compared to the right. On average, participants reported the target orientation as being more clockwise than its true orientation when it was

located on the left, and more counterclockwise when the target was located on the right. While we expected responses to be systematically biased away from the cardinal directions toward the oblique as reported by previous researchers (Taylor and Bays, 2018; Bae, 2021), the additional affects target location had on the parameters was not expected. Overall, response errors at each target orientation revealed a pronounced "oblique effect," with larger errors for oblique than cardinal orientations. Interestingly, guess rates and mean spikes showed the opposite with greater guessing and less certainty at the cardinal orientations than the oblique. The response precision as quantified by σ in the standard mixture model and κ in the stochastic model, replicated the finding by Bae (2021) that the cardinal locations were more precisely reported than the oblique. This effect did not seem to change with cue type and target location. It is notable that attention did not influence either model's parameter quantifying the quality of the orientation perceptual response (σ and κ). This implies that attention resulted in an increased likelihood of perceiving the target but did not alter the quality of the perception.

The bias away from cardinal orientation had been attributed to the anisotropic organization of orientation selective neurons in V1. Imaging and single-cell recording studies (Li, Peterson and Freeman, 2003; Huang *et al.*, 2006; Li *et al.*, 2015) have found that a larger proportion of the population are devoted to representing cardinal orientations and that such neurons are more narrowly tuned than obliquely-selective neurons (Taylor and Bays, 2018). However, while the cardinal orientations could be reproduced more accurately than the oblique as exemplified by bias values close to 0, increased response precision, and decreased variability, perceiving such targets was less likely or more difficult. Furthermore, this effect was amplified for targets oriented downward when they were located on the left and for targets oriented upward when they were located on the right. It is possible this is due to the right visual cortex having

more neurons tuned for downward orientations and the left visual cortex having more neurons tuned for upward orientations. This is difficult to determine though since the evidence for or against upward/downward orientation preferences in different hemispheres is sparse.

EEG Activity, Attention and Orientation Perception

Counter to previous reports, cueing spatial attention did not result in any detectable changes to the EEG activity in the contralateral posterior brain regions that process information from the upcoming relevant hemifield. Instead, there is an increasing negativity in the right occipital, parietal, and centroparietal brain areas in anticipation of target onset regardless of which hemifield the target will show up in (see Figure 3.5B). This sustained activity is comparable in time-course, waveform, and topography to the well-known contingent negative variation (CNV). The CNV appears when anticipating an incoming stimulus and is considered an indicator of attention to the task (Wright, Geffen and Geffen, 1995; Woodman, 2010; Baghdadi, Towhidkhah and Rajabi, 2021). Therefore, the enhanced CNV-like negativity in the current study, especially to informative cues, can be thought as an indicator of increased focused spatial attention.

The consistent negativity in the right hemisphere prior to target onset is also in accordance with previous research showing the bilateral control of attention by the right parietal cortex (Moos *et al.*, 2012). It has been proposed that the right hemisphere directs attention and transfers information in both visual hemifields, while the left hemisphere directs attention primarily for the right (Siman-Tov *et al.*, 2007). This leads to an overall asymmetry of visuospatial attention with the right visual hemifield having an advantage over the left due to a better bilateral representation in the parietal cortex. Because of this, we would expect participants to perform better when the target is on the right because the right hemifield has the

benefit of greater bilateral hemisphere engagement. Similarly, cues would have a greater impact on performance to left targets because left targets get the least attentional representation when the upcoming target location is unknown. It is analogous to why damage in the right parietal area leads to hemispatial neglect more often than similar damage in the left parietal area (Bartolomeo, 2006; Siman-Tov *et al.*, 2007).

As predicted, we found that the guess rate was lower when the cue was informative than non-informative, but only for targets presented in the left visual hemifield. Targets on the right always had a smaller guess rate than targets on the left regardless of whether there was an informative cue or not. Although there was little correspondence between those parameter values and brain activity measures, it is possible this could be due to the unexpected effects the target's orientation had on responses. However, there are too few trials per target orientation to test this statistically. On the other hand, while the model parameters response variability (σ) and precision (κ) showed no significant effects as a function of the experimental conditions, they did correlate with several measures of brain activity. For example, there were significant correlations between the stochastic model's precision (κ) and ERP contralateral minus ipsilateral difference waves when attention was cued toward the left (Figure 3.6A). The more the balance shifts towards contralateral (right) electrode voltage > ipsilateral (left) electrode voltage, the greater the precision of the response. This relationship was observed in the pre-target component CNV-1 and shortly after target onset in the P1 ERP component. Interestingly, the aperiodic exponent and offset also had a significant correlation with precision (κ) during the same time period as the CNV-1 when cues were informative and in the post-target time period when the cue was non-informative. It was found that the precision parameter increased as the 1/f exponent and broadband offset of the aperiodic activity decreased. A decrease in the aperiodic 1/f signal has

been attributed to a shift in the E:I balance towards excitation (Chini, Pfeffer and Hanganu-Opatz, 2021) which would lead to improved orientation perception. This is inline with a recent study that found selective attention in one sensory modality resulted in the reduction of the spectral exponent over the brain area typically associated with processing input in that modality (Waschke *et al.*, 2021). Furthermore, not only did we find that attention selectively reduced the EEG spectral aperiodic activity which coincided with a relative increase of excitatory neural activity in the posterior cortex, but we also show that this change in activity is associated with the improved quality of the target's representation by endogenous attentional processes when the cue is informative and exogenous, that is, automatic and stimulus-driven, attentional processes when the cue is non-informative. Notably, the 1/f aperiodic activity had a stronger association with attention modulation and task performance than alpha oscillations despite selective attention modulation and cortical excitability usually being attributed to alpha oscillations (Klimesch, Sauseng and Hanslmayr, 2007; Jensen and Mazaheri, 2010; Mathewson et al., 2011; Herring *et al.*, 2019; van Diepen, Foxe and Mazaheri, 2019).

While there was a complete absence of an interaction between hemisphere and cue type for power in the pre-defined frequency bands and aperiodic-adjusted power in the peak alpha and beta frequencies, the aperiodic 1/f activity showed significant effects. It seems that the significant interaction can be attributed to a large increase relative to fixation of the broadband offset and 1/f exponent in the right parietal electrode following target onset when the cue was non-informative. However, in the three-way interaction between electrode hemisphere, cue type, and target side, the exponent of the aperiodic 1/f activity only showed significant differences to left targets with the contralateral (right) electrode being significantly smaller than the ipsilateral (left) electrode when the cue was informative, and the contralateral (right) electrode being

significantly larger than ipsilateral (left) electrode when the cue was non-informative. So, while there was a large increase in the aperiodic activity in the right parietal area to non-informative cues, this was only significant for targets located on the left. Furthermore, the left electrode showed the same level of response to a target located on the left when the cue was non-informative as the right electrode showed to a left target when the cue was informative.

If a decrease in the aperiodic exponent reflects changes in E:I balance towards excitation, then the relatively equal decrease of the 1/f exponents in the right and left electrodes indicate that the increased excitation of the left parietal area to targets that appear in an unattended ipsilateral hemifield is equal to that of the right parietal area for targets that appear in an attended contralateral hemifield. In other words, the left parietal area does not seem to use an inhibitory mechanism to regulate its response when that upcoming target location is unknown. It remains in a high state of excitability until an upcoming target is known to appear in the ipsilateral visual hemifield after which the left parietal area shows the typical ipsilateral inhibition. It seems in our data that only the right parietal area shows an inhibitory response in anticipation of an unknown target's location though this difference is only detectable for targets in the left visual field. There are no significant changes in E:I balance of left and right parietal areas when targets appear in the right visual field regardless of having foreknowledge or not about the target's upcoming location.

This clear asymmetry in activity for targets in the left visual hemifield than the right is in line with the findings by Siman-Tov et al (2007) that both right and left parietal areas can mediate covert visuospatial attention to both visual hemifields (in contrast to attentional theories postulating only the right parietal cortex is capable of bilateral modulation (Kim *et al.*, 1999; Mesulam, 1999), but the right hemispheric dominance is the result of an asymmetric strength in

faciliatory connections that favor a right-to-left signal transfer between bilateral parietal areas thus the left electrode showing a continued state favoring excitation. They also postulate that this right hemisphere advantage reflects its dominance for attention processing and manifests as increased bilateral activation by left visual targets, but equal bilateral activation by right visual targets. As follows, the increase in the 1/f exponent of the right parietal electrode to non-informative cued left targets is likely due to an increase in top-down control of attentional responses. It had been shown that hyperpolarization through cathodal tDCS stimulation of the right parietal area improved attentional selection regardless of the stimuli's spatial position (Moos *et al.*, 2012) and neuroimaging studies have provided evidence for right hemispheric dominance of attentional networks predominantly associated with stimulus-driven control (Corbetta and Shulman, 2002; Pagnotta, Pascucci and Plomp, 2022).

The bias (μ) parameters from the standard mixture model and stochastic model were related to power in the 1-3 Hz and 8-14 Hz frequency bands (Figure 3.7C) as well as in the peak frequency of the alpha band (Figure 3.7C) prior to target onset. Overall, there seems to be a trend for power in the alpha frequency band prior to target onset modulating the degree to which responses were rotated too far clockwise from the target's actual orientation when targets were presented in the left visual hemifield. The response bias to right targets was also positively correlated to 1-3 Hz power at the left parietal electrode P7 so that less 1-3 Hz power was associated with responses having greater counterclockwise rotations away from the target's orientation. It is notable that increased power of both frequency bands have been linked to attentional and perceptual inhibitory processes (Harmony, 2013; Clayton, Yeung and Cohen Kadosh, 2018). While these correlations between the bias parameters and oscillatory power might hint at a mechanistic explanation for participants' biases to report orientation away from the closest cardinal axes,

there are not enough trials at each target orientation in the different trial conditions to statistically test this idea. The influence the target's orientation had on all the model parameter values is interesting and should be tested systemically. The effect of orientation on perception is well documented, but there is a gap between behavioral studies and single-unit recordings that future research can address.

References

Bae, G.-Y. (2021) 'Neural evidence for categorical biases in location and orientation representations in a working memory task', *NeuroImage*, 240, p. 118366. doi: https://doi.org/10.1016/j.neuroimage.2021.118366.

Baghdadi, G., Towhidkhah, F. and Rajabi, M. (2021) 'Chapter 2 - Anatomy and physiology of attention', in Baghdadi, G., Towhidkhah, F., and Rajabi, M. B. T.-N. M. of A. (eds) *Neurocognitive Mechanisms of Attention*. Academic Press, pp. 51–94. doi: https://doi.org/10.1016/B978-0-323-90935-8.00002-0.

Bartolomeo, P. (2006) 'A Parietofrontal Network for Spatial Awareness in the Right Hemisphere of the Human Brain', *Archives of Neurology*, 63(9), pp. 1238–1241. doi: 10.1001/archneur.63.9.1238.

Başar, E. *et al.* (1999) 'Are cognitive processes manifested in event-related gamma, alpha, theta and delta oscillations in the EEG?', *Neuroscience Letters*. Elsevier, 259(3), pp. 165–168. doi: 10.1016/S0304-3940(98)00934-3.

Başar, E. (2012) 'A review of alpha activity in integrative brain function: Fundamental physiology, sensory coding, cognition and pathology', *International Journal of Psychophysiology*, 86(1), pp. 1–24. doi: https://doi.org/10.1016/j.ijpsycho.2012.07.002.

Bays, P. M. (2014) 'Noise in Neural Populations Accounts for Errors in Working Memory', *The Journal of Neuroscience*, 34(10), pp. 3632–3645. doi: 10.1523/JNEUROSCI.3204-13.2014.

Bays, P. M. (2016) 'A signature of neural coding at human perceptual limits', *Journal of Vision*. Association for Research in Vision and Ophthalmology Inc., 16(11), p. Article 4. doi: 10.1167/16.11.4.

Bays, P. M., Catalao, R. F. G. and Husain, M. (2009) 'The precision of visual working memory is set by allocation of a shared resource', *Journal of Vision*. The Association for Research in Vision and Ophthalmology, 9(10), pp. 7–7. doi: 10.1167/9.10.7.

Benjamini, Y. and Yekutieli, D. (2001) 'The control of the false discovery rate in multiple testing under dependency', *Annals of Statistics*, 29(4), pp. 1165–1188. doi: 10.1214/aos/1013699998.

Berens, P. (2009) 'CircStat: a MATLAB toolbox for circular statistics', *Journal of Statistical Software*, 31(10), pp. 679–685. doi: 10.1016/j.amp.2012.05.023.

van den Berg, R. *et al.* (2012) 'Variability in encoding precision accounts for visual short-term memory limitations', *Proceedings of the National Academy of Sciences of the United States of America*. National Academy of Sciences, 109(22), pp. 8780–8785. doi: 10.1073/pnas.1117465109.

Blair, R. C. and Karniski, W. (1993) 'An alternative method for significance testing of waveform difference potentials', *Psychophysiology*. John Wiley & Sons, Ltd, 30(5), pp. 518–524. doi: 10.1111/j.1469-8986.1993.tb02075.x.

Bourgeois, A. *et al.* (2020) 'Pulvino-cortical interaction: An integrative role in the control of attention', *Neuroscience & Biobehavioral Reviews*, 111, pp. 104–113. doi: https://doi.org/10.1016/j.neubiorev.2020.01.005.

Brainard, D. H. (1997) 'The Psychophysics Toolbox.', *Spatial vision*, 10(4), pp. 433–436. Available at: http://www.ncbi.nlm.nih.gov/pubmed/9176952 (Accessed: 5 October 2017).

Carrasco, M. (2011) 'Visual attention: The past 25 years', *Vision Research*. Pergamon, 51(13), pp. 1484–1525. doi: 10.1016/J.VISRES.2011.04.012.

Chini, M., Pfeffer, T. and Hanganu-Opatz, I. L. (2021) 'Developmental increase of inhibition

drives decorrelation of neural activity', *bioRxiv*. Cold Spring Harbor Laboratory. doi: 10.1101/2021.07.06.451299.

Clayton, M. S., Yeung, N. and Cohen Kadosh, R. (2018) 'The many characters of visual alpha oscillations', *European Journal of Neuroscience*. Blackwell Publishing Ltd, 48(7), pp. 2498–2508. doi: 10.1111/ejn.13747.

Cohen, M. X. (2014) *Analyzing neural time series data: theory and practice*. Cambridge, Massachusetts: MIT Press.

Cohen, M. X. and Cavanagh, J. F. (2011) 'Single-trial regression elucidates the role of prefrontal theta oscillations in response conflict', *Frontiers in Psychology*, 2. doi: 10.3389/fpsyg.2011.00030.

Cohen, M. X. and Voytek, B. (2013) 'Linking nonlinear neural dynamics to single-trial human behavior', in Pesenson, M. (Meyer) Z. (ed.) *Multiscale Analysis and Nonlinear Dynamics*. Wiley-VCH Verlag GmbH & Co. KGaA., pp. 217–232. doi: 10.1002/9783527671632.

Cole, S. *et al.* (2019) 'NeuroDSP: A package for neural digital signal processing', *Journal of Open Source Software*, 4(36), p. 1272. doi: 10.21105/joss.01272.

Corbetta, M. and Shulman, G. L. (2002) 'Control of goal-directed and stimulus-driven attention in the brain', *Nature Reviews Neuroscience*, 3(3), pp. 201–215. doi: 10.1038/nrn755.

Dave, S., Brothers, T. A. and Swaab, T. Y. (2018) '1/f neural noise and electrophysiological indices of contextual prediction in aging', *Brain Research*, 1691, pp. 34–43. doi: https://doi.org/10.1016/j.brainres.2018.04.007.

Delorme, A. and Makeig, S. (2004) 'EEGLAB: An open source toolbox for analysis of single-trial EEG dynamics including independent component analysis', *Journal of Neuroscience*

Methods. Elsevier, 134(1), pp. 9–21. doi: 10.1016/J.JNEUMETH.2003.10.009.

Desimone, R. (1995) 'Neural mechanisms of selective visual attention', *Annual Review of Neuroscience*, 18(1), pp. 193–222. doi: 10.1146/annurev.neuro.18.1.193.

van Diepen, R. M., Foxe, J. J. and Mazaheri, A. (2019) 'The functional role of alpha-band activity in attentional processing: the current zeitgeist and future outlook', *Current Opinion in Psychology*. Elsevier, 29, pp. 229–238. doi: 10.1016/J.COPSYC.2019.03.015.

van Diepen, R. M. and Mazaheri, A. (2018) 'The Caveats of observing Inter-Trial Phase-Coherence in Cognitive Neuroscience', *Scientific Reports*. Nature Publishing Group, 8(1), p. 2990. doi: 10.1038/s41598-018-20423-z.

Donoghue, T. *et al.* (2020) 'Parameterizing neural power spectra into periodic and aperiodic components', *Nature Neuroscience 2020 23:12*. Nature Publishing Group, 23(12), pp. 1655–1665. doi: 10.1038/s41593-020-00744-x.

Donoghue, T., Dominguez, J. and Voytek, B. (2020) 'Electrophysiological Frequency Band Ratio Measures Conflate Periodic and Aperiodic Neural Activity', *eNeuro*. Society for Neuroscience, 7(6). doi: 10.1523/ENEURO.0192-20.2020.

Fields, E. C. (2017) 'Factorial Mass Univariate ERP Toolbox'. Available at: https://github.com/ericcfields/FMUT/releases.

Fields, E. C. and Kuperberg, G. R. (2019) 'Having your cake and eating it too: Flexibility and power with mass univariate statistics for ERP data', *Psychophysiology*. doi: 10.1111/psyp.13468.

Foster, J. J. and Awh, E. (2019) 'The role of alpha oscillations in spatial attention: limited evidence for a suppression account', *Current Opinion in Psychology*. Elsevier, 29, pp. 34–40. doi: 10.1016/J.COPSYC.2018.11.001.

Fougnie, D., Suchow, J. W. and Alvarez, G. A. (2012) 'Variability in the quality of visual working memory', *Nature Communications*. NIH Public Access, 3, p. 1229. doi: 10.1038/ncomms2237.

Gao, R., Peterson, E. J. and Voytek, B. (2017) 'Inferring synaptic excitation/inhibition balance from field potentials', *NeuroImage*, 158, pp. 70–78. doi: https://doi.org/10.1016/j.neuroimage.2017.06.078.

García-Pérez, M. A. (1998) 'Forced-choice staircases with fixed step sizes: asymptotic and small-sample properties', *Vision Research*, 38(12), pp. 1861–1881. doi: 10.1016/S0042-6989(97)00340-4.

Gould, I. C., Rushworth, M. F. and Nobre, A. C. (2011) 'Indexing the graded allocation of visuospatial attention using anticipatory alpha oscillations', *Journal of Neurophysiology*. American Physiological Society, 105(3), pp. 1318–1326. doi: 10.1152/jn.00653.2010.

Gratton, G., Coles, M. G. . and Donchin, E. (1983) 'A new method for off-line removal of ocular artifact', *Electroencephalography and Clinical Neurophysiology*, 55(4), pp. 468–484. doi: 10.1016/0013-4694(83)90135-9.

Groppe, D. M., Urbach, T. P. and Kutas, M. (2011) 'Mass univariate analysis of event-related brain potentials/fields I: A critical tutorial review', *Psychophysiology*. John Wiley & Sons, Ltd (10.1111), 48(12), pp. 1711–1725. doi: 10.1111/j.1469-8986.2011.01273.x.

Güntekin, B. and Başar, E. (2016) 'Review of evoked and event-related delta responses in the human brain', *International Journal of Psychophysiology*, 103, pp. 43–52. doi: https://doi.org/10.1016/j.ijpsycho.2015.02.001.

Gyurkovics, M. *et al.* (2021) 'The impact of 1/f activity and baseline correction on the results and interpretation of time-frequency analyses of EEG/MEG data: A cautionary tale',

NeuroImage. Academic Press, 237, p. Article 118192. doi: https://doi.org/10.1016/j.neuroimage.2021.118192.

Hakim, N. *et al.* (2019) 'Dissecting the Neural Focus of Attention Reveals Distinct Processes for Spatial Attention and Object-Based Storage in Visual Working Memory', *Psychological Science*. SAGE Publications Inc., 30(4), pp. 526–540. doi: 10.1177/0956797619830384.

Halgren, M. *et al.* (2019) 'The generation and propagation of the human alpha rhythm', *Proceedings of the National Academy of Sciences*. National Academy of Sciences, 116(47), pp. 23772–23782. doi: 10.1073/pnas.1913092116.

Harmony, T. (2013) 'The functional significance of delta oscillations in cognitive processing', *Frontiers in Integrative Neuroscience*. Frontiers, 7, p. Article 83. doi: 10.3389/fnint.2013.00083.

Harris, K. D. and Thiele, A. (2011) 'Cortical state and attention', *Nature Reviews Neuroscience*, 12(9), pp. 509–523. doi: 10.1038/nrn3084.

Herring, J. D. *et al.* (2019) 'Low-frequency alternating current stimulation rhythmically suppresses gamma-band oscillations and impairs perceptual performance', *NeuroImage*, 184, pp. 440–449. Available at: https://www.sciencedirect.com/science/article/pii/S1053811918318469 (Accessed: 27 November 2018).

Hong, X. *et al.* (2015) 'Normal aging selectively diminishes alpha lateralization in visual spatial attention', *NeuroImage*. Academic Press Inc., 106, pp. 353–363. doi: 10.1016/j.neuroimage.2014.11.019.

Huang, L. *et al.* (2006) 'Slab-like functional architecture of higher order cortical area 21a showing oblique effect of orientation preference in the cat', *NeuroImage*, 32(3), pp.

1365–1374. doi: https://doi.org/10.1016/j.neuroimage.2006.05.007.

Iemi, L. *et al.* (2019) 'Multiple mechanisms link prestimulus neural oscillations to sensory responses', *eLife*. eLife Sciences Publications Ltd, 8, p. Article e43620. doi: 10.7554/eLife.43620.001.

Jensen, O. and Mazaheri, A. (2010) 'Shaping functional architecture by oscillatory alpha activity: Gating by inhibition', *Frontiers in Human Neuroscience*. Frontiers Media S. A., 4, p. 186. doi: 10.3389/fnhum.2010.00186.

Jolicœur, P., Brisson, B. and Robitaille, N. (2008) 'Dissociation of the N2pc and sustained posterior contralateral negativity in a choice response task', *Brain Research*, 1215, pp. 160–172. doi: https://doi.org/10.1016/j.brainres.2008.03.059.

Kelly, S. P. *et al.* (2006) 'Increases in Alpha Oscillatory Power Reflect an Active Retinotopic Mechanism for Distracter Suppression During Sustained Visuospatial Attention', *Journal of Neurophysiology*, 95(6), pp. 3844–3851. doi: 10.1152/jn.01234.2005.

Kim, Y.-H. *et al.* (1999) 'The Large-Scale Neural Network for Spatial Attention Displays Multifunctional Overlap But Differential Asymmetry', *NeuroImage*, 9(3), pp. 269–277. doi: https://doi.org/10.1006/nimg.1999.0408.

Kingdom, F. A. A. and Prins, N. (2016) 'Chapter 5 – Adaptive Methods', in *Psychophysics*. Second Edi. San Diego: Academic Press, pp. 119–148. doi: 10.1016/B978-0-12-407156-8.00005-0.

Klimesch, W. (2012) 'Alpha-band oscillations, attention, and controlled access to stored information', *Trends in Cognitive Sciences*. Elsevier, 16(12), pp. 606–617. doi: 10.1016/j.tics.2012.10.007.

Klimesch, W., Sauseng, P. and Hanslmayr, S. (2007) 'EEG alpha oscillations: the inhibition–

timing hypothesis', *Brain Research Reviews*, 53(1), pp. 63–88. doi: 10.1016/j.brainresrev.2006.06.003.

Koivisto, M. and Revonsuo, A. (2010) 'Event-related brain potential correlates of visual awareness', *Neuroscience & Biobehavioral Reviews*. Pergamon, 34(6), pp. 922–934. doi: 10.1016/j.neubiorev.2009.12.002.

Li, B., Peterson, M. R. and Freeman, R. D. (2003) 'Oblique Effect: A Neural Basis in the Visual Cortex', *Journal of Neurophysiology*. American Physiological Society, 90(1), pp. 204–217. doi: 10.1152/jn.00954.2002.

Li, Y. *et al.* (2015) 'Synaptic Basis for Differential Orientation Selectivity between Complex and Simple Cells in Mouse Visual Cortex', *Journal of Neuroscience*. Society for Neuroscience, 35(31), pp. 11081–11093. doi: 10.1523/JNEUROSCI.5246-14.2015.

Luck, S. J. (2014) *An introduction to the event-related potential technique*. 2nd edn. Cambridge, Massachusetts: MIT Press. Available at: https://www.library.ualberta.ca/catalog/7776529 (Accessed: 9 November 2017).

Luck, S. J., Woodman, G. F. and Vogel, E. K. (2000) 'Event-related potential studies of attention', *Trends in Cognitive Sciences*. Elsevier Current Trends, 4(11), pp. 432–440. doi: 10.1016/S1364-6613(00)01545-X.

Mesulam, M.-M. (1999) 'Spatial attention and neglect: parietal, frontal and cingulate contributions to the mental representation and attentional targeting of salient extrapersonal events', *Philosophical Transactions of the Royal Society of London. Series B: Biological Sciences*. Edited by A. Howseman and S. Zeki, 354(1387), pp. 1325–1346. doi: 10.1098/rstb.1999.0482.

Michel, R., Dugué, L. and Busch, N. A. (2021) 'Distinct contributions of alpha and theta

rhythms to perceptual and attentional sampling', *European Journal of Neuroscience*. John Wiley & Sons, Ltd. doi: 10.1111/ejn.15154.

Moos, K. *et al.* (2012) 'Modulation of Top-Down Control of Visual Attention by Cathodal tDCS over Right IPS', *Journal of Neuroscience*. Society for Neuroscience, 32(46), pp. 16360–16368. doi: 10.1523/JNEUROSCI.6233-11.2012.

Nobre, A. C. and Kastner, S. (eds) (2014) *The Oxford Handbook of Attention.* New York, NY, US: Oxford University Press (Oxford library of psychology.).

Nobre, A. C., Sebestyen, G. N. and Miniussi, C. (2000) 'The dynamics of shifting visuospatial attention revealed by event-related potentials', *Neuropsychologia*, 38(7), pp. 964–974. doi: https://doi.org/10.1016/S0028-3932(00)00015-4.

Pagnotta, M. F., Pascucci, D. and Plomp, G. (2022) 'Selective attention involves a feature-specific sequential release from inhibitory gating', *NeuroImage*, 246, p. Article 118782. doi: https://doi.org/10.1016/j.neuroimage.2021.118782.

Pelli, D. G. (1997) 'The VideoToolbox software for visual psychophysics: transforming numbers into movies.', *Spatial vision*, 10(4), pp. 437–442. Available at: http://www.ncbi.nlm.nih.gov/pubmed/9176953 (Accessed: 5 October 2017).

Pouget, A., Dayan, P. and Zemel, R. (2000) 'Information processing with population codes', *Nature Reviews Neuroscience*, 1(2), pp. 125–132. doi: 10.1038/35039062.

R Core Team (2021) 'R: A language and environment for statistical computing'. Vienna, Austria: R Foundation for Statistical Computing. Available at: http://www.r-project.org/.

Rihs, T. A., Michel, C. M. and Thut, G. (2009) 'A bias for posterior α-band power suppression versus enhancement during shifting versus maintenance of spatial attention', *NeuroImage*, 44(1), pp. 190–199. doi: https://doi.org/10.1016/j.neuroimage.2008.08.022.

Di Russo, F. *et al.* (2021) 'Sustained visuospatial attention enhances lateralized anticipatory ERP activity in sensory areas', *Brain Structure and Function*, 226(2), pp. 457–470. doi: 10.1007/s00429-020-02192-6.

Samaha, J., Switzky, M. and Postle, B. R. (2019) 'Confidence boosts serial dependence in orientation estimation', *Journal of Vision*. Association for Research in Vision and Ophthalmology Inc., 19(4). doi: 10.1167/19.4.25.

Schneegans, S. and Bays, P. M. (2016) 'No fixed item limit in visuospatial working memory', *Cortex*, 83, pp. 181–193. doi: https://doi.org/10.1016/j.cortex.2016.07.021.

Schneegans, S., Taylor, R. and Bays, P. M. (2020) 'Stochastic sampling provides a unifying account of visual working memory limits', *Proceedings of the National Academy of Sciences*, 117(34), pp. 20959 LP – 20968. doi: 10.1073/pnas.2004306117.

Schürmann, M. *et al.* (2001) 'Delta responses and cognitive processing: Single-trial evaluations of human visual P300', *International Journal of Psychophysiology*. Elsevier, 39(2–3), pp. 229–239. doi: 10.1016/S0167-8760(00)00144-6.

Sheldon, S. S. and Mathewson, K. E. (2021) 'To see, not to see or to see poorly: Perceptual quality and guess rate as a function of electroencephalography (EEG) brain activity in an orientation perception task', *European Journal of Neuroscience*. John Wiley & Sons, Ltd, pp. 1–24. doi: https://doi.org/10.1111/ejn.15445.

Siman-Tov, T. *et al.* (2007) 'Bihemispheric Leftward Bias in a Visuospatial Attention-Related Network', *Journal of Neuroscience*. Society for Neuroscience, 27(42), pp. 11271–11278. doi: 10.1523/JNEUROSCI.0599-07.2007.

Sokoliuk, R. *et al.* (2019) 'Two Spatially Distinct Posterior Alpha Sources Fulfill Different Functional Roles in Attention', *Journal of Neuroscience*. Society for Neuroscience,

39(36), pp. 7183–7194. doi: 10.1523/JNEUROSCI.1993-18.2019.

Stouffer, S. A. *et al.* (1949) 'Studies in social psychology in World War II: the American soldier', in *Adjustment During Army Life*. Vol. 1. Princeton, NJ.: Princeton University Press. Available at: https://psycnet.apa.org/record/1950-00790-000.

Suchow, J. W. *et al.* (2013) 'Modeling visual working memory with the MemToolbox.', *Journal of Vision*. Association for Research in Vision and Ophthalmology, 13(10), pp. 1–8. doi: 10.1167/13.10.9.

Taylor, R. and Bays, P. M. (2018) 'Efficient Coding in Visual Working Memory Accounts for Stimulus-Specific Variations in Recall', *Journal of Neuroscience*. Society for Neuroscience, 38(32), pp. 7132–7142. doi: 10.1523/JNEUROSCI.1018-18.2018.

Taylor, R. and Bays, P. M. (2020) 'Theory of Neural Coding Predicts an Upper Bound on Estimates of Memory Variability', *Psychological Review*, 127(5), pp. 700–718. doi: 10.1037/rev0000189.

Thuwal, K., Banerjee, A. and Roy, D. (2021) 'Aperiodic and Periodic Components of Ongoing Oscillatory Brain Dynamics Link Distinct Functional Aspects of Cognition across Adult Lifespan', *eNeuro*. Society for Neuroscience, 8(5). doi: 10.1523/ENEURO.0224-21.2021.

VanRullen, R. (2016) 'How to Evaluate Phase Differences between Trial Groups in Ongoing Electrophysiological Signals', *Frontiers in Neuroscience*. Frontiers, 10, p. 426. doi: 10.3389/fnins.2016.00426.

Voytek, B. *et al.* (2015) 'Age-Related Changes in 1/f Neural Electrophysiological Noise', *Journal of Neuroscience*. Society for Neuroscience, 35(38), pp. 13257–13265. doi: 10.1523/JNEUROSCI.2332-14.2015.

Waschke, L. *et al.* (2021) 'Modality-specific tracking of attention and sensory statistics in the human electrophysiological spectral exponent', *eLife*. Edited by M. Chait et al. eLife Sciences Publications, Ltd, 10, p. e70068. doi: 10.7554/eLife.70068.

Woodman, G. F. (2010) 'A brief introduction to the use of event-related potentials in studies of perception and attention', *Attention, Perception, & Psychophysics*. Springer-Verlag, 72(8), pp. 2031–2046. doi: 10.3758/BF03196680.

Wright, M. J., Geffen, G. M. and Geffen, L. B. (1995) 'Event related potentials during covert orientation of visual attention: effects of cue validity and directionality', *Biological Psychology*, 41(2), pp. 183–202. doi: https://doi.org/10.1016/0301-0511(95)05128-7.

Zhang, W. and Luck, S. J. (2008) 'Discrete fixed-resolution representations in visual working memory.', *Nature*. NIH Public Access, 453(7192), pp. 233–235. doi: 10.1038/nature06860.

4

CONNECTING COVERT ATTENTION AND VISUAL PERCEPTION TO THE SPATIOTEMPORAL DYNAMICS OF ALPHA BAND ACTIVITY, CROSS-FREQUENCY COUPLING AND FUNCTIONAL CONNECTIVITY USING MULTIVARIATE PATTERN ANALYSIS

4.1 INTRODUCTION

Electroencephalography (EEG) is one of the oldest and most well-established neuroimaging techniques used by researchers and clinicians. Alpha oscillations (8-14 Hz) were the first EEG frequency band identified (Berger, 1929) and are particularly interesting to cognitive neuroscience researchers due to a plethora of evidence suggesting it has a critical role in visual perception and attention (Klimesch, Sauseng and Hanslmayr, 2007; Mathewson *et al.*, 2011, 2012; Klimesch, 2012; Clayton, Yeung and Cohen Kadosh, 2015; Frey, Ruhnau and Weisz, 2015; VanRullen, 2016b). Exactly what that role is, however, is still debated. For example, some researchers believe alpha oscillations inhibit the flow of irrelevant information into sensory areas or from sensory areas to higher order cortical locations (Klimesch, Sauseng and Hanslmayr, 2007; Jensen and Mazaheri, 2010; Foxe and Snyder, 2011; Mathewson *et al.*, 2011; Chaumon and Busch, 2014), while others think alpha oscillations indirectly control perception and attention by modulating the higher frequencies (e.g., gamma oscillations, >30 Hz) involved in sensory processing (Voytek, 2010; Jensen *et al.*, 2014; Zazio *et al.*, 2020). The purpose of the current research is to try elucidating the role of alpha oscillations in visual

perception and attention using the powerful new techniques offered by machine learning. It is now thought that one of the reasons the relationship between alpha oscillations and perception remains elusive after almost a century of research is that alpha's role in conscious perception has often been mistaken for sensory processing. For example, recent studies investigating the effect of prestimulus power on perception found that participants were more likely to report seeing a stimulus when prestimulus alpha (and low beta) power was low, even though the stimulus was not presented (Samaha, Iemi and Postle, 2017; Iemi and Busch, 2018; Samaha *et al.*, 2020). To account for these findings, Samaha et al (2020) proposed the baseline sensory excitability model (BSEM) which states that spontaneous alpha amplitude indiscriminately changes the baseline firing rate of sensory neurons such that the sensory response distribution is changed without changing the separability of the signal and noise representations. Furthermore, because it is thought that the internal fluctuations in sensory neuron excitability are not known by the higher-level decision-making areas (Samaha *et al.*, 2020), participants will fail to adjust their decision criteria accordingly so that participants are not only more likely to report stimulus presence and make more false alarms, but will also claim greater level of confidence in their decision even though their detection and discrimination sensitivity does not change. These predictions were confirmed by two studies designed for signal detection theory analysis (Samaha, Iemi and Postle, 2017; Iemi and Busch, 2018). Further support comes from Benwell et al (2018) who found that pre-stimulus alpha power correlated with participants' bias when judging the relative length of two line segments (landmark task) but not discrimination performance. Interestingly, the bias seemed to be partially driven by changes in pre-stimulus alpha power over the course of the experiment rather than trial-by-trial variability.

In contrast, another group has put forth the oscillation-based probability of response (OPR) model which states that the effects of alpha oscillations on perception are due to an alpha-gamma interaction modulating the probability of sensory neurons responding to a stimulus (Zazio *et al.*, 2020). Specially, the oscillation-based probability of response model proposes that there are two possible alpha-gamma cross-frequency interactions that effect the probability of responding to a visual stimulus: (1) alpha power modulates the power of gamma (amplitude–amplitude coupling; suppression of gamma amplitude), so that increased alpha power results in an increased threshold for responding (Chaumon and Busch, 2014); or, (2) alpha activity modulates the phase of gamma (phase–amplitude coupling,; desynchronization of gamma), so that increased alpha activity results in a decreased sensory response (Chaumon and Busch, 2014). In the current study, if amplitude–amplitude coupling activity is responsible for attentional modulation and visual perception, we would expect to see results like the baseline sensory excitability model (*i.e.,* alpha amplitude) since both propose alpha-related activity modulates the signal and noise similarly. On the other hand, we would expect phase–amplitude coupling to be strongly related to task performance and sensitive to the presence of an informative cue since it would modulate the signal to a larger extent than the noise. These ideas are supported by independent lines of research into the role of gamma oscillations for sensory enhancement (Pritchett *et al.*, 2015; Ni *et al.*, 2016) and the inverse relationship between alpha activity, cortical excitability, and sensory perception (Samuel *et al.*, 2018; de Graaf *et al.*, 2020), as well as research using transcranial stimulation that found stimulation at alpha frequency modulated gamma oscillation activity (Hamidi, 2009; Herring *et al.*, 2019; Okazaki, Mizuno and Kitajo, 2020).

There is also the possibility that coordinated activity across different brain areas underlie visual perception and attention. Rather than localized changes in brain activity, changes in the level of synchronization between brain areas might better explain attentional modulation and perceptual responses. Previous studies have reported alpha-mediated functional connectivity with regards to visual task performance and top-down attention. For example, authors found stimulus anticipation was related to occipital and medial frontal interactions in the alpha band and that participants with stronger network interactions were more likely to improve performance following an error (Cohen and van Gaal, 2013). Other studies have found alpha-mediated interactions between the parietal, frontal, and occipital areas during the control of task-related attentional processes (Plomp *et al.*, 2015; Doesburg, Bedo and Ward, 2016). These results suggests that alpha band activity might mediate top-down modulation of visual areas not only locally, but through the dynamic interactions of large-scale functional networks (Sadaghiani and Kleinschmidt, 2016).

It is important to note that the baseline sensory excitability model, the oscillation-based probability of response model, and functional connectivity are not necessarily mutually exclusive. It is possible that the oscillation-based probability of response model is a mechanistic explanation of the baseline sensory excitability model which is a result of coordination across different brain areas. It is also important to point out that neither model claims to explain attention, though both propose that their models could extend to, or are at least related to, attentional mechanisms. This leaves us with some interesting questions that need to be addressed. Namely, whether alpha power alone (baseline sensory excitability model), alpha modulated gamma (oscillation-based probability of response model), or functional connectivity best account for perceptual performance. Also, this paper sought to investigate if the same

pattern of brain activity that accounts for perceptual performance can predict performance when participants are actively engaged in visuospatial attention? To address these questions, the current study uses the combination of machine learning technique, EEG data collected from a combined orientation perception and spatial attention task and associated behavioral measures (see below for further details about the task). The idea is to determine whether alpha power, alpha-gamma cross-frequency coupling, or alpha-based functional connectivity could accurately classify trials as those with selective spatial attention (informative cue) and those without (non-informative cue). In addition, the current study would also test which set of EEG measures could predict perceptual performance on a cued orientation perception task.

4.2 Materials and Methods

This dataset and task have also been reported in Chapter 3.

Participants

Thirty-five participants from the University of Alberta community participated in the study (age range = 17-34 years). Seven participants were not included in the analysis due to 30% or more trials containing eye movement artifacts (see the EEG Preprocessing section for more details). One other participant was excluded from the analysis due to having extreme outlying performance on the task (see Behavioral Analysis in the Results section for more details). Participants were all right-handed and had normal or corrected normal vision and no history of neurological problems. All participants gave informed written consent, were either compensated at a rate of $10/hr or given research credit for their time. The study adhered to the tenets of the Declaration of Helsinki and was approved by the Internal Ethics Board at the University of Alberta.

Cued Orientation Perception Task

Participants were seated 57 cm away from a 1920 x 1080 pixel^2 ViewPixx/EEG LCD monitor (VPixx Technologies, Quebec, Canada) with a refresh rate of 120 Hz, simulating a CRT display with LED backlight rastering. The rastering, along with 8-bit digital TTL output triggers yoked to the onset and value of the top left pixel, allowed for submillisecond accuracy in pixel illumination times, which were confirmed with a photocell prior to the experiment. Stimuli were presented using a Windows 7 PC running MATLAB R2012b with the Psychophysics toolbox (Version 3; Brainard, 1997; Pelli, 1997). The code running the task was a modified version of the Orientation Perception Task code from Sheldon and Mathewson (2021). The original version of the code can be found here: https://github.com/APPLabUofA/OrientTask_paper. Video output was sent to the ViewPixx/EEG with an Asus Striker GTX760 (Fremont, CA) graphics processing unit.

Each trial began with a white fixation dot presented at the center of the monitor and two dark gray circles to the left and right of the fixation dot for 700 ms after which one of three possible cues appeared above the central fixation dot, vertically aligned to the top of the circles. Two cues were black triangles pointing towards the left or right, indicating the side the target will appear (*i.e.,* informative cues). The third cue was both black triangles pointed toward each other indicating that the target will appear to the left or right (*i.e.,* non-informative cue). The cues remained on screen for 1242, 1284, 1325, or 1367 ms. After the cue, the target appeared for 8.33 ms (one monitor refresh) in the center of the left or right circle. The target always appeared to the side indicated by the informative cue. For non-informative cues, the target could appear on the left or right with equal probability. The target was in the shape of a needle and was pointing toward one of 24 predefined evenly spaced directions so that all the orientations covered 360 degrees. The direction of the target was randomly selected on each trial. A backward mask

lasting for 8.33 ms with a constant 41.7 ms target-mask stimulus-onset asynchrony appeared in the center of both circles regardless of the side the target appeared. The mask was created by overlaying the target orientated in all 24 directions which created a star shape seen in Figure 4.1A. Following the mask offset, a 516.6 ms blank interval period occurred identical to the fixation.

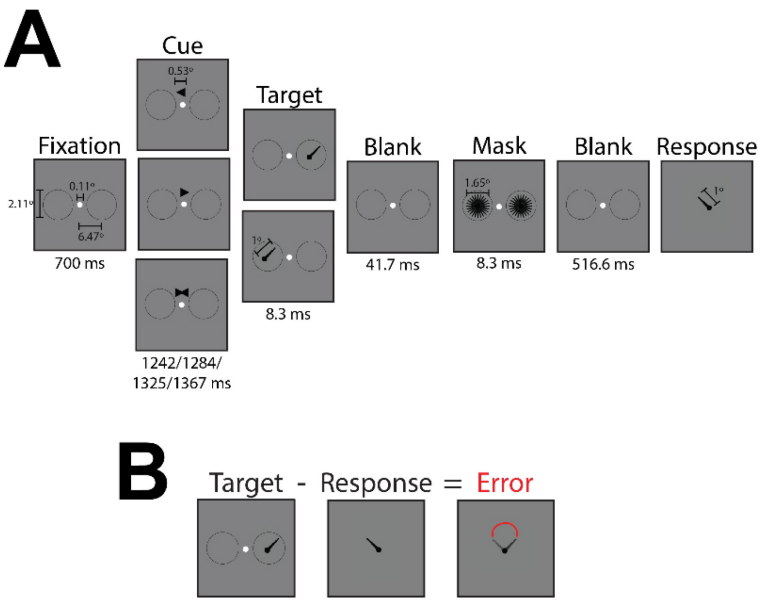

Figure 4.1. *Cued orientation perception task*

A) Sequence of task events with duration of each screen presentation and sizes of fixation, cues, target, mask, and response stimuli. Sizes are in degrees of visual angle. **B)** Example of response error calculation. Response errors are reported in degrees.

After the blank interval, a response screen appeared with the needle in the center of the screen. Using the computer mouse, participants were asked to rotate the needle so that it was pointed in the same direction as the previous target. If participants detected a target but could not remember its orientation, they were asked to guess the orientation of the target. Participants

could provide their response at their own pace. No feedback was given to participants. The next trial began immediately after a needle's orientation was selected. See Figure 4.1A for a summary of the task sequence and the stimulus dimensions.

Participants completed eight blocks consisting of 48 trials each, along with 20 practice trials at the beginning of the experiment. Participants ended completing a total of 404 trials with 33% of trials having a non-informative cue and about equal left and right targets, 33% of trials having a right target and informative cue, and 33% of trials having a left target and informative cue. Participants could rest at their own pace every 48 trials. Extensive written and verbal instructions were presented to participants prior to the practice trials. Instructions thoroughly explained and demonstrated each component that would compose a single trial.

Before the cued orientation perception task, participants performed a staircased cued target detection task that had the same parameters as the cued orientation perception task except that participants only reported whether they saw the target or not using the keyboard. The target color was a gray determined by a scalar value passed to the functions in Psychtoolbox. In the staircased cued target detection task, the target color value could range from the background color (making it not visible; corresponding value of 256) to black (making it the most visible; corresponding value of 0). This target gray value was adjusted throughout the task based on a 1-up/2-down staircasing procedure targeting a 0.65 target detection rate for each individual (García-Pérez, 1998; Kingdom and Prins, 2016). The staircased task consisted of three blocks of 48 trials. The target gray value was determined for each participant by taking the average target gray value across the last two blocks of trials. These final values came to be 56 on average (*SD* = 20) and were used as the target gray value in the cued orientation perception task.

The MATLAB code for the cued staircased target detection task and the cued orientation perception task are available at https://github.com/APPLabUofA/CuedOrientTask_paper/tree/main/Experiment_Code.

EEG Recording

During the experiment, EEG data was recorded from each participant with a Brain-Amp 32-channel amplifier (BrainVision) using gelled low-impedance electrodes (actiCAP passive electrodes kept below 5 kΩ). Inter-electrode impedances were measured at the start of each experiment. All electrodes were arranged in the same 10-20 positions (Fp2, Fp1, F4, F3, F8, F7, FC2, FC1, FC6, FC5, C4, C3, CP2, CP1, CP6 CP5, P4, P3 P6, P5, P8, P7, PO4, PO3, O2, O1, Fz, FCz, Cz, Pz, and Oz). In addition to the 31 EEG sensors, a ground electrode was used, positioned at AFz. Two reference electrodes and the vertical and horizontal bipolar EOG were recorded from passive Ag/AgCl easycap disk electrodes affixed on the mastoids, above and below the left eye, and 1 cm lateral from the outer canthus of each eye. The bipolar channels were recorded using the AUX ports of the Brain-Amp amplifier. SuperVisc electrolyte gel and mild abrasion with a blunted syringe tip were used to lower impedances. Gel was applied and inter-electrode impedances were lowered to less than 5 kΩ for all electrode sites. EEG data was recorded online referenced to an electrode attached to the left mastoid. Offline, the data were re-referenced to the arithmetically derived average of the left and right mastoid electrodes.

Data were digitized at 1000 Hz with a resolution of 24 bits. Data were filtered with an online bandpass with cutoffs of 0.1 Hz and 250 Hz. The experiment was run in a dimly lit, sound and radio frequency-attenuated chamber from Electromedical Instruments, with copper mesh covering the window. The only electrical devices in the chamber were an amplifier, speakers, keyboard, mouse, and monitor. The monitor ran on DC power from outside the chamber, the

keyboard and mouse were plugged into USB outside the chamber, and the speakers and amplifier were both powered from outside the chamber, and nothing was plugged into the internal power outlets. Any devices transmitting or receiving radio waves (e.g., cell phones) were removed from the chamber for the duration of the experiment.

Data Analyses

Data analyses were performed using MATLAB R2021a (The MathWorks Inc, Natick, MA, USA), EEGLAB 14.1.2b (Delorme & Makeig, 2004), FieldTrip 20160928 (Oostenveld *et al.*, 2011), Python 3.7.9 (Python Software Foundation, https://www.python.org/) via the Spyder IDE (version 5.0.5; Raybaut, 2009), and custom scripts. All statistical analyses were conducted using MATLAB R2021a. Red-white-blue colormaps were created using the redblue.m function by Auton (2009) found here: https://www.mathworks.com/matlabcentral/fileexchange/25536-red-blue-colormap. The functional connectivity topographic plots were made with code adapted from the FCLAB toolbox (Pezoulas *et al.*, 2018) found here: https://github.com/ramsys28/FCLAB. The raw behavior and EEG data files are available at https://osf.io/u6fgm/.

Behavioral Data

Response errors on each trial were calculated by subtracting the orientation of the response stimulus, as reported by the participant, from the orientation of the target stimulus (see Figure 4.1B). The response errors and absolute response errors were submitted to a repeated-measures factorial ANOVA (target side and cue type the within-subject factors) using the permutation-based *Fmax* test which is a mass univariate approach for factorial ANOVAs. The *Fmax* test has the advantages of permutation tests in there are a lot less assumptions about the data than traditional statistical approaches, and has been shown to be very good at controlling

Type I errors without a great cost in power (Fields and Kuperberg, 2019). The implementation of the *Fmax* test was done with code modified from the Factorial Mass Univariate Toolbox (FMUT; Fields, 2017). The original code can be found here: https://github.com/ericcfields/FMUT.

Follow-up pairwise comparisons of significant interactions and main effects were done with a repeated-measures, two-tailed permutation test based on the *tmax* statistic (Blair & Karniski, 1993) using the mxt_perm1() function from the Mass Univariate ERP Toolbox (Groppe et al., 2011). *P*-values were then corrected for multiple comparisons using the false discovery rate (FDR) procedure described in Benjamini and Yekutieli (2001). Effects that satisfied a 5% FDR criterion were considered significant. 10,000 random within-participant permutations were used to estimate the distribution of the null hypothesis for all permutation-based tests (*i.e., Fmax* and *tmax*) and the familywise alpha (α) was set to 0.05.

EEG Data

Preprocessing. After the data had been re-referenced offline, the bandpass FIR filter from EEGLAB was applied with lower and upper cut-offs of 0.1 Hz and 50 Hz. Data was segmented into 3000 ms epochs aligned to target onset (-2400 ms pre-target onset to 1400 ms post-target onset). The average voltage in the 200 ms baseline following fixation onset was subtracted on each trial for every electrode, and trials with absolute voltage fluctuations on any channel greater than 1000 μV were discarded. Eye movements were then corrected with a regression-based procedure developed by Gratton, Coles, and Donchin (1983). After a second baseline subtraction with 200 ms following fixation onset, trials with remaining absolute voltage fluctuations on any channel greater than 500 μV were removed from further analysis.

Data was then subjected to visual inspection and manual rejection of trials (both EEG and behavioral data) contaminated by blocking (*i.e.,* amplifier saturation), blinks, muscle noise, or

skin potentials. To ensure there were no horizontal eye movements during the trial, we use a split-half sliding window approach on the HEOG signal. We slid a 100 ms time window in steps of 10 ms from 1600 ms prior to target onset (at least 200 ms before the first cue appears) to the response screen onset 600 ms after target onset. If the change in voltage from the first half to the second half of the window was greater than 25 μV, it was marked as an eye movement and rejected (Hong *et al.*, 2015; Hakim *et al.*, 2019). Seven participants had to be removed from further analysis after this procedure because more than 30% of trials got rejected indicating that they did not use covert attention as instructed.

Periodic and Aperiodic Components. Because neural power spectra consist of overlapping periodic and aperiodic components, it is important to consider the aperiodic activity when measuring a signal's oscillatory properties. For this reason, the FOOOF toolbox (version 1.0.0; Donoghue et al., 2020) was used to identify peaks within the alpha (8-14 Hz) frequency range after adjusting for the aperiodic component. FOOOF is a spectral parameterization algorithm which decomposes the power spectrum into periodic and aperiodic components via an iterative process of model fitting (see Donoghue et al., (2020) for detailed description). The FOOOF toolbox is available on https://github.com/fooof-tools/fooof.

Before FOOOF, the power spectral density (PSD) was estimated using Welch's method by applying the pwelch function from MATLAB's Signal Processing Toolbox to the 1000 ms before target onset for each participant, electrode, and trial separately. The PSD was calculated using a Hamming window based on a 500 ms periodogram to perform spectral decomposition at each frequency. The PSD data was then submitted to FOOOF in Python.

Settings for the FOOOF algorithm were set as: peak width limits: [1,5]; max number of peaks: 7; minimum peak height: 0.22; peak threshold: 0.20; and aperiodic mode: fixed. Power

spectra were parameterized across the frequency range 3.9 to 48.8 Hz with a frequency resolution of 1.9 Hz.

The aperiodic component measures offset and exponent and the measures quantifying the quality of fit, r^2 and fit error, were submitted to a repeated-measures factorial ANOVA (target side and cue type the within-subject factors) using the permutation-based *Fmax* statistic. The implementation of the *Fmax* test was done with code modified from the Factorial Mass Univariate Toolbox (FMUT; Fields, 2017). All brain electrodes were included in the analysis 10,000 random within-participant permutations were used to estimate the distribution of the null hypothesis and the familywise alpha (α) was set to 0.0125 (Bonferroni corrected alpha level α_{corr} = 0.05/4 to account for the two aperiodic component measures and the two quality of fit measures).

Alpha (8-14 Hz) Peak Detection. Alpha peaks were identified on a trial-by-trial basis for each electrode and participant separately using the FOOOF algorithm. The final alpha peak frequencies used in subsequent analyses were the median frequency of the trials in each trial category (*i.e.,* informative cue, right target; non-informative cue, right target; informative cue, left target; and, non-informative cue, right target). This meant that each participant, electrode, and trial category had a peak alpha frequency that could be used in later analyses.

EEG Signal Metrics. All EEG metrics were calculated for each trial type, electrode, and participant separately. All features depend on both band-pass filtering and applying Hilbert transform to obtain instantaneous phase, amplitude, and frequency. Because both models are concerned with the influence of alpha oscillations on stimulus perception, only brain activity before target onset was considered. It was also important to use a time window starting at least 200 ms after the last cue onset to prevent contamination from the visual evoked potential (Luck,

2014). Thus, all EEG features were calculated for the 1000 ms prior to target onset (*i.e.,* -1000 to 0 ms) with the condition that the time windows over which the metrics were calculated never exceeded 0 ms.

To prevent edge artifacts, the data was zero-padded so that filtering was done on an additional 2000 ms (1400 ms data + 600 ms zero-padding) on either side of the selected window (Cohen, 2008). The filter type used was a 4^{th} order Butterworth Infinite Impulse Response (IIR) filter implemented using Fieldtrip's ft_preproc_bandpassfilter() function (Oostenveld *et al.*, 2011). To remove any phase distortion caused by filtering in the original signal, we used a backward forward zero phase filtering method. A variable width filter was used for the cross-frequency coupling (CFC) calculations (see Cross-Frequency Coupling (CFC) section for more details), and an 8-14 Hz wide filter was used for the functional connectivity analysis. Afterward, the Hilbert transform was applied using Fieldtrip's ft_preproc_hilbert() function (Oostenveld *et al.*, 2011) or the Hilbert() function from MATLAB's Signal Processing Toolbox. The reason both functions were utilized was that the code calculating the cross-frequency coupling (CFC) metrics originated from different sources who used either Fieldtrip's or MATLAB's function. In other words, when code was adapted from other sources, that function was not changed (see below for more details).

The instantaneous amplitude extracted after filtering ±1 Hz of the median peak alpha frequency was used as the metric of instantaneous alpha amplitude submitted to the decoding analysis along with the cross-frequency coupling metrics describe below. Because of the Hilbert transformation, there were 1001 time points (-1000 to 0 relative to target onset) for the alpha metric.

Cross-Frequency Coupling. Cross-frequency coupling metrics are used to quantify the interactions between frequency bands. There are two types relevant to the current study: phase–amplitude coupling and amplitude–amplitude coupling (Jensen and Colgin, 2007; Cohen, 2014; Davoudi, Ahmadi and Daliri, 2020). Both were calculated using a 250 ms time window, the minimum needed to capture two full cycles of the lowest frequency oscillation at the 1000 sampling rate, and a 1 ms time step.

The bandwidth of a filter used is a crucial parameter when calculating CFC. For extracting the instantaneous amplitude, filters need to be wide enough to capture the amplitude fluctuations. However, extracting the instantaneous phase requires a narrow band filter for accurate estimation (Davoudi, Ahmadi and Daliri, 2020). For this reason, a variable bandwidth, defined as ±0.4 times the center frequency was used on the faster 30-45 Hz frequency range (Aru *et al.*, 2015; Seymour, Rippon and Kessler, 2017), and a precise ±1 Hz of the median peak alpha frequency was used for the slower frequency range (Seymour, Rippon and Kessler, 2017).

Amplitude-amplitude coupling was measured using Spearman's rho which assess the correlation between the instantaneous amplitude of alpha and gamma (Cohen, 2014). Values can range between 1 and -1 where 0 indicates no coupling and ±1 indicated complete coupling.

Since there is little agreement about the best way to quantify phase-amplitude coupling, several different metrics were chosen, each with their own benefits and limitations. For instance, the phase-locking value (which will be referred to as PAC_{PLV}) described by Cohen (2008) was calculated using a modified version of the pacMEG.m function by Seymour and colleagues (2017). The PAC_{PLV} represents the degree to which the faster (gamma) oscillations are comodulated with the slower frequency's (alpha) phase. It was originally developed as a flexible way to identify PAC across time without requiring *a priori* assumptions about the frequency

bands at which coupling will be assessed (Cohen, 2008). The value of 1 represents complete coupling and 0 represents no coupling.

The Modulation Index (MI), as proposed by Tort and colleagues (2008, 2010), measures cross-frequency coupling based on Shannon entropy and Kullback-Leibler (KL) divergence. When the mean amplitude is uniformly distributed over the phases (*i.e.*, lack of phase-amplitude coupling), MI = 0. As the amplitude distribution deviates further from a uniform distribution, the closer MI gets to 1 indicating the existence of phase-amplitude coupling. The MI was calculated with a modified version of code from the EEGLAB extension PACTools (version 1.0.1; Martinez-Cancino et al., 2020). The original code can be found here: https://github.com/sccn/PACTools. The number of bins was 18 except when that resulted in empty bins. To avoid having empty bins (which results in a null value), the number of bins was iteratively decreased by half until none of the bins were empty.

Alternatively, the mean vector length (MVL) created by Canolty et al (2006) is calculated by multiplying slow oscillation phase time series by fast oscillation amplitude and then averaging the vectors across time. The length of the average vector represents the amount of phase-amplitude coupling and the direction represents the mean phase where amplitude is strongest. When no coupling is present, all vectors cancel each other out and the mean vector will be short (Hülsemann, Naumann and Rasch, 2019). The problem with the MVL is that it can be dependent on the absolute amplitude of the high frequency oscillation (Tort *et al.*, 2010). To address this caveat, Özkurt and Schnitzler (2011) proposed a direct MVL (which will be referred to as $MVL_{Özkurt}$) which is amplitude-normalized and ranges between 0 and 1. $MVL_{Özkurt}$ was used as a phase-amplitude coupling measure and it was calculated using a modified version of the pacMEG.m function by Seymour and colleagues (2017).

Finally, Penny et al (2008) created a measure of phase-amplitude coupling based on the general linear model (GLM). This measure, which will be referred to as PAC_{GLM}, uses multiple regression to estimate (via least squares solutions) the regression coefficients of a model relating the amplitude of the faster frequency to the phase of the slower frequency (see Penny et al (2008) for details). The final PAC_{GLM} metric is the proportion of variance explained by the model (r^2_{GLM}) which ranges between 0 and 1. The PAC_{GLM} was meant as an improvement to the envelope-to-signal correlation measure by Bruns and Eckhorn (2004) by removing sensitivity to amplitude co-modulation and allowing coupling to be detected at all phases of the slower oscillation (Penny *et al.*, 2008). The PAC_{GLM} was calculated with a modified version of code from the EEGLAB extension PACTools (version 1.0.1; Martinez-Cancino et al., 2020). The original code can be found here: https://github.com/sccn/PACTools.

Functional Connectivity. Functional connectivity metrics are used to quantify the synchronization of neural responses across electrodes. Volume conduction is a possible confound in functional connectivity analysis that can be dealt with in several ways. One method is to use measurements that are relatively insensitive to the effects of volume conduction such as phase-lag index (PLI), weighted PLI, and imaginary coherence (iCOH) (Cohen, 2014). These measures were calculated for all electrode pairs following the bandpass filtering and Hilbert transform.

Another method is to apply a spatial filter, like the surface Laplacian, which minimizes volume-conduction effects (Kayser and Tenke, 2015). This was done prior to the bandpass filtering using the algorithm described by Perrin and colleagues (1989) and the function laplacian_perrinX.m written by Cohen (2014) which can be found at https://github.com/mikexcohen/AnalyzingNeuralTimeSeries. The function's default settings were used which had the Legendre polynomial order set to 20 and the G smoothing parameter

(lambda) set to 1e-5. After spatial and frequency filtering and the Hilbert transform, phase-locking values (PLV) and amplitude envelope correlations were calculated for all electrode pairs. All functional connectivity measurements were calculated between -1000 ms and 0 ms (relative to target onset) in 375 ms time windows, the minimum segment length for at least three cycles of the lowest frequency band as recommended by Cohen (2014), and 5 ms time steps.

There are several other metrics used to quantify functional connectivity. There are a lot more ways to quantify functional connectivity than the measures used here, but the metrics chosen, which are summarized below, were those that best balanced computational intensity with suitability for the experimental design and research question.

Phase lag index (PLI) aims to obtain reliable estimates of phase synchronization that are unaffected by volume conduction. The central idea is to discard phase differences that center around 0 mod π since zero phase delay between two points is one of the properties of volume conduction. It is calculated as the average number of phase angle differences that are positive or negative in the complex plane (Cohen, 2015). The weighted phase lag index (wPLI) is an extension of the phase lag index (PLI) proposed by Vinck et al (2011) where the vectors closest to the real axis are given less weight, thus, have a smaller influence on the final connectivity estimate (Cohen, 2015). The wPLI in the current study was corrected for sample-size bias using the debiased estimator introduced by Vinck *et al* (2011). wPLI was calculated using modified code based on Fieldtrip's (Oostenveld *et al.*, 2011) implementation found here: https://github.com/fieldtrip/fieldtrip/tree/master/connectivity; and, online code by Cohen (2014) found here: https://github.com/mikexcohen/AnalyzingNeuralTimeSeries.

Imaginary coherence (iCOH) was developed by Nolte et al (2004) as a way to measure spectral coherence without the influence of volume conduction (Cohen, 2014). The iCOH was

calculated using a modified version of the online code provided by Cohen (2014) found here: https://github.com/mikexcohen/AnalyzingNeuralTimeSeries.

Phase-locking value (PLV) described by Lachaux *et al* (1999) measures the uniformity of the distribution of phase angle difference between two electrodes. However, instead of calculating the phase difference across trials, the phase difference between electrodes was calculated across time within each trial. So, if the phase difference varies little within a time window, the PLV is close to one. If there is a lot of variability within a time window, the PLV is close to 0. The PLV was calculated using a modified version of the pn_eegPLV.m function from the FCLAB toolbox (Pezoulas *et al.*, 2018). The original code can be found here: https://github.com/ramsys28/FCLAB.

Like the cross-frequency coupling metric AAC, the amplitude envelope correlations were calculated using Spearman's rho because it does not rely on an assumption of normally distributed data. The only difference in the calculation was that the amplitude envelope correlations were done between electrode pairs rather than between two different frequencies at the same electrode.

Multivariate Pattern Analysis (MVPA)

Traditionally, data analysis has primarily been limited to a univariate approach such as detecting differences in activity between experimental conditions. In contrast, MVPA is concerned with how multivariate neural patterns comprising spatial and temporal combinations might collectively correspond to a cognitive event or state of interest (Kuntzelman *et al.*, 2021). As such, MVPA is a powerful technique to demonstrate the availability of discriminatory or predictive information, without requiring many assumptions about the underlying spatial or temporal extent of that information (Hogendoorn, 2015). Another important advantage of this

approach is that it does not require averaging over space, time, trials, or participants. Furthermore, MVPA can be applied at individual time points, allowing for the investigation of how the information content changes over time (Hogendoorn, 2015).

A linear support vector machine (SVM) was chosen for the current MVPA. The SVM is a generalization of the maximal margin classifier developed in the 1990s by computer scientist (James *et al.*, 2021). Because the goal of the current study was not high prediction accuracy, the linear SVM was preferrable to the more sophisticated nonlinear algorithms because the linear SVM is simpler, making interpretation less complex (Grootswagers, Wardle and Carlson, 2017).

It should be noted that finding discriminatory or predictive information in EEG activity patterns using MVPA does not mean that those activity patterns are how the brain represents that information. In other words, it should not be assumed MVPA represents a biologically plausible mechanism employed by the brain. At best, MVPA shows that information about the experimental conditions is latent in brain activity patterns, not that the information is being used by the brain (Ritchie, Kaplan and Klein, 2019).

With regards to the current analysis, each metric was *z*-score normalized across trials at each time window for each participant before SVM classification and regression because it can speed up calculations and help increase accuracy (Ben-Hur and Weston, 2010).

Support Vector Machine (SVM) Classification

The goal of the SVM classification analysis was to determine the patterns of brain activity before target onset that best distinguish between informative and non-informative cued trials (left and right targets separately). Support vector machine (SVM) classification works by finding the hyperplane which maximizes the margin between categories. The margins are

determined by the support vectors which are, in this case, the closest points to the hyperplane (Taghizadeh-Sarabi, Daliri and Niksirat, 2014).

To perform classification, we used C-SVM (implemented by the LIBSVM Toolbox; Chang & Lin, 2011) with a linear kernel and the regularizing/cost parameter C = 1. This was implemented with the Decision Decoding Toolbox (DDTBOX; Bode et al., 2019) code and custom script. The number of trials were balanced between the two conditions before classification because a trained classifier could achieve high accuracy in an unbalanced dataset by predicting the more frequent trial category (Grootswagers, Wardle and Carlson, 2017).

Support Vector Regression (SVR). When the variables of interest are continuous rather than categorical, an alternative to support vector machine (SVM) classification is support vector regression (SVR). SVR allows for trial-by-trial values of a continuous variable (in this case, response errors) to be mapped to predicted values of that variable (Bode *et al.*, 2019). The goal of this analysis was to determine the patterns of brain activity before target onset that best predict response errors (done separately for each individual and the following four conditions: informative cue, right target; non-informative cue, right target; informative cue, left target; and, non-informative cue, left target).

Support vector regression (SVR) works a little differently than support vector machine (SVM) classification in that the support vectors of SVR are the data points (*i.e.,* EEG signal metrics calculated at each electrode and timepoint) with relatively large residuals (*i.e.,* furthest from the regression line) rather than the closest (Bishop, 2006). However, in both cases, the data points that are hardest to categorize (closest together) or predict (furthest from their predicted values) are the support vectors used to determine the solution (Bode *et al.*, 2019).

Support vector regression (SVR) analyses was implemented with the Decision Decoding Toolbox (DDTBOX; Bode et al., 2019) code and custom script. The SVR model was calculated using LIBSVM with a standard cost parameter C = 0.1 (Chang and Lin, 2011).

Cross-Validation. A 10-fold cross-validation procedure repeated 10 times was used to assess performance of the support vector machine (SVM) classifier/model for each participant and set of conditions. In this method, the data are divided into 10 subsets. The classifier/model is trained on nine subsets and tested using the left-out subset. This procedure is then independently repeated with each subset serving at the test data once while training on the remaining nine data sets. The average 10 cross-validation steps and 10 repetitions of the entire cross-validated analysis results in 100 analyses which was averaged, giving the final classification/prediction accuracy (Grootswagers, Wardle and Carlson, 2017; Bode et al., 2019).

For support vector regression (SVR), the only difference to the classification analysis was that the results of SVR are individual correlation coefficients between the predicted variable based on the regression model and their true values, averaged across all 100 analyses (10-fold cross-validation and 10 repetitions). Finally, the Fisher-Z transformation was applied to the correlation coefficients so that the final values could approach a normal distribution (Bode *et al.*, 2019).

Permuted-labels analyses can be used to estimate a distribution for the null hypothesis (in this case the null hypothesis is that the data patterns associated with each category are exchangeable). This was done by repeating all original analyses with the same data and category labels, but with assignment of labels independently randomized for each iteration. The only difference between the actual classification accuracy and the permuted-labels/chance accuracy was that 20 repetitions were used in the permuted-labels calculations rather than 10. The final

statistical chance level was obtained by averaging the estimates from 200 analyses (e.g., 10-fold cross-validation with 20 full repetitions). Then this chance accuracy was compared with the actual classification accuracy to check the statistical significance (Bode *et al.*, 2019). The same permuted-labels analyses were applied to the support vector regression (SVR) analyses for each participant and each condition to obtain a distribution of regression results under the null hypothesis.

For SVM classification and SVR, a moving time window was used to perform the cross-validation calculations and analyses over the pre-target time-period. The choice in window width and step size was based on balancing data size and temporal resolution. All the CFC measures used a 15 ms time window and 15 ms step size which meant that there were 50 timepoints at each electrode. The alpha amplitude metric used a 20 ms time window and 20 ms step size which resulted 50 timepoints at each electrode. All the functional connectivity metrics used a 50 ms (10 timepoints multiplied by the step size of the original calculations) time window and 50 ms (10 timepoints multiplied by the step size of the original calculations) step size which meant that there were 12 timepoints at each electrode. It should be noted that the timepoints in the cross-validation analysis are CFC and functional connectivity measurements calculated from larger time windows so there is less temporal precision than it might appear.

For group level statistical analysis, t-tests using a threshold of $p < 0.05$ were used to compare the empirical results with permuted-labels results (Bode *et al.*, 2019). Subsequently, right-tailed *tmax* permutation testing (number of iterations = 10000, α level = 0.05) was conducted for multiple comparisons correction (Blair and Karniski, 1993).

Feature Weight Analysis. Support vector machine (SVM) feature weights are measures of the relative importance of each feature for classification or regression. Feature weights

describe the contribution of each feature in determining the decision boundary or regression line (Bode *et al.*, 2019). Importantly, a weight parameter does not reflect the contribution of each feature in isolation. Instead, the weight parameter directly reflects the usefulness of that feature to the discrimination or prediction process in the context of the other features (Hebart and Baker, 2018).

For the feature weight analysis, the absolute feature weights were extracted for each electrode at time windows showing significance at the group level. Each electrode weight was calculated as the average feature weight across the time window at that channel. Raw feature weights were transformed using the method introduced by Haufe et al (2014) to ensure accurate topographies. Then the transformed feature weights were converted into *z*-scores and submitted to a right-tailed *tmax* permutation testing (number of iterations = 10000, α level = 0.05) for multiple comparisons correction (Blair and Karniski, 1993). It is important to note that the reliability of activity patterns depends on the quality of the weights which, in turn, rely on classification/prediction performance. If accuracy is low, weights are likely suboptimal, and reconstructed activation patterns have to be interpreted with caution (Haufe *et al.*, 2014; Grootswagers, Wardle and Carlson, 2017).

4.3 RESULTS

Behavioral Data

As can be seen in Figure 4.2, The response errors showed no significant main effects (target side: $Fmax(1,27) = 2.04$ (critical $Fmax = \pm 4.03$), $p = 0.15$; cue type: $Fmax(1,27) < 1$) or interactions ($Fmax(1,27) = 1.36$ (critical $Fmax = \pm 4.16$), $p = 0.25$). In contrast, the absolute response errors, which can be thought of as the magnitude of the response error, had a significant main effect for target side ($Fmax(1,27) = 13.78$ (critical $Fmax = \pm 4.16$), $p < 0.001$), cue type

(*Fmax*(1,27) = 9.80 (critical *Fmax* = ±4.27), $p < 0.01$), and a significant interaction between target side and cue type (*Fmax*(1,27) = 17.19 (critical *Fmax* = ±4.06), $p < 0.001$).

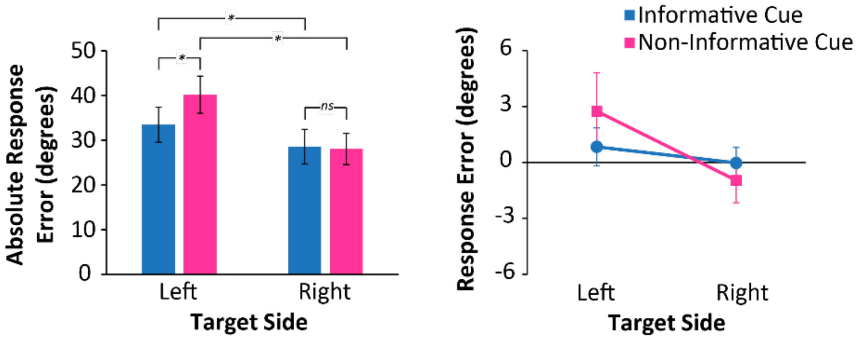

Figure 4.2. *Summary of behavioral results*
Left, significant effects of experimental conditions on the absolute values or magnitude of the response errors. Error bars are the ± *SEM. Right,* the interaction and main effects were not significant for participants' response errors. Error bars are the ±*SEM*

Aperiodic Component

The aperiodic offset and exponent showed no significant main effects or interactions (mean critical *Fmax*(1,27) = +/-14.67 and mean critical *Fmax*(1,27) = +/-15.05, respectively). The quality of fit measures r^2 and fit error also showed no significant main effects or interactions (mean critical *Fmax*(1,27) = +/-13.74 and mean critical *Fmax*(1,27) = +/-16.27, respectively).

Support Vector Machine (SVM) Classification

As shown in Figure 4.3A, the SVM was able to accurately distinguish between trials that had an informative cue from those with a non-informative cue by the spatiotemporal pattern of alpha amplitude before target onset. The classification accuracy was significantly above chance at most of the time windows regardless of whether the target was to appear on the left or right. Feature weight analysis averaged over the entire epoch revealed that the major contributors to the

discrimination process were the central and medial electrodes in the centroparietal, parietal, parietooccipital and occipital brain areas. However, when the targets would appear on the left, the left and central occipital electrodes were not significant contributors to the classification analysis whereas they were for when the upcoming targets would to appear on the right (Figure 4.3B).

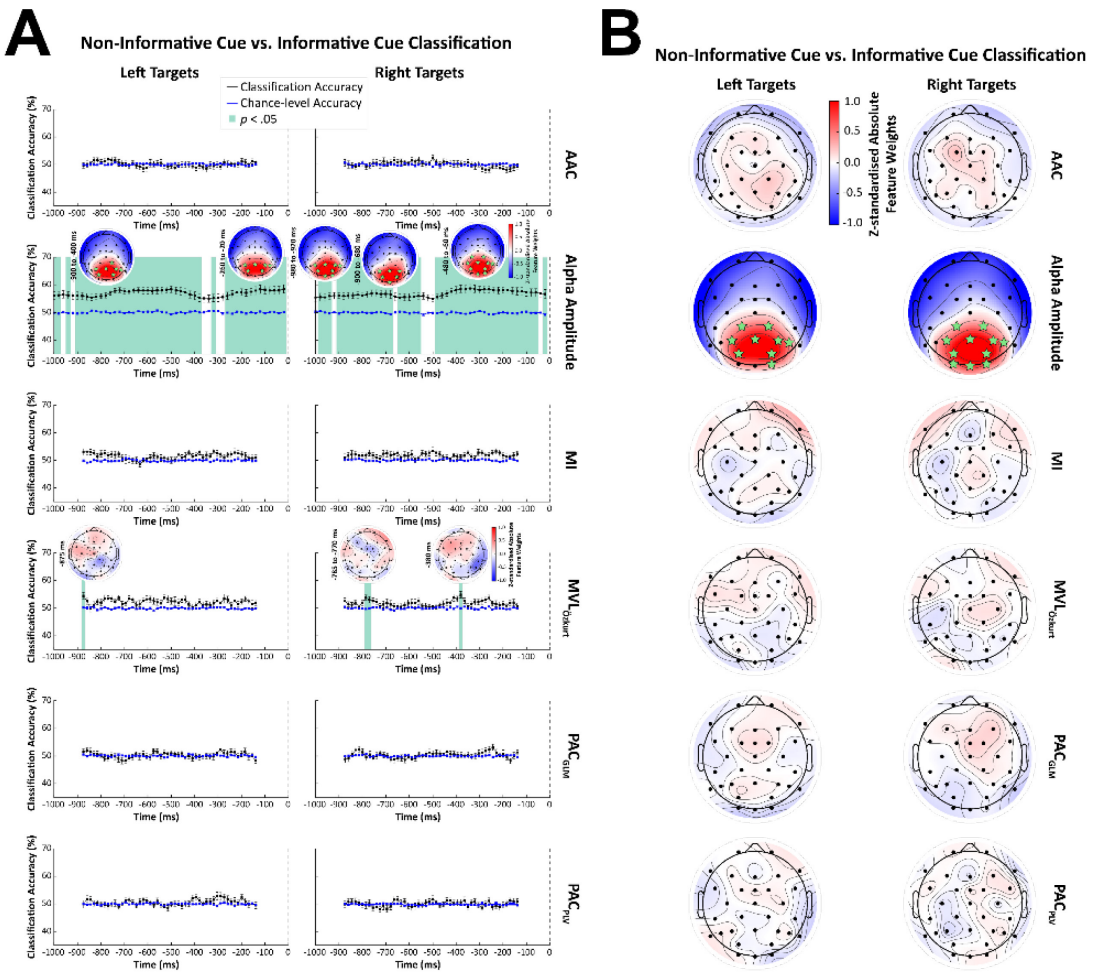

Figure 4.3. *Results from spatiotemporal SVM classification and corresponding feature weight analysis based on alpha amplitude and cross-frequency coupling (CFC) measures*

A) Spatiotemporal classification accuracy of trials with non-informative vs informative cues across all electrodes from alpha amplitude and cross-frequency coupling (CFC) measures. The SVM was trained separately on trials with left targets and trials with

right targets. The black and blue lines show the actual accuracy, and the permutation test results, respectively. Error bars indicate standard error of the mean. The green shaded regions indicate the classification accuracy was significant at these time points ($p < 0.05$, corrected for multiple comparison). The dashed gray line indicates target onset. Topographic plots are the z-standardized absolute feature weights at or across the significant time points indicated by the text to the left of the heads. Green stars on the topographic plots are electrodes found to be significant features after correction for multiple comparisons. **B)** Topographic maps of the *z*-standardized absolute feature weights averaged over the -1000 ms epoch prior to target onset. Green stars indicate the electrodes with *z*-score feature weights significantly above zero after correction for multiple comparisons. Only measures with classification accuracy scores significantly above chance have stars indicating the electrodes with significant feature weight *z*-scores. AAC = amplitude-amplitude coupling; MI = modulation index; MVL = mean vector length; PAC = phase-amplitude coupling.

Cross-Frequency Coupling (CFC)

The only CFC measure with an activity pattern that trained the support vector machine (SVM) to classify trials significantly better than chance was the $MVL_{Özkurt}$ (Figure 4.3A). For left targets, this was at -875 ms relative to target onset; for right targets, this was for the time window -785 to -770 ms and at -380 ms relative to target onset. The feature weights calculated for the entire epoch and at the significant time windows were not significant contributors to determining the decision boundary (Figure 4.3B). Note that because feature weights are only as useful as the information represented by the pattern of activity they are derived from (*e.g.,* the relative importance of electrode activity for classification is meaningless if there is no way to accurately classify trials in the first place), only measures that had classification accuracies above chance are discussed.

Functional Connectivity

The only functional connectivity measure that had classification accuracies above chance was the weighted phase lag index (wPLI). As can be seen in Figure 4.4A, the significantly above chance classification accuracy (black solid line) was only for targets on the right and at -462.5 ms relative to target onset. Feature weight analysis revealed that none of the electrode connections were significant contributors to the decision boundary. The same was for the feature analysis over the entire epoch (Figure 4.4B).

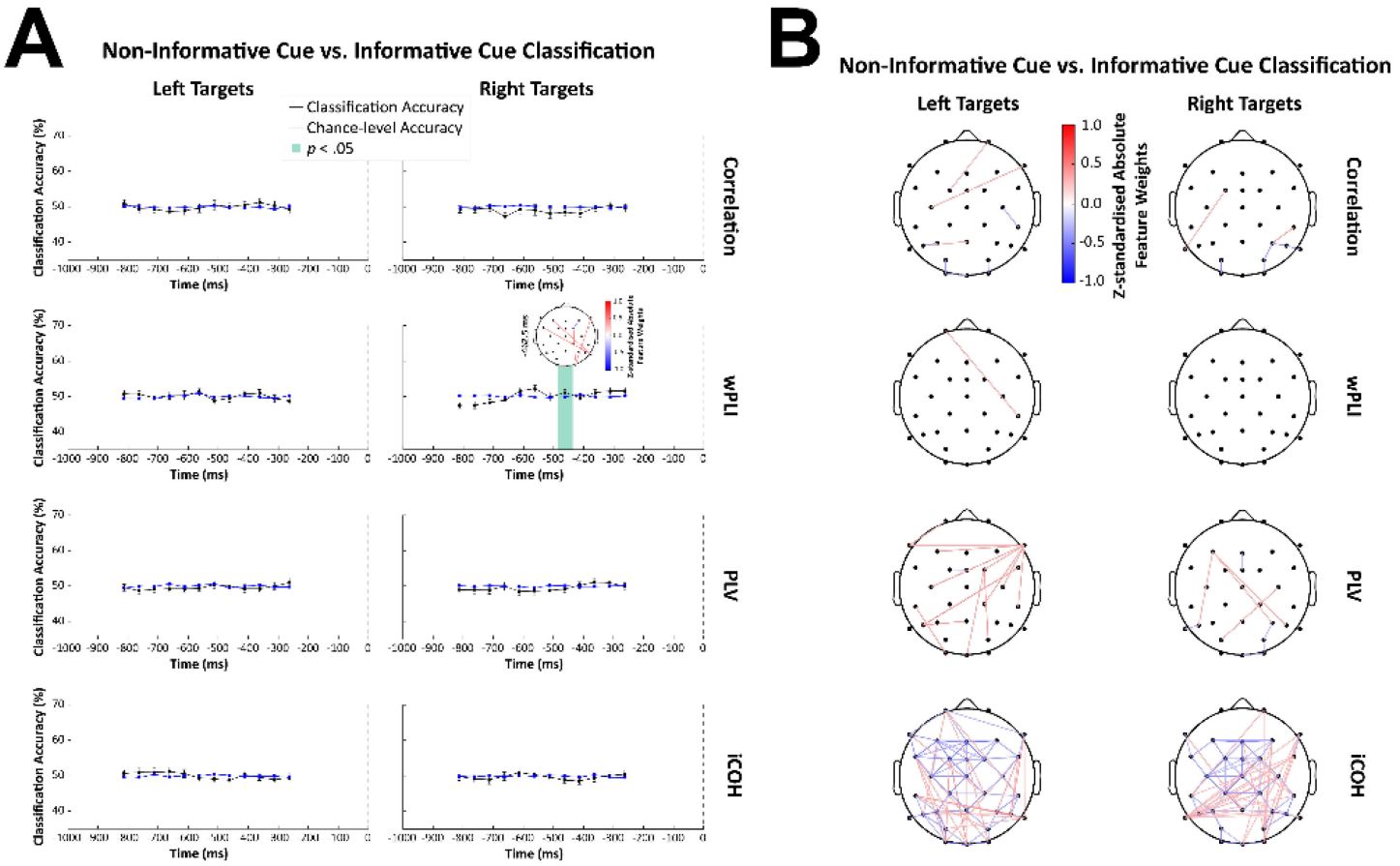

Figure 4.4. *Results from spatiotemporal SVM classification and corresponding feature weight analysis based on functional connectivity metrics*

A) Spatiotemporal classification accuracy of trials with non-informative vs informative cues across all electrodes from functional connectivity measures. The support vector machine (SVM) was trained separately on trials with left targets and trials with right targets. The black and blue lines show the actual accuracy, and the permutation test

results, respectively. The green shaded region indicates the classification accuracy was significant at this time point ($p < 0.05$, corrected for multiple comparison). Error bars indicate standard error of the mean. The dashed gray line indicates target onset. Topographic plot is the z-standardized absolute feature weights at the time point indicated by the text to the left of the head. Only feature weights with a *z*-score exceeding ± 0.45 are shown. **B)** Topographic maps of the *z*-standardized absolute feature weights averaged over the -1000 ms epoch prior to target onset. Only feature weights with a *z*-score exceeding ± 0.3 are shown. Correlation = amplitude envelope correlations; wPLI = weighted phase lag index; PLV = phase locking value; iCOH = imaginary coherence.

Support Vector Regression (SVR)

Support vector regression (SVR) analysis was used to determine whether the spatiotemporal pattern of EEG activity before target onset was predictive of the degree of responsive error on a given trial. As seen in Figure 4.5, predictions of response errors on trials with a right target and non-informative cue from spatiotemporal alpha amplitude patterns were significantly above chance at -640 ms prior to target onset. Feature weight analysis showed that the biggest contributors to prediction accuracy at -640 ms were the occipital, parietooccipital, and parietal electrodes. However, the most lateral parietal electrodes (P7 and P8) were not significant features as well as the next most lateral parietal electrode on the left (P5). The average feature weights across the entire epoch found the same electrodes to be significant contributors as well as the medial centroparietal electrodes CP1 and CP2 (Figure 4.5B). Note that because feature weights are only as useful as the information represented by the pattern of activity they are derived from (*e.g.,* the relative importance of electrode activity to prediction accuracy is meaningless if there is no way to predict response errors in the first place), only measures that had prediction accuracies above chance are discussed.

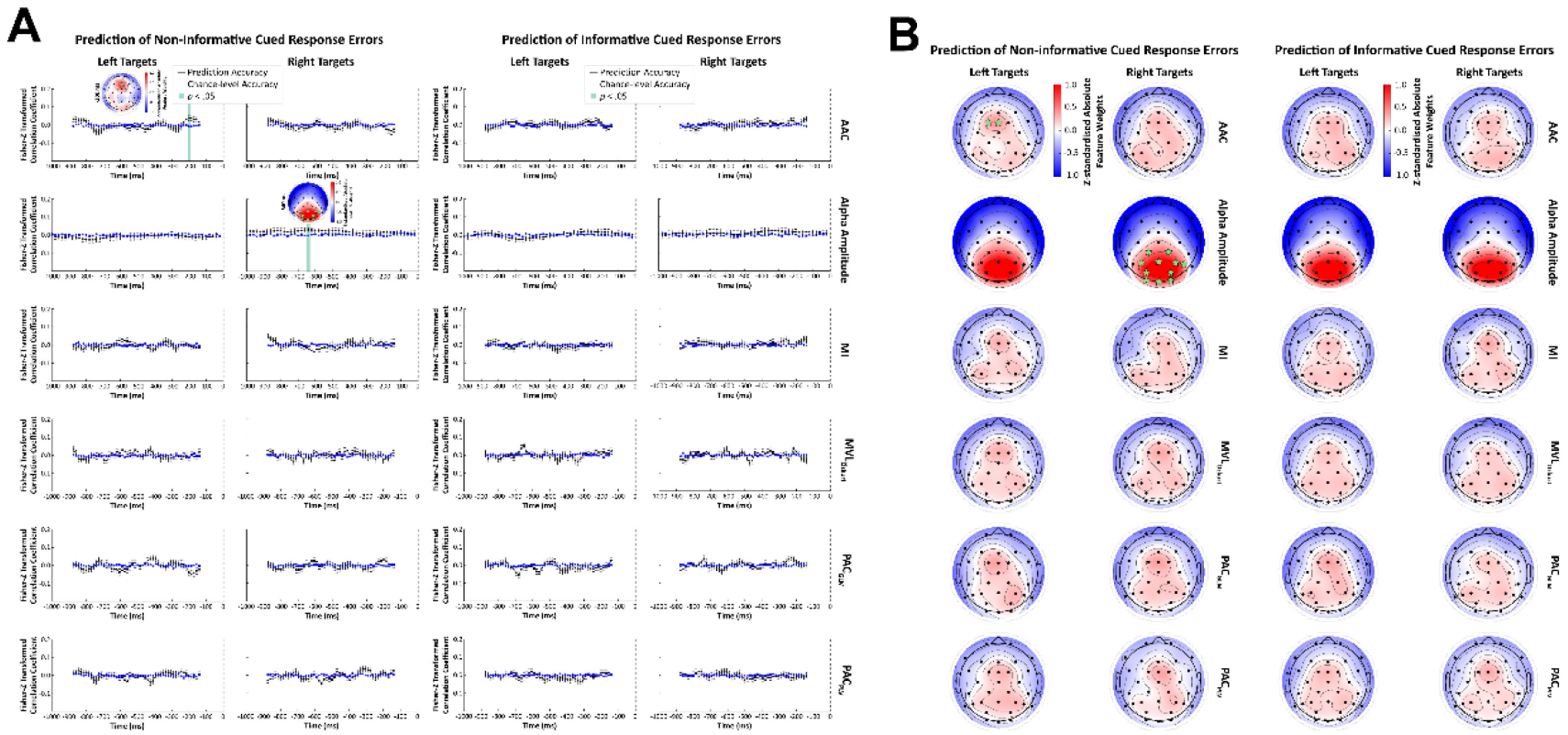

Figure 4.5. *Results from spatiotemporal SVR prediction analysis and corresponding feature weight analysis based on alpha amplitude and cross-frequency coupling (CFC) measures*

A) Spatiotemporal prediction accuracy of response errors across all electrodes for alpha amplitude and cross-frequency coupling (CFC) measures when cues were non-informative (*left*) and informative (*right*). For the non-informative cue and informative cue groups, columns are subdivided by targets on the left and targets on the right. The black and blue lines show the actual accuracy, and the permutation test results, respectively. Error bars indicate standard error of the mean. The dashed gray line indicates target onset. The green shaded regions indicate the prediction accuracy was significant at these time points ($p < 0.05$, corrected for multiple

comparison). Topographic plots are the *z*-standardized absolute feature weights at or across the significant time points indicated by the text to the left of the heads. Green stars on the topographic plots are electrodes found to be significant features after correction for multiple comparisons. **B)** Topographic maps of the *z*-standardized absolute feature weights averaged over the -1000 ms epoch prior to target onset. Green stars indicate the electrodes with z-score feature weights significantly above zero after correction for multiple comparisons. Only the trial condition and measure with prediction accuracy scores significantly above chance have stars indicating the electrodes with significant feature weight *z*-scores. AAC = amplitude-amplitude coupling; MI = modulation index; MVL = mean vector length; PAC = phase-amplitude coupling.

Cross-Frequency Coupling (CFC)

Using the spatiotemporal pattern of amplitude-amplitude coupling (AAC) activity, predictions of response errors on trials with left targets and non-informative cues were significantly above chance at -200 ms relative to target onset (see Figure 4.5A). Feature weight analysis found that the biggest contributor to support vector regression (SVR) accuracy at -200 ms was the frontal electrode Fz. For the entire epoch, the most important features were the left frontocentral electrode FC1 and the frontocentral electrode FCz (Figure 4.5B). No other CFC metric was able to predict response errors above chance level.

Functional Connectivity

The only functional connectivity measure that predicted response errors above chance was the correlation metric (Figure 4.6A). The significant effect was only for trials with a non-informative cue and targets on the left at -562.5 ms relative to target onset. Feature weight analysis revealed that none of the electrode connections were significant contributors to the decision boundary (Figure 4.6B). The same were for feature analysis over the entire epoch.

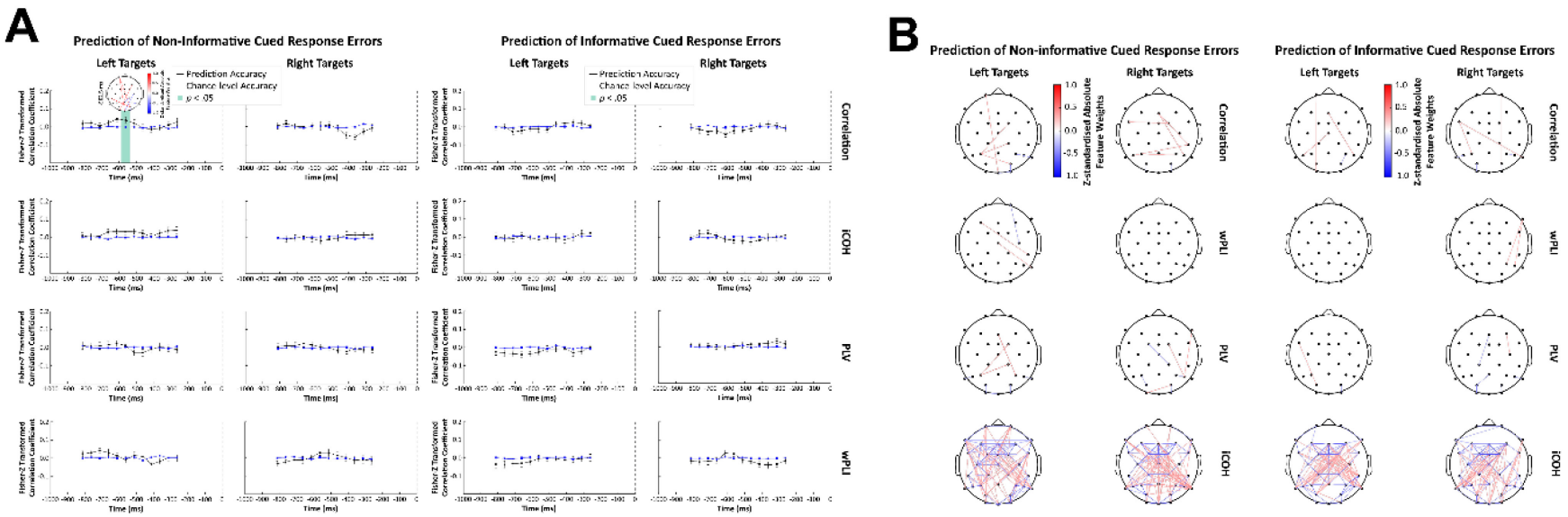

Figure 4.6. *Results from spatiotemporal SVR prediction analysis and corresponding feature weight analysis based on functional connectivity measures*

A) Spatiotemporal prediction accuracy of response errors across all electrodes for the functional connectivity measures when cues were non-informative (*left*) and informative (*right*). For the non-informative cue and informative cue groups, columns are subdivided by targets on the left and targets on the right. The black and blue lines show the actual accuracy, and the permutation test results, respectively. Error bars indicate standard error of the mean. The dashed gray line indicates target onset. The green shaded region indicates the prediction accuracy was significant at that time point ($p < 0.05$, corrected for multiple comparison). Topographic plots are the *z*-standardized absolute feature weights at the significant time point indicated by the text to the left of the heads. Only feature weights with a *z*-score exceeding ± 0.45 are shown. **B)** Topographic maps of the *z*-standardized absolute feature weights averaged over the -1000 ms epoch prior to target onset. Only feature weights with a *z*-score exceeding ± 0.3 are shown. Correlation = amplitude envelope correlations; wPLI = weighted phase lag index; PLV = phase locking value; iCOH = imaginary coherence.

4.4 DISCUSSION

In the current study, we used multivariate pattern analysis (MVPA) to test whether alpha activity, cross-frequency coupling (CFC) between alpha and gamma frequencies, or functional connectivity in alpha could better classify trials with covert spatial attention from those without. We also investigated the amount of underlying predictive information each type of alpha activity contained using MVPA. In line with the baseline sensory excitability model (BSEM) proposed by Samaha et al (2020), alpha activity alone could train a linear support vector machine (SVM) to accurately classify trials prior to the target onset. This means that the spatiotemporal pattern of alpha activity 1000 ms before the target is presented provides the best information for discriminating trials with and without endogenous covert spatial attention. Interestingly, the same activity was only predictive of response errors in trials with a non-informative cue at a very brief time window. This too is in line with the baseline sensory excitability model (BSEM) that predicts changes in alpha amplitude affect the stimulus response and alternative responses (*i.e.,* noise) equally so that discriminability does not change, or, in current study, response errors do not improve.

We also found that the phase-amplitude coupling (PAC) metric $MVL_{Özkurt}$ had a pattern of activity predictive of attention, but only for brief time windows. None of the feature weights were significant making it unclear which electrode or electrodes contributed most to determining the decision boundary although the distribution of feature weight z-scores in the frontal areas suggests that those electrodes contain more information than other spatial locations. Regardless, the support vector regression (SVR) analysis did not find $MVL_{Özkurt}$ activity predictive of response errors which is counter to what we would predict about alpha-gamma phase-amplitude

coupling (PAC) based on the oscillation-based probability of response (OPR) model (Zazio *et al.*, 2020). In contrast, the spatial pattern of amplitude-amplitude coupling between alpha and gamma activity was predictive of response errors on non-informative cued trials towards the end of cue-target interval which is in accordance with the oscillation-based probability of response (OPR) model (Zazio *et al.*, 2020). Feature weight analysis found Fz to be a significant contributor to the determination of the regression line. For the overall time course, FCz and FC1 were significant features in the support vector regression (SVR) prediction analysis of response errors on non-informative cued trials. However, as with the alpha amplitude, amplitude-amplitude coupling activity was found to be a significant predictor of response errors only on trials with a non-informative cue at a very brief time window. Unlike alpha amplitude, amplitude-amplitude coupling did not contain discriminating information with respect to the presence of covert spatial attention suggesting a role in the temporal anticipation for the upcoming target that provides only modest benefits to task performance.

It might seem counterintuitive that the support vector regression (SVR) results were specific to left targets or right targets when the cue was non-informative. Afterall, a non-informative cue means that participants did not know where the target will appear so they could not be influenced by the target's location during the analyzed time window. However, the SVR analysis is using the EEG data to predict response errors which are influenced by the target's location (see Behavioral Data section under Results). Furthermore, response errors showed an interaction between cue type and target side which might, in part, be attributed to the complex spatiotemporal pattern of alpha-related brain activity prior to target onset.

Even though we did not find as strong of evidence supporting the oscillation-based probability of response (OPR) model (Zazio *et al.*, 2020), that does not mean it should be

discarded. Many findings on alpha-gamma phase-amplitude coupling (PAC) are for the high gamma frequency range, something that surface EEGs are not suitable for recording due to attenuation of the electrical signals by skull and scalp. For example, Voytek (2010) found phase-amplitude coupling between theta/alpha and 80-150 Hz gamma in two participants with implanted subdural electrocorticography in visual cortical regions during visual tasks. Bonnefond and Jensen (2015) also found that the phase of alpha oscillations was coupled with the power of 80-120 Hz gamma band activity in visual sensory regions during an anticipatory pre-distractor period. Therefore, it is possible alpha-gamma phase-amplitude coupling (PAC) is important to attentional modulation. However, at least in the current study, measuring gamma oscillations with scalp EEG has methodological difficulties due to contamination by eye- and muscle-related artifacts at the same frequencies. These artifacts coupled with gamma's inherently low amplitude means that PAC may be important to attentional modulation, but the gamma frequency this occurs at is too fast to be studied with recordings from outside the head.

It is important to note that while the EEG signal was filtered around the peak frequency of the aperiodic-adjusted alpha band activity, the instantaneous amplitudes extracted from the filtered signal were not aperiodic-adjusted since the FOOOF algorithm is not designed or easily adaptable for time-resolved analysis (Donoghue *et al.*, 2020). However, we did not find the aperiodic activity to vary significantly with the experimental conditions suggesting that the current results cannot be attributed to changes in the broadband activity. At the same time, the aperiodic component was not removed from the EEG signal so it cannot be discounted entirely.

The current study only focused on activity in the alpha frequency band and its interactions with gamma band activity since it has been the major focus of research on visual spatial attention and perception. However, activity patterns within and between other frequency

bands have been implicated in attentional and perceptual functioning (Clayton, Yeung and Cohen Kadosh, 2015; Yuan *et al.*, 2021). For example, previous research has found that prestimulus theta activity (4-7 Hz) is also associated with perceptual outcomes and attentional modulation (Landau *et al.*, 2015; Fiebelkorn and Kastner, 2019). In the current study, the cue-target interval was a little too short to adequately capture frequencies below alpha, but this is something that future studies can easily change by making small adjustments to the task design. Longer cue-target intervals would have the additional benefit of being long enough for time-resolved versions of other types of connectivity analysis such as those that test for directionality like Granger causality and phase transfer entropy (Cohen and van Gaal, 2013; Bastos and Schoffelen, 2016; O'Neill *et al.*, 2018).

The functional connectivity metrics used in the current study are a small subset of the methods that are available. Most recent studies combining brain connectivity estimations with machine learning methods focus on various neurological conditions with much less extensive evidence on functional connectivity influencing perceptual responses (Cao *et al.*, 2022; Sadaghiani, Brookes and Baillet, 2022). It is very possible that functional connectivity contains more decodable information about the task conditions and performance measures than these results suggest. If temporal order or coupling direction contain the most decodable information about covert spatial attention and task performance, our functional connectivity measures would not be able to capture it. Furthermore, research has found theta band activity to also be important for coordinating different attention-related brain regions (Gootjes *et al.*, 2006; Clayton, Yeung and Cohen Kadosh, 2015; Fiebelkorn, Pinsk and Kastner, 2018; Fiebelkorn and Kastner, 2019) which would explain why we found little evidence for alpha functional connectivity.

Summary

Overall, we find more evidence supporting the baseline sensory excitability model (BSEM) proposed by Samaha *et al* (2020) than the oscillation-based probability of response (OPR) model put forth by Zazio *et al* (2020). However, the inherent limitations in the current study mean that this should not be taken as invaliding the oscillation-based probability of response (OPR) model. Instead, these results highlight the need for further investigation into the role of cross-frequency coupling (CFC) and functional connectivity in attention and visual perception. Future research can expand on our multivariate approach by investigating a wider range of frequencies whose role might have gone unnoticed due to complex spatiotemporal dynamics that are difficult to detect with traditional univariate approaches.

References

Aru, Juhan *et al.* (2015) 'Untangling cross-frequency coupling in neuroscience', *Current Opinion in Neurobiology*. Elsevier Ltd, 31, pp. 51–61. doi: 10.1016/j.conb.2014.08.002.

Bastos, A. M. and Schoffelen, J.-M. (2016) 'A Tutorial Review of Functional Connectivity Analysis Methods and Their Interpretational Pitfalls', *Frontiers in Systems Neuroscience*. Frontiers, 9, p. Article 175. doi: 10.3389/fnsys.2015.00175.

Ben-Hur, A. and Weston, J. (2010) 'A User's Guide to Support Vector Machines', in Carugo, O. and Eisenhaber, F. (eds) *Data Mining Techniques for the Life Sciences*. Totowa, NJ: Humana Press, pp. 223–239. doi: 10.1007/978-1-60327-241-4_13.

Benwell, C. S. Y. *et al.* (2018) 'Trial-by-trial co-variation of pre-stimulus EEG alpha power and visuospatial bias reflects a mixture of stochastic and deterministic effects', *European Journal of Neuroscience*. Blackwell Publishing Ltd, 48(7), pp. 2566–2584. doi: 10.1111/ejn.13688.

Berger, H. (1929) 'Über das Elektrenkephalogramm des Menschen', *Archiv für Psychiatrie und Nervenkrankheiten*. Springer-Verlag, 87(1), pp. 527–570. doi: 10.1007/BF01797193.

Bishop, C. M. (2006) *Pattern Recognition and Machine Learning (Information Science and Statistics)*. New York, NY: Springer.

Blair, R. C. and Karniski, W. (1993) 'An alternative method for significance testing of waveform difference potentials', *Psychophysiology*. John Wiley & Sons, Ltd, 30(5), pp. 518–524. doi: 10.1111/j.1469-8986.1993.tb02075.x.

Bode, S. *et al.* (2019) 'The Decision Decoding ToolBOX (DDTBOX) – A Multivariate Pattern Analysis Toolbox for Event-Related Potentials', *Neuroinformatics*. Humana Press Inc., 17(1), pp. 27–42. doi: 10.1007/s12021-018-9375-z.

Bonnefond, M. and Jensen, O. (2015) 'Gamma Activity Coupled to Alpha Phase as a Mechanism for Top-Down Controlled Gating', *PLOS ONE*. Public Library of Science, 10(6), p. e0128667. Available at: https://doi.org/10.1371/journal.pone.0128667.

Brainard, D. H. (1997) 'The Psychophysics Toolbox.', *Spatial vision*, 10(4), pp. 433–436. Available at: http://www.ncbi.nlm.nih.gov/pubmed/9176952 (Accessed: 5 October 2017).

Bruns, A. and Eckhorn, R. (2004) 'Task-related coupling from high- to low-frequency signals among visual cortical areas in human subdural recordings', *International Journal of Psychophysiology*, 51(2), pp. 97–116. doi: https://doi.org/10.1016/j.ijpsycho.2003.07.001.

Canolty, R. T. *et al.* (2006) 'High gamma power is phase-locked to theta oscillations in human neocortex', *Science*, 313(5793), pp. 1626–1628. doi: 10.1126/SCIENCE.1128115.

Cao, J. *et al.* (2022) 'Brain functional and effective connectivity based on electroencephalography recordings: A review', *Human Brain Mapping*. John Wiley & Sons, Ltd, 43(2), pp. 860–879. doi: https://doi.org/10.1002/hbm.25683.

Chang, C.-C. and Lin, C.-J. (2011) 'LIBSVM: a library for support vector machines', *ACM Transactions on Intelligent Systems and Technology*, 2(3), pp. 1–27. Available at: http://www.csie.ntu.edu.tw/~cjlin/libsvm.

Chaumon, M. and Busch, N. A. (2014) 'Prestimulus neural oscillations inhibit visual perception via modulation of response gain', *Journal of Cognitive Neuroscience*. MIT Press Journals, 26(11), pp. 2514–2529. doi: 10.1162/jocn_a_00653.

Clayton, M. S., Yeung, N. and Cohen Kadosh, R. (2015) 'The roles of cortical oscillations in sustained attention', *Trends in Cognitive Sciences*. Elsevier Ltd, pp. 188–195. doi: 10.1016/j.tics.2015.02.004.

Cohen, M. X. (2008) ‘Assessing transient cross-frequency coupling in EEG data’, *Journal of Neuroscience Methods*. Elsevier, 168(2), pp. 494–499. doi: 10.1016/j.jneumeth.2007.10.012.

Cohen, M. X. (2014) *Analyzing neural time series data: theory and practice*. Cambridge, Massachusetts: MIT Press.

Cohen, M. X. (2015) ‘Effects of time lag and frequency matching on phase-based connectivity’, *Journal of Neuroscience Methods*, 250, pp. 137–146. doi: https://doi.org/10.1016/j.jneumeth.2014.09.005.

Cohen, M. X. and van Gaal, S. (2013) ‘Dynamic interactions between large-scale brain networks predict behavioral adaptation after perceptual errors’, *Cerebral Cortex*. 2012/04/18. Oxford University Press, 23(5), pp. 1061–1072. doi: 10.1093/cercor/bhs069.

Davoudi, S., Ahmadi, A. and Daliri, M. R. (2020) ‘Frequency–amplitude coupling: a new approach for decoding of attended features in covert visual attention task’, *Neural Computing and Applications*. Springer, pp. 1–16. doi: 10.1007/s00521-020-05222-w.

Doesburg, S. M., Bedo, N. and Ward, L. M. (2016) ‘Top-down alpha oscillatory network interactions during visuospatial attention orienting’, *NeuroImage*, 132, pp. 512–519. doi: https://doi.org/10.1016/j.neuroimage.2016.02.076.

Donoghue, T. *et al.* (2020) ‘Parameterizing neural power spectra into periodic and aperiodic components’, *Nature Neuroscience 2020 23:12*. Nature Publishing Group, 23(12), pp. 1655–1665. doi: 10.1038/s41593-020-00744-x.

Fiebelkorn, I. C. and Kastner, S. (2019) ‘A Rhythmic Theory of Attention’, *Trends in Cognitive Sciences*. Elsevier Current Trends, 23(2), pp. 87–101. doi: 10.1016/j.tics.2018.11.009.

Fiebelkorn, I. C., Pinsk, M. A. and Kastner, S. (2018) ‘A Dynamic Interplay within the

Frontoparietal Network Underlies Rhythmic Spatial Attention', *Neuron*, 99(4), pp. 842-853.e8. doi: https://doi.org/10.1016/j.neuron.2018.07.038.

Fields, E. C. (2017) 'Factorial Mass Univariate ERP Toolbox'. Available at: https://github.com/ericcfields/FMUT/releases.

Fields, E. C. and Kuperberg, G. R. (2019) 'Having your cake and eating it too: Flexibility and power with mass univariate statistics for ERP data', *Psychophysiology*. doi: 10.1111/psyp.13468.

Foxe, J. J. and Snyder, A. C. (2011) 'The role of alpha-band brain oscillations as a sensory suppression mechanism during selective attention', *Frontiers in Psychology*. Frontiers Media SA, 2, p. Article 154. doi: 10.3389/fpsyg.2011.00154.

Frey, J. N., Ruhnau, P. and Weisz, N. (2015) 'Not so different after all: The same oscillatory processes support different types of attention', *Brain Research*. Elsevier, 1626, pp. 183–197. doi: 10.1016/J.BRAINRES.2015.02.017.

García-Pérez, M. A. (1998) 'Forced-choice staircases with fixed step sizes: asymptotic and small-sample properties', *Vision Research*, 38(12), pp. 1861–1881. doi: 10.1016/S0042-6989(97)00340-4.

Gootjes, L. *et al.* (2006) 'Attention modulates hemispheric differences in functional connectivity: Evidence from MEG recordings', *NeuroImage*, 30(1), pp. 245–253. doi: https://doi.org/10.1016/j.neuroimage.2005.09.015.

de Graaf, T. A. *et al.* (2020) 'Does alpha phase modulate visual target detection? Three experiments with tACS-phase-based stimulus presentation', *European Journal of Neuroscience*. Blackwell Publishing Ltd, 51(11), pp. 2299–2313. doi: 10.1111/ejn.14677.

Grootswagers, T., Wardle, S. G. and Carlson, T. A. (2017) 'Decoding dynamic brain patterns

from evoked responses: A tutorial on multivariate pattern analysis applied to time series neuroimaging data', *Journal of Cognitive Neuroscience*. MIT Press Journals, 29(4), pp. 677–697. doi: 10.1162/jocn_a_01068.

Hakim, N. *et al.* (2019) 'Dissecting the Neural Focus of Attention Reveals Distinct Processes for Spatial Attention and Object-Based Storage in Visual Working Memory', *Psychological Science*. SAGE Publications Inc., 30(4), pp. 526–540. doi: 10.1177/0956797619830384.

Hamidi, M. (2009) 'Repetitive transcranial magnetic stimulation affects behavior by biasing endogenous cortical oscillations', *Frontiers in Integrative Neuroscience*. Frontiers, 3(JUN), p. 14. doi: 10.3389/neuro.07.014.2009.

Haufe, S. *et al.* (2014) 'On the interpretation of weight vectors of linear models in multivariate neuroimaging', *NeuroImage*. Academic Press Inc., 87, pp. 96–110. doi: 10.1016/j.neuroimage.2013.10.067.

Hebart, M. N. and Baker, C. I. (2018) 'Deconstructing multivariate decoding for the study of brain function', *NeuroImage*. Academic Press, pp. 4–18. doi: 10.1016/j.neuroimage.2017.08.005.

Herring, J. D. *et al.* (2019) 'Low-frequency alternating current stimulation rhythmically suppresses gamma-band oscillations and impairs perceptual performance', *NeuroImage*, 184, pp. 440–449. Available at: https://www.sciencedirect.com/science/article/pii/S1053811918318469 (Accessed: 27 November 2018).

Hogendoorn, H. (2015) 'From sensation to perception: Using multivariate classification of visual illusions to identify neural correlates of conscious awareness in space and time', *Perception*, 44(1), pp. 71–78. doi: 10.1068/p7832.

Hong, X. *et al.* (2015) 'Normal aging selectively diminishes alpha lateralization in visual spatial attention', *NeuroImage*. Academic Press Inc., 106, pp. 353–363. doi: 10.1016/j.neuroimage.2014.11.019.

Hülsemann, M. J., Naumann, E. and Rasch, B. (2019) 'Quantification of phase-amplitude coupling in neuronal oscillations:comparison of phase-locking value, mean vector length, modulation index, and generalized-linear-modeling-cross-frequency-coupling', *Frontiers in Neuroscience*. Frontiers Media S.A., 13, p. Article 573. doi: 10.3389/fnins.2019.00573.

Iemi, L. and Busch, N. A. (2018) 'Moment-to-moment fluctuations in neuronal excitability bias subjective perception rather than strategic decision-making', *eNeuro*. Society for Neuroscience, 5(3). doi: 10.1523/ENEURO.0430-17.2018.

James, G. *et al.* (2021) *An Introduction to Statistical Learning*. 2nd edn. New York, NY: Springer US (Springer Texts in Statistics). doi: 10.1007/978-1-0716-1418-1.

Jensen, O. *et al.* (2014) 'Temporal coding organized by coupled alpha and gamma oscillations prioritize visual processing', *Trends in Neurosciences*. Elsevier Ltd, 37(7), pp. 357–369. doi: 10.1016/j.tins.2014.04.001.

Jensen, O. and Colgin, L. L. (2007) 'Cross-frequency coupling between neuronal oscillations', *Trends in Cognitive Sciences*, 11(7), pp. 267–269. doi: 10.1016/j.tics.2007.05.003.

Jensen, O. and Mazaheri, A. (2010) 'Shaping functional architecture by oscillatory alpha activity: Gating by inhibition', *Frontiers in Human Neuroscience*. Frontiers Media S. A., 4, p. 186. doi: 10.3389/fnhum.2010.00186.

Kayser, J. and Tenke, C. E. (2015) 'Issues and considerations for using the scalp surface Laplacian in EEG/ERP research: A tutorial review', *International Journal of*

Psychophysiology, 97(3), pp. 189–209. doi: 10.1016/j.ijpsycho.2015.04.012.

Kingdom, F. A. A. and Prins, N. (2016) 'Chapter 5 – Adaptive Methods', in *Psychophysics*. Second Edi. San Diego: Academic Press, pp. 119–148. doi: 10.1016/B978-0-12-407156-8.00005-0.

Klimesch, W. (2012) 'Alpha-band oscillations, attention, and controlled access to stored information', *Trends in Cognitive Sciences*. Elsevier, 16(12), pp. 606–617. doi: 10.1016/j.tics.2012.10.007.

Klimesch, W., Sauseng, P. and Hanslmayr, S. (2007) 'EEG alpha oscillations: the inhibition–timing hypothesis', *Brain Research Reviews*, 53(1), pp. 63–88. doi: 10.1016/j.brainresrev.2006.06.003.

Kuntzelman, K. M. *et al.* (2021) 'Deep-Learning-Based Multivariate Pattern Analysis (dMVPA): A Tutorial and a Toolbox', *Frontiers in Human Neuroscience*, 15, p. Article 89. doi: 10.3389/fnhum.2021.638052.

Lachaux, J.-P. *et al.* (1999) 'Measuring phase synchrony in brain signals', *Human Brain Mapping*, 8(4), pp. 194–208. Available at: https://onlinelibrary.wiley.com/doi/epdf/10.1002/%28SICI%291097-0193%281999%298%3A4%3C194%3A%3AAID-HBM4%3E3.0.CO%3B2-C.

Landau, A. N. *et al.* (2015) 'Distributed Attention Is Implemented through Theta-Rhythmic Gamma Modulation', *Current Biology*. Cell Press, 25(17), pp. 2332–2337. doi: 10.1016/j.cub.2015.07.048.

Luck, S. J. (2014) *An introduction to the event-related potential technique*. 2nd edn. Cambridge, Massachusetts: MIT Press. Available at: https://www.library.ualberta.ca/catalog/7776529 (Accessed: 9 November 2017).

Martinez-Cancino, R. *et al.* (2020) 'Computing Phase Amplitude Coupling in EEGLAB: PACTools', *Proceedings - IEEE 20th International Conference on Bioinformatics and Bioengineering, BIBE 2020*. Institute of Electrical and Electronics Engineers Inc., pp. 387–394. doi: 10.1109/BIBE50027.2020.00070.

Mathewson, K. E. *et al.* (2011) 'Pulsed out of awareness: EEG alpha oscillations represent a pulsed-inhibition of ongoing cortical processing.', *Frontiers in Psychology*, 2, p. Article 99. doi: 10.3389/fpsyg.2011.00099.

Mathewson, K. E. *et al.* (2012) 'Making waves in the stream of consciousness: entraining oscillations in EEG alpha and fluctuations in visual awareness with rhythmic visual stimulation', *Journal of Cognitive Neuroscience*. MIT Press, 24(12), pp. 2321–2333. doi: 10.1162/jocn_a_00288.

Ni, J. *et al.* (2016) 'Gamma-Rhythmic Gain Modulation', *Neuron*. Cell Press, 92(1), pp. 240–251. doi: 10.1016/j.neuron.2016.09.003.

Nolte, G. *et al.* (2004) 'Identifying true brain interaction from EEG data using the imaginary part of coherency', *Clinical Neurophysiology*, 115(10), pp. 2292–2307. doi: https://doi.org/10.1016/j.clinph.2004.04.029.

O'Neill, G. C. *et al.* (2018) 'Dynamics of large-scale electrophysiological networks: A technical review', *NeuroImage*, 180, pp. 559–576. doi: https://doi.org/10.1016/j.neuroimage.2017.10.003.

Okazaki, Y. O., Mizuno, Y. and Kitajo, K. (2020) 'Probing dynamical cortical gating of attention with concurrent TMS-EEG', *Scientific Reports*. Nature Research, 10(1), pp. 1–10. doi: 10.1038/s41598-020-61590-2.

Oostenveld, R. *et al.* (2011) 'FieldTrip: Open source software for advanced analysis of MEG,

EEG, and invasive electrophysiological data', *Computational Intelligence and Neuroscience*. Hindawi Limited, 2011, p. Article 156869. doi: 10.1155/2011/156869.

Özkurt, T. E. and Schnitzler, A. (2011) 'A critical note on the definition of phase–amplitude cross-frequency coupling', *Journal of Neuroscience Methods*. Elsevier, 201(2), pp. 438–443. doi: 10.1016/J.JNEUMETH.2011.08.014.

Pelli, D. G. (1997) 'The VideoToolbox software for visual psychophysics: transforming numbers into movies.', *Spatial vision*, 10(4), pp. 437–442. Available at: http://www.ncbi.nlm.nih.gov/pubmed/9176953 (Accessed: 5 October 2017).

Penny, W. D. *et al.* (2008) 'Testing for nested oscillation', *Journal of Neuroscience Methods*. Elsevier, 174(1), pp. 50–61. doi: 10.1016/j.jneumeth.2008.06.035.

Perrin, F. *et al.* (1989) 'Spherical splines for scalp potential and current density mapping', *Electroencephalography and Clinical Neurophysiology*, 72(2), pp. 184–187. doi: 10.1016/0013-4694(89)90180-6.

Pezoulas, V. C. *et al.* (2018) 'FCLAB: An EEGLAB module for performing functional connectivity analysis on single-subject EEG data', in *2018 IEEE EMBS International Conference on Biomedical & Health Informatics (BHI)*. IEEE, pp. 96–99. doi: 10.1109/BHI.2018.8333378.

Plomp, G. *et al.* (2015) 'Early recurrence and ongoing parietal driving during elementary visual processing', *Scientific reports*. Nature Publishing Group, 5, p. 18733. doi: 10.1038/srep18733.

Pritchett, D. L. *et al.* (2015) 'For things needing your attention: The role of neocortical gamma in sensory perception', *Current Opinion in Neurobiology*. Elsevier Ltd, pp. 254–263. doi: 10.1016/j.conb.2015.02.004.

Raybaut, P. (2009) 'Spyder-documentation', *Available online at: pythonhosted.org*. Available at: https://www.spyder-ide.org/.

Ritchie, J. B., Kaplan, D. M. and Klein, C. (2019) 'Decoding the Brain: Neural Representation and the Limits of Multivariate Pattern Analysis in Cognitive Neuroscience', *The British Journal for the Philosophy of Science*, 70(2), pp. 581–607. doi: 10.1093/bjps/axx023.

Sadaghiani, S., Brookes, M. J. and Baillet, S. (2022) 'Connectomics of human electrophysiology', *NeuroImage*, 247, p. 118788. doi: https://doi.org/10.1016/j.neuroimage.2021.118788.

Sadaghiani, S. and Kleinschmidt, A. (2016) 'Brain Networks and α-Oscillations: Structural and Functional Foundations of Cognitive Control', *Trends in Cognitive Sciences*, 20(11), pp. 805–817. doi: https://doi.org/10.1016/j.tics.2016.09.004.

Samaha, J. *et al.* (2020) 'Spontaneous Brain Oscillations and Perceptual Decision-Making', *Trends in Cognitive Sciences*. Elsevier Ltd, 24(8), pp. 639–653. doi: 10.1016/j.tics.2020.05.004.

Samaha, J., Iemi, L. and Postle, B. R. (2017) 'Prestimulus alpha-band power biases visual discrimination confidence, but not accuracy', *Consciousness and Cognition*. Academic Press, 54, pp. 47–55. doi: 10.1016/J.CONCOG.2017.02.005.

Samuel, I. B. H. *et al.* (2018) 'The frequency of alpha oscillations: Task-dependent modulation and its functional significance', *NeuroImage*. Academic Press Inc., 183, pp. 897–906. doi: 10.1016/j.neuroimage.2018.08.063.

Seymour, R. A., Rippon, G. and Kessler, K. (2017) 'The Detection of Phase Amplitude Coupling during Sensory Processing', *Frontiers in Neuroscience*. Frontiers Media S.A., 11(SEP), p. 487. doi: 10.3389/fnins.2017.00487.

Sheldon, S. S. and Mathewson, K. E. (2021) 'To see, not to see or to see poorly: Perceptual quality and guess rate as a function of electroencephalography (EEG) brain activity in an orientation perception task', *European Journal of Neuroscience*. John Wiley & Sons, Ltd, pp. 1–24. doi: https://doi.org/10.1111/ejn.15445.

Taghizadeh-Sarabi, M., Daliri, M. R. and Niksirat, K. S. (2014) 'Decoding Objects of Basic Categories from Electroencephalographic Signals Using Wavelet Transform and Support Vector Machines', *Brain Topography*. Springer, 28(1), pp. 33–46. doi: 10.1007/S10548-014-0371-9.

Tort, A. B. L. *et al.* (2008) 'Dynamic cross-frequency couplings of local field potential oscillations in rat striatum and hippocampus during performance of a T-maze task', *Proceedings of the National Academy of Sciences*. National Academy of Sciences, 105(51), pp. 20517–20522. doi: 10.1073/PNAS.0810524105.

Tort, A. B. L. *et al.* (2010) 'Measuring Phase-Amplitude Coupling Between Neuronal Oscillations of Different Frequencies', *Journal of Neurophysiology*, 104(2), pp. 1195–1210. doi: 10.1152/jn.00106.2010.

VanRullen, R. (2016) 'Perceptual cycles', *Trends in Cognitive Sciences*. Elsevier Current Trends, 20(10), pp. 723–735. doi: 10.1016/j.tics.2016.07.006.

Vinck, M. *et al.* (2011) 'An improved index of phase-synchronization for electrophysiological data in the presence of volume-conduction, noise and sample-size bias', *NeuroImage*, 55(4), pp. 1548–1565. doi: https://doi.org/10.1016/j.neuroimage.2011.01.055.

Voytek, B. (2010) 'Shifts in gamma phase–amplitude coupling frequency from theta to alpha over posterior cortex during visual tasks', *Frontiers in Human Neuroscience*. Frontiers Media S. A., 4, p. 191. doi: 10.3389/fnhum.2010.00191.

Yuan, Z. *et al.* (2021) 'The Modulating Effect of Top-down Attention on the Optimal Pre-target Onset Oscillatory States of Bottom-up Attention', *Neuroscience*. Pergamon, 466, pp. 186–195. doi: 10.1016/J.NEUROSCIENCE.2021.03.036.

Zazio, A. *et al.* (2020) 'Modelling the effects of ongoing alpha activity on visual perception: The oscillation-based probability of response', *Neuroscience & Biobehavioral Reviews*. Elsevier Ltd, 112, pp. 242–253. doi: 10.1016/j.neubiorev.2020.01.037.

5

CONCLUSION

In this dissertation, we have examined new methods for investigating the neural mechanisms that connect visual perception and attention to perceptual performance. These new methods include the novel application of probabilistic models from the visual working memory literature to quantify performance on the basic and cued attention versions of our orientation perception task. We also applied a new algorithm that parameterizes neural power spectra (Donoghue *et al.*, 2020) to examine the task-related changes in the alpha (8-14 Hz) and low beta (15-22 Hz) oscillatory component and the 1/f aperiodic component of the electrophysiological brain data. Finally, we used a type of machine learning called multivariate pattern analysis (MVPA) to investigate the spatiotemporal dynamics of alpha band activity in covert attention and visual perception and determine whether some of the popular models about alpha oscillation functioning can hold up to the information-rich evidence provided by MVPA.

The primary purpose of this research was to better understand visual perception, attention, and their underlying neural mechanisms. Specifically, the current experiments sought to address these three main questions: (1) what is the role of EEG recorded activity in visual perception; (2) what is the role of EEG brain activity in visual attention; and (3) what is the best way to associate these relationships to behavior? The first step in addressing these questions was the experiment in Chapter 2 which used an orientation perception task to introduce the concept of applying models from the working memory literature to studying the relationship between brain activity and visual perception. Through this application, it was found that the relationship between perceptual performance and EEG brain activity could be quantified using the standard

mixture model (Zhang and Luck, 2008). This led to the finding that participants' response errors have a fixed amount of variability and that the actual error values are modulated by the level of 2-3 Hz brain activity after target onset. Together, these results imply that there is a lower limit to forming or stabilizing a perceptual representation which is related, at least in part, to the level of 2-3 Hz EEG activity following target onset.

Addressing the second question was the primary goal of Chapter 3. This was done by modifying the orientation perception task to include a cued attention component and extending the application of the standard mixture model to investigate the relationship between attention, perceptual performance, and EEG brain activity. The first notable finding was that visuospatial attention asymmetry manifests as a right negativity starting during the cue-target interval, and that the continuation of this negativity into the post-target time period underlies how left attentional cues improved perceptual performance more than the right attentional cues. The second notable finding was that a similar shift in the E:I balance as reflected by changes in the aperiodic 1/f activity (Gao, Peterson and Voytek, 2017) also coincided with attention modulation and task performance, possibly providing a mechanistic explanation for these results. While hemispheric lateralization during visuospatial attention have been noted by many other researchers (Kim *et al.*, 1999; Bartolomeo, 2006; Siman-Tov *et al.*, 2007), these results suggests that the underlying explanation for these observations is a persistent state of excitation in the left parietal area which can be well captured by the aperiodic component of EEG brain activity.

Finally, Chapter 4 sought to directly test the role of pre-target EEG brain activity in visual perception and attention. Through the application of multivariate statistics, it was found that the spatiotemporal pattern of alpha activity best represents the differences between trials with and without covert attention though it did not predict how that attention affects subsequent

perceptual performance. On the other hand, it was found that without informative cues, perceptual performance is likely related to the level of amplitude-amplitude coupling between alpha and gamma prior to target onset. Together, these results support the hypothesis that attentional effects before target onset are mediated by changes in alpha activity alone which, in turn, modulates baseline cortical excitability and the probability of a responding to a stimulus without improving the quality of the perceptual response (Samaha *et al.*, 2020).

Overall, these results demonstrate that there is more complexity to the relationship between EEG brain activity and visual perception and attention than was previously thought. Most previous work has focused on alpha band (8-14 Hz) activity which might be limiting the full scope of spatial and temporal mechanisms responsible for these processes. Undoubtedly alpha activity plays an important role in covert attention, and, to some degree, perceptual responses as shown in Chapter 4. However, there remains a lot of unknowns about how pre-target brain activity and anticipatory attentional modulation relates to variations in task performance. While the previous studies and proposed theories have been of great value, the current research highlights the need to think beyond a single frequency band in the EEG spectra. Specifically, the research in Chapter 3 shows that periodic oscillatory activity is not the only type of task-relevant activity in the EEG signal. We show that the often ignored 1/f aperiodic component plays an important role in covert visual attention and that it may better reflect changes in the brain's level of cortical excitability than the index of alpha activity. In fact, alpha activity that has not been separated from the aperiodic component could be showing effects due to aperiodic activity changes rather than the rhythmic alpha activity. This could also explain why the researchers have had such a hard time understanding the functional role of alpha oscillations even after nearly a century of study. Regardless, the current work emphasizes the importance for

future researchers to consider multiple aspects of brain activity including multiple oscillatory frequencies and aperiodic activity.

The overarching goal of this work is to better understand visual perception, attention, and their underlying neural mechanisms. By adapting visual working memory probabilistic models, we show how simple performance measures can be turned in metrics that quantify the cognitive and behavioral state of a participant. The visual working memory models used in this thesis allowed us to go beyond questions of response errors and target detection to how the quality or precision of the target's perceptual representation changed as a function of neural activity. In Chapter 4, we show the advantages of using the information-rich multivariate approach for investigating the complex dynamics of EEG brain activity such as those found leading up to the onset of a stimulus. The biggest advantage EEG has over other neuroimaging methods is its temporal resolution. Multivariate methods such as SVM classification and prediction are powerful techniques that make full use of the spatial and temporal extent of that information. While the research in this thesis moves us one step closer to improving our understanding of visual perception, attention, and their underlying neural mechanisms, it also highlights how much work remains for us to truly comprehend that which is fundamental to our ability to interact with and thrive in the world: vision.

References

Bartolomeo, P. (2006) 'A Parietofrontal Network for Spatial Awareness in the Right Hemisphere of the Human Brain', *Archives of Neurology*, 63(9), pp. 1238–1241. doi: 10.1001/archneur.63.9.1238.

Donoghue, T. *et al.* (2020) 'Parameterizing neural power spectra into periodic and aperiodic components', *Nature Neuroscience 2020 23:12*. Nature Publishing Group, 23(12), pp. 1655–1665. doi: 10.1038/s41593-020-00744-x.

Gao, R., Peterson, E. J. and Voytek, B. (2017) 'Inferring synaptic excitation/inhibition balance from field potentials', *NeuroImage*, 158, pp. 70–78. doi: https://doi.org/10.1016/j.neuroimage.2017.06.078.

Kim, Y.-H. *et al.* (1999) 'The Large-Scale Neural Network for Spatial Attention Displays Multifunctional Overlap But Differential Asymmetry', *NeuroImage*, 9(3), pp. 269–277. doi: https://doi.org/10.1006/nimg.1999.0408.

Samaha, J. *et al.* (2020) 'Spontaneous Brain Oscillations and Perceptual Decision-Making', *Trends in Cognitive Sciences*. Elsevier Ltd, 24(8), pp. 639–653. doi: 10.1016/j.tics.2020.05.004.

Siman-Tov, T. *et al.* (2007) 'Bihemispheric Leftward Bias in a Visuospatial Attention-Related Network', *Journal of Neuroscience*. Society for Neuroscience, 27(42), pp. 11271–11278. doi: 10.1523/JNEUROSCI.0599-07.2007.

Zhang, W. and Luck, S. J. (2008) 'Discrete fixed-resolution representations in visual working memory.', *Nature*. NIH Public Access, 453(7192), pp. 233–235. doi: 10.1038/nature06860.

BIBLIOGRAPHY

Adrian, E. D. and Mathews, B. H. (1934) 'The Berger rhythm: potential changes from the occipital lobes in man', *Brain*, 57(4), pp. 355–385. Available at: https://backyardbrains.com/experiments/files/AdrianMathews-1934-EEG-recordings.pdf.

Aru, Juhan *et al.* (2015) 'Untangling cross-frequency coupling in neuroscience', *Current Opinion in Neurobiology*. Elsevier Ltd, 31, pp. 51–61. doi: 10.1016/j.conb.2014.08.002.

Auton, A. (2009) 'Red Blue Colormap'. MATLAB Central File Exchange. Available at: https://www.mathworks.com/matlabcentral/fileexchange/25536-red-blue-colormap.

Bae, G.-Y. (2021) 'Neural evidence for categorical biases in location and orientation representations in a working memory task', *NeuroImage*, 240, p. 118366. doi: https://doi.org/10.1016/j.neuroimage.2021.118366.

Bae, G.-Y. and Luck, S. J. (2018) 'Dissociable decoding of spatial attention and working memory from EEG oscillations and sustained potentials', *Journal of Neuroscience*. Society for Neuroscience, 38(2), pp. 409–422. doi: 10.1523/JNEUROSCI.2860-17.2017.

Baghdadi, G., Towhidkhah, F. and Rajabi, M. (2021) 'Chapter 2 - Anatomy and physiology of attention', in Baghdadi, G., Towhidkhah, F., and Rajabi, M. B. T.-N. M. of A. (eds) *Neurocognitive Mechanisms of Attention*. Academic Press, pp. 51–94. doi: https://doi.org/10.1016/B978-0-323-90935-8.00002-0.

Bartolomeo, P. (2006) 'A Parietofrontal Network for Spatial Awareness in the Right Hemisphere of the Human Brain', *Archives of Neurology*, 63(9), pp. 1238–1241. doi: 10.1001/archneur.63.9.1238.

Başar, E. *et al.* (1997) 'Alpha oscillations in brain functioning: an integrative theory',

International Journal of Psychophysiology, 26(1), pp. 5–29. doi: https://doi.org/10.1016/S0167-8760(97)00753-8.

Başar, E. *et al.* (1999) 'Are cognitive processes manifested in event-related gamma, alpha, theta and delta oscillations in the EEG?', *Neuroscience Letters*. Elsevier, 259(3), pp. 165–168. doi: 10.1016/S0304-3940(98)00934-3.

Başar, E. *et al.* (2001) 'Gamma, alpha, delta, and theta oscillations govern cognitive processes', *International Journal of Psychophysiology*. Elsevier, 39(2–3), pp. 241–248. doi: 10.1016/S0167-8760(00)00145-8.

Başar, E. (2012) 'A review of alpha activity in integrative brain function: Fundamental physiology, sensory coding, cognition and pathology', *International Journal of Psychophysiology*, 86(1), pp. 1–24. doi: https://doi.org/10.1016/j.ijpsycho.2012.07.002.

Başar, E. and Düzgün, A. (2016) 'Links of Consciousness, Perception, and Memory by Means of Delta Oscillations of Brain', *Frontiers in Psychology*, 7, p. Article 275. doi: 10.3389/fpsyg.2016.00275.

Bastos, A. M. and Schoffelen, J.-M. (2016) 'A Tutorial Review of Functional Connectivity Analysis Methods and Their Interpretational Pitfalls', *Frontiers in Systems Neuroscience*. Frontiers, 9, p. Article 175. doi: 10.3389/fnsys.2015.00175.

Bays, P. M. (2014) 'Noise in Neural Populations Accounts for Errors in Working Memory', *The Journal of Neuroscience*, 34(10), pp. 3632–3645. doi: 10.1523/JNEUROSCI.3204-13.2014.

Bays, P. M. (2016) 'A signature of neural coding at human perceptual limits', *Journal of Vision*. Association for Research in Vision and Ophthalmology Inc., 16(11), p. Article 4. doi: 10.1167/16.11.4.

Bays, P. M., Catalao, R. F. G. and Husain, M. (2009) 'The precision of visual working memory is set by allocation of a shared resource', *Journal of Vision*. The Association for Research in Vision and Ophthalmology, 9(10), pp. 7–7. doi: 10.1167/9.10.7.

Bazanova, O. M. and Vernon, D. J. (2014) 'Interpreting EEG alpha activity', *Neuroscience & Biobehavioral Reviews*, 44, pp. 94–110. doi: 10.1016/j.neubiorev.2013.05.007.

Ben-Hur, A. and Weston, J. (2010) 'A User's Guide to Support Vector Machines', in Carugo, O. and Eisenhaber, F. (eds) *Data Mining Techniques for the Life Sciences*. Totowa, NJ: Humana Press, pp. 223–239. doi: 10.1007/978-1-60327-241-4_13.

Benjamini, Y. and Yekutieli, D. (2001) 'The control of the false discovery rate in multiple testing under dependency', *Annals of Statistics*, 29(4), pp. 1165–1188. doi: 10.1214/aos/1013699998.

Benwell, C. S. Y. *et al.* (2017) 'Prestimulus EEG Power Predicts Conscious Awareness But Not Objective Visual Performance.', *eNeuro*. Society for Neuroscience, 4(6). doi: 10.1523/ENEURO.0182-17.2017.

Benwell, C. S. Y. *et al.* (2018) 'Trial-by-trial co-variation of pre-stimulus EEG alpha power and visuospatial bias reflects a mixture of stochastic and deterministic effects', *European Journal of Neuroscience*. Blackwell Publishing Ltd, 48(7), pp. 2566–2584. doi: 10.1111/ejn.13688.

Benwell, C. S. Y. *et al.* (2019) 'Frequency and power of human alpha oscillations drift systematically with time-on-task', *NeuroImage*. Academic Press, 192, pp. 101–114. doi: 10.1016/J.NEUROIMAGE.2019.02.067.

Benwell, C. S. Y. *et al.* (2021) 'Low pre-stimulus EEG alpha power amplifies visual awareness but not visual sensitivity', *European Journal of Neuroscience*. John Wiley & Sons, Ltd,

00, pp. 1–16. doi: 10.1111/EJN.15166.

Berens, P. (2009) ‘CircStat: a MATLAB toolbox for circular statistics’, *Journal of Statistical Software*, 31(10), pp. 679–685. doi: 10.1016/j.amp.2012.05.023.

van den Berg, R. *et al.* (2012) ‘Variability in encoding precision accounts for visual short-term memory limitations’, *Proceedings of the National Academy of Sciences of the United States of America*. National Academy of Sciences, 109(22), pp. 8780–8785. doi: 10.1073/pnas.1117465109.

Berger, H. (1929) ‘Über das Elektrenkephalogramm des Menschen’, *Archiv für Psychiatrie und Nervenkrankheiten*. Springer-Verlag, 87(1), pp. 527–570. doi: 10.1007/BF01797193.

Bishop, C. M. (2006) *Pattern Recognition and Machine Learning (Information Science and Statistics)*. New York, NY: Springer.

Blair, R. C. and Karniski, W. (1993) ‘An alternative method for significance testing of waveform difference potentials’, *Psychophysiology*. John Wiley & Sons, Ltd, 30(5), pp. 518–524. doi: 10.1111/j.1469-8986.1993.tb02075.x.

Bode, S. *et al.* (2019) ‘The Decision Decoding ToolBOX (DDTBOX) – A Multivariate Pattern Analysis Toolbox for Event-Related Potentials’, *Neuroinformatics*. Humana Press Inc., 17(1), pp. 27–42. doi: 10.1007/s12021-018-9375-z.

Bonnefond, M. and Jensen, O. (2015) ‘Gamma Activity Coupled to Alpha Phase as a Mechanism for Top-Down Controlled Gating’, *PLOS ONE*. Public Library of Science, 10(6), p. e0128667. Available at: https://doi.org/10.1371/journal.pone.0128667.

Bonnefond, M., Kastner, S. and Jensen, O. (2017) ‘Communication between brain areas based on nested oscillations’, *eNeuro*, 4(2). doi: 10.1523/ENEURO.0153-16.2017.

Bourgeois, A. *et al.* (2020) ‘Pulvino-cortical interaction: An integrative role in the control of

attention', *Neuroscience & Biobehavioral Reviews*, 111, pp. 104–113. doi: https://doi.org/10.1016/j.neubiorev.2020.01.005.

Brainard, D. H. (1997) 'The Psychophysics Toolbox.', *Spatial vision*, 10(4), pp. 433–436. Available at: http://www.ncbi.nlm.nih.gov/pubmed/9176952 (Accessed: 5 October 2017).

Brüers, S. and VanRullen, R. (2017) 'At what latency does the phase of brain oscillations influence perception?', *eNeuro*. Society for Neuroscience, 4(3). doi: 10.1523/ENEURO.0078-17.2017.

Bruns, A. and Eckhorn, R. (2004) 'Task-related coupling from high- to low-frequency signals among visual cortical areas in human subdural recordings', *International Journal of Psychophysiology*, 51(2), pp. 97–116. doi: https://doi.org/10.1016/j.ijpsycho.2003.07.001.

Busch, N. A., Dubois, J. and VanRullen, R. (2009) 'The phase of ongoing EEG oscillations predicts visual perception', *Journal of Neuroscience*, 29(24), pp. 7869–7876. doi: https://doi.org/10.1523/JNEUROSCI.0113-09.2009.

Buzsáki, G., Anastassiou, C. A. and Koch, C. (2012) 'The origin of extracellular fields and currents — EEG, ECoG, LFP and spikes', *Nature Reviews Neuroscience*, 13(6), pp. 407–420. doi: 10.1038/nrn3241.

Buzsaki, G. and Buzsáki, G. (2006) *Rhythms of the Brain*. Oxford, UK: Oxford university press. doi: 10.1093/acprof:oso/9780195301069.001.0001.

Buzsáki, G. and Draguhn, A. (2004) 'Neuronal oscillations in cortical networks', *Science*. American Association for the Advancement of Science, 304(5679), pp. 1926–1929. doi: 10.1126/science.1099745.

Canolty, R. T. *et al.* (2006) 'High gamma power is phase-locked to theta oscillations in human

neocortex', *Science*, 313(5793), pp. 1626–1628. doi: 10.1126/SCIENCE.1128115.

Cao, J. *et al.* (2022) 'Brain functional and effective connectivity based on electroencephalography recordings: A review', *Human Brain Mapping*. John Wiley & Sons, Ltd, 43(2), pp. 860–879. doi: https://doi.org/10.1002/hbm.25683.

Carrasco, M. (2011) 'Visual attention: The past 25 years', *Vision Research*. Pergamon, 51(13), pp. 1484–1525. doi: 10.1016/J.VISRES.2011.04.012.

Chang, C.-C. and Lin, C.-J. (2011) 'LIBSVM: a library for support vector machines', *ACM Transactions on Intelligent Systems and Technology*, 2(3), pp. 1–27. Available at: http://www.csie.ntu.edu.tw/~cjlin/libsvm.

Chaumon, M. and Busch, N. A. (2014) 'Prestimulus neural oscillations inhibit visual perception via modulation of response gain', *Journal of Cognitive Neuroscience*. MIT Press Journals, 26(11), pp. 2514–2529. doi: 10.1162/jocn_a_00653.

Chini, M., Pfeffer, T. and Hanganu-Opatz, I. L. (2021) 'Developmental increase of inhibition drives decorrelation of neural activity', *bioRxiv*. Cold Spring Harbor Laboratory. doi: 10.1101/2021.07.06.451299.

Clayton, M. S., Yeung, N. and Cohen Kadosh, R. (2015) 'The roles of cortical oscillations in sustained attention', *Trends in Cognitive Sciences*. Elsevier Ltd, pp. 188–195. doi: 10.1016/j.tics.2015.02.004.

Clayton, M. S., Yeung, N. and Cohen Kadosh, R. (2018) 'The many characters of visual alpha oscillations', *European Journal of Neuroscience*. Blackwell Publishing Ltd, 48(7), pp. 2498–2508. doi: 10.1111/ejn.13747.

Cohen, M. X. (2008) 'Assessing transient cross-frequency coupling in EEG data', *Journal of Neuroscience Methods*. Elsevier, 168(2), pp. 494–499. doi:

10.1016/j.jneumeth.2007.10.012.

Cohen, M. X. (2014) *Analyzing neural time series data: theory and practice*. Cambridge, Massachusetts: MIT Press.

Cohen, M. X. (2015) 'Effects of time lag and frequency matching on phase-based connectivity', *Journal of Neuroscience Methods*, 250, pp. 137–146. doi: https://doi.org/10.1016/j.jneumeth.2014.09.005.

Cohen, M. X. and Cavanagh, J. F. (2011) 'Single-trial regression elucidates the role of prefrontal theta oscillations in response conflict', *Frontiers in Psychology*, 2. doi: 10.3389/fpsyg.2011.00030.

Cohen, M. X. and van Gaal, S. (2013) 'Dynamic interactions between large-scale brain networks predict behavioral adaptation after perceptual errors', *Cerebral Cortex*. 2012/04/18. Oxford University Press, 23(5), pp. 1061–1072. doi: 10.1093/cercor/bhs069.

Cohen, M. X. and Voytek, B. (2013) 'Linking nonlinear neural dynamics to single-trial human behavior', in Pesenson, M. (Meyer) Z. (ed.) *Multiscale Analysis and Nonlinear Dynamics*. Wiley-VCH Verlag GmbH & Co. KGaA., pp. 217–232. doi: 10.1002/9783527671632.

Cole, S. *et al.* (2019) 'NeuroDSP: A package for neural digital signal processing', *Journal of Open Source Software*, 4(36), p. 1272. doi: 10.21105/joss.01272.

Compton, R. J. *et al.* (2011) 'Cognitive control in the intertrial interval: Evidence from EEG alpha power', *Psychophysiology*. Blackwell Publishing Inc., 48(5), pp. 583–590. doi: 10.1111/j.1469-8986.2010.01124.x.

Compton, R. J., Bissey, B. and Worby-Selim, S. (2014) 'Task motivation influences alpha suppression following errors', *Psychophysiology*. Blackwell Publishing Inc., 51(7), pp.

585–595. doi: 10.1111/psyp.12212.

Compton, R. J., Heaton, E. and Ozer, E. (2017) 'Intertrial interval duration affects error monitoring', *Psychophysiology*. Blackwell Publishing Inc., 54(8), pp. 1151–1162. doi: 10.1111/psyp.12877.

Corbetta, M. and Shulman, G. L. (2002) 'Control of goal-directed and stimulus-driven attention in the brain', *Nature Reviews Neuroscience*, 3(3), pp. 201–215. doi: 10.1038/nrn755.

Dave, S., Brothers, T. A. and Swaab, T. Y. (2018) '1/f neural noise and electrophysiological indices of contextual prediction in aging', *Brain Research*, 1691, pp. 34–43. doi: https://doi.org/10.1016/j.brainres.2018.04.007.

Davoudi, S., Ahmadi, A. and Daliri, M. R. (2020) 'Frequency–amplitude coupling: a new approach for decoding of attended features in covert visual attention task', *Neural Computing and Applications*. Springer, pp. 1–16. doi: 10.1007/s00521-020-05222-w.

Delorme, A. and Makeig, S. (2004) 'EEGLAB: An open source toolbox for analysis of single-trial EEG dynamics including independent component analysis', *Journal of Neuroscience Methods*. Elsevier, 134(1), pp. 9–21. doi: 10.1016/J.JNEUMETH.2003.10.009.

Desimone, R. (1995) 'Neural mechanisms of selective visual attention', *Annual Review of Neuroscience*, 18(1), pp. 193–222. doi: 10.1146/annurev.neuro.18.1.193.

van Diepen, R. M., Foxe, J. J. and Mazaheri, A. (2019) 'The functional role of alpha-band activity in attentional processing: the current zeitgeist and future outlook', *Current Opinion in Psychology*. Elsevier, 29, pp. 229–238. doi: 10.1016/J.COPSYC.2019.03.015.

van Diepen, R. M. and Mazaheri, A. (2018) 'The Caveats of observing Inter-Trial Phase-Coherence in Cognitive Neuroscience', *Scientific Reports*. Nature Publishing Group, 8(1), p. 2990. doi: 10.1038/s41598-018-20423-z.

van Dijk, H. *et al.* (2008) 'Prestimulus Oscillatory Activity in the Alpha Band Predicts Visual Discrimination Ability', *The Journal of Neuroscience*, 28(8), pp. 1816–1823. doi: 10.1523/JNEUROSCI.1853-07.2008.

Doesburg, S. M., Bedo, N. and Ward, L. M. (2016) 'Top-down alpha oscillatory network interactions during visuospatial attention orienting', *NeuroImage*, 132, pp. 512–519. doi: https://doi.org/10.1016/j.neuroimage.2016.02.076.

Donoghue, T. *et al.* (2020) 'Parameterizing neural power spectra into periodic and aperiodic components', *Nature Neuroscience 2020 23:12*. Nature Publishing Group, 23(12), pp. 1655–1665. doi: 10.1038/s41593-020-00744-x.

Donoghue, T., Dominguez, J. and Voytek, B. (2020) 'Electrophysiological Frequency Band Ratio Measures Conflate Periodic and Aperiodic Neural Activity', *eNeuro*. Society for Neuroscience, 7(6). doi: 10.1523/ENEURO.0192-20.2020.

Doradzińska, Ł. *et al.* (2020) 'Unconscious perception of one's own name modulates amplitude of the P3B ERP component', *Neuropsychologia*. Elsevier Ltd, 147, p. 107564. doi: 10.1016/j.neuropsychologia.2020.107564.

Dube, B. and Golomb, J. D. (2020) 'Revisiting mixture models of memory', *Nature Human Behaviour*, 4(11), pp. 1098–1099. doi: 10.1038/s41562-020-00947-z.

Ergenoglu, T. *et al.* (2004) 'Alpha rhythm of the EEG modulates visual detection performance in humans', *Cognitive Brain Research*, 20(3), pp. 376–383. doi: https://doi.org/10.1016/j.cogbrainres.2004.03.009.

Van Essen, D. C. *et al.* (1990) 'Modular and hierarchical organization of extrastriate visual cortex in the macaque monkey', *Cold Spring Harbor symposia on quantitative biology*, 55, pp. 679–696. Available at: https://www-webofscience-

com.login.ezproxy.library.ualberta.ca/wos/woscc/full-record/WOS:A1990HB91800063.

Faraway, J. J. (2016). *Linear Models with R* (2nd ed.). Chapman and Hall/CRC. https://doi.org/10.1201/b17144.

Fiebelkorn, I. C. *et al.* (2013) 'Cortical cross-frequency coupling predicts perceptual outcomes', *NeuroImage*. Academic Press, 69, pp. 126–137. doi: 10.1016/j.neuroimage.2012.11.021.

Fiebelkorn, I. C. and Kastner, S. (2019) 'A Rhythmic Theory of Attention', *Trends in Cognitive Sciences*. Elsevier Current Trends, 23(2), pp. 87–101. doi: 10.1016/j.tics.2018.11.009.

Fiebelkorn, I. C., Pinsk, M. A. and Kastner, S. (2018) 'A Dynamic Interplay within the Frontoparietal Network Underlies Rhythmic Spatial Attention', *Neuron*, 99(4), pp. 842-853.e8. doi: https://doi.org/10.1016/j.neuron.2018.07.038.

Fields, E. C. (2017) 'Factorial Mass Univariate ERP Toolbox'. Available at: https://github.com/ericcfields/FMUT/releases.

Fields, E. C. and Kuperberg, G. R. (2019) 'Having your cake and eating it too: Flexibility and power with mass univariate statistics for ERP data', *Psychophysiology*. doi: 10.1111/psyp.13468.

Fischer, J. and Whitney, D. (2014) 'Serial dependence in visual perception', *Nature Neuroscience*. Nature Publishing Group, 17(5), pp. 738–743. doi: 10.1038/nn.3689.

Förster, J., Koivisto, M. and Revonsuo, A. (2020) 'ERP and MEG correlates of visual consciousness: The second decade', *Consciousness and Cognition*. Academic Press Inc., 80, p. Article 102917. doi: 10.1016/j.concog.2020.102917.

Foster, J. J. and Awh, E. (2019) 'The role of alpha oscillations in spatial attention: limited evidence for a suppression account', *Current Opinion in Psychology*. Elsevier, 29, pp. 34–40. doi: 10.1016/J.COPSYC.2018.11.001.

Fougnie, D., Suchow, J. W. and Alvarez, G. A. (2012) 'Variability in the quality of visual working memory', *Nature Communications*. NIH Public Access, 3, p. 1229. doi: 10.1038/ncomms2237.

Foxe, J. J. and Snyder, A. C. (2011) 'The role of alpha-band brain oscillations as a sensory suppression mechanism during selective attention', *Frontiers in Psychology*. Frontiers Media SA, 2, p. Article 154. doi: 10.3389/fpsyg.2011.00154.

Frey, J. N., Ruhnau, P. and Weisz, N. (2015) 'Not so different after all: The same oscillatory processes support different types of attention', *Brain Research*. Elsevier, 1626, pp. 183–197. doi: 10.1016/J.BRAINRES.2015.02.017.

Fries, P. *et al.* (2008) 'The Effects of Visual Stimulation and Selective Visual Attention on Rhythmic Neuronal Synchronization in Macaque Area V4', *The Journal of Neuroscience*, 28(18), pp. 4823–4835. doi: 10.1523/JNEUROSCI.4499-07.2008.

Gao, R., Peterson, E. J. and Voytek, B. (2017) 'Inferring synaptic excitation/inhibition balance from field potentials', *NeuroImage*, 158, pp. 70–78. doi: https://doi.org/10.1016/j.neuroimage.2017.06.078.

García-Pérez, M. A. (1998) 'Forced-choice staircases with fixed step sizes: asymptotic and small-sample properties', *Vision Research*, 38(12), pp. 1861–1881. doi: 10.1016/S0042-6989(97)00340-4.

Gootjes, L. *et al.* (2006) 'Attention modulates hemispheric differences in functional connectivity: Evidence from MEG recordings', *NeuroImage*, 30(1), pp. 245–253. doi: https://doi.org/10.1016/j.neuroimage.2005.09.015.

Gould, I. C., Rushworth, M. F. and Nobre, A. C. (2011) 'Indexing the graded allocation of visuospatial attention using anticipatory alpha oscillations', *Journal of Neurophysiology*.

American Physiological Society, 105(3), pp. 1318–1326. doi: 10.1152/jn.00653.2010.

de Graaf, T. A. *et al.* (2020) 'Does alpha phase modulate visual target detection? Three experiments with tACS-phase-based stimulus presentation', *European Journal of Neuroscience*. Blackwell Publishing Ltd, 51(11), pp. 2299–2313. doi: 10.1111/ejn.14677.

Grandchamp, R. and Delorme, A. (2011) 'Single-trial normalization for event-related spectral decomposition reduces sensitivity to noisy trials.', *Frontiers in psychology*. Frontiers Media SA, 2, p. 236. doi: 10.3389/fpsyg.2011.00236.

Gratton, G., Coles, M. G. . and Donchin, E. (1983) 'A new method for off-line removal of ocular artifact', *Electroencephalography and Clinical Neurophysiology*, 55(4), pp. 468–484. doi: 10.1016/0013-4694(83)90135-9.

Grootswagers, T., Wardle, S. G. and Carlson, T. A. (2017) 'Decoding dynamic brain patterns from evoked responses: A tutorial on multivariate pattern analysis applied to time series neuroimaging data', *Journal of Cognitive Neuroscience*. MIT Press Journals, 29(4), pp. 677–697. doi: 10.1162/jocn_a_01068.

Groppe, D. M., Urbach, T. P. and Kutas, M. (2011) 'Mass univariate analysis of event-related brain potentials/fields I: A critical tutorial review', *Psychophysiology*. John Wiley & Sons, Ltd (10.1111), 48(12), pp. 1711–1725. doi: 10.1111/j.1469-8986.2011.01273.x.

Güntekin, B. and Başar, E. (2016) 'Review of evoked and event-related delta responses in the human brain', *International Journal of Psychophysiology*, 103, pp. 43–52. doi: https://doi.org/10.1016/j.ijpsycho.2015.02.001.

Gyurkovics, M. *et al.* (2021) 'The impact of 1/f activity and baseline correction on the results and interpretation of time-frequency analyses of EEG/MEG data: A cautionary tale', *NeuroImage*. Academic Press, 237, p. Article 118192. doi:

https://doi.org/10.1016/j.neuroimage.2021.118192.

Haegens, S. *et al.* (2014) 'Inter- and intra-individual variability in alpha peak frequency', *NeuroImage*. Academic Press, 92, pp. 46–55. doi: 10.1016/J.NEUROIMAGE.2014.01.049.

Hakim, N. *et al.* (2019) 'Dissecting the Neural Focus of Attention Reveals Distinct Processes for Spatial Attention and Object-Based Storage in Visual Working Memory', *Psychological Science*. SAGE Publications Inc., 30(4), pp. 526–540. doi: 10.1177/0956797619830384.

Halgren, M. *et al.* (2019) 'The generation and propagation of the human alpha rhythm', *Proceedings of the National Academy of Sciences*. National Academy of Sciences, 116(47), pp. 23772–23782. doi: 10.1073/pnas.1913092116.

Hamidi, M. (2009) 'Repetitive transcranial magnetic stimulation affects behavior by biasing endogenous cortical oscillations', *Frontiers in Integrative Neuroscience*. Frontiers, 3(JUN), p. 14. doi: 10.3389/neuro.07.014.2009.

Hanslmayr, S. *et al.* (2007) 'Prestimulus oscillations predict visual perception performance between and within subjects', *NeuroImage*, 37(4), pp. 1465–1473. doi: https://doi.org/10.1016/j.neuroimage.2007.07.011.

Harel, A. *et al.* (2016) 'The temporal dynamics of scene processing: A multifaceted EEG investigation', *eNeuro*. Society for Neuroscience, 3(5), p. Article e0139-16.2016. doi: 10.1523/ENEURO.0139-16.2016.

Harmony, T. (2013) 'The functional significance of delta oscillations in cognitive processing', *Frontiers in Integrative Neuroscience*. Frontiers, 7, p. Article 83. doi: 10.3389/fnint.2013.00083.

Harper, J., Malone, S. M. and Bernat, E. M. (2014) 'Theta and delta band activity explain N2 and

P3 ERP component activity in a go/no-go task', *Clinical Neurophysiology*. Elsevier, 125(1), pp. 124–132. doi: 10.1016/j.clinph.2013.06.025.

Harris, K. D. and Thiele, A. (2011) 'Cortical state and attention', *Nature Reviews Neuroscience*, 12(9), pp. 509–523. doi: 10.1038/nrn3084.

Haufe, S. *et al.* (2014) 'On the interpretation of weight vectors of linear models in multivariate neuroimaging', *NeuroImage*. Academic Press Inc., 87, pp. 96–110. doi: 10.1016/j.neuroimage.2013.10.067.

Hebart, M. N. and Baker, C. I. (2018) 'Deconstructing multivariate decoding for the study of brain function', *NeuroImage*. Academic Press, pp. 4–18. doi: 10.1016/j.neuroimage.2017.08.005.

Helfrich, R. F. *et al.* (2017) 'Prefrontal cortex modulates posterior alpha oscillations during top-down guided visual perception', *Proceedings of the National Academy of Sciences of the United States of America*. National Academy of Sciences, 114(35), pp. 9457–9462. doi: 10.1073/pnas.1705965114.

Helfrich, R. F. *et al.* (2018) 'Neural mechanisms of sustained attention are rhythmic', *Neuron*. Elsevier Inc., 99(4), pp. 854–865. doi: 10.1016/j.neuron.2018.07.032.

Helfrich, R. F., Breska, A. and Knight, R. T. (2019) 'Neural Entrainment and Network Resonance in Support of Top-down guided Attention', *Current Opinion in Psychology*. Elsevier. doi: 10.1016/J.COPSYC.2018.12.016.

Helfrich, R. F. and Knight, R. T. (2019) 'Cognitive neurophysiology: Event-related potentials', in *Handbook of Clinical Neurology*. Elsevier B.V., pp. 543–558. doi: 10.1016/B978-0-444-64032-1.00036-9.

Herring, J. D. *et al.* (2019) 'Low-frequency alternating current stimulation rhythmically

suppresses gamma-band oscillations and impairs perceptual performance', *NeuroImage*, 184, pp. 440–449. Available at: https://www.sciencedirect.com/science/article/pii/S1053811918318469 (Accessed: 27 November 2018).

Herrmann, C. S. *et al.* (2014) 'Time–frequency analysis of event-related potentials: A brief tutorial', *Brain Topography*. Springer US, 27(4), pp. 438–450. doi: 10.1007/s10548-013-0327-5.

Herweg, N. A., Solomon, E. A. and Kahana, M. J. (2020) 'Theta Oscillations in Human Memory', *Trends in Cognitive Sciences*, 24(3), pp. 208–227. doi: https://doi.org/10.1016/j.tics.2019.12.006.

Hillyard, S. A. and Anllo-Vento, L. (1998) 'Event-related brain potentials in the study of visual selective attention.', *Proceedings of the National Academy of Sciences of the United States of America*. National Academy of Sciences, 95(3), pp. 781–787. doi: 10.1073/pnas.95.3.781.

Hillyard, S. A., Vogel, E. K. and Luck, S. J. (1998) 'Sensory gain control (amplification) as a mechanism of selective attention: electrophysiological and neuroimaging evidence', *Philosophical Transactions of the Royal Society of London. Series B: Biological Sciences*. The Royal Society, 353(1373), pp. 1257–1270. doi: 10.1098/RSTB.1998.0281.

Hogendoorn, H. (2015) 'From sensation to perception: Using multivariate classification of visual illusions to identify neural correlates of conscious awareness in space and time', *Perception*, 44(1), pp. 71–78. doi: 10.1068/p7832.

Hong, X. *et al.* (2015) 'Normal aging selectively diminishes alpha lateralization in visual spatial attention', *NeuroImage*. Academic Press Inc., 106, pp. 353–363. doi:

10.1016/j.neuroimage.2014.11.019.

Huang, L. *et al.* (2006) 'Slab-like functional architecture of higher order cortical area 21a showing oblique effect of orientation preference in the cat', *NeuroImage*, 32(3), pp. 1365–1374. doi: https://doi.org/10.1016/j.neuroimage.2006.05.007.

Hülsemann, M. J., Naumann, E. and Rasch, B. (2019) 'Quantification of phase-amplitude coupling in neuronal oscillations:comparison of phase-locking value, mean vector length, modulation index, and generalized-linear-modeling-cross-frequency-coupling', *Frontiers in Neuroscience*. Frontiers Media S.A., 13, p. Article 573. doi: 10.3389/fnins.2019.00573.

Iemi, L. *et al.* (2017) 'Spontaneous neural oscillations bias perception by modulating baseline excitability', *Journal of Neuroscience*. Society for Neuroscience, 37(4), pp. 807–819. doi: 10.1523/JNEUROSCI.1432-16.2016.

Iemi, L. *et al.* (2019) 'Multiple mechanisms link prestimulus neural oscillations to sensory responses', *eLife*. eLife Sciences Publications Ltd, 8, p. Article e43620. doi: 10.7554/eLife.43620.001.

Iemi, L. and Busch, N. A. (2018) 'Moment-to-moment fluctuations in neuronal excitability bias subjective perception rather than strategic decision-making', *eNeuro*. Society for Neuroscience, 5(3). doi: 10.1523/ENEURO.0430-17.2018.

İşoğlu-Alkaç, Ü. and Strüber, D. (2006) 'Necker cube reversals during long-term EEG recordings: Sub-bands of alpha activity', *International Journal of Psychophysiology*, 59(2), pp. 179–189. doi: https://doi.org/10.1016/j.ijpsycho.2005.05.002.

Jackson, A. F. and Bolger, D. J. (2014) 'The neurophysiological bases of EEG and EEG measurement: A review for the rest of us', *Psychophysiology*. John Wiley & Sons, Ltd,

51(11), pp. 1061–1071. doi: 10.1111/PSYP.12283.

James, G. *et al.* (2021) *An Introduction to Statistical Learning*. 2nd edn. New York, NY: Springer US (Springer Texts in Statistics). doi: 10.1007/978-1-0716-1418-1.

Jensen, O. *et al.* (2014) 'Temporal coding organized by coupled alpha and gamma oscillations prioritize visual processing', *Trends in Neurosciences*. Elsevier Ltd, 37(7), pp. 357–369. doi: 10.1016/j.tins.2014.04.001.

Jensen, O. and Colgin, L. L. (2007) 'Cross-frequency coupling between neuronal oscillations', *Trends in Cognitive Sciences*, 11(7), pp. 267–269. doi: 10.1016/j.tics.2007.05.003.

Jensen, O. and Mazaheri, A. (2010) 'Shaping functional architecture by oscillatory alpha activity: Gating by inhibition', *Frontiers in Human Neuroscience*. Frontiers Media S. A., 4, p. 186. doi: 10.3389/fnhum.2010.00186.

Jokisch, D. and Jensen, O. (2007) 'Modulation of Gamma and Alpha Activity during a Working Memory Task Engaging the Dorsal or Ventral Stream', *Journal of Neuroscience*. Society for Neuroscience, 27(12), pp. 3244–3251. doi: 10.1523/JNEUROSCI.5399-06.2007.

Jolicœur, P., Brisson, B. and Robitaille, N. (2008) 'Dissociation of the N2pc and sustained posterior contralateral negativity in a choice response task', *Brain Research*, 1215, pp. 160–172. doi: https://doi.org/10.1016/j.brainres.2008.03.059.

Kader, G. D. and Perry, M. (2007) 'Variability for Categorical Variables', *Journal of Statistics Education*, 15(2). Available at: https://eric.ed.gov/?id=EJ842705 (Accessed: 16 March 2021).

Karakaş, S. (2020) 'A review of theta oscillation and its functional correlates', *International Journal of Psychophysiology*. Elsevier B.V. doi: 10.1016/j.ijpsycho.2020.04.008.

Karakaş, S., Erzengin, Ö U. and Başar, E. (2000) 'A new strategy involving multiple cognitive

paradigms demonstrates that ERP components are determined by the superposition of oscillatory responses', *Clinical Neurophysiology*. Elsevier, 111(10), pp. 1719–1732. doi: 10.1016/S1388-2457(00)00418-1.

Karakaş, S., Erzengin, Ömer Utku and Başar, E. (2000) 'The genesis of human event-related responses explained through the theory of oscillatory neural assemblies', *Neuroscience Letters*. Elsevier, 285(1), pp. 45–48. doi: 10.1016/S0304-3940(00)01022-3.

Kastner, S. and Ungerleider, L. G. (2000) 'Mechanisms of visual attention in the human cortex', *Annual Review of Neuroscience*. Annual Reviews 4139 El Camino Way, P.O. Box 10139, Palo Alto, CA 94303-0139, USA, pp. 315–341. doi: 10.1146/annurev.neuro.23.1.315.

Kayser, J. and Tenke, C. E. (2015) 'Issues and considerations for using the scalp surface Laplacian in EEG/ERP research: A tutorial review', *International Journal of Psychophysiology*, 97(3), pp. 189–209. doi: 10.1016/j.ijpsycho.2015.04.012.

Keitel, C. *et al.* (2018) 'No changes in parieto-occipital alpha during neural phase locking to visual quasi-periodic theta-, alpha-, and beta-band stimulation', *European Journal of Neuroscience*, pp. 1–15. doi: 10.1111/ejn.13935.

Kelly, S. P. *et al.* (2006) 'Increases in Alpha Oscillatory Power Reflect an Active Retinotopic Mechanism for Distracter Suppression During Sustained Visuospatial Attention', *Journal of Neurophysiology*, 95(6), pp. 3844–3851. doi: 10.1152/jn.01234.2005.

Kelly, S. P., Gomez-Ramirez, M. and Foxe, J. J. (2009) 'The strength of anticipatory spatial biasing predicts target discrimination at attended locations: a high-density EEG study', *European Journal of Neuroscience*. John Wiley & Sons, Ltd, 30(11), pp. 2224–2234. doi: https://doi.org/10.1111/j.1460-9568.2009.06980.x.

Key, A. P. F., Dove, G. O. and Maguire, M. J. (2005) 'Linking brainwaves to the brain: An ERP primer', *Developmental Neuropsychology*, 27(2), pp. 183–215. doi: 10.1207/s15326942dn2702_1.

Kim, Y.-H. *et al.* (1999) 'The Large-Scale Neural Network for Spatial Attention Displays Multifunctional Overlap But Differential Asymmetry', *NeuroImage*, 9(3), pp. 269–277. doi: https://doi.org/10.1006/nimg.1999.0408.

Kingdom, F. A. A. and Prins, N. (2016) 'Chapter 5 – Adaptive Methods', in *Psychophysics*. Second Edi. San Diego: Academic Press, pp. 119–148. doi: 10.1016/B978-0-12-407156-8.00005-0.

Kizuk, S. A. D. and Mathewson, K. E. (2017) 'Power and Phase of Alpha Oscillations Reveal an Interaction between Spatial and Temporal Visual Attention', *Journal of Cognitive Neuroscience*. MIT PressOne Rogers Street, Cambridge, MA 02142-1209USAjournals-info@mit.edu, 29(3), pp. 480–494. doi: 10.1162/jocn_a_01058.

Klimesch, W. (1999) 'EEG alpha and theta oscillations reflect cognitive and memory performance: a review and analysis', *Brain Research Reviews*. Elsevier, 29(2–3), pp. 169–195. doi: 10.1016/S0165-0173(98)00056-3.

Klimesch, W. (2012) 'Alpha-band oscillations, attention, and controlled access to stored information', *Trends in Cognitive Sciences*. Elsevier, 16(12), pp. 606–617. doi: 10.1016/j.tics.2012.10.007.

Klimesch, W., Sauseng, P. and Hanslmayr, S. (2007) 'EEG alpha oscillations: the inhibition–timing hypothesis', *Brain Research Reviews*, 53(1), pp. 63–88. doi: 10.1016/j.brainresrev.2006.06.003.

Knakker, B., Weiss, B. and Vidnyánszky, Z. (2015) 'Object-based attentional selection

modulates anticipatory alpha oscillations', *Frontiers in Human Neuroscience*, 8, p. Article 1048. doi: 10.3389/fnhum.2014.01048.

Koenig, L. and Ro, T. (2019) 'Dissociations of conscious and unconscious perception in TMS-induced blindsight', *Neuropsychologia*. Elsevier Ltd, 128, pp. 215–222. doi: 10.1016/j.neuropsychologia.2018.03.028.

Koivisto, M. and Revonsuo, A. (2003) 'An ERP study of change detection, change blindness, and visual awareness', *Psychophysiology*. Society for Psychophysiological Research, 40(3), pp. 423–429. doi: 10.1111/1469-8986.00044.

Koivisto, M. and Revonsuo, A. (2010) 'Event-related brain potential correlates of visual awareness', *Neuroscience & Biobehavioral Reviews*. Pergamon, 34(6), pp. 922–934. doi: 10.1016/j.neubiorev.2009.12.002.

Kuntzelman, K. M. *et al.* (2021) 'Deep-Learning-Based Multivariate Pattern Analysis (dMVPA): A Tutorial and a Toolbox', *Frontiers in Human Neuroscience*, 15, p. Article 89. doi: 10.3389/fnhum.2021.638052.

Lachaux, J.-P. *et al.* (1999) 'Measuring phase synchrony in brain signals', *Human Brain Mapping*, 8(4), pp. 194–208. Available at: https://onlinelibrary.wiley.com/doi/epdf/10.1002/%28SICI%291097-0193%281999%298%3A4%3C194%3A%3AAID-HBM4%3E3.0.CO%3B2-C.

Landau, A. N. *et al.* (2015) 'Distributed Attention Is Implemented through Theta-Rhythmic Gamma Modulation', *Current Biology*. Cell Press, 25(17), pp. 2332–2337. doi: 10.1016/j.cub.2015.07.048.

Lange, J., Oostenveld, R. and Fries, P. (2013) 'Reduced Occipital Alpha Power Indexes Enhanced Excitability Rather than Improved Visual Perception', *The Journal of*

Neuroscience, 33(7), pp. 3212–3220. doi: 10.1523/JNEUROSCI.3755-12.2013.

Laufs, H. *et al.* (2003) 'EEG-correlated fMRI of human alpha activity', *NeuroImage*, 19(4), pp. 1463–1476. doi: 10.1016/S1053-8119(03)00286-6.

Li, B., Peterson, M. R. and Freeman, R. D. (2003) 'Oblique Effect: A Neural Basis in the Visual Cortex', *Journal of Neurophysiology*. American Physiological Society, 90(1), pp. 204–217. doi: 10.1152/jn.00954.2002.

Li, Y. *et al.* (2015) 'Synaptic Basis for Differential Orientation Selectivity between Complex and Simple Cells in Mouse Visual Cortex', *Journal of Neuroscience*. Society for Neuroscience, 35(31), pp. 11081–11093. doi: 10.1523/JNEUROSCI.5246-14.2015.

Limbach, K. and Corballis, P. M. (2016) 'Prestimulus alpha power influences response criterion in a detection task', *Psychophysiology*. Blackwell Publishing Inc., 53(8), pp. 1154–1164. doi: 10.1111/psyp.12666.

Liu, Y. *et al.* (2016) 'Top-down Modulation of Neural Activity in Anticipatory Visual Attention: Control Mechanisms Revealed by Simultaneous EEG-fMRI.', *Cerebral cortex*. Oxford University Press, 26(2), pp. 517–529. doi: 10.1093/cercor/bhu204.

Lobier, M., Palva, J. M. and Palva, S. (2018) 'High-alpha band synchronization across frontal, parietal and visual cortex mediates behavioral and neuronal effects of visuospatial attention', *NeuroImage*, 165, pp. 222–237. doi: https://doi.org/10.1016/j.neuroimage.2017.10.044.

Lopes da Silva, F. (1991) 'Neural mechanisms underlying brain waves: from neural membranes to networks', *Electroencephalography and Clinical Neurophysiology*, 79(2), pp. 81–93. doi: https://doi.org/10.1016/0013-4694(91)90044-5.

Lopes da Silva, F. H. *et al.* (1980) 'Relative contributions of intracortical and thalamo-cortical

processes in the generation of alpha rhythms, revealed by partial coherence analysis', *Electroencephalography and Clinical Neurophysiology*, 50(5), pp. 449–456. doi: https://doi.org/10.1016/0013-4694(80)90011-5.

Luck, S. J. *et al.* (1997) 'Neural Mechanisms of Spatial Selective Attention in Areas V1, V2, and V4 of Macaque Visual Cortex', *Journal of Neurophysiology*, 77(1), pp. 24–42. doi: 10.1152/jn.1997.77.1.24.

Luck, S. J. (2014) *An introduction to the event-related potential technique*. 2nd edn. Cambridge, Massachusetts: MIT Press. Available at: https://www.library.ualberta.ca/catalog/7776529 (Accessed: 9 November 2017).

Luck, S. J., Woodman, G. F. and Vogel, E. K. (2000) 'Event-related potential studies of attention', *Trends in Cognitive Sciences*. Elsevier Current Trends, 4(11), pp. 432–440. doi: 10.1016/S1364-6613(00)01545-X.

Lutz, A. *et al.* (2009) 'Mental Training Enhances Attentional Stability: Neural and Behavioral Evidence', *Journal of Neuroscience*. Society for Neuroscience, 29(42), pp. 13418–13427. doi: 10.1523/JNEUROSCI.1614-09.2009.

Martinez-Cancino, R. *et al.* (2020) 'Computing Phase Amplitude Coupling in EEGLAB: PACTools', *Proceedings - IEEE 20th International Conference on Bioinformatics and Bioengineering, BIBE 2020*. Institute of Electrical and Electronics Engineers Inc., pp. 387–394. doi: 10.1109/BIBE50027.2020.00070.

Martinez-Trujillo, J. C. and Treue, S. (2004) 'Feature-Based Attention Increases the Selectivity of Population Responses in Primate Visual Cortex', *Current Biology*, 14(9), pp. 744–751. doi: https://doi.org/10.1016/j.cub.2004.04.028.

Mathewson, K. E. *et al.* (2009) 'To See or Not to See: Prestimulus Phase Predicts Visual

Awareness', *Journal of Neuroscience*, 29(9), pp. 2725–2732. doi: 10.1523/JNEUROSCI.3963-08.2009.

Mathewson, K. E. *et al.* (2011) 'Pulsed out of awareness: EEG alpha oscillations represent a pulsed-inhibition of ongoing cortical processing.', *Frontiers in Psychology*, 2, p. Article 99. doi: 10.3389/fpsyg.2011.00099.

Mathewson, K. E. *et al.* (2012) 'Making waves in the stream of consciousness: entraining oscillations in EEG alpha and fluctuations in visual awareness with rhythmic visual stimulation', *Journal of Cognitive Neuroscience*. MIT Press, 24(12), pp. 2321–2333. doi: 10.1162/jocn_a_00288.

Mathewson, K. E. *et al.* (2014) 'Dynamics of Alpha Control: Preparatory Suppression of Posterior Alpha Oscillations by Frontal Modulators Revealed with Combined EEG and Event-related Optical Signal', *Journal of Cognitive Neuroscience*. MIT PressOne Rogers Street, Cambridge, MA 02142-1209USAjournals-info@mit.edu, 26(10), pp. 2400–2415. doi: 10.1162/jocn_a_00637.

Maunsell, J. H. R. and Treue, S. (2006) 'Feature-based attention in visual cortex', *Trends in Neurosciences*, 29(6), pp. 317–322. doi: https://doi.org/10.1016/j.tins.2006.04.001.

McAdams, C. J. and Maunsell, J. H. R. (1999) 'Effects of Attention on Orientation-Tuning Functions of Single Neurons in Macaque Cortical Area V4', *Journal of Neuroscience*. Society for Neuroscience, 19(1), pp. 431–441. doi: 10.1523/JNEUROSCI.19-01-00431.1999.

Mesulam, M.-M. (1999) 'Spatial attention and neglect: parietal, frontal and cingulate contributions to the mental representation and attentional targeting of salient extrapersonal events', *Philosophical Transactions of the Royal Society of London. Series*

B: Biological Sciences. Edited by A. Howseman and S. Zeki, 354(1387), pp. 1325–1346. doi: 10.1098/rstb.1999.0482.

Michel, R., Dugué, L. and Busch, N. A. (2021) 'Distinct contributions of alpha and theta rhythms to perceptual and attentional sampling', *European Journal of Neuroscience*. John Wiley & Sons, Ltd. doi: 10.1111/ejn.15154.

Mierau, A., Klimesch, W. and Lefebvre, J. (2017) 'State-dependent alpha peak frequency shifts: experimental evidence, potential mechanisms and functional implications', *Neuroscience*. Pergamon, 360, pp. 146–154. doi: 10.1016/J.NEUROSCIENCE.2017.07.037.

Miller, E. K. and Buschman, T. J. (2013) 'Cortical circuits for the control of attention', *Current Opinion in Neurobiology*, 23(2), pp. 216–222. doi: https://doi.org/10.1016/j.conb.2012.11.011.

Miller, K. J. *et al.* (2014) 'Broadband changes in the cortical surface potential track activation of functionally diverse neuronal populations', *NeuroImage*, 85, pp. 711–720. doi: https://doi.org/10.1016/j.neuroimage.2013.08.070.

Moos, K. *et al.* (2012) 'Modulation of Top-Down Control of Visual Attention by Cathodal tDCS over Right IPS', *Journal of Neuroscience*. Society for Neuroscience, 32(46), pp. 16360–16368. doi: 10.1523/JNEUROSCI.6233-11.2012.

Moosmann, M. *et al.* (2003) 'Correlates of alpha rhythm in functional magnetic resonance imaging and near infrared spectroscopy', *NeuroImage*, 20(1), pp. 145–158. doi: 10.1016/S1053-8119(03)00344-6.

Motter, B. C. (1993) 'Focal attention produces spatially selective processing in visual cortical areas V1, V2, and V4 in the presence of competing stimuli', *Journal of Neurophysiology*. American Physiological Society, 70(3), pp. 909–919. doi: 10.1152/jn.1993.70.3.909.

Ni, J. *et al.* (2016) 'Gamma-Rhythmic Gain Modulation', *Neuron*. Cell Press, 92(1), pp. 240–251. doi: 10.1016/j.neuron.2016.09.003.

Nobre, A. C. and Kastner, S. (eds) (2014) *The Oxford Handbook of Attention.* New York, NY, US: Oxford University Press (Oxford library of psychology.).

Nobre, A. C., Sebestyen, G. N. and Miniussi, C. (2000) 'The dynamics of shifting visuospatial attention revealed by event-related potentials', *Neuropsychologia*, 38(7), pp. 964–974. doi: https://doi.org/10.1016/S0028-3932(00)00015-4.

Nolte, G. *et al.* (2004) 'Identifying true brain interaction from EEG data using the imaginary part of coherency', *Clinical Neurophysiology*, 115(10), pp. 2292–2307. doi: https://doi.org/10.1016/j.clinph.2004.04.029.

O'Neill, G. C. *et al.* (2018) 'Dynamics of large-scale electrophysiological networks: A technical review', *NeuroImage*, 180, pp. 559–576. doi: https://doi.org/10.1016/j.neuroimage.2017.10.003.

Okazaki, Y. O., Mizuno, Y. and Kitajo, K. (2020) 'Probing dynamical cortical gating of attention with concurrent TMS-EEG', *Scientific Reports*. Nature Research, 10(1), pp. 1–10. doi: 10.1038/s41598-020-61590-2.

Oostenveld, R. *et al.* (2011) 'FieldTrip: Open source software for advanced analysis of MEG, EEG, and invasive electrophysiological data', *Computational Intelligence and Neuroscience*. Hindawi Limited, 2011, p. Article 156869. doi: 10.1155/2011/156869.

Özkurt, T. E. and Schnitzler, A. (2011) 'A critical note on the definition of phase–amplitude cross-frequency coupling', *Journal of Neuroscience Methods*. Elsevier, 201(2), pp. 438–443. doi: 10.1016/J.JNEUMETH.2011.08.014.

Pagnotta, M. F., Pascucci, D. and Plomp, G. (2022) 'Selective attention involves a feature-

specific sequential release from inhibitory gating', *NeuroImage*, 246, p. Article 118782. doi: https://doi.org/10.1016/j.neuroimage.2021.118782.

Palomäki, J. *et al.* (2012) 'Brain oscillatory 4-35 Hz EEG responses during an n-back task with complex visual stimuli', *Neuroscience Letters*. Elsevier, 516(1), pp. 141–145. doi: 10.1016/j.neulet.2012.03.076.

Pelli, D. G. (1997) 'The VideoToolbox software for visual psychophysics: transforming numbers into movies.', *Spatial vision*, 10(4), pp. 437–442. Available at: http://www.ncbi.nlm.nih.gov/pubmed/9176953 (Accessed: 5 October 2017).

Penny, W. D. *et al.* (2008) 'Testing for nested oscillation', *Journal of Neuroscience Methods*. Elsevier, 174(1), pp. 50–61. doi: 10.1016/j.jneumeth.2008.06.035.

Perrin, F. *et al.* (1989) 'Spherical splines for scalp potential and current density mapping', *Electroencephalography and Clinical Neurophysiology*, 72(2), pp. 184–187. doi: 10.1016/0013-4694(89)90180-6.

Peylo, C., Hilla, Y. and Sauseng, P. (2021) 'Cause or consequence? Alpha oscillations in visuospatial attention', *Trends in Neurosciences*, 44(9), pp. 705–713. doi: https://doi.org/10.1016/j.tins.2021.05.004.

Pezoulas, V. C. *et al.* (2018) 'FCLAB: An EEGLAB module for performing functional connectivity analysis on single-subject EEG data', in *2018 IEEE EMBS International Conference on Biomedical & Health Informatics (BHI)*. IEEE, pp. 96–99. doi: 10.1109/BHI.2018.8333378.

Pfurtscheller, G., Stancák, A. and Neuper, C. (1996) 'Event-related synchronization (ERS) in the alpha band - An electrophysiological correlate of cortical idling: A review', *International Journal of Psychophysiology*. Elsevier B.V., 24(1–2), pp. 39–46. doi: 10.1016/S0167-

8760(96)00066-9.

Plomp, G. *et al.* (2015) 'Early recurrence and ongoing parietal driving during elementary visual processing', *Scientific reports*. Nature Publishing Group, 5, p. 18733. doi: 10.1038/srep18733.

Popov, T. *et al.* (2019) 'Spatial specificity of alpha oscillations in the human visual system', *Human Brain Mapping*. John Wiley & Sons, Ltd, 40(15), pp. 4432–4440. doi: https://doi.org/10.1002/hbm.24712.

Potts, G. F. and Tucker, D. M. (2001) 'Frontal evaluation and posterior representation in target detection', *Cognitive Brain Research*. Elsevier, 11(1), pp. 147–156. doi: 10.1016/S0926-6410(00)00075-6.

Pouget, A., Dayan, P. and Zemel, R. (2000) 'Information processing with population codes', *Nature Reviews Neuroscience*, 1(2), pp. 125–132. doi: 10.1038/35039062.

Pritchett, D. L. *et al.* (2015) 'For things needing your attention: The role of neocortical gamma in sensory perception', *Current Opinion in Neurobiology*. Elsevier Ltd, pp. 254–263. doi: 10.1016/j.conb.2015.02.004.

R Core Team (2021) 'R: A language and environment for statistical computing'. Vienna, Austria: R Foundation for Statistical Computing. Available at: http://www.r-project.org/.

Rawls, E., Miskovic, V. and Lamm, C. (2020) 'Delta phase reset predicts conflict-related changes in P3 amplitude and behavior', *Brain Research*. Elsevier B.V., 1730, p. 146662. doi: 10.1016/j.brainres.2020.146662.

Raybaut, P. (2009) 'Spyder-documentation', *Available online at: pythonhosted.org*. Available at: https://www.spyder-ide.org/.

Reteig, L. C. *et al.* (2019) 'Sustaining attention for a prolonged period of time increases temporal

variability in cortical responses', *Cortex*, 117, pp. 16–32. doi: https://doi.org/10.1016/j.cortex.2019.02.016.

Riddle, J. *et al.* (2020) 'Causal Evidence for a Role of Theta and Alpha Oscillations in the Control of Working Memory', *Current Biology*, 30(9), pp. 1748–1754. doi: https://doi.org/10.1016/j.cub.2020.02.065.

Rihs, T. A., Michel, C. M. and Thut, G. (2009) 'A bias for posterior α-band power suppression versus enhancement during shifting versus maintenance of spatial attention', *NeuroImage*, 44(1), pp. 190–199. doi: https://doi.org/10.1016/j.neuroimage.2008.08.022.

Ritchie, J. B., Kaplan, D. M. and Klein, C. (2019) 'Decoding the Brain: Neural Representation and the Limits of Multivariate Pattern Analysis in Cognitive Neuroscience', *The British Journal for the Philosophy of Science*, 70(2), pp. 581–607. doi: 10.1093/bjps/axx023.

Romei, V. *et al.* (2008) 'Spontaneous Fluctuations in Posterior α-Band EEG Activity Reflect Variability in Excitability of Human Visual Areas', *Cerebral Cortex*, 18(9), pp. 2010–2018. doi: 10.1093/cercor/bhm229.

Ronconi, L., Busch, N. A. and Melcher, D. (2018) 'Alpha-band sensory entrainment alters the duration of temporal windows in visual perception', *Scientific Reports*. Nature Publishing Group, 8(1), p. 11810. doi: 10.1038/s41598-018-29671-5.

Ronconi, L. and Melcher, D. (2017) 'Alpha oscillation phase determines the timing of perception: evidence from sensory entrainment', *Journal of Vision*, 17(10), p. 726. doi: 10.1167/17.10.726.

Di Russo, F. *et al.* (2019) 'Normative event-related potentials from sensory and cognitive tasks reveal occipital and frontal activities prior and following visual events', *NeuroImage*. Academic Press Inc., 196, pp. 173–187. doi: 10.1016/j.neuroimage.2019.04.033.

Di Russo, F. *et al.* (2021) 'Sustained visuospatial attention enhances lateralized anticipatory ERP activity in sensory areas', *Brain Structure and Function*, 226(2), pp. 457–470. doi: 10.1007/s00429-020-02192-6.

Ruzzoli, M. *et al.* (2019) 'The relevance of alpha phase in human perception', *Cortex*. Elsevier BV, 120, pp. 249–268. doi: 10.1016/j.cortex.2019.05.012.

Saalmann, Y. B. *et al.* (2012) 'The Pulvinar Regulates Information Transmission Between Cortical Areas Based on Attention Demands', *Science*, 337(6095), pp. 753–756. doi: 10.1126/science.1223082.

Sadaghiani, S., Brookes, M. J. and Baillet, S. (2022) 'Connectomics of human electrophysiology', *NeuroImage*, 247, p. 118788. doi: https://doi.org/10.1016/j.neuroimage.2021.118788.

Sadaghiani, S. and Kleinschmidt, A. (2016) 'Brain Networks and α-Oscillations: Structural and Functional Foundations of Cognitive Control', *Trends in Cognitive Sciences*, 20(11), pp. 805–817. doi: https://doi.org/10.1016/j.tics.2016.09.004.

Salti, M., Bar-Haim, Y. and Lamy, D. (2012) 'The P3 component of the ERP reflects conscious perception, not confidence', *Consciousness and Cognition*. Academic Press, 21(2), pp. 961–968. doi: 10.1016/j.concog.2012.01.012.

Samaha, J. *et al.* (2020) 'Spontaneous Brain Oscillations and Perceptual Decision-Making', *Trends in Cognitive Sciences*. Elsevier Ltd, 24(8), pp. 639–653. doi: 10.1016/j.tics.2020.05.004.

Samaha, J., Gosseries, O. and Postle, B. R. (2017) 'Distinct Oscillatory Frequencies Underlie Excitability of Human Occipital and Parietal Cortex', *Journal of Neuroscience*. Society for Neuroscience, 37(11), pp. 2824–2833. doi: 10.1523/JNEUROSCI.3413-16.2017.

Samaha, J., Iemi, L. and Postle, B. R. (2017) 'Prestimulus alpha-band power biases visual discrimination confidence, but not accuracy', *Consciousness and Cognition*. Academic Press, 54, pp. 47–55. doi: 10.1016/J.CONCOG.2017.02.005.

Samaha, J., Sprague, T. C. and Postle, B. R. (2016) 'Decoding and Reconstructing the Focus of Spatial Attention from the Topography of Alpha-band Oscillations', *Journal of Cognitive Neuroscience*. MIT PressOne Rogers Street, Cambridge, MA 02142-1209USAjournals-info@mit.edu, 28(8), pp. 1090–1097. doi: 10.1162/jocn_a_00955.

Samaha, J., Switzky, M. and Postle, B. R. (2019) 'Confidence boosts serial dependence in orientation estimation', *Journal of Vision*. Association for Research in Vision and Ophthalmology Inc., 19(4). doi: 10.1167/19.4.25.

Samuel, I. B. H. *et al.* (2018) 'The frequency of alpha oscillations: Task-dependent modulation and its functional significance', *NeuroImage*. Academic Press Inc., 183, pp. 897–906. doi: 10.1016/j.neuroimage.2018.08.063.

Sauseng, P. *et al.* (2004) 'Theta coupling in the human electroencephalogram during a working memory task', *Neuroscience Letters*. Elsevier Ireland Ltd, 354(2), pp. 123–126. doi: 10.1016/j.neulet.2003.10.002.

Sauseng, P. *et al.* (2005) 'A shift of visual spatial attention is selectively associated with human EEG alpha activity', *European Journal of Neuroscience*. John Wiley & Sons, Ltd, 22(11), pp. 2917–2926. doi: https://doi.org/10.1111/j.1460-9568.2005.04482.x.

Sauseng, P. and Klimesch, W. (2008) 'What does phase information of oscillatory brain activity tell us about cognitive processes?', *Neuroscience & Biobehavioral Reviews*, 32(5), pp. 1001–1013. doi: https://doi.org/10.1016/j.neubiorev.2008.03.014.

Schalk, G. (2015) 'A general framework for dynamic cortical function: the function-through-

biased-oscillations (FBO) hypothesis', *Frontiers in Human Neuroscience*, 9, p. Article 352. doi: 10.3389/fnhum.2015.00352.

Scheeringa, R. *et al.* (2011) 'Modulation of Visually Evoked Cortical fMRI Responses by Phase of Ongoing Occipital Alpha Oscillations', *The Journal of Neuroscience*, 31(10), pp. 3813–3820. doi: 10.1523/JNEUROSCI.4697-10.2011.

Schneegans, S. and Bays, P. M. (2016) 'No fixed item limit in visuospatial working memory', *Cortex*, 83, pp. 181–193. doi: https://doi.org/10.1016/j.cortex.2016.07.021.

Schneegans, S., Taylor, R. and Bays, P. M. (2020) 'Stochastic sampling provides a unifying account of visual working memory limits', *Proceedings of the National Academy of Sciences*, 117(34), pp. 20959 LP – 20968. doi: 10.1073/pnas.2004306117.

Schroeder, C. E. and Lakatos, P. (2009) 'Low-frequency neuronal oscillations as instruments of sensory selection', *Trends in Neurosciences*, 32(1), pp. 9–18. doi: https://doi.org/10.1016/j.tins.2008.09.012.

Schurgin, M. W., Wixted, J. T. and Brady, T. F. (2020) 'Psychophysical scaling reveals a unified theory of visual memory strength', *Nature Human Behaviour*, 4(11), pp. 1156–1172. doi: 10.1038/s41562-020-00938-0.

Schürmann, M. *et al.* (1995) 'A new metric for analyzing single-trial event-related potentials (ERPs): application to human visual P300 delta response', *Neuroscience Letters*. Elsevier, 197(3), pp. 167–170. doi: 10.1016/0304-3940(95)11912-G.

Schürmann, M. *et al.* (2001) 'Delta responses and cognitive processing: Single-trial evaluations of human visual P300', *International Journal of Psychophysiology*. Elsevier, 39(2–3), pp. 229–239. doi: 10.1016/S0167-8760(00)00144-6.

Seymour, R. A., Rippon, G. and Kessler, K. (2017) 'The Detection of Phase Amplitude Coupling

during Sensory Processing', *Frontiers in Neuroscience*. Frontiers Media S.A., 11(SEP), p. 487. doi: 10.3389/fnins.2017.00487.

Sheldon, S. S. and Mathewson, K. E. (2021) 'To see, not to see or to see poorly: Perceptual quality and guess rate as a function of electroencephalography (EEG) brain activity in an orientation perception task', *European Journal of Neuroscience*. John Wiley & Sons, Ltd, pp. 1–24. doi: https://doi.org/10.1111/ejn.15445.

Shen, S. and Ma, W. J. (2019) 'Variable precision in visual perception', *Psychological Review*, 126(1), pp. 89–132. doi: 10.1037/rev0000128.

Silva, L. R., Amitai, Y. and Connors, B. W. (1991) 'Intrinsic Oscillations of Neocortex Generated by Layer 5 Pyramidal Neurons', *Science*, 251(4992), pp. 432–435. doi: 10.1126/science.1824881.

Siman-Tov, T. *et al.* (2007) 'Bihemispheric Leftward Bias in a Visuospatial Attention-Related Network', *Journal of Neuroscience*. Society for Neuroscience, 27(42), pp. 11271–11278. doi: 10.1523/JNEUROSCI.0599-07.2007.

Sokoliuk, R. *et al.* (2019) 'Two Spatially Distinct Posterior Alpha Sources Fulfill Different Functional Roles in Attention', *Journal of Neuroscience*. Society for Neuroscience, 39(36), pp. 7183–7194. doi: 10.1523/JNEUROSCI.1993-18.2019.

Spitzer, H., Desimone, R. and Moran, J. (1988) 'Increased Attention Enhances Both Behavioral and Neuronal Performance', *Science*. American Association for the Advancement of Science, 240(4850), pp. 338–340. doi: 10.1126/science.3353728.

Stouffer, S. A. *et al.* (1949) 'Studies in social psychology in World War II: the American soldier', in *Adjustment During Army Life*. Vol. 1. Princeton, NJ.: Princeton University Press. Available at: https://psycnet.apa.org/record/1950-00790-000.

Suchow, J. W. *et al.* (2013) 'Modeling visual working memory with the MemToolbox.', *Journal of Vision*. Association for Research in Vision and Ophthalmology, 13(10), pp. 1–8. doi: 10.1167/13.10.9.

Taghizadeh-Sarabi, M., Daliri, M. R. and Niksirat, K. S. (2014) 'Decoding Objects of Basic Categories from Electroencephalographic Signals Using Wavelet Transform and Support Vector Machines', *Brain Topography*. Springer, 28(1), pp. 33–46. doi: 10.1007/S10548-014-0371-9.

Tallon-Baudry, C. (2012) 'On the neural mechanisms subserving consciousness and attention', *Frontiers in Psychology*. Frontiers, 2, p. 397. doi: 10.3389/fpsyg.2011.00397.

Taylor, R. and Bays, P. M. (2018) 'Efficient Coding in Visual Working Memory Accounts for Stimulus-Specific Variations in Recall', *Journal of Neuroscience*. Society for Neuroscience, 38(32), pp. 7132–7142. doi: 10.1523/JNEUROSCI.1018-18.2018.

Taylor, R. and Bays, P. M. (2020) 'Theory of Neural Coding Predicts an Upper Bound on Estimates of Memory Variability', *Psychological Review*, 127(5), pp. 700–718. doi: 10.1037/rev0000189.

Thut, G. *et al.* (2006) 'α-Band Electroencephalographic Activity over Occipital Cortex Indexes Visuospatial Attention Bias and Predicts Visual Target Detection', *Journal of Neuroscience*. Society for Neuroscience, 26(37), pp. 9494–9502. doi: 10.1523/JNEUROSCI.0875-06.2006.

Thuwal, K., Banerjee, A. and Roy, D. (2021) 'Aperiodic and Periodic Components of Ongoing Oscillatory Brain Dynamics Link Distinct Functional Aspects of Cognition across Adult Lifespan', *eNeuro*. Society for Neuroscience, 8(5). doi: 10.1523/ENEURO.0224-21.2021.

Tort, A. B. L. *et al.* (2008) 'Dynamic cross-frequency couplings of local field potential oscillations in rat striatum and hippocampus during performance of a T-maze task', *Proceedings of the National Academy of Sciences*. National Academy of Sciences, 105(51), pp. 20517–20522. doi: 10.1073/PNAS.0810524105.

Tort, A. B. L. *et al.* (2010) 'Measuring Phase-Amplitude Coupling Between Neuronal Oscillations of Different Frequencies', *Journal of Neurophysiology*, 104(2), pp. 1195–1210. doi: 10.1152/jn.00106.2010.

VanRullen, R. (2011) 'Four common conceptual fallacies in mapping the time course of recognition.', *Frontiers in Psychology*. Frontiers Media SA, 2, p. Article 365. doi: 10.3389/fpsyg.2011.00365.

VanRullen, R. (2016a) 'How to Evaluate Phase Differences between Trial Groups in Ongoing Electrophysiological Signals', *Frontiers in Neuroscience*. Frontiers, 10, p. 426. doi: 10.3389/fnins.2016.00426.

VanRullen, R. (2016b) 'Perceptual cycles', *Trends in Cognitive Sciences*. Elsevier Current Trends, 20(10), pp. 723–735. doi: 10.1016/j.tics.2016.07.006.

van de Vijver, I. and Cohen, M. X. (2019) *Electrophysiological phase synchrony in distributed brain networks as a promising tool in the study of cognition*, *New Methods in Cognitive Psychology*. doi: 10.4324/9780429318405-8.

Vinck, M. *et al.* (2011) 'An improved index of phase-synchronization for electrophysiological data in the presence of volume-conduction, noise and sample-size bias', *NeuroImage*, 55(4), pp. 1548–1565. doi: https://doi.org/10.1016/j.neuroimage.2011.01.055.

Voytek, B. (2010) 'Shifts in gamma phase–amplitude coupling frequency from theta to alpha over posterior cortex during visual tasks', *Frontiers in Human Neuroscience*. Frontiers

Media S. A., 4, p. 191. doi: 10.3389/fnhum.2010.00191.

Voytek, B. *et al.* (2015) 'Age-Related Changes in 1/f Neural Electrophysiological Noise', *Journal of Neuroscience*. Society for Neuroscience, 35(38), pp. 13257–13265. doi: 10.1523/JNEUROSCI.2332-14.2015.

De Vries, I. E. J. *et al.* (2018) 'Priority switches in visual working memory are supported by frontal delta and posterior alpha interactions', *Cerebral Cortex*. Oxford University Press, 28(11), pp. 4090–4104. doi: 10.1093/cercor/bhy223.

Wagner, J. *et al.* (2019) 'Can Oscillatory Alpha-Gamma Phase-Amplitude Coupling be Used to Understand and Enhance TMS Effects?', *Frontiers in Human Neuroscience*, 13, p. Article 263. doi: 10.3389/fnhum.2019.00263.

Wandell, B. A., Dumoulin, S. O. and Brewer, A. A. (2009) 'Visual cortex in humans', *Encyclopedia of Neuroscience*, 10, pp. 251–257. Available at: https://www.spinozacentre.nl/dumoulin/PDFs/Wandell-Encyclopedia-2009.pdf.

Waschke, L. *et al.* (2021) 'Modality-specific tracking of attention and sensory statistics in the human electrophysiological spectral exponent', *eLife*. Edited by M. Chait et al. eLife Sciences Publications, Ltd, 10, p. e70068. doi: 10.7554/eLife.70068.

Woodman, G. F. (2010) 'A brief introduction to the use of event-related potentials in studies of perception and attention', *Attention, Perception, & Psychophysics*. Springer-Verlag, 72(8), pp. 2031–2046. doi: 10.3758/BF03196680.

Worden, M. S. *et al.* (2000) 'Anticipatory Biasing of Visuospatial Attention Indexed by Retinotopically Specific α-Bank Electroencephalography Increases over Occipital Cortex', *Journal of Neuroscience*. Society for Neuroscience, 20(6), p. RC63. doi: 10.1523/JNEUROSCI.20-06-j0002.2000.

Wright, M. J., Geffen, G. M. and Geffen, L. B. (1995) 'Event related potentials during covert orientation of visual attention: effects of cue validity and directionality', *Biological Psychology*, 41(2), pp. 183–202. doi: https://doi.org/10.1016/0301-0511(95)05128-7.

Yuan, Z. *et al.* (2021) 'The Modulating Effect of Top-down Attention on the Optimal Pre-target Onset Oscillatory States of Bottom-up Attention', *Neuroscience*. Pergamon, 466, pp. 186–195. doi: 10.1016/J.NEUROSCIENCE.2021.03.036.

Zazio, A. *et al.* (2020) 'Modelling the effects of ongoing alpha activity on visual perception: The oscillation-based probability of response', *Neuroscience & Biobehavioral Reviews*. Elsevier Ltd, 112, pp. 242–253. doi: 10.1016/j.neubiorev.2020.01.037.

Zazio, A. *et al.* (2021) 'Pre-stimulus alpha-band power and phase fluctuations originate from different neural sources and exert distinct impact on stimulus-evoked responses', *European Journal of Neuroscience*. John Wiley & Sons, Ltd, 00, pp. 1–13. doi: https://doi.org/10.1111/ejn.15138.

Zhang, W. and Luck, S. J. (2008) 'Discrete fixed-resolution representations in visual working memory.', *Nature*. NIH Public Access, 453(7192), pp. 233–235. doi: 10.1038/nature06860.

Zhou, H., Schafer, R. J. and Desimone, R. (2016) 'Pulvinar-Cortex Interactions in Vision and Attention', *Neuron*, 89(1), pp. 209–220. doi: https://doi.org/10.1016/j.neuron.2015.11.034.

Appendix A

FITTED PARAMETER VALUES FROM WORKING MEMORY MODELS

Appendix Table A.1. *Fitted parameter values from working memory models*

	Standard Mixture Model		
	Guess Rate (g)	SD (σ)	Bias (μ)
Model	0.19 ± 0.04	11.15 ± 0.51	-
Model + Bias	0.19 ± 0.04	11.04 ± 0.51	0.14 ± 0.29

	Variable Precision Model (Gaussian over SD)		
	Guess Rate (g)	meanSD (σ_{mn})	stdSD (σ_{std})
Model	0.18 ± 0.03	11.26 ± 0.54	2.82 ± 0.31
Model − Guess Rate	-	10.23 ± 5.72	33.48 ± 5.26

	Variable Precision Model (Gamma over Precision)		
	Guess Rate (g)	modePrecision (J_{mod}) / Shape	stdPrecision (J_{std}) / Scale
Model	0.17 ± 0.03	0.012 ± 0.001 / 13.62 ± 5.42	0.009 ± 0.002 / 0.005 ± 0.001
Model − Guess Rate	-	0.011 ± 0.002 / 1.59 ± 0.12	0.061 ± 0.017 / 0.056 ± 0.018

Note. All values are *Mean* ± *SEM*. Scale and shape are the traditional parameters of the Gamma distribution.

Appendix B

STEPWISE MULTIPLE REGRESSION

B.1 METHODS

Stepwise multiple regression analyses were performed for the standard mixture model parameters from "high" and "low" trials separately. For the guess rate parameter, predictor variables were the guess rates on 2-3 Hz, 4-7 Hz, and 8-40 Hz log power trials averaged across the time windows used for each ERP component that showed significant effects in the previous analyses: 200-255 ms (P2), 255-360 ms (N2), and 360-500 ms (P3). The predicted variables were the guess rates on trials with high or low amplitudes in their P2, N2, and P3 ERP components. For the standard deviation parameter, the predictor variables were the same in the guess rate analyses except only the 360-500 ms (P3) time window was used. Similarly, the only predicted variables were the standard deviation parameters from trials split by their P3 ERP component. A Bonferroni type adjustment was made for inflated Type 1 error, α for each electrode site was assigned the value of 0.0028 for each $b*$ among a set of $b*$ such that α for each set did not exceed the critical value of 0.05 (Karakaş et al., 2000) The cumulative proportion of explained variances adjusted for number of predictors (referred to as the adjusted coefficient of determination; R^2_{adj}) and the standardized regression coefficients ($b*$) for the regression equations at each step of the multivariate analysis for guess rates and standard deviation parameters are summarized in Table B.1 and Table B.2, respectively.

It should be noted that multicollinearity, that is, a high correlation between two or most predictor variables, is present in the stepwise multiple regression analyses described above. This is the most likely cause of the negative standardized regression coefficients seen in Tables B.1

and B2. While this is considered an issue that could interfere with the multiple regression analyses, we are using these results to get a rough estimate of the relative contributions from each predictor variable. The presence of multicollinearity usually means that it is harder to reject the null hypothesis, thus one might miss the importance of the predictors (Faraway, 2016). With regards to the current dataset, this means that some predictors might have greater relative importance than indicated by their $b*$.

B.2 RESULTS

As Table B.1 shows, the guess rate parameter from 2-3 Hz, 4-7 Hz and higher frequencies amply account for the guess rate values on trials with high and low ERP amplitudes. The proportion of explained variances were between 0.935-0.990. Table B.2 shows a similar result for the standard deviation (σ) parameter except the proportion of explained variances were smaller, being between 0.700-0.928.

Appendix Table B.1. *Stepwise regression results for guess rate (g) parameter.*

Trial Category	Predicted Model	P2 (200-255 ms) $b*$	P2 (200-255 ms) R^2_{adj}	N2 (255-360 ms) $b*$	N2 (255-360 ms) R^2_{adj}	P3 (360-500 ms) $b*$	P3 (360-500 ms) R^2_{adj}
			Fp1				
High	Step 1		0.953		0.961		0.958
	2-3 Hz	0.98		0.98		0.98	
	Step 2		0.956		0.965		0.956
	2-3 Hz	0.34		0.29		0.90	
	4-7 Hz	0.64		0.70		0.08	
	Step 3		0.953		0.963		0.955
	2-3 Hz	0.35		0.35		1.06	
	4-7 Hz	0.58		0.81		0.24	
	8-40 Hz	0.06		-0.17		-0.32	
Low	Step 1		0.963		0.970		0.966
	2-3 Hz	0.98		0.99		0.98	
	Step 2		0.966		0.974		0.965
	2-3 Hz	0.31		0.26		0.74	
	4-7 Hz	0.67		0.73		0.25	
	Step 3		0.965		0.973		0.964

	2-3 Hz	0.30		0.29	0.94	
	4-7 Hz	0.58		0.75	0.38	
	8-40 Hz	0.11		-0.05	-0.34	
			FC2			
High	Step 1		0.953		0.977	0.935
	2-3 Hz	0.98		0.99	0.97	
	Step 2		0.954		0.977	0.935
	2-3 Hz	0.67		1.16	0.67	
	4-7 Hz	0.31		-0.18	0.30	
	Step 3		0.952		0.980	0.935
	2-3 Hz	0.70		0.99	0.50	
	4-7 Hz	0.41		-0.57	0.09	
	8-40 Hz	-0.13		0.56	0.38	
Low	Step 1		0.975		0.982	0.965
	2-3 Hz	0.99		0.99	0.98	
	Step 2		0.976		0.983	0.967
	2-3 Hz	0.70		1.23	0.63	
	4-7 Hz	0.29		-0.24	0.36	
	Step 3		0.975		0.984	0.970
	2-3 Hz	0.71		1.07	0.36	
	4-7 Hz	0.33		-0.49	0.05	
	8-40 Hz	-0.05		0.41	0.58	
			P5			
High	Step 1		0.954		0.972	0.963
	2-3 Hz	0.98		0.99	0.98	
	Step 2		0.965		0.971	0.964
	2-3 Hz	0.31		1.09	0.70	
	4-7 Hz	0.68		-0.10	0.29	
	Step 3		0.990		0.972	0.962
	2-3 Hz	0.23		1.04	0.70	
	4-7 Hz	-0.44		-0.42	0.28	
	8-40 Hz	1.21		0.37	0.01	
Low	Step 1		0.950		0.980	0.981
	2-3 Hz	0.98		0.99	0.99	
	Step 2		0.960		0.981	0.981
	2-3 Hz	0.29		1.23	0.79	
	4-7 Hz	0.70		-0.24	0.20	
	Step 3		0.986		0.980	0.980
	2-3 Hz	0.20		1.22	0.79	
	4-7 Hz	-0.41		-0.30	0.19	

	8-40 Hz	1.20		0.07	0.01	
			P7			
High	Step 1		0.943	0.968		0.955
	2-3 Hz	0.97		0.98	0.98	
	Step 2		0.956	0.967		0.958
	2-3 Hz	0.05		0.85	0.44	
	4-7 Hz	0.93		0.13	0.55	
	Step 3		0.988	0.966		0.957
	2-3 Hz	-0.13		0.84	0.48	
	4-7 Hz	-0.11		0.03	0.71	
	8-40 Hz	1.23		0.12	-0.21	
Low	Step 1		0.942	0.971		0.961
	2-3 Hz	0.97		0.99	0.98	
	Step 2		0.950	0.970		0.967
	2-3 Hz	0.25		1.02	0.09	
	4-7 Hz	0.73		-0.04	0.89	
	Step 3		0.987	0.969		0.967
	2-3 Hz	-0.02		0.96	0.23	
	4-7 Hz	-0.27		-0.21	1.11	
	8-40 Hz	1.29		0.25	-0.36	
			P8			
High	Step 1		0.952	0.955		0.964
	2-3 Hz	0.98		0.98	0.98	
	Step 2		0.950	0.954		0.975
	2-3 Hz	1.12		0.72	0.15	
	4-7 Hz	-0.15		0.26	0.84	
	Step 3		0.973	0.960		0.976
	2-3 Hz	0.39		0.52	-0.06	
	4-7 Hz	-0.77		-0.44	0.62	
	8-40 Hz	1.36		0.90	0.43	
Low	Step 1		0.943	0.967		0.982
	2-3 Hz	0.97		0.98	0.99	
	Step 2		0.941	0.966		0.983
	2-3 Hz	1.13		0.85	0.64	
	4-7 Hz	-0.16		0.14	0.35	
	Step 3		0.964	0.969		0.984
	2-3 Hz	0.27		0.62	0.32	
	4-7 Hz	-0.70		-0.45	0.23	
	8-40 Hz	1.41		0.82	0.44	
			O1			

High	Step 1		0.959		0.958		0.950
	2-3 Hz	0.98		0.98		0.98	
	Step 2		0.957		0.956		0.956
	2-3 Hz	0.76		1.05		0.47	
	4-7 Hz	0.22		-0.07		0.51	
	Step 3		0.967		0.958		0.958
	2-3 Hz	0.29		0.80		0.29	
	4-7 Hz	-0.13		-0.31		0.21	
	8-40 Hz	0.83		0.49		0.49	
Low	Step 1		0.957		0.967		0.972
	2-3 Hz	0.98		0.98		0.99	
	Step 2		0.956		0.966		0.975
	2-3 Hz	0.71		1.10		0.53	
	4-7 Hz	0.27		-0.12		0.46	
	Step 3		0.967		0.971		0.982
	2-3 Hz	0.26		0.90		0.28	
	4-7 Hz	-0.09		-0.64		-0.18	
	8-40 Hz	0.82		0.72		0.90	
			O2				
High	Step 1		0.932		0.956		0.954
	2-3 Hz	0.97		0.98		0.98	
	Step 2		0.945		0.954		0.960
	2-3 Hz	0.01		0.98		0.36	
	4-7 Hz	0.97		0.00		0.62	
	Step 3		0.964		0.969		0.963
	2-3 Hz	-0.23		0.41		0.14	
	4-7 Hz	-0.06		-0.54		0.27	
	8-40 Hz	1.28		1.12		0.58	
Low	Step 1		0.910		0.960		0.972
	2-3 Hz	0.96		0.98		0.99	
	Step 2		0.938		0.960		0.975
	2-3 Hz	-0.17		0.74		0.52	
	4-7 Hz	1.14		0.24		0.47	
	Step 3		0.959		0.972		0.979
	2-3 Hz	-0.37		0.25		0.25	
	4-7 Hz	0.10		-0.44		0.10	
	8-40 Hz	1.25		1.18		0.64	

Note. Predictors in each model are the guess rate parameters from fitting the standard mixture model to trials categorized as high or low log power in the specified frequency band and time windows. Predicted values are the guess rate parameters from fitting the standard mixture model to trials categorized as high or low ERP amplitudes in the specified time windows. $b*$ = estimated values of standardized regression coefficients; R^2_{adj} = adjusted coefficient of determination (*i.e.,* coefficient of determination adjusted for number of predictors).

The guess rate from the P2 (200-255 ms) ERP trials (both high and low) had a clear difference in its major contributor between the frontal electrodes (Fp1 and FC2) and the parietal and occipital electrodes. The guess rates from 2-3 Hz and 2-7 Hz trials accounted for most of the variance (0.954-0.976) in the frontal electrodes and the addition of higher frequencies was redundant or detrimental (0.952-0.975). In comparison, the addition of higher frequencies in the parietal and occipital electrodes regression models added some small benefit to the proportion of explained variances (increased 0.009-0.036).

Interestingly, the guess rate from the N2 (255-360 ms) ERP trials (both high and low) had most of its variance accounted for by the guess rates from 2-3 Hz trials (0.955-0.982). According to the standardized regression coefficients, whose values can be thought of as indicators of relative importance in the regression model, the 2-3 Hz guess rates were the “best” predictors in all cases except for Fp1 which indicates 4-7 Hz as the best predictor, and O2 which has the 8-40 Hz variable as the best predictor.

Unlike the other ERPs, guess rate from the P3 (360-500 ms) ERP trials had a difference in the proportion of explained variances between the high and low trials. That is, at all

electrodes, the trials categorized as "low" had more explained variance by the set of predictors than trials categorized as "high" (0.964-0.980 and 0.935-0.976, respectively). In all cases, the majority of the proportion of explained variances came from the 2-3 Hz guess rates though 4-7 Hz was often a relatively important predictor. The exceptions were O1 and O2 which consistently had 8-40 Hz as the most important predictor variable.

Like the results from the guess rate analyses of the P3 (360-500 ms) ERP trials, the standard deviation (σ) parameter indicated that the proportion of explained variances differed between trials categorized as "low" compared to "high." However, Fp1 and FC2 had more explained variance for the low category of trials than the high (see Table B.2), whereas the parietal and occipital electrodes were the reverse (low: 0.700-0.898; high: 0.867-0.928). Interestingly, the most important predictor variables tended to differ between the high and low categories. Most of the time, 4-7 Hz was ranked the most important predictor in the high category, whereas 2-3 Hz was ranked the most important predictor in the low category. The notable exception was the low category of the O2 electrode which had the proportion of explained variance increase from 0.570 to 0.709 with the addition of the 4-7 Hz predictor.

Appendix Table B.2. *Stepwise regression results for the standard deviation (σ) parameter.*

Trial Category	Predicted P3 (360-500 ms)		
	Model	$b*$	R^2_{adj}
	Fp1		
High	Step 1		0.865
	2-3 Hz	0.93	
	Step 2		0.904
	2-3 Hz	0.34	
	4-7 Hz	0.63	
	Step 3		0.899
	2-3 Hz	0.29	
	4-7 Hz	0.56	

	8-40 Hz	0.11	
Low	Step 1		0.884
	2-3 Hz	0.94	
	Step 2		0.916
	2-3 Hz	0.64	
	4-7 Hz	0.35	
	Step 3		0.912
	2-3 Hz	0.65	
	4-7 Hz	0.37	
	8-40 Hz	-0.02	
	FC2		
High	Step 1		0.879
	2-3 Hz	0.94	
	Step 2		0.880
	2-3 Hz	0.75	
	4-7 Hz	0.21	
	Step 3		0.906
	2-3 Hz	0.24	
	4-7 Hz	0.09	
	8-40 Hz	0.65	
Low	Step 1		0.893
	2-3 Hz	0.95	
	Step 2		0.913
	2-3 Hz	0.53	
	4-7 Hz	0.44	
	Step 3		0.915
	2-3 Hz	0.34	
	4-7 Hz	0.35	
	8-40 Hz	0.29	
	P5		
High	Step 1		0.921
	2-3 Hz	0.96	
	Step 2		0.931
	2-3 Hz	0.42	
	4-7 Hz	0.55	
	Step 3		0.928
	2-3 Hz	0.51	
	4-7 Hz	0.60	
	8-40 Hz	-0.13	
Low	Step 1		0.787

	2-3 Hz	0.89	
	Step 2		0.791
	2-3 Hz	1.33	
	4-7 Hz	-0.46	
	Step 3		0.788
	2-3 Hz	1.79	
	4-7 Hz	-0.42	
	8-40 Hz	-0.49	
	P7		
High	Step 1		0.849
	2-3 Hz	0.93	
	Step 2		0.870
	2-3 Hz	0.02	
	4-7 Hz	0.92	
	Step 3		0.867
	2-3 Hz	0.24	
	4-7 Hz	1.09	
	8-40 Hz	-0.39	
Low	Step 1		0.721
	2-3 Hz	0.86	
	Step 2		0.722
	2-3 Hz	1.45	
	4-7 Hz	-0.61	
	Step 3		0.738
	2-3 Hz	1.69	
	4-7 Hz	-1.43	
	8-40 Hz	0.62	
	P8		
High	Step 1		0.911
	2-3 Hz	0.96	
	Step 2		0.913
	2-3 Hz	0.68	
	4-7 Hz	0.29	
	Step 3		0.924
	2-3 Hz	0.45	
	4-7 Hz	0.10	
	8-40 Hz	0.43	
Low	Step 1		0.875
	2-3 Hz	0.94	
	Step 2		0.890
	2-3 Hz	0.66	

	4-7 Hz	0.31	
	Step 3		0.898
	2-3 Hz	0.71	
	4-7 Hz	-0.12	
	8-40 Hz	0.40	
	O1		
High	Step 1		0.903
	2-3 Hz	0.95	
	Step 2		0.919
	2-3 Hz	0.40	
	4-7 Hz	0.57	
	Step 3		0.926
	2-3 Hz	0.00	
	4-7 Hz	0.49	
	8-40 Hz	0.49	
Low	Step 1		0.859
	2-3 Hz	0.93	
	Step 2		0.855
	2-3 Hz	0.81	
	4-7 Hz	0.12	
	Step 3		0.880
	2-3 Hz	1.54	
	4-7 Hz	0.01	
	8-40 Hz	-0.64	
	O2		
High	Step 1		0.850
	2-3 Hz	0.93	
	Step 2		0.881
	2-3 Hz	0.43	
	4-7 Hz	0.52	
	Step 3		0.875
	2-3 Hz	0.37	
	4-7 Hz	0.51	
	8-40 Hz	0.07	
Low	Step 1		0.570
	2-3 Hz	0.77	
	Step 2		0.709
	2-3 Hz	-0.20	
	4-7 Hz	1.04	
	Step 3		0.700
	2-3 Hz	0.10	

4-7 Hz	1.14
8-40 Hz	-0.40

Note. Predictors in each model are the guess rate parameters from fitting the standard mixture model to trials categorized as high or low log power in the specified frequency band and time windows. Predicted values are the standard deviation parameters from fitting the standard mixture model to trials categorized as high or low ERP amplitudes in the specified time windows. $b*$ = estimated values of standardized regression coefficients; R^2_{adj} = adjusted coefficient of determination (*i.e.,* coefficient of determination adjusted for number of predictors).

References

Faraway, J. J. (2016). *Linear Models with R* (2nd ed.). Chapman and Hall/CRC. https://doi.org/10.1201/b17144

Karakaş, S., Erzengin, Ö. U., & Başar, E. (2000). The genesis of human event-related responses explained through the theory of oscillatory neural assemblies. *Neuroscience Letters*, *285*(1), 45–48. https://doi.org/10.1016/S0304-3940(00)01022-3